Republic of Iraq

Ministry of Higher Education & Scientific Research

University of Kerbala

College of Engineering

Civil Engineering Department

Flexural Performance of Bilayer Concrete Beams Reinforced with Different Types of Rebars

A Thesis Submitted to the Council of Civil Engineering Department/College of Engineering/University of Kerbala in Partial Fulfillment of the Requirements for Master Degree of Sciens in Civil Engineering/Structure

Prepared by :

Salam Hussein Madloul

(B. Sc. in Civil Engineering-2019)

Supervised by :

Asst. Prof. Dr. Zainab M. R. Abdul Rasoul

Asst. Prof. Dr. Mushtaq Sadiq Radhi

April 2025 Shawwal 1446

بسم الله الرحمن الرحيم

يَرْفَعِ اللَّهُ الَّذِينَ آمَنُوا مِنكُمْ وَالَّذِينَ أُوتُوا الْعِلْمَ دَرَجَاتٍ

صدق الله العلي العظيم

(المجادلة: من الآية 11)

Supervisor certificate

We certify that the thesis entitled **"Flexural Performance of Bilayer Concrete Beams Reinforced with Different Types of Rebars "** was prepared by **Salam Huusein Madloul** under our supervision at the Department of Civil Engineering, Faculty of Engineering, University of Kerbala as a partial of fulfilment of the requirements for the Degree of Master of Science in Civil Engineering.

Signature:

Asst. Prof. Dr. Zainab M. R. Abdul Rasoul

Date: / / 2025

Signature: M. S. Radh

Asst. Prof. Dr. Mushtaq Sadiq Radhi

Date: / / 2025

Linguistic certificate

I certify that the thesis entitled "**Flexural Performance of Bilayer Concrete Beams Reinforced with Different Types of Rebars** ," which has been submitted by Salam Hussein Madloul, has been proofread, and its language has been amended to meet the English style.

Signature:

Linguistic Supervisor: Dr. Hawraa Jabbar Rahi

Date: / / 2025

Examination Committee Certification

We certify that this thesis entitled "**Flexural Performance of Bilayer Concrete Beams Reinforced with Different Types of Rebars**" and as an examining committee examined the student "**Salam Hussein Madloul**" in its content and in what is related to it, and that in our opinion it meets the standards of a dissertation for the degree of Master of Science in Civil Engineering (Structural Engineering Branch).

Supervisor

Signature:

Name: Assist. Prof. Zainab M. R. Abdul Rasoul

Date: / / 2025

Supervisor

Signature:

Name: Assist. Prof. Mushtaq Sadiq Radhi

Date: / / 2025

Member

Signature:

Name: Assist. Prof. Dr. Wail A.M. Hussain

Date: / / 2025

Member

Signature:

Name: Lec. Dr. Kamal Darweesh Ibrahim

Date: / / 2025

Chairman

Signature:

Name: Prof. Dr. Haitham H. Muteb

Data: / / 2025

Approval of the Department of Civil Engineering

Signature:

Name: Assist. Prof. Dr. Aysar Tuama Al-Awadi

Date: / / 2025

Approval Deanery of the College of Engineering University of Kerbala

Signature:

Name: Prof. Dr. Haider Nadhom Azziz

Data: / / 2025

Undertaking

I certify that research work titled **"Flexural Performance of Bilayer Concrete Beams Reinforced with Different Types of Rebars "** is my own work. The work has not been presented elsewhere for assessment. Where material has been used from other sources, it has been properly acknowledged / referred.

Signature: 

Salam Hussein Madloul

Date: / / 2025

Dedication

To the light of sacrifice and steadfastness, **Imam Hussain (peace be upon him)**, whose eternal stand inspires resilience and purpose; To my awaited hope, **Imam Al-Mahdi (may Allah hasten his reappearance)**, for whom we strive with sincerity and knowledge; To my dearest parents, whose love, prayers, and endless support have shaped every step of this journey; to my family, for their patience and encouragement through every challenge; and to all those who guided me along the path of learning .. I dedicate this humble work with deep gratitude and love.

Signature: 

Salam Hussein Madloul

Date: / / 2025

Acknowledgments

All praise is due to Allah, the Most Gracious, the Most Merciful, who granted me the strength, determination, and patience to complete this research journey. I want to express my sincere gratitude and appreciation to my supervisors, **Asst. Prof. Dr. Zainab M. R. Abdul Rasoul** and **Asst. Prof. Dr. Mushtaq Sadiq Radhi**, for their valuable guidance, continuous support, and insightful advice throughout this study. Their encouragement and expertise have been instrumental in shaping the direction and quality of this work. My heartfelt thanks go to the Head of the Civil Engineering Department at the University of Karbala and all its respected faculty and staff for their support, facilities, and contributions, which made this research possible.

I would like to extend my special gratitude to **"Dr. Bahaa Hussein"** for his assistance during the experimental work. I would also like to sincerely thank **"Dr. Sadjad Amir"** for his valuable support and encouragement during my academic journey at the University of Karbala. I am especially thankful to my dear friend **"Alhussain Basim Jaafar"**, whose generous help and assistance in the experimental phase were crucial and genuinely appreciated. I am deeply indebted to my beloved parents and family for their endless love, prayers, and sacrifices. Their support has been a cornerstone throughout my academic path.

Finally, I dedicate this work to the symbol of sacrifice and steadfastness, **Imam Al-Hussain** (peace be upon him), and to the hope of justice and truth, **Imam Al-Mahdi** (may Allah hasten his reappearance), asking Allah to accept this humble effort in their honor.

Signature: 

Salam Hussein Madloul

Date: / / 2025

Abstract

A bilayer concrete beam is a specialized structural element composed of two types of concrete layers. This configuration is designed to improve structural efficiency by providing enhanced flexural strength, durability, and ultimate load capacity throughout different operating situations. However, combining glass, carbon fiber reinforced polymer (GFRP, CFRP), steel, and hybrid reinforcement in bilayer concrete beams was a suitable substitute for standard steel reinforcing due to its impressive ratio of strength to weight and improved flexural performance and crack resistance. This study aims to experimentally and numerically evaluate the flexural performance (load capacity, crack propagation, and deflection) of bilayer concrete beams reinforced with different types of rebars (steel, CFRP, GFRP, or hybrid) under two-point loading. Fifteen models measuring (150, 200, and 1400) mm were fabricated on-site, six models consisted of a single layer of concrete, whereas nine models were constructed from bilayers of concrete. Normal-strength concrete (NSC) generally used in the tension zone, whereas high-strength concrete (HSC) applied in the compression zone to enhance material performance and structural behavior. The subjects were planned to be classified into four sections according to the reinforcement employed: steel, CFRP, GFRP, and different type of rebars. The nonlinear beam behavior was modeled using ABAQUS numerical analysis. An average difference in a maximum load of 2.1% and a maximum deflection of 4.93% showed that the numerical model matched experimental measurements. The findings indicated that the bilayer concrete system models exhibited an enhancement in ultimate load and the magnitude of the first crack load by 12.77% and 30.95%, respectively, compared to models built with a single layer of concrete. The hybrid reinforcement models exhibit a 7.3% greater ductility than those reinforced with a one type of rebar. The suggested hybrid designs improved structural performance, presenting a feasible method for sustainable and robust concrete structures.

Table of Contents

Chapter Three: The Experimental Work

List of Tables

List of Figures

Chapter One: Introduction

Chapter Two: Literature Review

Chapter Three: The Experimental Work

Chapter Four: Results and Discussion (Experimental)

Chapter Five: Finite Element Analysis

List of Abbreviations

ACI	**American Concrete Institute**
AFRP	Aramid fiber reinforced polymer
ASTM	American Society for Testing and Materials
CC	Control combination
CFRP	Carbon fiber-reinforced polymer
DOF	degrees of freedom
EFNARC	European guidelines for self-compacting concrete
et al.	others
FEA	Finite Element Analysis
FEM	Finite Element Method
FRCC	Fiber-reinforced cementitious composites
FRP	Fibre reinforcement polymer
GFRP	Glass fiber-reinforced polymer
GHG	greenhouse house gas
HSC	High Strength Concrete
HVFA	high-volume fly ashes
HVFAC	high-volume fly ash concrete
IQS	Iraqi specification
LVDT	Linear Variable Differential Transformer
LWA	lightweight aggregate
LWAC	lightweight aggregate concrete
mm	Millimeter
NC	Normal concrete
No.	Number
NSC	Normal Strength Concrete
NSM	Near-surface mounted
NVC	Normal vibrated concrete
PC	Portland Cement

RC	Reinforced Concrete
S4R	Shell Element Four-Node Reduces Integration
SCC	Self-compacted concrete
SCMs	Supplemental Cementitious Materials

List of Symbols

F'_c	**Compressive Strength of Concrete (N/mm^2)**
A	The Cross-Sectional Area of a Section (mm^2)
A_v	Area of Vertical Shear Reinforcing Bar (mm^2)
d	Effective Depth of Beam (mm)
f_y	Yield Stress of Steel (N/mm^2)
M_n	Nominal Moment Capacity (kN.m)
M_u	Ultimate Moment Capacity (kN.m)
$P_{max.}$	Maximum Applied Load (kN)
V_c	Shear Strength of Concrete (kN)
V_n	Nominal Shear Strength (kN)
V_s	Shear Strength of Steel Bar (kN)
V_u	Ultimate Shear Strength (kN)
ρ	The Ratio of Longitudinal Tensile Reinforcement
ρ_{min}	Minimum Ratio of Longitudinal Tensile Reinforcement
ϕ	Size of the Bar (mm)
C3D8R	8-Node Linear Brick
T3D2	2-Node Linear Displacement
Φ	Reduction Factor According to ACI

Chapter One: Introduction

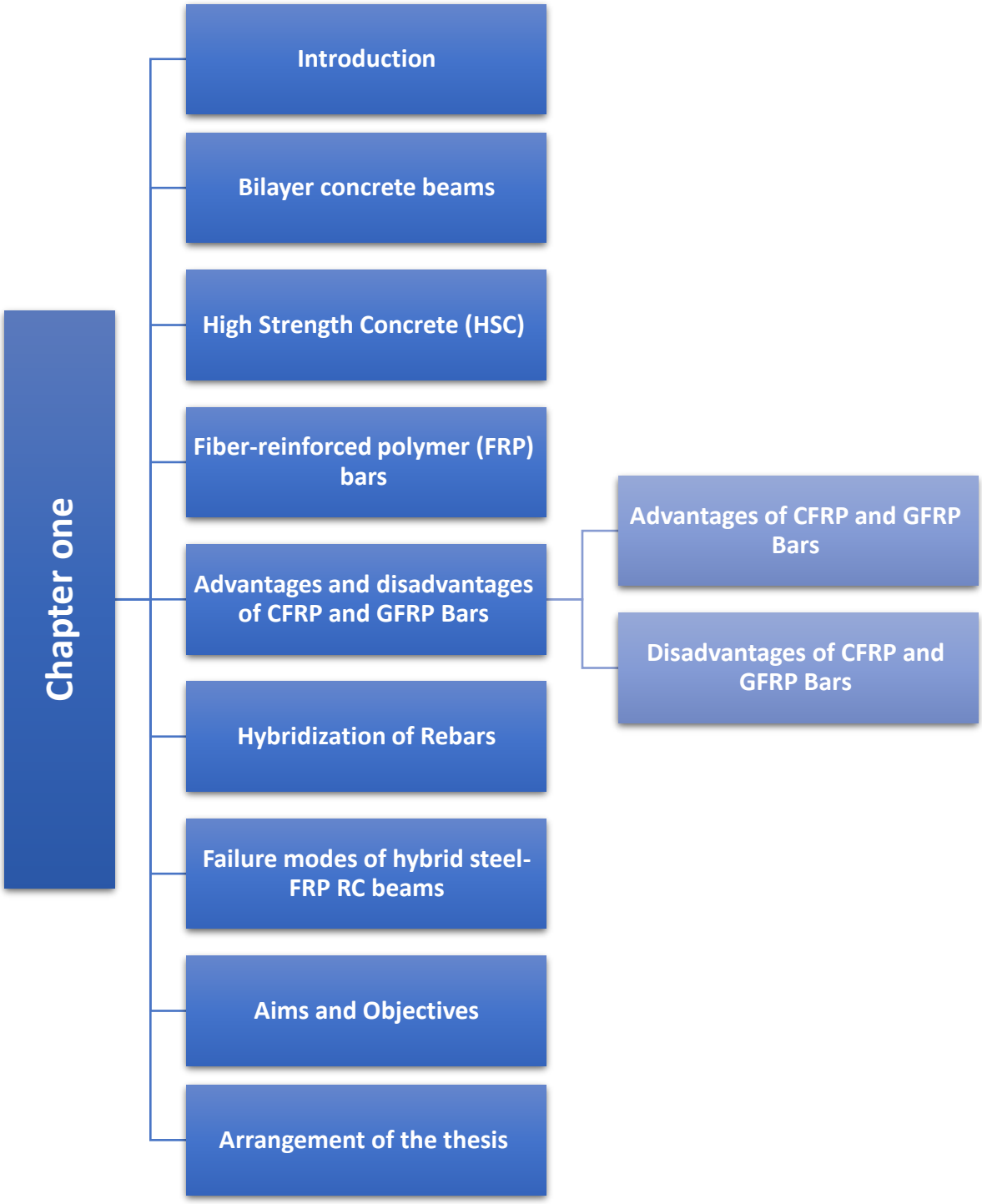

Chapter One
Introduction

1.1 Introduction

A concrete beam is a structural element used in engineering that extends over an open space. It is a structural component designed to transmit a load. Due to concrete's low tensile strength and high compressive strength, applied load will ultimately initiate a fracture at the bottom of the beam, progressing upward. These beams, which are known as reinforced concrete beams, are created by embedding steel bars, plates, or fibres into the concrete **(Martin Perry Associates, 2022)**.

In civil engineering construction, choosing any material aims to optimize its qualities to provide optimal performance for the constructed structure. The material's advantages depend on availability, structural integrity, durability, workability, and cost-effectiveness. Due to the challenge of identifying a material that exhibits all these features to the required degree, the engineer's task involves optimising several materials and building techniques. High-strength concrete (HSC) reduces beam dimensions while enhancing strength, leading to increased expenses compared to normal-strength concrete. In contrast, using normal-strength concrete (NSC) leads to excessive concrete (layer thickness) for the beam section. For balance. The correlation between the cost and dimensions of beams facilitates the efficient use of materials through a dual-layer configuration: HSC in the compression zone (upper layer) increases beam strength, while NSC in the tension zone (lower layer) is adequate, eliminating the need for HSC in that region **(Najm & Fahmi, 2023)**.

1.2 Bilayer concrete beams

Reinforced concrete beams, composed of two layers of different strengths, are classified as composite constructions and may, therefore, be analyzed using established techniques for composite materials. In these beams, high-strength concrete (HSC) is used just in the compression zone since the tensile zone's concrete resistance can often be disregarded **(Iskhakov & Ribakov, 2007, 2013).**

Expanding the construction business has necessitated the enhancement of affordability in building components via cost retention, leading to the use of composite sections. A composite member integrates several materials to form a composite structural component with advantageous material characteristics. The rationale is to optimize the use of construction resources since no single material can satisfy all structural criteria independently. Common examples include steel-reinforced concrete constructions. A member with two or more concrete kinds is categorized as a composite structure. High-strength concrete (HSC) reduces beam dimensions and increases strength, leading to an excessive volume of concrete in the beam section. A bilayer technique maximises the balance between cost and beam dimensions, employing high-strength concrete (HSC) in the compression zone (upper layer) to augment beam strength. Conversely, NSC is employed in the tension zone (lower layer), as HSC is superfluous in this area. Combining plain concrete and fibre-reinforced concrete in beams as dual-layer composite elements may significantly improve flexural performance and reduce the cost of these structural components **(Iskhakov & Ribakov, 2007).**

1.3 High strength concrete (HSC)

The use of HSC in the planning industry has risen owing to its superior mechanical qualities relative to conventional concrete. The shear refusal of concrete beams is a significant focus of study **(Sudheer & Ramana, 2011)**. The current advancement in concrete technology yields high compressive strength concrete ranging from 40 to 150 MPa. High-strength concrete may be achieved by incorporating extensive combinations of water-reducing compounds (superplasticizers) and additional admixtures (silica fume or fly ash) into Portland cement concrete **(Newman & Choo, 2003)**. Superplasticizer chemicals significantly diminish the water used to create a workable mixture, enabling concretes with water-cement ratios around 0.25 or lower to flow effortlessly without considerable bleeding and segregation. High-strength concrete in construction facilitates the design of smaller sections, reduces dead weight, and permits longer spans and increased usable areas in buildings, exemplified by prestressed concrete beams, bridges, high-rise structures, and structural repairs **(ACI Committee 363, 1992)**.

1.4 Fiber reinforced polymer (FRP) bar

This bar is regarded as an ideal material for competitive applications. It has a significant strength and stiffness-to-density ratio, along with corrosion resistance. Furthermore, FRP bars possess a low weight, exhibit fatigue resistance, and are impervious to magnetic and electrical forces. Due to these characteristics, together with the increased tensile strength of FRP bars, they may serve as a substitute for steel bar reinforcement. FRP bars exhibit no plastic deformation (yielding) when subjected to tensile loading before failure. Carbon, glass, and aramid fibres are the predominant fibres used. This study used two types, Carbon Fibre fibre-reinforced polymer (CFRP) and Glass Fibre fibre-reinforced polymer (GFRP), in both experimental and

numerical investigations—the two types of bars (CFRP and GFRP). **Figures (1.1)** and **(1.2)** show the strain-stress relations for these FRP types**.**

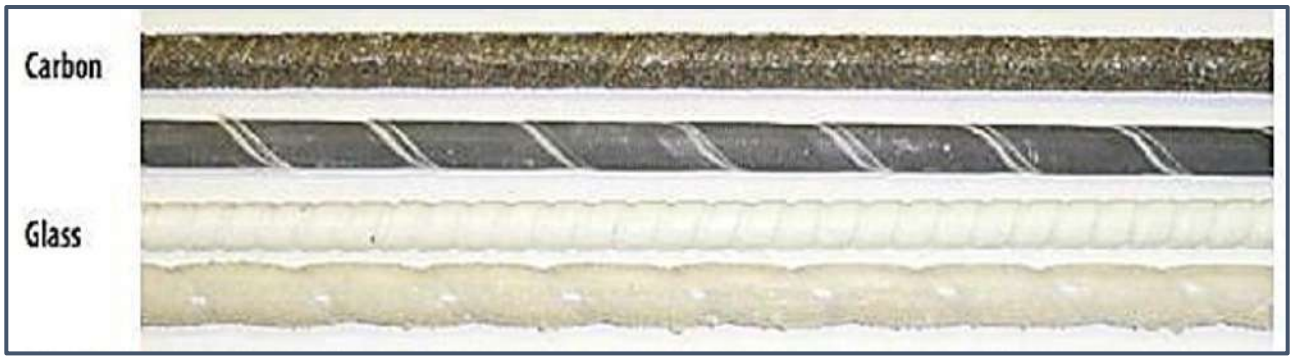

Figure (1.1): FRP bars with various surface preparations: CFRP (top two), GFRP (middle two), and BFRP (bottom two) (Szabó, 2013).

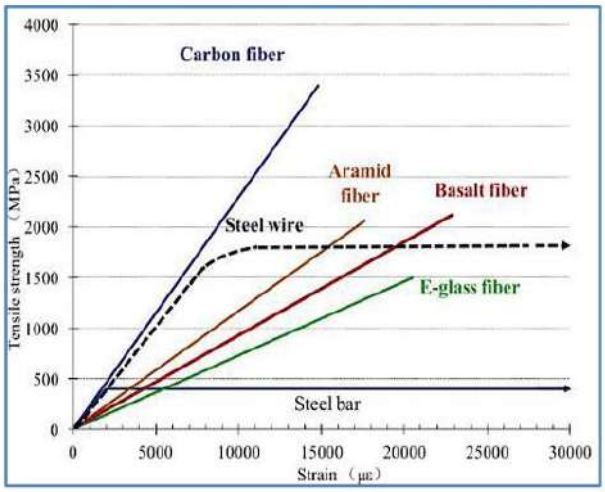

Figure (1.2): Stress-strain relation for various FRP types (Ramakrishnan et al., 2019).

Table (1.1): Rebar Material Properties

Material	Yield Strength (MPa)	Young's Modulus (GPa)	Ultimate Strain (%)
Steel	420–550	200–210	10–15
CFRP	– (no yield)	120–600	1.2–2.0
GFRP	– (no yield)	35–55	1.5–3.0
BFRP	– (no yield)	45–55	2.0–3.0
Aramid FRP	– (no yield)	70–130	2.5–4.0

1.5. Advantages and disadvantages of CFRP and GFRP Bars

Structural engineers increasingly use composite materials like GFRP and CFRP instead of steel reinforcement. These materials excel in extreme environments and specialty applications because of their high strength-to-weight ratios, electromagnetic neutrality, and corrosion resistance. However, their ubiquitous usage has limitations, such as brittle failure modes, high pricing, and low fire resistance.

1.5.1 Advantages of CFRP and GFRP Bars

Some of the FRP advantages are listed, compared with the traditional steel reinforcement according to **(ACI 440.1r, 2015):**

- Exceptional longitudinal tensile strength.
- Resistance against corrosion.
- Nonmagnetic.
- Exceptional fatigue endurance.
- Lightweight (about 1/5 to 1/4 the density of steel).
- Reduced thermal and electrical conductivity.

1.5.2 Disadvantages of CFRP and GFRP Bars

Some of the FRP disadvantages are listed, compared with the traditional steel reinforcement according to **(ACI 440.1r, 2015):**

- Before brittle rupture, there must be no yielding.
- Low crosswise strength.
- Low modulus of elasticity (150,50 Gpa) for CFRP, GFRP, respectively.
- Vulnerability of polymeric resins and fibers to deterioration from UV light exposure.
- Elevated coefficient of thermal expansion orthogonal to the fibers, compared to concrete.

- Potential vulnerability to fire, contingent upon the kind of matrix and concrete cover thickness.

1.6 Hybridization of Rebars

FRP intrinsically lacks flexibility but has many advantages depending on the construction material. Hence, the composite system formed by FRP bars and reinforced concrete (RC), named FRP-reinforced concrete fiber-reinforced polymer reinforced concrete (FRPRC), generally has low elasticity **(Bank,2013)**. To enhance the flexibility of such composite techniques, it is suggested to improve a specific volume of steel bars in FRPRC techniques such that the brittleness of FRP bars may be reimbursed by the malleable nature of the added steel reinforcement RC beams that contain both FRP and steel bars are indicated as hybrid FRPRC beams. However, the performance of the structure of such hybrid beams has not been wholly examined so far. An enhancement of the performance of structural concrete beams may be achieved by using a combination of FRP and steel reinforcement or, instead, FRP rebars produced by combining two or more diverse materials. Ductility is significant because it yields a noticeable warning before failure; consequently, the loss of the soul's life may be significantly decreased. With the ductility of limited FRPRC beams, engineers are reluctant to depend on FRP bars in building production, as shown in **Figure (1.3) (Lau & Pam, 2010).**

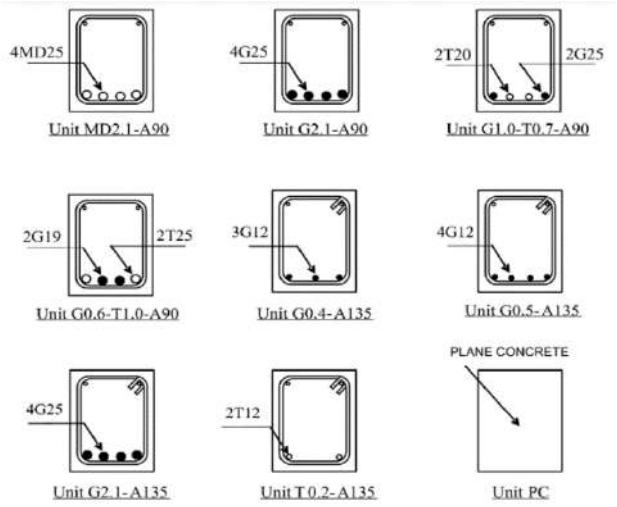

Figure (1.3): Cross-section details of all the beam specimens (Lau & Pam, 2010).

1.7 Failure modes of hybrid steel-FRP RC beams

The beam fails due to concrete under compression and either the rupture of FRP or steel yielding under tension, concurrently with reinforced concrete beams that use FRP or steel as stable reinforcement. The ratio has been attained. However, the simultaneous occurrence of steel bar yielding, concrete cracking, and FRP rupture in hybrid (FRP/steel) reinforced concrete beams is a very problematic failure condition. The steel bar may be manufactured far in advance of the failure of FRP reinforcement. Consequently, the stability condition for hybrid FRP-steel reinforced concrete beams is proposed by a method, such as simultaneous failure of FRP reinforcement and concrete compression failure. At the same time, steel bars would have already been produced **(Kara & Köroğlu, 2015).**

1.8 Aims and Objectives

This study aims to survey the flexural behaviors of supported (bilayer and composite with hybrid reinforcement) beams. Bilayer beams were cast of two concrete types, normal concrete and high-strength concrete. High-strength concrete was used in compression layer near to the plastic zones to benefit from HSC properties where it is required. The beams are reinforced using steel bars, FRP bars reinforcement of two types of bars to estimate the effect of reinforcement kind on the behavior of the bilayer beams.

In light of this, this study aims to accomplish the following objectives:

- Examining the flexural behavior of supported beams (bilayer and composite with various reinforcements) subjected to static loads by analyzing the impact of different concrete layer types in compression zones (under compression) and the type of primary reinforcement (steel, FRP, or hybrid) on the structure.
- Examining the influence of the high-strength layer on the performance and ultimate load capacity of supported hybrid beams.

- Study the impact of introducing different types of reinforcement on the bilayer concrete beam and determine the pattern and form of failure.
- Will be utilize ABAQUS finite element software to simulate the flexural behavior of bilayer concrete beams and to perform a parametric analysis after validating the numerical model with experimental results.

1.9 Arrangement of the thesis

There are six chapters to the thesis:

Chapter One, which is the current chapter, explains a general introduction to the bilayer concrete beam with different rebars, its applications, failure modes of hybrid steel-FRPRC beams, and the problem and aim of the present work.

Chapter Two summarizes past researches on properties or reviews of theoretical and experimental studies relevant to hybrid beams to observe the latest studies.

Chapter Three details the experimental work, which includes material properties, concrete mix ratios, reinforcing and formworks, casting and curing, and conducting laboratory tests.

Chapter Four includes the results obtained from the tests conducted on the experimental models in the current study. Deep discussions of all results have been presented to give a good idea about the behavior of hybrid beams. Moreover, some parametric studies have investigated the effect of some controlling parameters for this type of bilayer beams.

Chapter Five implements the results of the nonlinear analysis of selected beams tested under static loads using ABAQUS software and compares the results with available practical values. It also studies some parameters' influence on the bilayer beams' flexural behavior.

Chapter Six summarises the main conclusions obtained from the present research in addition to several suggestions for future work studies in connection with the topic of this study.

Chapter Two: Literature Review

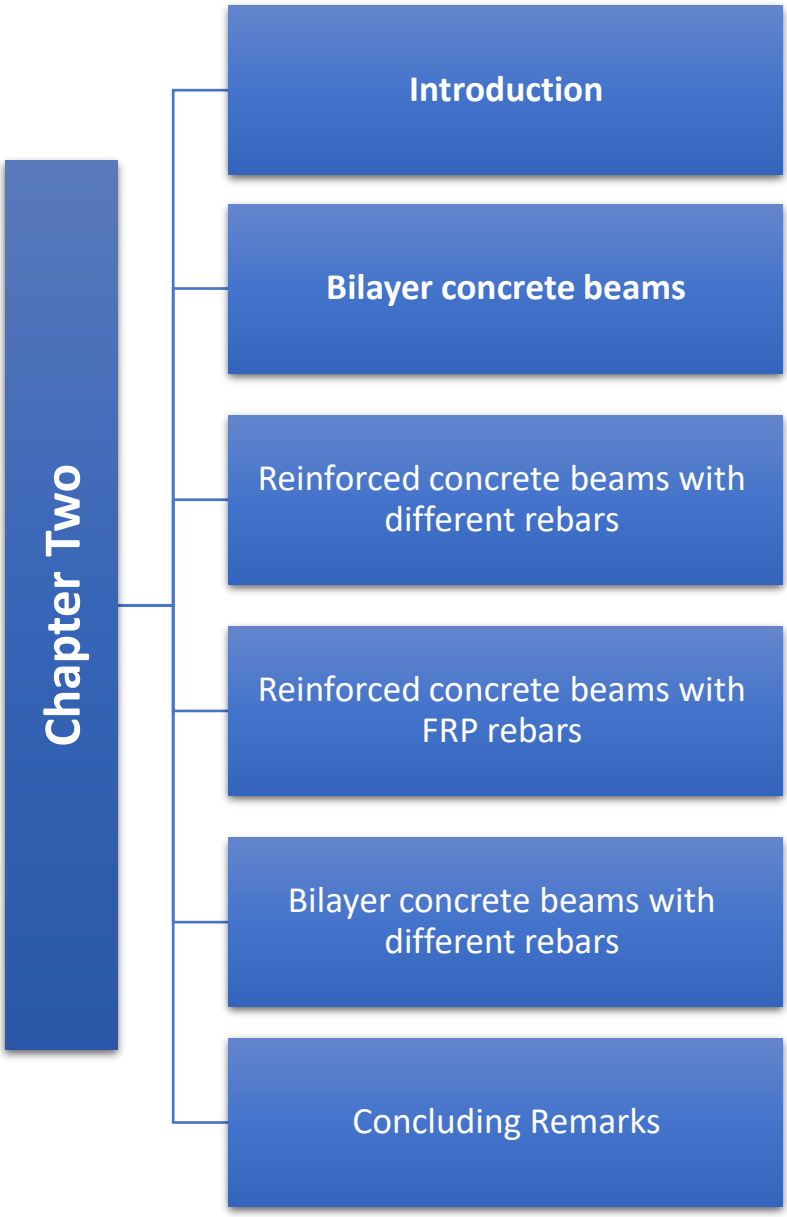

Chapter two
Literature review

2.1 Introduction

This chapter reviews previous studies published on bilayer concrete beams with different rebars. Both experimental and theoretical works have been considered. Other parameters that were of concern in previous studies have been discussed. The researchers have reported the most significant findings for each study on bilayer beams with different rebars worldwide, and the studies have been grouped into four categories. The **first** concern is those published on bilayer concrete beams. The **second** regarded reinforced concrete beams with hybrid bars. The **third** group discussed studies concerning FRP bars in concrete beams. The **last** group discussed bilayer concrete beams with different rebar. Furthermore, a summary of the investigations about hybrid beams with different rebar has been reported.

2.2 Bilayer Concrete Beams

Certain studies examined hybrid beams, employing multiple concrete types within the beam; high-strength concrete is utilized to minimize beam dimensions and enhance strength, resulting in inflated costs relative to NSC, whereas the use of normal-strength concrete results in an excessive volume of concrete (layer size) in the beam section. A dual-layer approach is employed to optimize the balance between cost and beam dimensions: HSC is used in the compression zone (upper layer) to enhance beam strength. In contrast, regular-strength concrete is applied in the tension zone (lower layer) **(Najm & Fahmi, 2023)**.

Grepstad and Overli (2007) were tested ten hybrid reinforced concrete beams. A variety of hybrid concrete beams with different diameters were tested for

flexural performance. These beams included lightweight concrete on top and fiber reinforced concrete on bottom, with a thickness of 50 mm. The beams were bent in four different directions. Half of the beams in the testing program had steel fiber reinforcement and the other half had synthetic fibers in the bottom layer. The small size beams were 600 × 150 × 150 mm, while the large beams measured 3000 × 150 × 250 mm. The beams were also statistically analyzed using DIANA, a finite element program. Scientists found that moment failures and a single fracture zone were the primary factors affecting the small beams' behavior. In the large beams, the ultimate capacity was decided by moment and shear failures, and a distributed fracture pattern was seen. The global response of the beams was well approximated by the numerical simulations.

An experimental investigation of hybrid-strength concrete beams was presented by **(Kheder et al., 2010)**. The flexural and cracking behavior of hybrid strength concrete beams, having compressive strengths of 20 and 70 MPa, was compared to regular 20 MPa and high strength 70 MPa beams. The hybrid beams exhibited superior load-bearing capacity at cracking, yielding, and ultimate loading compared to conventional strength beams. The enhancement in load-bearing capacity was 1.80–70.8% more than standard strength beams and just 3.3–9.8% less than comparable high compressive strength beams. Experimental results demonstrate that the fracture spacing in hybrid beams is intermediate between that of normal strength and high strength beams; nevertheless, the crack width in hybrid beams is consistently shorter than that of both types at all loading stages. In the service and ultimate loading phases, the fracture width in the hybrid beams was 19.5–26.0% smaller than that of the equivalent normal strength beams and 9.2–15.1% narrower than that of the high strength beams.

An experimental investigation was presented by **(Sarsam & Mohammed, 2014)** to study the response for twenty-four supported RC beams with rectangular sections. Three beams were constructed with conventional concrete, five using Reactive Powder Concrete (RPC), and the others were hybrid beams, including both concrete kinds. At 10 specimens of hybrid beams, RPC was used at the bottom (tension zones), whereas in other hybrid beams, RPC was employed at the top (compression zone), as seen in Figure (2.1). From the experimental results that the load-deflection response became stiffer with an increase in the thickness of the RPC layer, the volumetric ratio of steel fibers, and the percentage of steel reinforcement for both kinds of hybrid beams. Furthermore, it was determined that RPC had greater compression efficacy than tension zones.

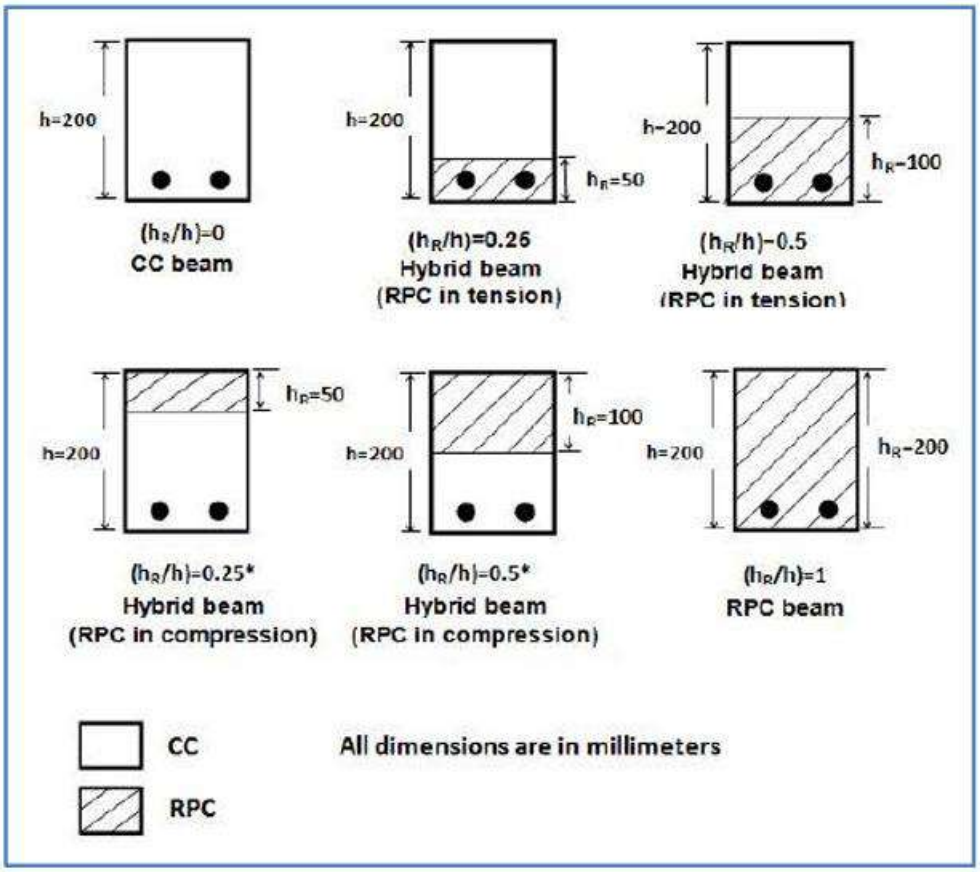

Figure (2.1): Types of Beams Used in Sarsam and Mohammed's Paper (Sarsam & Mohammed, 2014)

(Hassan, 2015) Twelve specimens of supported deep beams were evaluated, including three conventional concrete, three high-performance concrete (RPC), and six of a hybrid of standard and high-performance composite concrete in the compression zone, as shown in Figure 2.2. Utilizing varying quantities of steel fibers (0%, 0.5%, 1%). The findings indicated that a more rigid load-deflection response was achieved with increased UHPC layer thickness. Using 0.52% and 1% steel fibers embellished the cracking load (26.13% and 58.42%), whereas the ultimate load was increased by 25.49% and 44.33%, respectively.

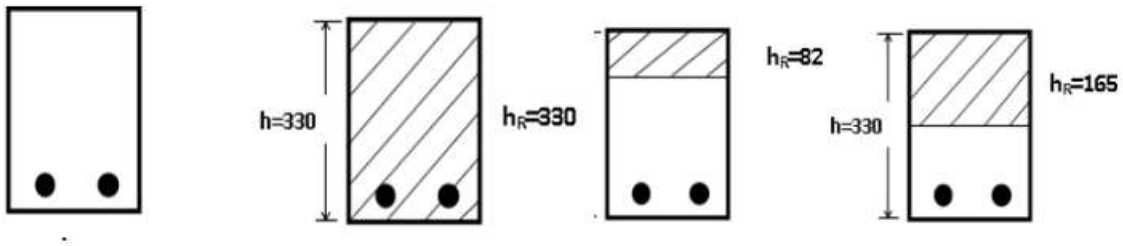

Figure (2.2): Types of the Tested Beams (Hassan, 2015)

(Hassan and Faroun, 2016) Examined the behavior of hybrid deep beams subjected to monotonic and cyclic loading. Two varieties of concrete were utilized: coarse concrete was applied on both faces of the beam inside the shear region, while normal concrete was positioned in the center. The variables included the loading type, quantity of steel reinforcement, and percentage of steel fibers (0, 1, 2) %. The ratio of shear span to effective depth (a/d) is 1.14. The ultimate load ratio under repeated loading diminishes by 27.08% and 25.09% for fiber ratios of 1% and 2%, respectively, and drops by 20.81% and 18.81% when comparing regular concrete to fibrous concrete.

(Nguyen et al., 2020) test-based analyses were conducted of the action of hybrid deep beams, including two varieties of steel fibers, long and short, at varying ratios of 0%, 1%, and 2%. At the same time, the compressive strength of the concrete varied from 66 to 72 MPa. The variable examined was the impact of both categories

of steel fibers. The load was high by 67% plus 114%, adding 1% and 2% fibers, respectively, compared to the standard deep beam.

(Sada, 2021) investigated the response of changing the section area and using hybrid concrete on the deep beam capacity. The experimental study included fourteen deep beams with a trapezoidal section, categorized based on concrete compressive strength (25, 50, 70 MPa), with high-strength concrete positioned at the top and normal concrete at the bottom of each beam, as seen in Figures 2.3 and 2.4. The findings indicated that shear strength enhanced with the expansion of HSC in the upper zone, with gains ranging from 3.66% to 8.63% relative to control specimens. The load at which diagonal cracking occurred decreased, and the hybrid exhibited significant ductility.

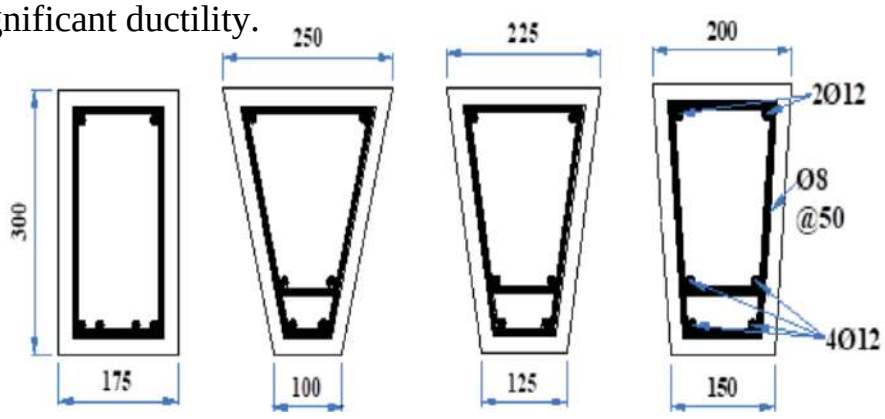

Figure (2.3): Steel reinforcement distribution (Sada, 2021).

Figure (2.4): Specimen matrix (Sada, 2021).

2.3 Reinforced concrete beams with different rebars

As was mentioned in chapter one, the problem of steel corrosion may be resolved by using FRP (fiber-reinforced polymers) bars as the primary reinforcement in concrete members instead of conventional steel. Nonetheless, an additional issue arose with applying FRP bars due to FRP's linear elastic stress-strain behavior under tension until reaching ultimate loads. This results in the brittle failure of FRP. Consequently, the flexural performance of FRP bars in reinforced concrete beams demonstrates limited ductility. FRP bars have significant tensile strength but lack yielding properties. As a result, beams reinforced with them exhibit minimal ductility but possess high resistance moments. Various beams may provide a balanced method for attaining the requisite ductility by permitting a defined degree of force dissipation for a particular application. **(Nachiappan et al., 2014)**. Few researchers have experimentally tested the behavior of continuous composite concrete beams with FRP bar reinforcement, compared with supported beams **(Cheung & Tsang, 2010).**

(Harris et al., 1998), conducted experimental studies on hybrid FRP rebars to replicate the elastic-plastic behavior of steel by using pseudo-ductile materials (demonstrating a progressive failure mechanism that resembles ductility, offering a warning before fracture while being intrinsically brittle) via the combination of two or more distinct FRP reinforcing materials. The ductility index of the beam was almost equivalent to that of the standard steel-reinforced beams. The elevated cost of the hybrid bars and the intricate production process limited their practical usage. ultimate failure strain between 2% and 3%.

(Aiello and Ombres, 2002), experimentally studied the structural performances of concrete beams with hybrid fiber-reinforced polymer-steel (FRP) reinforcement using six beams with rectangular cross-sections. The study pertains

to the capacity of tested concrete beams to safeguard steel bars from corrosion when FRP rebars, with minimal thickness cover, are positioned at the exterior face of the tensile zone. In contrast, steel rebars, with substantial thickness cover, are situated at the inner level of the tensile zone. Reinforcing the beams in this way improves their structural performance without sacrificing stiffness or flexibility. The results of both theoretical and experimental studies are presented and discussed. Deflection, curvature, ductility, fracture width, and spacing are some of the important structural behavior traits that are found. The impact of mechanical and geometrical parameters on the performance of hybrid reinforced concrete beams is highlighted while the examination of serviceability and ultimate needs takes place.

(Zhang & Huang, 2009) investigated experimentally and analytically the behavior of reinforcement concrete beams with hybrid steel and GFRP bars. Eight reinforced concrete examples were evaluated, and two control specimens were strengthened only with GFRP or steel bars. The primary parameters examined were the GFRP to steel ratio and the reinforcement amount. Test results demonstrated the incorporation of steel reinforcement alongside the GFRP bar. Improved the flexural performance of GFRP-reinforced concrete sample. Additionally, the beams were found to be hybrid GFRP/steel reinforced concrete, and they had standard effective reinforcement. Final load capacity, flexibility, and serviceability were all shown to be adequate by the ratios. The results of the numerical analysis were used to predict how the hybrid concrete specimens would behave accurately.

Pam (2010) introduced an experimental study of hybrid FRP beams; twelve beams, including regular concrete specimens, steel-reinforced concrete (RC) specimens, hybrid FRP-reinforced concrete specimens, and pure FRP-RC specimens, were tested for failure. The flexibility of hybrid FRPRC specimens exceeded that of pure FRPRC specimens. Specimens with increased ductility exhibited a greater extent of over-reinforcement. Furthermore, using steel rebar

enhanced the flexural ductility of FRPRC components, and over-reinforcement was a preferred strategy in the design of these members.

Experimentally and analytically, the flexural strength and deflection of high-strength concrete beams reinforced with multiple layers, hybrid, and combinations of different reinforcement types (steel, GFRP, and CFRP bars) were evaluated by **(Yoon et al., 2011)**. Three beam examples were reinforced with a singular form of reinforcement, while three other specimens were strengthened with a mix of various types of reinforcement, as seen in Figure (2.5). An examination was conducted on the impact of hybrid reinforcement using several layers of steel or FRP flexural reinforcements on load-carrying capacity, post-cracking stiffness, cracking pattern, and flexibility. Hybrid reinforcement using steel bars effectively enhanced poor post-cracking stiffness, excessive deflection, extensive crack propagation, significant fracture breadth, and reduced flexibility of FRP bar-reinforced beams. The test results were juxtaposed with the cracking and ultimate moment forecasts of the ACI Code, as well as the service deflection projections of ACI 440.1R-06. Furthermore, new service deflection prediction models for hybrid reinforced concrete beams, including several layers of steel or FRP bars, were developed based on the effective moment of inertia methodology outlined in ACI 440.1R-06.

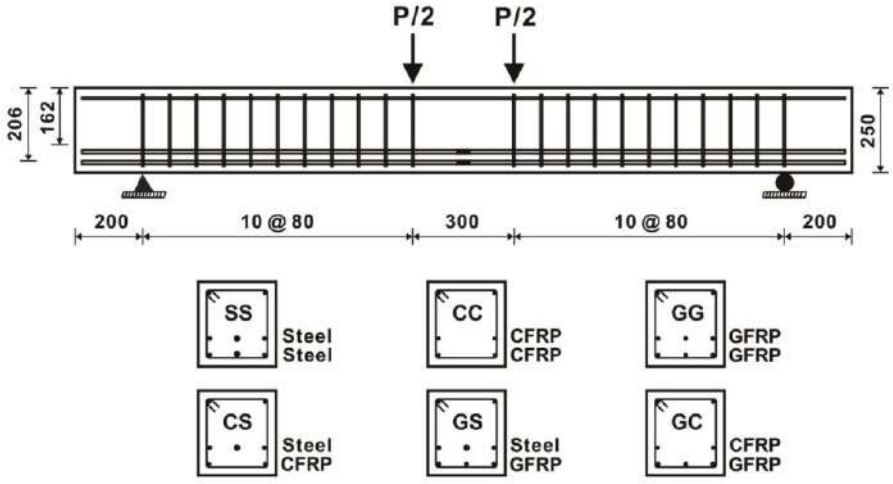

Figure (2.5): Details of test specimens (Yoon et al., 2011).

An experimental investigation was presented by **(Nachiappan et al., 2014)** to experimentally study the combination of RC with steel and BFRP bars. The outcomes were compared with two beams. The first beam included conventional steel reinforcement, whereas the second used BFRP bar reinforcement. The findings for the three examined beams indicated that the flexibility of a reinforced beam, including a BFRP bar, may be enhanced by adding steel bars, resulting in a bi-linear load-deflection curve. Beams reinforced with basalt FRP bars exhibited reduced stiffness compared to their steel equivalents, resulting in more rapid deflection.

(Hawileh, 2015) studied how concrete beams reinforced with a mix of steel and AFRP (Aramid fiber-reinforced polymer) fared. This research added to the existing literature on reinforced concrete (RC) beams tested with a combination of steel and AFRP bars by developing a three-dimensional (3D) finite element (FE) model to predict the load-versus-mid-span deflection response. Results showed that the suggested finite element models account for component material nonlinearities and bond-slip behavior between adjacent concrete surfaces and reinforcing bars. The load of specimens with AFRP bars of 10 mm, 12 mm, and 14 mm increased by 24.84%, 39.92%, and 40.40%, respectively, compared to those with 8 mm diameter bars. The ductility of the beams with AFRP bars of diameters 10 mm, 12 mm, and 14 mm decreased by 4.02%, 6.32%, and 26.49%, respectively, compared to those with 8 mm diameter bars. FRP bars exhibited varied reactions to the beams while using different materials. The beam reinforced with a hybrid bar exhibited superior performance to those reinforced with AFRP, GFRP, and steel bars.

(Kara et al., 2015) presented a flexural performance of hybrid FRP and steel RC beams. The test results indicated that increased steel reinforcement improved the beam stiffness and ductility of FRP-reinforced concrete specimens. Furthermore, it was determined that the FRP reinforcement had a significant role in resisting loads after steel yielding in over-reinforced portions. In contrast to previous hybrid

specimens, the hybrids showed a significant softening of the steel reinforcement and the initial fracture after it started. The moment capacity, curvature, and deflection of hybrid FRP/steel reinforced concrete beams may be correctly assessed using the suggested numerical technique, according to a review of theoretical and empirical data from alternative testing. The ductility and rigidity of FRP-reinforced concrete beams are improved by adding steel reinforcement, according to the simulation findings.

(Osman et al., 2015) tested 15 specimens containing different reinforcement (steel, glass, hybrid carbon, hybrid glass) bars. The primary factors of the research were concrete strength, reinforcement ratio, and carbon fiber volume percent in the bar. The findings indicated that specimens reinforced with hybrid bars exhibited linear behavior post-cracking stress, followed by a significant reduction in stiffness while demonstrating linearity up to the cracking load with elevated starting stiffness. As the carbon fiber volume fraction grew, the beam deflection at load capacity decreased. The beams using hybrid bars (40 and 50% carbon) with medium-strength concrete exhibited greater failure loads than those with steel at equivalent concrete strength, typically resulting in fewer cracks.

Experimental and theoretical investigation of flexural behaviors of hybrid concrete beams reinforced with BFRP and steel bars, shown by **(Ge et al., 2015).** Five separate beams made of hybrid reinforced concrete were built. Based on the results of the trials, BFRP bars have a higher tensile strength but a lower elastic modulus than steel bars. As an example of effective bond performance, BFRP bars and concrete exhibited a bond strength that was on par with that of steel bars and concrete. It is assumed that BFRP bars have a relative bond strength coefficient of 1.0. The crack width and spacing were measured, and suitable calculation techniques were proposed. It looked at the flexural capacity of appropriate hybrid reinforced beams and proposed a simplified way to calculate it. According to the

findings, the experimental value was quite similar to the flexural capacity obtained from the proposed simplified formula. This proves that the formula works when applied correctly. The ductility of hybrid reinforced beams may meet the requirements for typical service circumstances if the reinforcement ratio and Af/As values are controlled appropriately.

(Pang et al., 2016) reported the results of an extensive study to investigate the feasibility of concrete beams with different reinforcement (FRP and steel bars). The research examined reinforced concrete beams with various reinforcements that integrate the benefits of concrete beams with fiber-reinforced polymer reinforcement (elevated ultimate strength) and traditional concrete beams reinforced with steel (enhanced flexibility). It is essential to improve concrete strength and ultimate compressive strain to enhance the flexibility of hybrid-RC beams. However, enhancements in steel strength and effective stiffness negatively impact flexibility, akin to conventional steel-reinforced concrete beams.

(Mustafa and Hassan, 2018), presented a nonlinear finite element model to investigate the behavior of concrete beams reinforced with hybrid steel and FRP composites. Various forms of Carbon and Glass FRP, CFRP, and GFRP were pushed in conjunction with steel reinforcement bars in the analyzed RC beams. The research was performed with the nonlinear finite element software "ANSYS." Three-dimensional finite element models used nonlinear material models for the concrete beam components. The results derived from finite element analysis were validated in opposition to experimental findings. A comprehensive parametric analysis investigated the impact of substituting steel reinforcement with various FRP bars. Incorporating steel rebars into FRP rebars inside concrete beams improved beam flexibility and reduced the detrimental brittle failure, according to the study. It is

also better to use steel rebars as the principal reinforcement in hybrid reinforced concrete beams. After the first fracture appeared and the steel reinforcement yielded, the stiffness of hybrid GFRP/steel reinforced concrete beams significantly decreased and the deflection significantly increased. Conversely, hybrid CFRP/steel reinforced concrete beams exhibited superior performance at the start and propagation of cracking, as shown in Figures (2.6) and (2.7).

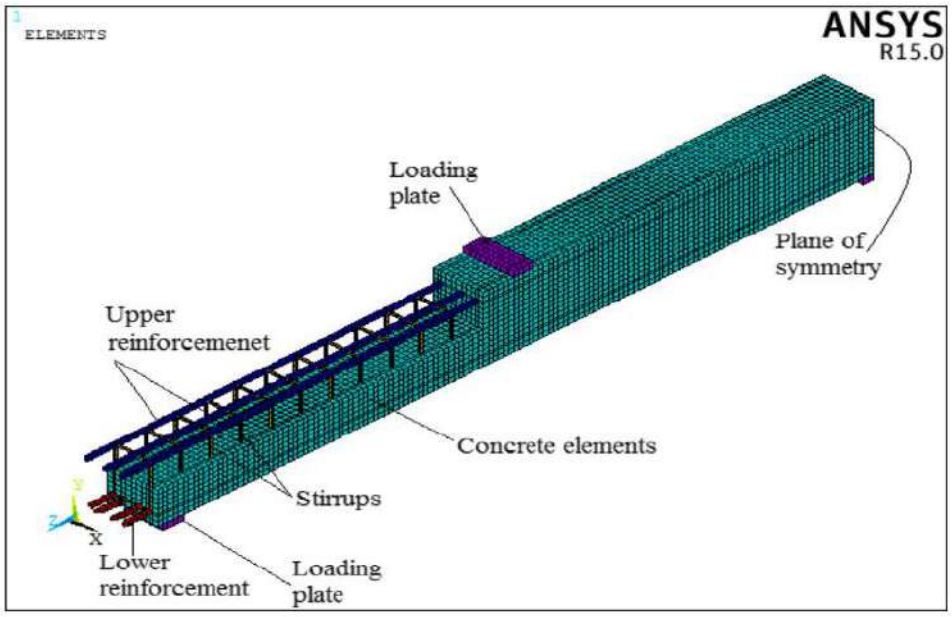

Figure (2.6): A typical figure of the 3-D FE mesh (selected concrete elements were removed to illustrate reinforcement) (Mustafa & Hassan, 2018).

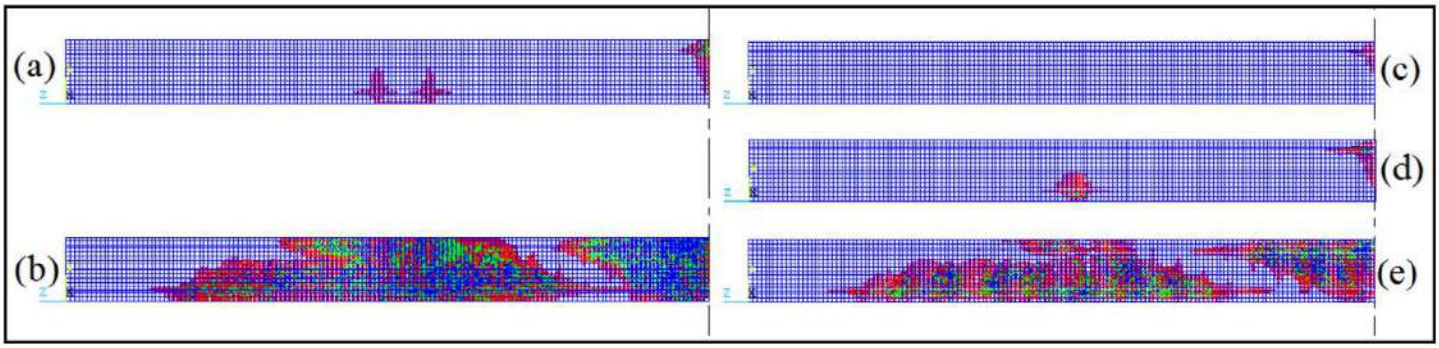

Figure (2.7): Typical cracking/crushing pattern in FRP/steel reinforced concrete beams (Mustafa & Hassan, 2018).

(Sun et al., 2019), experimental studies were conducted on five concrete beams with different bundled reinforcements. The test results showed that all the beams exhibited concrete crushing failure modes after the steel bar yielded, and the elastic FRP bar's plastic development was restrained. The bond strength between the longitudinal reinforcement and the adjacent concrete decreased with increased reinforcement density. Furthermore, the post-cracking stiffness and the number of cracks in the concrete beam that experienced cracking decreased, but the crack line expanded. The first stiffness and after-yield stiffness of the RC beam with three-bar bundles were about 15 percent of those of the beam with double-bar bundles. The displacement ductility's of each concrete beam significantly exceeded those of the other three. The ultimate displacements of the beams with 3-bar and 6-bar bundles were about 1.6 and 1.9 times greater than the ultimate displacement of the beam with single-bar reinforcement, respectively. This resulted from alterations in the binding behavior between the two beam types.

(Maranan et al., 2019), presented the flexural behavior of geopolymer-concrete beams longitudinally reinforced with GFRP and steel hybrid reinforcements shown in Figure (2.8). Seven different specimens were evaluated until failure was reached. Several important properties were investigated, such as the proportions and arrangements of GFRP and steel bars. According to the results, the hybrid specimens improved the ductility and toughness of the reinforced concrete beams while increasing their strength. When the hybrid beams were compared to specimens that had just been reinforced with GFRP bars, the bending moment of the hybrid beams rose by about 15%. Compared to specimens with hybrid tensile reinforcement, hybrid specimens that included GFRP bars at the bottom portion and steel bars at the top part demonstrated significantly higher levels of strength and stiffness when subjected to concrete crushing.

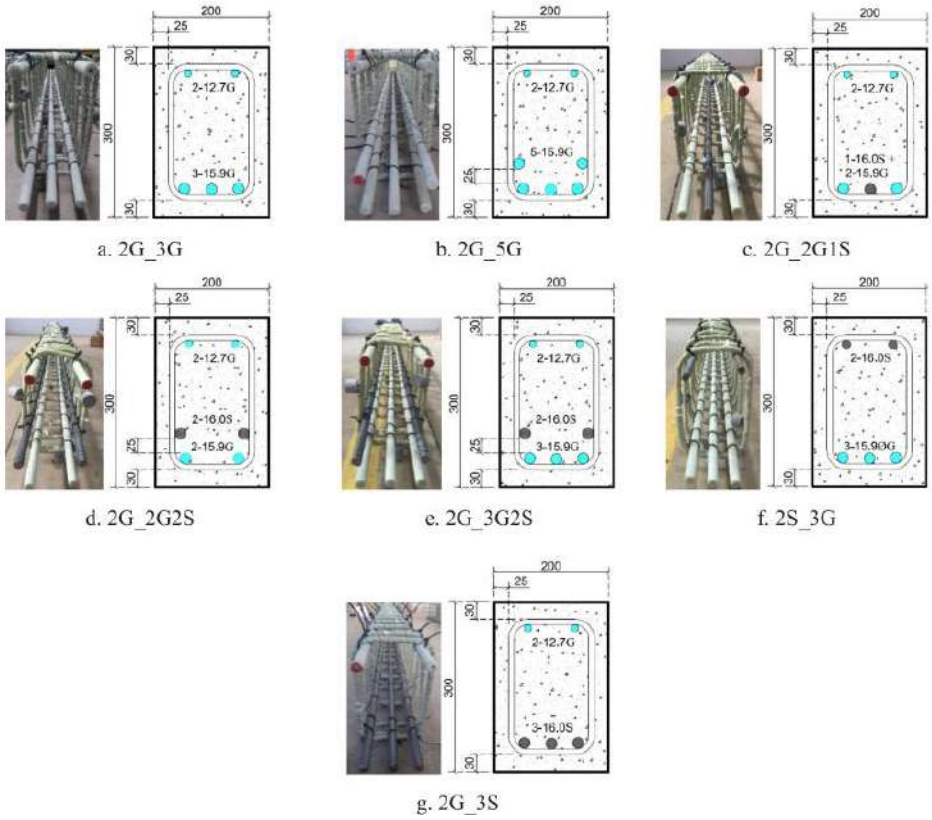

Figure (2.8): Cross-sectional details of the tested beams(Maranan et al., 2019).

(Ge et al., 2020), investigated the flexural performance of concrete beams reinforced with Steel Fiber Composite Bars (SFCB). Eight concrete beams, each reinforced with distinct bar types—one with steel bars, one with fiber-reinforced polymer (FRP) bars, four with steel fiber composite bars (SFCB), and the last two with hybrid FRP/steel bars—were subjected to failure testing. Test findings indicated that SFCB/hybrid reinforced materials had enhanced stiffness, decreased fracture width, and increased bending capability compared to FRP-reinforced specimens. Based on strain compatibility, material constitutive relationships, and force equilibrium, two balanced states, three distinct failure modes, and balanced reinforcement ratios were established, along with analytical methods for forecasting the loading process. Proposed simplified formulae for an effective moment of inertia

and fracture breadth. The anticipated outcomes aligned well with the test findings, as seen in Figure (2.9), validating the suggested formulae for practical use.

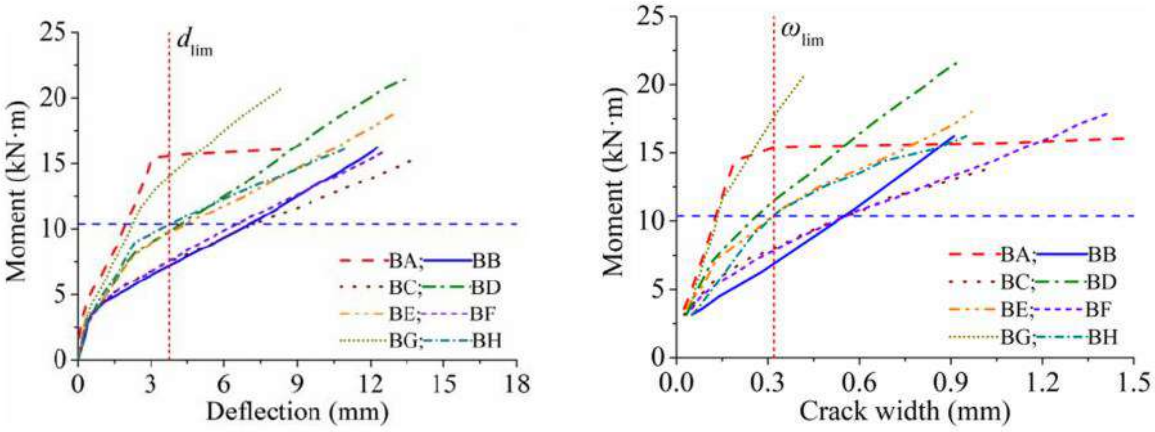

Figure (2.9): Moment–defection curves and Moment–crack width curves (Ge et al., 2020)

2.4 Reinforced concrete beams with FRP rebars

Fiber-reinforced polymer (FRP) is extensively used in concrete constructions owing to its exceptional tensile strength and improved corrosion resistance. Nevertheless, FRP-reinforced concrete (FRPRC) has worse ductility than traditional steel-reinforced concrete. This research examines two varieties of FRP: Glass Fiber Reinforced Polymer (GFRP) and Carbon Fiber Reinforced Polymer (CFRP). The linear elastic characteristics of FRP exhibit a tensile strength ranging from 2400 to 3400 MPa. The characteristics of the matrix constrain the shear forces generated inside the fibers. The matrix restricts vertical forces applied to the fibers. **(Valerio, 2009).** The many benefits of fiber-reinforced plastic (FRP) bars over more traditional building materials like steel and concrete have led to their increased acceptance as viable alternatives for strengthening and modifying existing concrete structures.

(Duthinh and Starnes, 2001) exhibited the ductility and tensile strengths of a prismatic concrete beam reinforced with steel and carbon fiber. Following the fracture of seven concrete beams due to service loads, they were internally

strengthened with varied quantities of steel and externally with carbon fiber reinforced polymer (FRP) laminates. The beam's curvature in the constant moment region was ascertainable by measuring stresses at different depths along the beam. The findings indicate that FRP functions well as flexural reinforcement. The enhanced strength of carbon FRP laminates diminishes as the steel percentage increases. Beams reinforced with carbon and steel have much more deformation capacity than those reinforced just with steel, notwithstanding their tendency to fracture in a brittle manner. The strength of adhesively bonded FRP anchoring is enhanced by clamping or encasing the laminate edges. The design formulas for anchorage, permissible stress, ductility, and reinforcement amount were discussed. Beams reinforced with carbon FRP and steel have an ultimate load curvature that is 1.43 to 1.86 times greater than that of beams reinforced with a steel reinforcement ratio of 75% of the balanced ratio. Despite their vulnerability to brittle failure modes such as delamination, concrete crushing, and laminate debonding, steel and carbon FRP-reinforced beams possess sufficient deformation capacity.

Flexural strengthening of reinforced concrete beams studied by **(Lamanna et al., 2004)**. Currently, the process of attaching FRP reinforcing strips to concrete buildings takes a long time and involves some level of unskilled labor. Another option is to attach the FRP strips to the concrete using a powder-actuated fastening mechanism that is commercially available. Tests for flexural strength were conducted on fifteen beams made of reinforced concrete. This beam measures (304, 304, and 3657 mm). The impacts of three different strip moduli, different fastener lengths and designs, pre-drilling procedures, and twelve reinforced beams with mechanically fastened FRP strips and one reinforced beam with a bonded FRP strip were evaluated. The beams were either unreinforced or had some kind of reinforcement. There was no significant difference in the strength of three beams reinforced with bonded and mechanically attached fiber-reinforced plastic strips. In

comparison to beams reinforced with bonded FRP strips, the ductility of three similar beams reinforced with mechanically linked FRP strips was much higher.

The flexural behavior of concrete beams reinforced with glass fiber-reinforced polymer bars was presented by **(Sam & Swamy, 2005)** , RC beam measuring 150 x 255 x 2400 mm. Failure testing was done on three RC beams. GFRP-reinforced specimens had reduced stiffness, shear strengthening, and deflection at the same load level as the reference specimen. GFRP bars' low modulus of elasticity caused them to behave differently from stainless steel bars. A stirrup made of stainless steel mesh improved the performance of the GFRP-reinforced concrete sample. In Figure (2.10), load-bearing capacity, deflection, concrete strain, reinforcement strain, cracking, and failure mode were assessed for the beams. GFRP-reinforced beams showed lower ultimate load, stiffness, and stronger deflection than control beams at the same load level. The performance of GFRP-reinforced concrete beams improved somewhat with stainless steel mesh shear reinforcement.

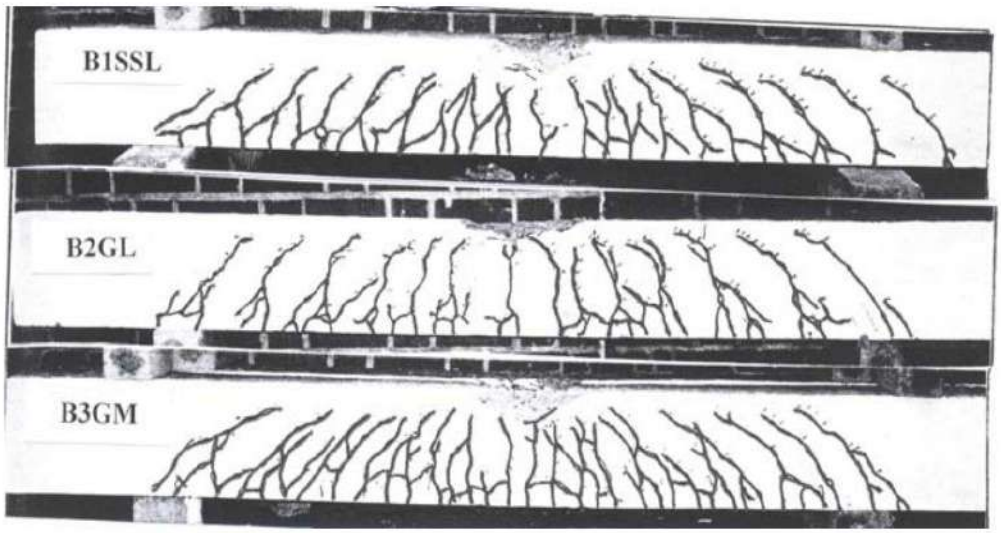

Figure (2.10): Mode of failure and crack pattern of all the beams tested (Sam & Swamy, 2005)

The behavior of concrete beams reinforced with GFRP bars was presented by **(Kalpana & Subramanian, 2011).** Using various concrete grades and bar diameters, nine specimens reinforced with steel and GFRP bars were evaluated under two-point loading. The failure causes, and fracture widths at each loading stage are shown in Figure (2.11). The properties of load-deflection and load-crack width were delineated. The fracture pattern of the GFRP beams under stress has been recorded. Theoretical and experimental approaches compared the flexural capacity of GFRP and steel beams. Finite Element models are created with ANSYS software to validate the structural performance of tested Glass Fiber fiber-reinforced polymer beams. The test findings demonstrated that the GFRP bars implanted in high-strength concrete exhibited superior deflection and load capacity performance compared to those in normal-strength concrete, attributable to their elevated tensile strength. The reduction in stiffness of the GFRP bars led to an enhancement in breadth, although the variations in the final widths of cracks were minor as the concrete strength rose.

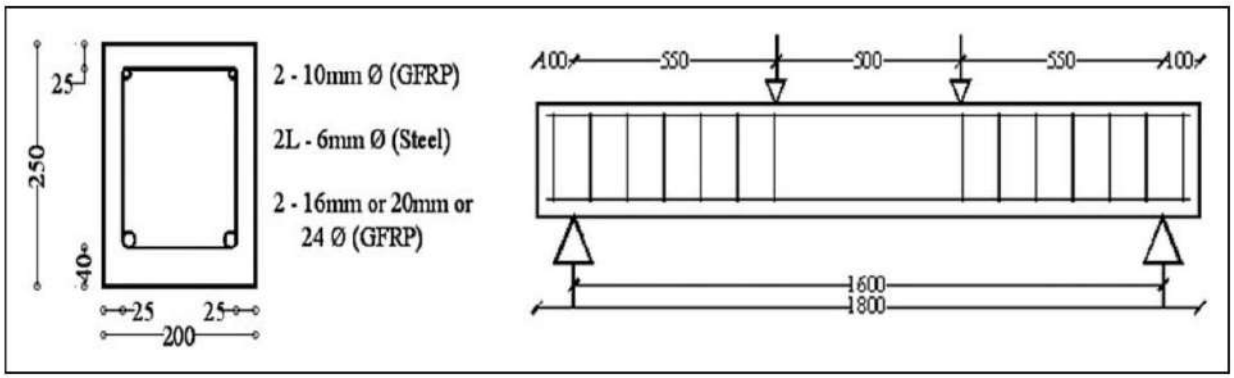

Figure (2.11): Cross-section detail and test setup of beam (Kalpana and Subramanian, 2011)

(Miàs Oller et al., 2013) showed the results of an experimental study of GFRP- RC beams tested at service load. The experimental procedure included casting eight reinforced concrete beams that were subjected to failure testing. The primary parameters consisted of two distinct quantities of GFRP reinforcement and

two sustained load intensities. The test findings indicated that the loading-unloading processes and the reinforcement ratio affected both short-term and time-dependent deflections. No significant impact on the sustained load level was seen.

The behavior of high-strength concrete and flexure-strength specimens reinforced with carbon fiber reinforcement rebars with and without chopped carbon fiber was investigated by **(Aziz and Taha, 2013).** Twenty-seven beams underwent failure testing. The primary factors were the reinforcing ratio ρ, the compressive strength of the concrete, and the volume percent of chopped carbon fiber. The maximum load capacity was shown to improve with higher reinforcement ratios, greater volume fractions of chopped carbon concrete, and enhanced compressive strength. The fracture spacing of the fiber-reinforced concrete beams was about 20% less than that of plain concrete specimens under service load (30% shear strengthening). Although fibers significantly enhanced the system's ductility, the ductility index was contingent upon the amount of reinforcement (more reinforcement permits less deformation, resulting in a lower ductility index).

Experimentally, numerically, and analytically, the flexural behavior of RC specimens with locally created glass fiber-reinforced polymer bars was tested by **(Adam et al., 2015).** Ten specimens were subjected to failure testing. The primary variables were reinforcement ratio, reinforcing material (steel and GFRP), and concrete compressive. The enhancement of the percent of reinforcement dramatically decreased the deflection and breadth of cracks. The loading capacity increased from 47% to 97% when the reinforcement ratio escalated from 1.7 to 2.7. Furthermore, it was observed that enhancing the concrete compressive strength from 25 to 45 MPa resulted in a reduction in crack width by around 52%, but an increase in compressive strength from 25 to 70 MPa led to a drop in fracture width by nearly 80%.

(El Refai et al., 2015) presented an investigation to study the flexural behavior of hybrid-RC- beams. Six concrete specimens reinforced with a hybrid of steel and (GFRP) bars and three other specimens reinforced with GFRP bars only were tested in flexure. The main section included the percent of reinforcement and steel to GFRP bars used to reinforce the test specimens. It was concluded that using steel reinforcement in combination with GFRP bars improved the behavior of purely GFRP-reinforced concrete specimens in terms of ultimate load, cracking load, deformability, and stiffness. Also, it was found that the improvement in availability aspects was more marked at service loads before steel yielding.

Twelve full-scale reinforced beams were tested by **(El-Nemr et al., 2016)** to examine the flexural behavior of GFRP-reinforced concrete beams of various grades, measuring 4,250 mm long, 200 mm wide, and 400 mm deep (see Figure 2.12). Testing demonstrated that FRP-reinforced concrete members' behavior was influenced by axial stiffness. The greater axial stiffness (E_fA_f) means superior flexural performance (greater load capacity, reduced deflection, smaller fracture widths). Maintaining the same for specimens reinforced with the same GFRP bars was predicted to give equal ultimate capacity and deflection. However, greater GFRP bar diameters were projected to produce fewer flexural fractures and wider cracks.

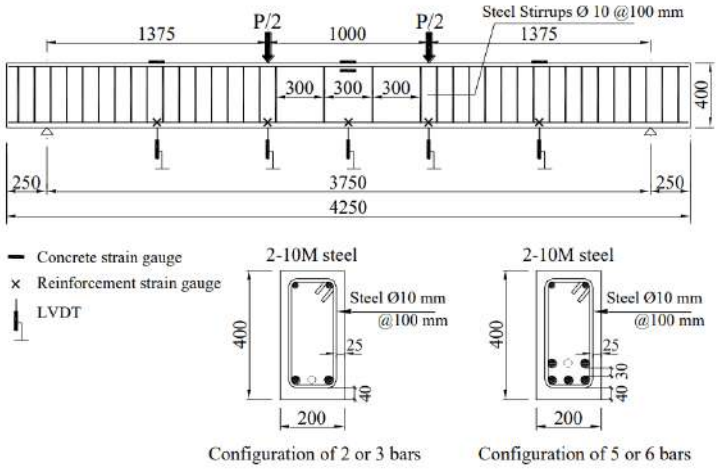

Figure (2.12): Dimensions and Reinforcement Details(El-Nemr et al., 2016).

Kabashi et al. (2018) presented the flexural behavior and cracks in specimens strengthened with (GFRP) bars. The two sets of beams, including varying percentages of reinforcement with GFRP bars, were evaluated to investigate the effects of reinforcement ratio and concrete compressive strength on strengthening, failure modes, cracking, and bending. Concrete specimens reinforced with GFRP bars had significantly greater deflections and fracture widths than those reinforced with traditional steel. The use of smaller diameter GFRP bars demonstrated superior deflection enhancement compared to larger diameter bars at the same reinforcement ratios for the behavior of structural components.

Experimental study of reinforced concrete beams with (CFRP) bars presented by **(Karayannis et al., 2018)**. Seven thin concrete beams strengthened with CFRP bars were experimentally examined under progressively increasing static loads. examined and discussed ultimate load, deflections, after-cracking, sudden local strength decreases, failure processes, and crack patterns. The anchoring length bond conditions of the tensile carbon-FRP bars were given special attention. Some specimens seem to have different cracking behaviors depending on whether local confinement conditions are applied along the anchoring lengths of the carbon-FRP bars. Nevertheless, this topic requires more research. Additionally, presented and discussed comparative assessments of experimental results for CFRP beams and beams reinforced with GFRP bars, all drawn from the most recent research. The experimental results are compared to predictions derived from ACI 440.1R-15 and CSA S806-12 in this publication.

Barris et al. (2020) discussed the flexural behavior of FRP-reinforced concrete beams. The research reported findings from an experimental program examining the flexural performance of internally reinforced concrete beams enhanced with carbon-FRP strips using the Near-Surface Mounted approach, as seen in Figure 2.13. NSM CFRP has shown to be a successful technique for augmenting

the bending capacity of RC beams internally reinforced with glass bars, notwithstanding the significant deformability of glass RC. Enhancing the reinforcement ratio and mechanical qualities, whether internal or near-surface mounted (NSM), augments the flexural capacity. Nonetheless, parameter alterations may variably influence the rise rates and induce distinct failure modes, as seen in Figure (2.14). The findings demonstrate that analytical assumptions accurately forecasted the laboratory failure load, yielding a mean ratio of 0.95 between the laboratory and philosophical loads. The fluctuation of this percent may be ascribed to the final concrete strain of less than 0.003 found in some beams, as accounted for in the theoretical calculations.

Figure (2.13): Bar types used for internal reinforcement (Barris et al., 2020)

Figure (2.14): Failure modes: (a) Concrete crushing, (b) NSM CFRP rupture, (c) Concrete cover separation(Barris et al., 2020).

2.5 Bilayer concrete beams with different rebars

It is possible to improve flexural performance and reduce the cost of beams by integrating plain concrete with fiber-reinforced concrete as two-layer composite members. Rebar made of glass fiber reinforced polymer (GFRP) has a better strength-to-weight ratio than steel rebar, therefore it might be used in reinforced concrete beams instead of steel rebar.

Experimental and theoretical investigation of hybrid reinforced concrete deep beams was presented by **(Al-Amry,2013)**. Nine variants of hybrid reinforced concrete deep beams were tested with double-point loads. One beam was tested as a pilot, while the other eight beams were categorized into two groups, designated as group (A) and group (B), to examine the impacts of the following parameters: high-strength concrete (HSC) layer thickness and the influence of web reinforcing presence. The experimental test results derived from the implemented hybridization technique of HSC and NSC indicate that for beams composed of HSC (approximately 45 MPa) with a compression zone layer thickness of 25-50% of the total beam depth, the ultimate shear strength increased by approximately 11.2-19.5% for beams lacking web reinforcement and by 16.75-22.25% for beams with minimal web reinforcement. The first cracking load rose by about 32.8% to 48% for beams without web reinforcement and 43.4% to 57.9% for beams with web reinforcement. The hybrid concrete beams cast monolithically demonstrated an increase in flexibility of around 13.3% to 22.6% for specimens without web reinforcement and 17.3% to 26.3% for those with web reinforcement. The hybrid concrete beams with construction joints and epoxy resin layers around 1mm thick demonstrated a significant improvement in flexibility, with increases of 28.7% and 30.2% for specimens lacking and incorporating web reinforcement, respectively.

(Ge et al., 2015), analyzed the flexural behaviors of hybrid reinforced concrete beams by static flexural experiments of five different hybrid reinforced concrete beams. The testing indicated that Basalt Fiber fiber-reinforced polymer (BFRP) bars had superior tensile force and a lower modulus of elasticity than steel bars. The bond strength of BFRP bars and concrete is comparable to steel bars and concrete, demonstrating effective bond behavior. The bond force relative coefficient of BFRP bars is regarded as 1.0. The crack spacing and breadth were examined, and appropriate methods for computation were suggested. The flexural capacity of suitable hybrid reinforced beams is analyzed, and a simpler method for its calculation is presented. The results indicated that the flexural capacity derived from the suggested simplified formula closely approximated the experimental value. This demonstrates that the formula may be effectively used. By correctly regulating the reinforcement ratio and the value of Af/As, the flexibility of hybrid reinforced beams may satisfy the demands of standard service conditions.

(Ge et al., 2019), investigated the flexural behavior of engineered cementitious composite (ECC) –concrete hybrid composite beams reinforced with fiber-reinforced polymer (FRP) bars and steel bars, as shown in **Figure (2.15)**. Thirty-two hybrid reinforced composite beams, including diverse ECC height replacement ratios and combinations of BFRP and steel reinforcements, were subjected to experimental testing for flexural failure. Test findings indicated that the cracking, yield, ultimate moments, and stiffness of hybrid and ECC beams were enhanced relative to conventional concrete beams with the same reinforcing, attributable to the superior tensile capabilities of ECC materials. The mean crack spacing and breadth diminish as the ECC height replacement ratio increases. The flexibility of hybrid reinforced composite beams exceeded that of standard reinforced concrete beams, but their practical reinforcement ratios were comparable. Reinforced ECC beams have significant energy dissipation capacity owing to the

superior deformation capability of ECC. Formulas were constructed to forecast cracking, yield, ultimate moments, and deflections of hybrid reinforced ECC–concrete composite beams, considering the constitutive models of materials, compatibility, and equilibrium circumstances. The suggested formulae aligned well with the experimental data.

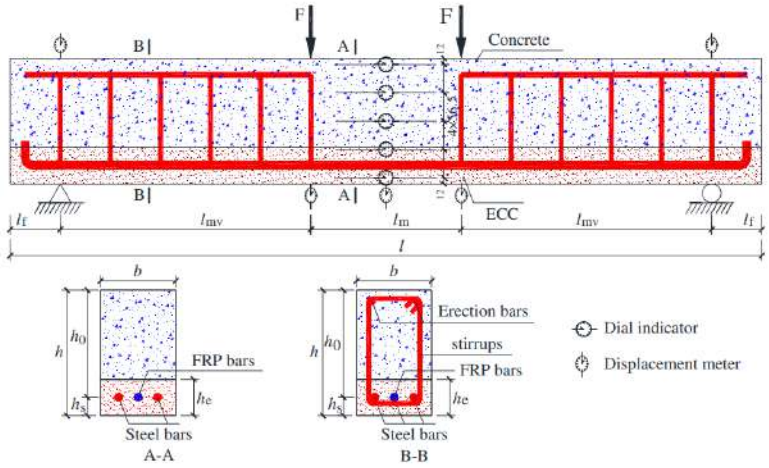

Figure (2.15): Hybrid Reinforced ECC–Concrete Composite Beams(Ge et al., 2019).

Analytical and experimental study of the structural behavior of steel and GFRP rebar-reinforced two-layer fiber-reinforced concrete beams given by **(Nematzadeh & Fallah, 2021).** Figure (2.16) shows the produced concrete beams with one and two layers that include varying volumes of steel fibers (Vf = 0, 0.75, and 1.5%), but without shear reinforcement. Reinforcing three sets of concrete beams using glass fiber reinforced plastic (GFRP) and four sets with steel rebars was the procedure used. There was a longitudinal reinforcement ratio of 0.37 and 0.73% for the GFRP and 1.05 and 2.1% for the steel rebars, respectively. The concrete has a total compressive strength of 33 to 64 MPa throughout the building. Then, a three-point bending test was performed on the manufactured beams. Beams reinforced with either GFRP or steel rebar were found to be more flexible after having fibers added to the section's compression zone, according to the results of the layered

concrete experiment. Conversely, the beams' ultimate flexural strength was enhanced by incorporating fibers into the tensile zone. Their flexural performance in load-carrying capacity, flexural stiffness, and flexibility were enhanced by increasing the ratio of glass fiber to steel reinforcement and improving the concrete compressive strength of the multilayer beams. However, these characteristics were reduced when GFRP rebars were used instead of steel rebars. Sectional analysis and empirical equations derived from the mechanical properties of the component materials were used to predict the flexural response of the layered concrete beams reinforced with GFRP and steel rebars. Figure (2.17), which displays the analytical findings, demonstrates that the experimental data and the suggested model were in excellent agreement. This agreement was to the extent that the model could correctly predict the flexural performance of the stage layers concrete beams in terms of the ultimate load and deflection.

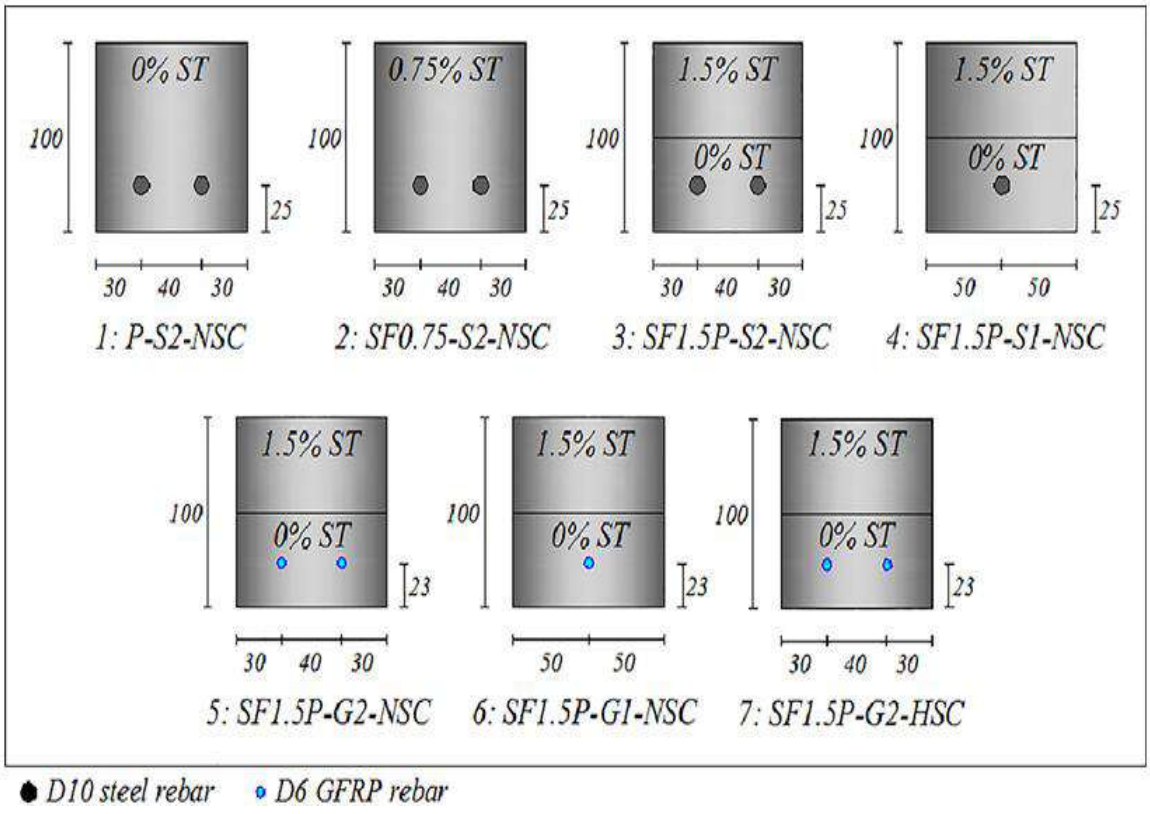

Figure (2.16): Details of beam specimens (unit: mm) (Nematzadeh & Fallah, 2021).

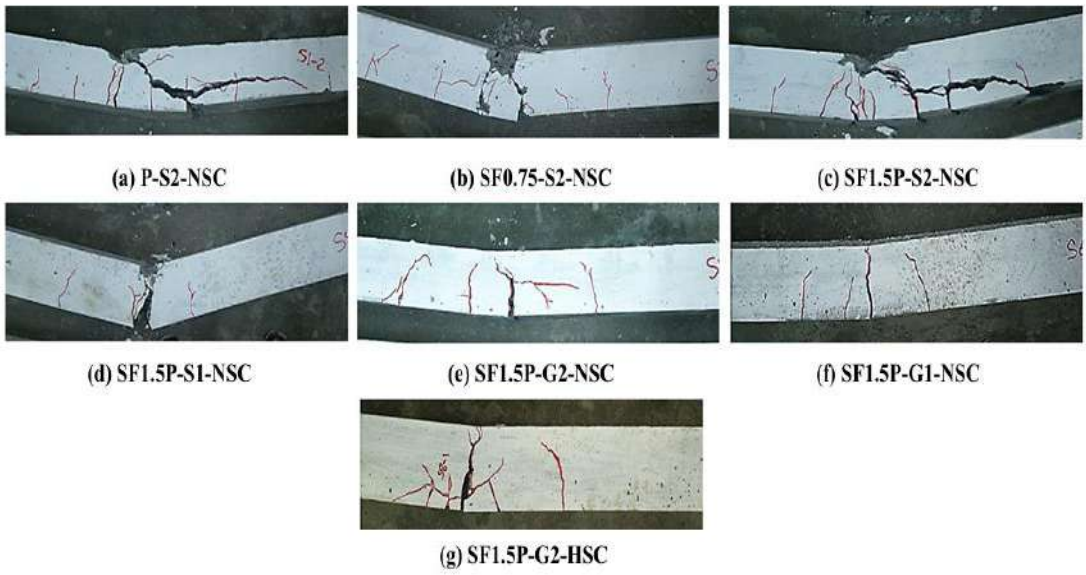

Figure (2.17): (a) the impact of adding and stacking fibers, (b) GFRP rebar is used in place of steel rebar, and (c) Concrete strength is taken into account (Nematzadeh & Fallah, 2021).

(Fallah and Nematzadeh,2022), presented experiments and predictions of the flexural performance of bilayer concrete beams with steel and GFRP rebars. Stress-strain relationships are shown in Figure (2.18). Fourteen beam specimens reinforced with GFRP and steel fibers were manufactured in seven experimental groups without shear reinforcement details for the test beam section shown in Figure (2.19). An investigation was conducted to determine the extent to which the performance of bilayer beams was affected by major elements such as the reinforcement ratio, the volumetric content of steel fibers, and the compressive strength of concrete. The examination of flexural specimens via the use of three-point flexural testing was the major experiment that was conducted for this study. The data were used to establish the important factors that impact the flexural behavior of beams. These characteristics include flexural resistance, stiffness, toughness, fracture energy, and the load-displacement curve. The results demonstrated that incorporating 0.75 percent steel fibers into concrete beams

improved the flexural properties of the beams. However, compared to one-layer fibrous concrete beam specimens, bilayer fibrous beam specimens demonstrated a lower level of flexural performance at the same fiber ratio. When the GFRP bar in the bilayer concrete flexural specimen was replaced with a steel bar, the results showed a decrease in the specimen's flexural resistance, toughness, fracture energy, and stiffness. During the same period, there was a significant increase in the deflection of the peak load. Compared to the usage of normal-strength concrete (NSC), the use of high-strength concrete (HSC) in bilayer GFRP-reinforced beams resulted in an approximately 28% improvement in the flexural properties of the elements. Once the formulation for assessing the flexural capacity of beam specimens across various specifications is compared to the findings of this study, it is determined that ACI 440.1R-06 and CAN/CSA S806-12 accurately predict service mode deformation for beams reinforced with FRP. In contrast, ACI 318, CAN/CSA A23.3, and ACI 440.1R-15 effectively predict the same for steel-reinforced beams. This conclusion was reached after the formulation was evaluated.

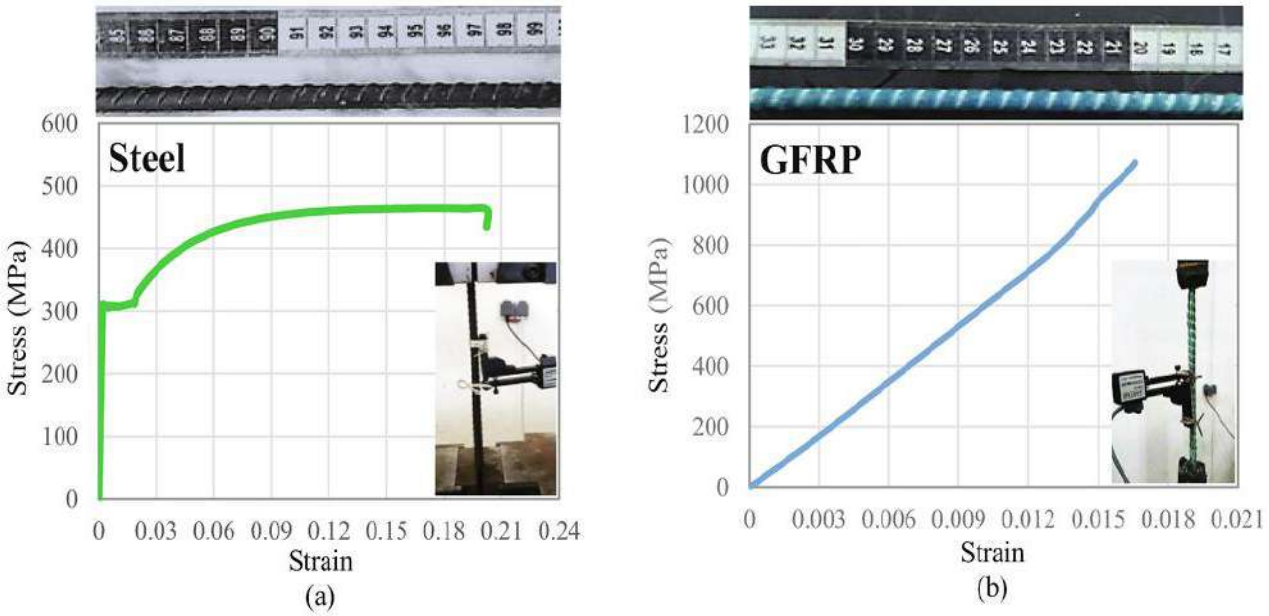

Figure (2.18): Stress-Strain Relationships for (a) Steel Rebar and (b) GFRP Rebar (Fallah & Nematzadeh,2022).

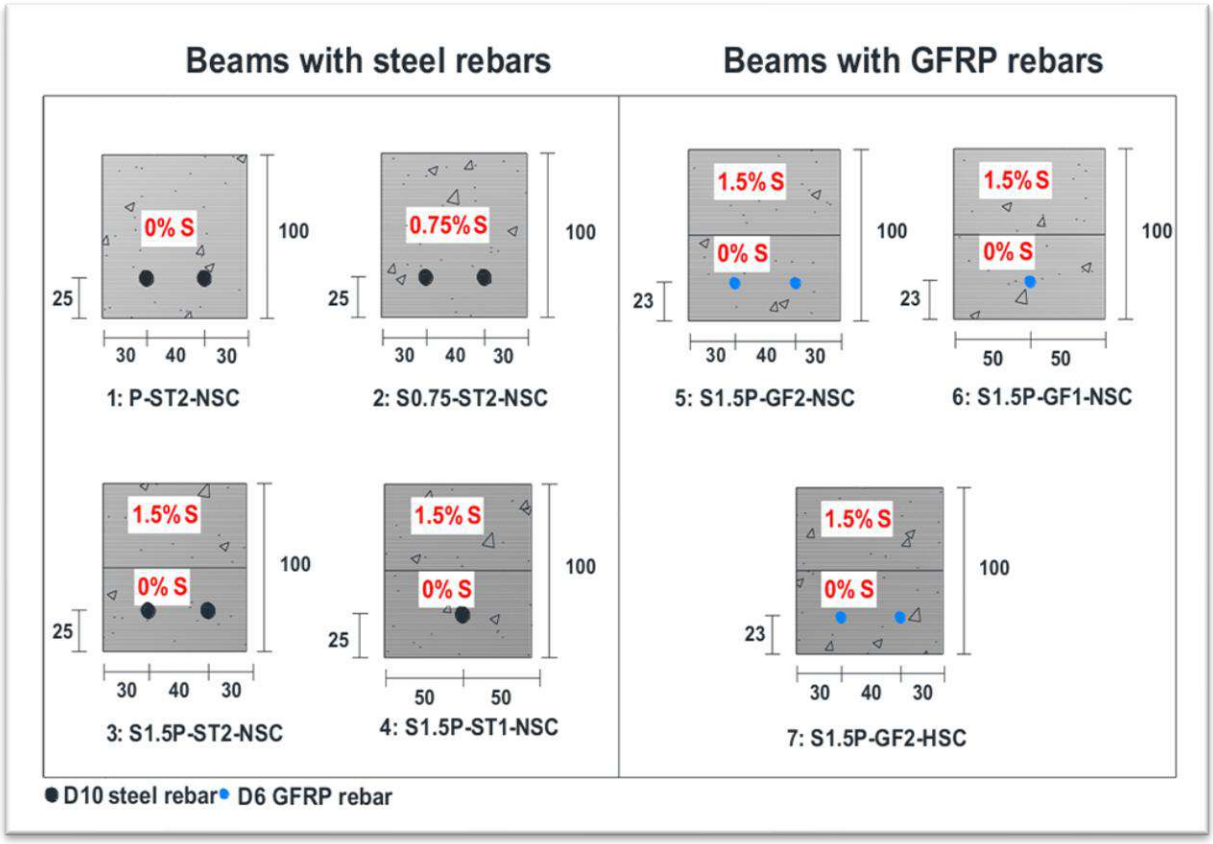

Figure (2.19): Details for Test Beam Section(Fallah & Nematzadeh,2022).

2.6 Concluding Remarks

By reviewing previous research on hybrid concrete beams with different rebar, the following points can be drawn:

1. The hybrid specimens with average effective reinforcement ratios demonstrated satisfactory serviceability.
2. The ultimate load of the bilayer concrete beams was flexural enhanced with a higher reinforcing ratio, while it diminished upon substituting steel rebar with GFRP rebar.
3. The use of High-Strength Concrete (HSC) in two-layer beams reinforced with Glass Fiber fiber-reinforced polymer (GFRP) rebar enhanced the flexural load-carrying capacity and flexibility compared to Normal-Strength Concrete (NSC).

4. The use of High-Strength Concrete (HSC) in two-layer beams reinforced with Glass Fiber fiber-reinforced polymer (GFRP) rebar yielded a 22% increase in the deformability index compared to Normal Strength Concrete (NSC).
5. The deformability of the RC GFRP bar is augmented with a higher percent of reinforcement.
6. In hybrid RC beams, the quantity of cracks escalates, although the average crack spacing and breadth diminish as the height replacement ratio rises.
7. The deflection of bilayer RC beams diminishes as the ratio of Af to As falls correspondingly.
8. The BFRP bars are distinct from steel bars in that they undergo sudden tensile destruction and have a low elastic modulus despite their high tensile strength.
9. In hybrid GFRP/steel-reinforced concrete beams, the steel reinforcement enhanced beam stiffness, flexibility, and load-bearing capacity after cracking.
10. The higher the amount of GFRP reinforcement, the less the increase of the ultimate capacity of the concrete beam.
11. The higher the percentage of the GFRP bars concerning the steel bars, the lower the beam strength.
12. FRP-reinforced concrete beams display wider cracks and large deflection.
13. FRP-reinforced concrete beams improve tensile strength and ultimate load capacity.

After studying and reading the conclusions reached by previous researchers on various research topics, unanswered questions and knowledge gaps were the driving forces for the present investigation into reinforced concrete, after a comprehensive literature evaluation of related studies and their findings. Despite the abundance of research on individual reinforcing types and bilayer concrete systems, there has been surprisingly little exploration into the combined effects of these two factors, especially when subjected to flexural load. Without considering a bilayer concrete system, most previous research has either concentrated on full-depth beams using high-strength concrete (HSC) investigated the mechanical behavior of various reinforcing materials, such as fiber-reinforced polymer bars. Furthermore, there has been a lack of adequate investigation into the potential interactions between HSC and NSC in bilayer beam reinforced with various bars such as carbon, glass, or hybrid composites. Understanding the influence of these combinations on flexural behavior, initial crack load, ultimate load, and overall ductility is significantly lacking in the existing studies. By examining the flexural performance of bilayer concrete beams reinforced with various bar types, this work aims to address this gap. By using the material qualities more efficiently, this dual-layer arrangement increases structural integrity at a reduced cost. HSC improves the load-bearing capacity in compression, while NSC offers suitable resistance in tension.

Chapter Three: The Experimental Work

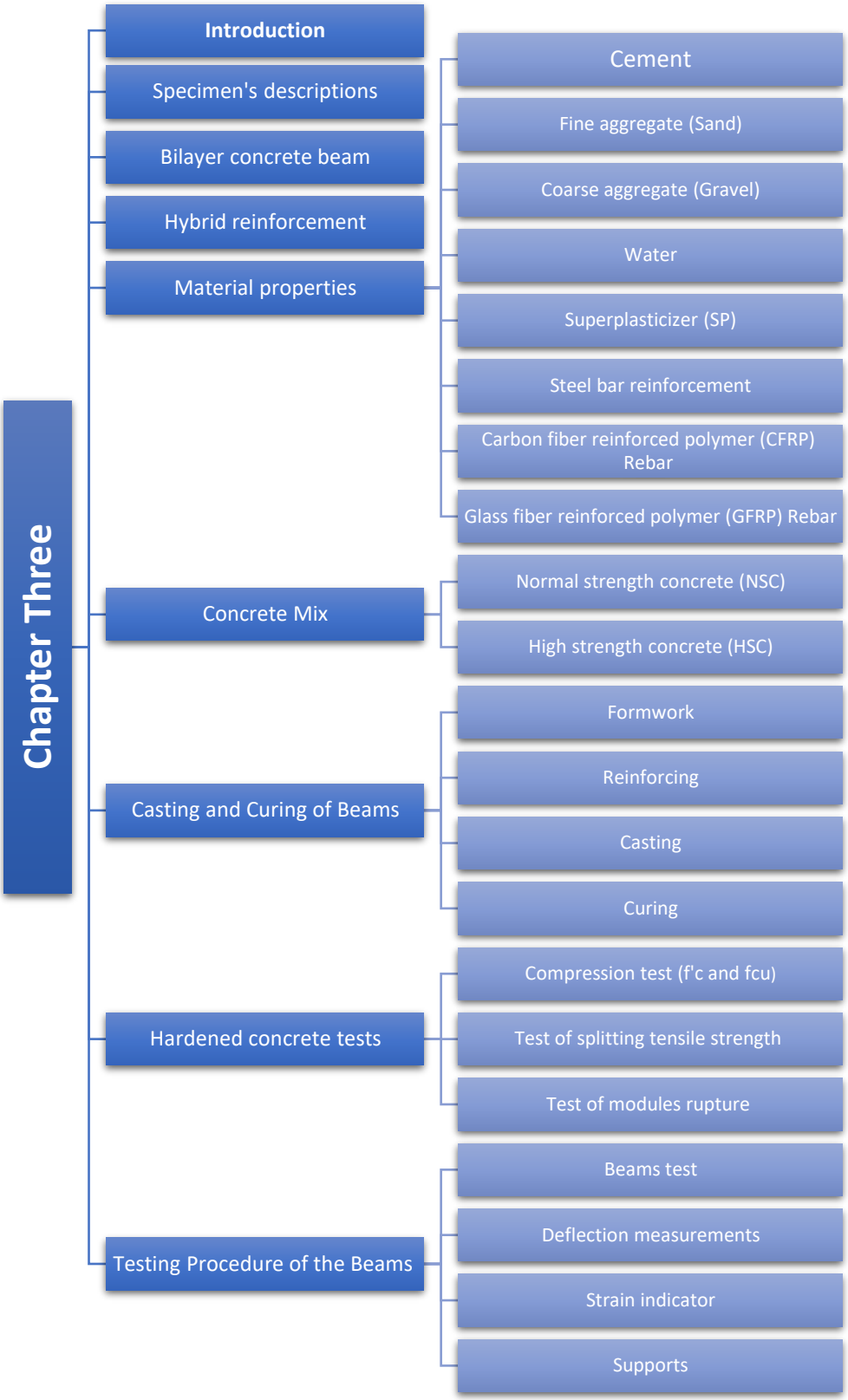

Chapter Three

The Experimental Work

3.1 Introduction

This chapter presents details of the experimental work achieved in the current study, which includes preparing the materials for making the various mixtures used in the research. Two types of concrete were used to pour the hybrid concrete beams and conduct the necessary tests to increase the concrete strength in the compression zone. Several variables have been examined in this study, including the use of (CFRP-GFRP) bars and high-strength concrete (HSC). This chapter describes the reinforced concrete beam test specimens, the mechanical characteristics of the concrete samples, and the qualities of the materials utilized. All tests on the beam specimens and materials had been completed in the engineering college of the University of Kerbala's laboratories.

3.2 Specimen's descriptions

The study has investigated the variables used in the study experiment on a specimen of fifteen reinforcement concrete beams. Table (3.1) shows details of specimens. The total length of the beams is 1400 mm, with rectangular cross-sections of 150 mm in width and 200 mm in height. Six specimens were made with a single layer concrete (three NSC, three HSC). In comparison, nine specimens were made with bilayers of reinforced concrete beams, where the top layer consists of high-strength concrete representing the compression zone. In contrast, the bottom layer comprises normal concrete, representing the tension zone. Different reinforcement

(steel, CFRP, and GFRP) bars were used in this specimen, as shown in the detailed layers, and the specimens were reinforced in **Figures (3.1) (3.4).**

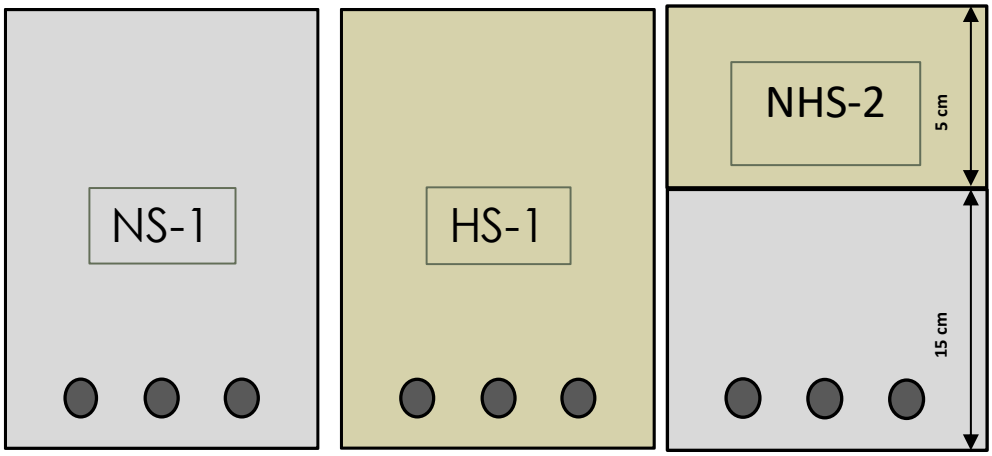

Figure (3.1): Details of Steel Bar Specimens.

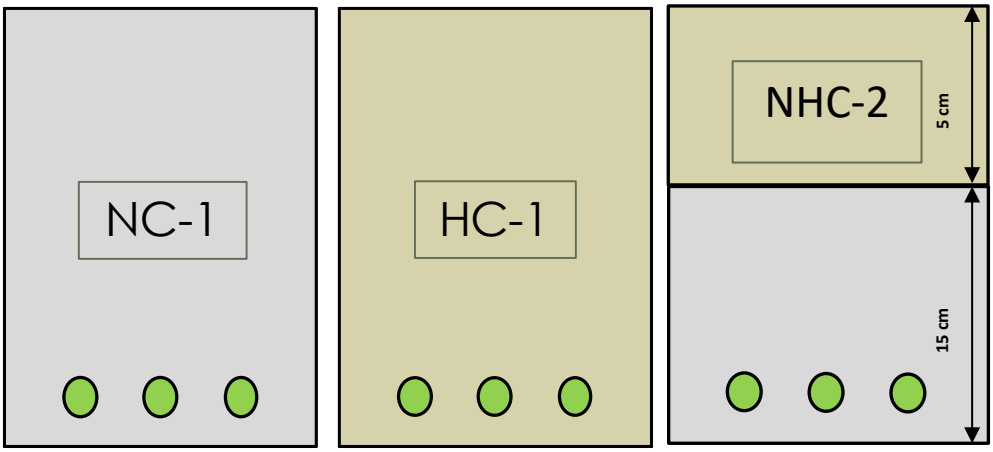

Figure (3.2): Details of Carbon Bar Specimens.

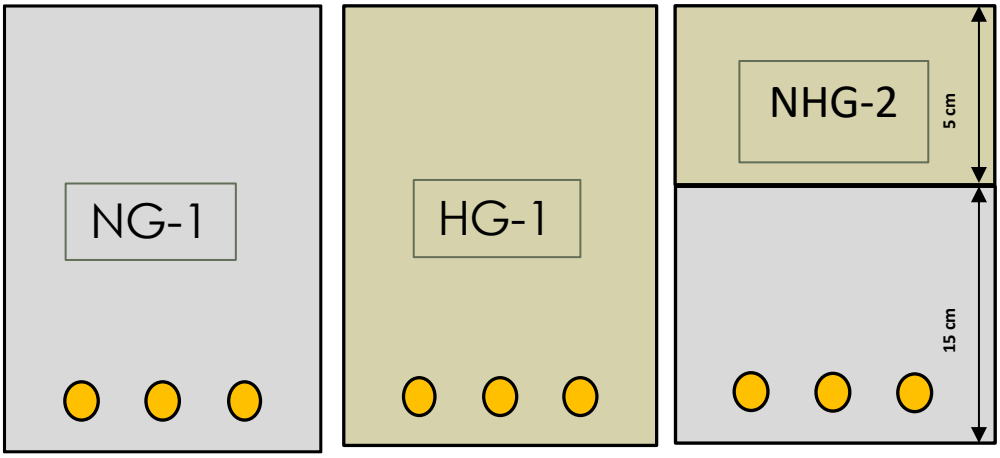

Figure (3.3): Details of Glass Bar Specimens.

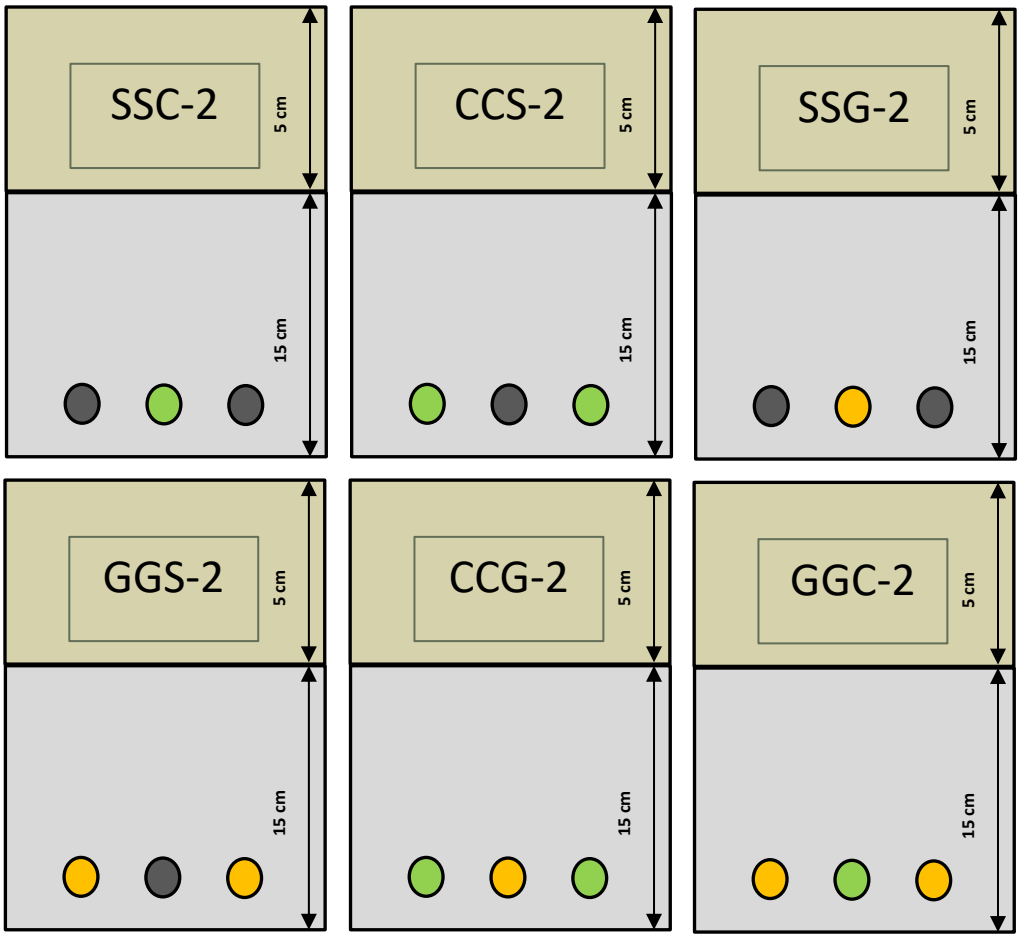

Figure (3.4): Details of Bilayer Concrete with Different Rebars Specimens.

Key Details of the above Figures.

- *C: CFRP bar*
- *G: GFRP bar*
- *1: One-layer*
- *2: Bilayer*
- *N: Normal*
- *H: High*
- *S: Steel bar*

Steel bar
CFRP bar
GFRP bar

Compressive strengths of 38 and 71 MPa were prepared for the concrete. The beams that were manufactured were then subjected to two-point load bending tests. The main reinforcement was a steel rebar with a top diameter of 2Ø10 mm and a bottom diameter of 3Ø10 mm, with stirrups Ø8 mm placed 65 mm apart and beginning 50 mm from each end. Presented in **Figure (3.5). Appendix A: Design of Reinforced Concrete Beam.**

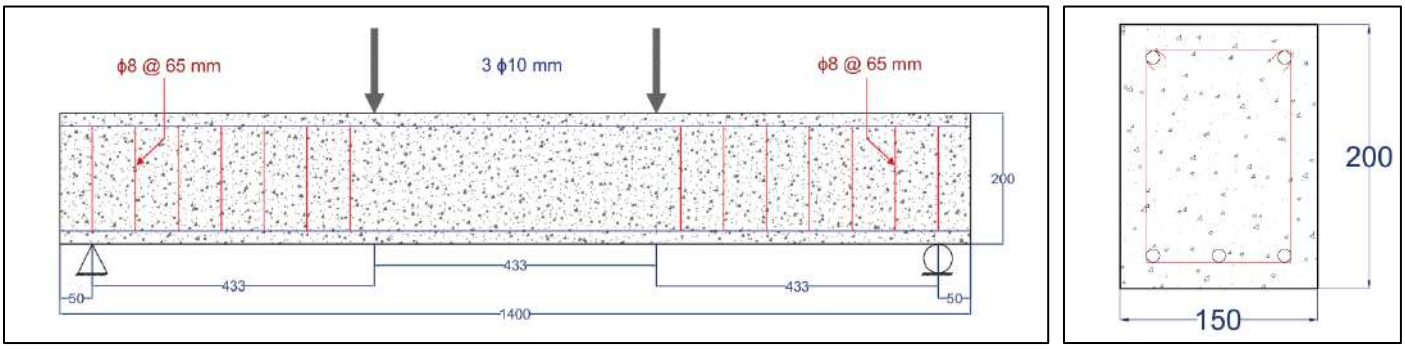

Figure (3.5): Cross-section and reinforcement of specimens.

Table 3.1: The Specimen's Description

Group	Beams specimen	No. of layers	Type of Reinforcement	Longitudinal reinforcement
Group 1	NS-1	Single	Steel Bar	3Ø10 mm Steel
	HS-1	Single	Steel Bar	3Ø10 mm Steel
	NHS-2	Bilayer	Steel Bar	3Ø10 mm Steel
Group 2	NC-1	Single	CFRP bar	3Ø 6 mm CFRP
	HC-1	Single	CFRP bar	3Ø 6 mm CFRP
	NHC-2	Bilayer	CFRP bar	3Ø 6 mm CFRP
Group 3	NG-1	Single	GFRP bar	3Ø 8 mm GFRP
	HG-1	Single	GFRP bar	3Ø 8 mm GFRP
	NHG-2	Bilayer	GFRP bar	3Ø 8 mm GFRP
Group 4	SSC-2	Bilayer	Steel & CFRP	2Ø10 mm Steel & 1Ø 6 mm CFRP
	CCS-2	Bilayer	Steel & CFRP	1Ø10 mm Steel & 2Ø 6 mm CFRP
	SSG-2	Bilayer	Steel & GFRP	2Ø10 mm Steel & 1Ø 8 mm GFRP
	GGS-2	Bilayer	Steel & GFRP	1Ø10 mm Steel & 2Ø 8 mm GFRP
	CCG-2	Bilayer	CFRP & GFRP	2Ø 6 mm CFRP & 1Ø 8 mm GFRP
	GGC-2	Bilayer	CFRP & GFRP	1Ø 6 mm CFRP & 2Ø 8 mm GFRP

3.3 Bilayer concrete beam

Nine models were cast as bilayer concrete beams with different concrete compressive strengths of 38 and 71 MPa. The position of the neutral axis adopted the thickness of layers. It detected the depth of the compression zone (top layer), about 50 mm from the top edge of the beam, while the tension zone (bottom layer) presents the remaining part of the beam, about 150 mm. The top layer was poured using a high-strength concrete mix of about 71 MPa, while the bottom layer was poured using a normal concrete mix of about 38 MPa.

3.4 Hybrid reinforcement

The exceptional corrosion resistance and high tensile strength of FRP bars have led to their recent use into concrete flexure reinforcement. But fiber-reinforced plastics are fragile. Consequently, RC beams reinforced with these materials would not be as ductile as RC beams reinforced with regular steel **(Wei et al., 2024)**. In this study, six specimens were cast in bilayer concrete with different hybrid reinforcement uses (steel, CFRP, GFRP) bars. Two steel bars with one CFRP bar, two CFRP bars with one steel bar, two steel bars with one GFRP bar, two GFRP bars with one steel bar, two CFRP bars with one GFRP bar, and two GFRP bars with one CFRP bar. Usually, a stand-alone bar is put in the middle to make balance in reinforcement, as shown in **Figure (3.6)**.

Figure (3.6): Detail of hybrid reinforcement of specimens.

3.5 Material properties

3.5.1 Cement

Cement is well recognized as a fundamental component in the formulation of concrete mixes. During this investigation and throughout the experimental procedures, the prevailing variant of cement used was the locally available ordinary Portland cement sourced from the Lafarge cement factory, complying with the Iraqi Standard Specification **(Iraqi Standards Organization, 2019)**. Used in this study. The cement was made in Karbala, Iraq. **Tables (B.1) and (B.2)** detail the cement's physical and chemical properties, as shown in **Appendix B**.

3.5.2 Fine aggregate (Sand)

In this study, clean sand was sourced from a specific local area, AL-Akhaidir, to conduct the experimental procedures. **Table (B.3)** in **Appendix B** shows that the grading test results follow **(Iraqi Standards Organization, 1984).**

3.5.3 Coarse aggregate (Gravel)

The present study used black-crushed gravel sourced from a specific geographical area known as Al-Niba'ai as an ingredient in the concrete mixture. Water was used for cleaning and washing the gravel, which was then allowed to dry in the air before use. The gravel used according to **(Iraqi Standards Organization, 1984). Appendix B**, **Table (B.4)** shows this type of aggregate's grading and other characteristics.

3.5.4 Water

Potable water was utilized to mix and cure concrete.

3.5.5 Superplasticizer (SP)

Concrete compositions containing Master Glenium54 have had the percentage of water reduced. Produce concrete with high ultimate strength, little voids, and good workability without bleeding or segregation. It is utilized in all concrete mixtures that meet **(ASTM C494/C494M, 2013)** Type F & G superplasticizer standards, as indicated in **Appendix B, Table (B.5)** properties of superplasticizer and that are equipped by the producer as shown in **Figure (3.7)**.

Figure (3.7): Master Glenium54 Superplasticizer (SP).

3.5.6 Steel bar reinforcement

This study tested Steel reinforcement according to **(ASTM A496/A496M, 2004)**. **Figure (3.8)** shows two different steel reinforcement sizes that have been used. Primary reinforcement consisted of Ø10 mm steel reinforcement, and stirrups were Ø8 mm. The experiment was conducted at the University of Kerbala using a tensile testing apparatus. The tensile strengths of each reinforcement are shown in **Table (3.2)**.

Table 3.2: Specification and Test Results of Steel Reinforcing Bars.

Diameter of Bar (mm)	Actual diameter (mm)	Yield stress (MPa)	Ultimate strength (MPa)	Elongation Ratio %
10	9.98	547	616	18.3
8	8.00	513	632	32.2

Figure (3.8): Steel Bar Reinforcement.

3.5.7 Carbon fiber reinforced polymer (CFRP) Rebar

Carbon fiber Rebar (CFRP), a reinforced polymer (CFRP) rebar, is a reinforcement material used in construction and civil engineering projects. It is a lightweight and high-strength alternative to traditional steel reinforcement, which provides exceptional tensile strength, stiffness, and corrosion resistance **(Vijayan et al., 2023)**. Combining these properties makes carbon fiber rebar an attractive choice for applications where weight reduction, high strength, and durability are desired. In

this study, one side of the carbon bar (CFRP) was Ø6mm, presented in **Figure (3.9)**. According to the manufacturer, the properties (CFRP) are outlined in **Appendix B**, **Fig (B.2)**.

Figure (3.9): CFRP Bar Reinforcement.

3.5.8 Glass fiber reinforced polymer (GFRP) Rebar

Fiberglass rebar, also known as GFRP (Glass Fiber Reinforced Polymer) rebar, is used in construction projects as an alternative to traditional steel reinforcement. It is made by impregnating glass fibers with a polymer resin, typically epoxy or vinyl ester, forming them into bars or rods of various diameters. Fiberglass rebar is commonly used in multiple construction applications, including bridge decks, marine structures, parking garages, foundation slabs, and concrete walls. It offers long-term durability and can extend the service life of concrete structures while reducing maintenance and repair costs associated with corrosion **(Hosseini & Sadeghian, 2025)**. In this study, one size of the glass bar (GFRP) was Ø 8mm, as

planned in **Figure (3.10)**. According to the manufacturer, the properties (GFRP) are outlined in **Appendix B, Fig (B.1).**

Figure (3.10): GFRP Bar Reinforcement.

3.6 Concrete Mix

3.6.1 Normal strength concrete (NSC)

The primary ingredients of this kind of concrete mixture are cement, sand, gravel, and water. Previous research indicated that this material's compressive strength of between 30 and 40 MPa was ideal **(AL-Khafaji et al., 2018)**. Normal-strength concrete was utilized for the tension zone (bottom layer) and reference beams. A tiny concrete mixture was used to cast the concrete. The concrete has a compressive strength of 38 MPa. **Table (3.3)** shows the material requirements for each cubic meter based on the mix.

Table 3.3: Mix Proportion of (NSC)

Cement kg/ m^3	Sand kg/ m^3	Gravel kg/ m^3	Water kg/ m^3	Superplasticizer kg/ m^3	Compressive strength MPa
320	786	1139	140	4.5	38

3.6.2 High strength concrete (HSC)

High-strength concrete has a specified compressive strength of 55 MPa (8000 psi) or higher. In many markets today, concrete having a specified compressive strength over 69 MPa (10,000 psi) is routinely produced daily **(ACI 363R, 2002)**. The design of high-strength concrete is more crucial than that of normal-strength mixes because to the chemical admixtures (Superplasticizer), low water-cement ratio, and high cement content that are used. So far, in our current effort, we have developed a number of experimental mixes. According to **Table (3.4)**, the high-strength concrete mix is given a compressive strength of about (71 MPa) after 28 days of mixing.

Table 3.4: Mix Proportion of (HSC)

Cement kg/ m^3	Sand kg/ m^3	Gravel kg/ m^3	Water kg/ m^3	Superplasticizer kg/ m^3
418	**736**	**1089**	**140**	**5.4**

3.7 Casting and Curing of Beams

3.7.1 Formwork

This study used eight steel molds to cast the models in two stages. Screws and nuts can move the side plate of molds for ease of dimension control and reusability. The internal dimensions of the mold were (200 mm in height, 150 mm in width, and 1400 mm in length), as shown in **Figure (3.11)**.

Figure (3.11): The steel mold used in this study.

3.7.2 Reinforcing

In the present study, three types of longitudinal reinforcement were utilized, namely steel, carbon, and glass, each varying in size, with Ø10 mm steel, Ø6 mm CFRP, and Ø8 mm GFRP employed. The steel reinforcement was precisely cut to a length of 1600mm, whereas the overall dimension of the model stood at 1400 mm,

with a flexure introduced at a height of 10 cm at both ends. Similarly, the steel, carbon, and glass were all cut along a length of 1400 mm, matching the model's dimensions. The primary reinforcement consisted of steel, carbon, and glass bars. In the case of hybrid reinforcement, two bars of one type of reinforcement were paired with a single bar of another kind, strategically positioning the single bar in the middle to ensure equilibrium in the distribution of reinforcement, with the end bars mirroring the type of reinforcement steel showcased in **Figure (3.12)** and **(3.13)**. Furthermore, an 8 mm reinforcing steel was designated for the stirrups, and following the design specifications outlined in Appendix A, the distance between the stirrups was set at 65 mm, commencing from the support zone up to one-third of the beam, equipped with hooks (closure) for each stirrup.

Figure (3.12): Reinforcement details in this study.

Figure (3.13): Hybrid reinforcement in this study.

3.7.3 Casting

The chosen materials were ready and weighed by the mix's volume before casting. They were thoroughly cleaned and oiled to prevent concrete from sticking to the interior surfaces of the cube, cylinder, prism, and beam molds once they had hardened. Next, as indicated in **Figure (3.14)**, the reinforcement was carefully positioned inside each beam steel mold, ensuring the necessary sides and bottom covers were kept in place. Before that, the

template dimensions were adjusted to match the design dimensions of the model by tightening the screws to secure the side edges.

Figure (3.14): Beam specimens, steel moulds, and reinforcement bars.

A mixing machine was used to accomplish the mixing of the concrete. Sand and gravel were added to the concrete mixture, and the mixer was started after the mixing tank had been cleaned and the quantities of the components of the concrete mixture had been weighed according to the proportions stated. Following that, cement was used to bring the components into uniformity. After that, the concrete was gradually combined with water and super-plasticizer until it achieved the desired level of consistency for workability, as shown in **Figure (3.15).**

Figure (3.15): Concrete mixer.

The process of casting models is carried out in layers according to the type of model as follows:

3.7.3.1 One layer of concrete beam

Six moulds were filled with one-layer normal-strength concrete with compaction. A vibrator was employed to eliminate air and voids from the sample. For the cube, cylinder, and prism moulds, standard techniques were used to comply with conventional concrete regarding layer count and rod length. After casting, the standard concrete's upper surface was smoothed down using a hand trowel, as shown in **Figure (3.16).**

Figure (3.16): Casting the Specmines.

3.7.3.2 Bilayer of concrete beam

Nine moulds were cast with two types of concrete: Normal strength concrete in the bottom (tension zone) at 150 mm depth and using a vibrator to eliminate air and voids from the sample and waiting about 15 minutes to obtain light hardening for this layer, and fill the other layer 50 mm from the top end by high strength concrete represent compression zone. Standard techniques were used for the cube, cylinder, and prism moulds. After casting, the standard concrete's upper surface was smoothed down using a hand trowel, as shown in **Figure (3.17).**

Figure (3.17): Formwork and casting of the bilayer concrete.

For concrete tests, three cubes for each (NSC and HSC) were cast to assess the compressive strength, while three cylinders for each (NSC and HSC) were casted to find the splitting tensile strength. Additionally, three prisms for each (NSC and HSC) were made to examine the flexural strength, as shown in **Figure (3.18).**

Figure (3.18): Casting of the cube, cylinder, and prism for concrete tests.

3.7.4 Curing

After the casting process, all the models were covered with nylon to reduce water evaporation and complete the curing process. After 24 hours, the moulds were opened, and the models were covered with nylon with continuous water spraying, as shown in **Figure (3.19)**. However, the concrete test specimens were opened and placed in a water tank using a heater device to maintain the water temperature suitable for curing due to the cold weather, which led to the cooling of the water in the tank used for curing, and using water pump to distribution the water inside tank as shown in **Figure (3.20)**.

Figure (3.19): Curing of the specimens.

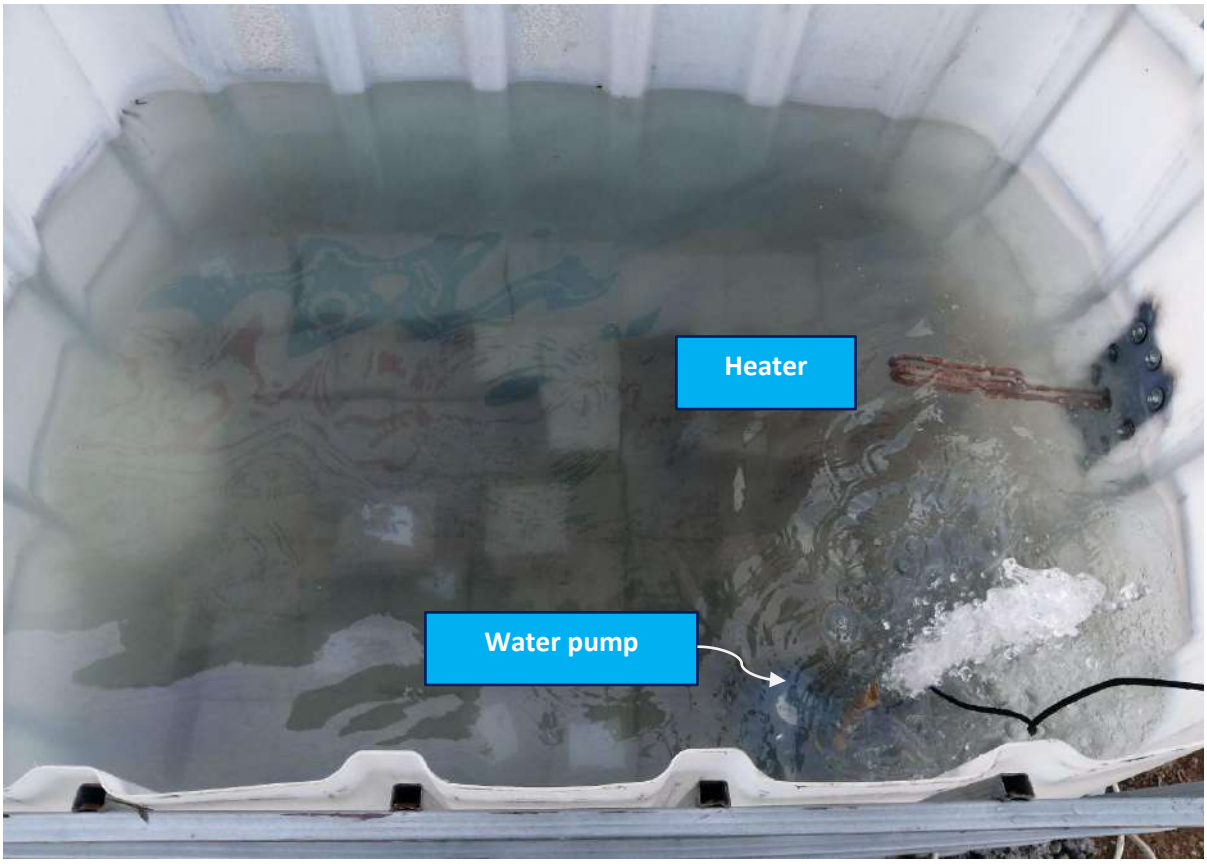

Figure (3.20): Curing of the cube, cylinder, and prism for concrete tests.

3.8 Hardened concrete tests

Three specimens (cubes, cylinders, and prisms) for each type of concrete mix (normal and high strength) were tested in the Structural Laboratory of the University of Kerbala's Civil Engineering Department. Specifically, the compressive strength of the cubes (100 mm) sample was analyzed, while the splitting tensile strength of the cylinders (100 mm diameter x 200 mm hight) and the flexure strength of the prisms (100 mm x 100 mm x 400 mm) were assessed for their mechanical properties in this experimental study. The tests encompassed an evaluation of various parameters for the concrete types utilized in this research, such as the splitting tensile strength and compressive strength of cubes and cylinders. The comprehensive examination aimed to provide valuable insights into the performance and characteristics of the different concrete mixes, shedding light on their suitability for various structural applications and construction projects.

3.8.1 Compression test (f'c and fcu)

As seen in **Figure (3.21)**, cubes with dimensions of (100 mm) are used to obtain the compressive strength (fcu) by **(BS 1881-116 1983)**. Each cube was loaded continually until it failed using the 2000 KN digital test machine (ELE). For each blend, a three-cube average compressive strength was used. All of the cubes were tested following a 28-day water curing period. A static load was applied at a loading rate of 0.6 MPa/s. The NSC and HSC compressive strengths were represented by the value of each of the three specimens.

Figure (3.21): Compressive strength tests of Cube.

3.8.2 Test of splitting tensile strength

Three standard cylinders, each 100 mm in diameter and 200 mm in length, were used to test the splitting tensile strength for each concrete variant used in this experiment. per the **(ASTM C496/C496M, 2011)** specification. During the study, the cylindrical samples underwent a 28-day duration of water submersion to enhance the curing process. A mean of three specimens was employed as a proxy for the ultimate tensile strength of NSC and HSC. The computation of this test can be derived by using equation (3.1). The testing machine had a 2000 kN capacity, and the load was delivered steadily and without shock until the cylinder failed, as shown in **Figure (3.22)**.

$$F_{st} = \frac{2P}{\pi DL} \quad \text{..... (3.1)}$$

Where:

- F_{st} = Splitting tensile strength (MPa).
- **P =** Max. The applied load was recorded by the testing machine (N).
- **D** = Cylinder Diameter (mm).
- **L** = Cylinder length (mm).

Figure (3.22): Splitting Tensile Strength Test.

3.8.3 Test of modules rupture

Prisms of concrete measuring (100 mm×100 mm ×400 mm) were fabricated following the specifications outlined in **(ASTM C78, 2010)**. Three prisms for each concrete mix underwent testing utilizing a universal hydraulic machine with a maximum capacity of 2000 KN. The load application was executed continuously,

steadily escalating consistently until failure ensued. This testing was carried out at the Structural Laboratory of the Department of Civil Engineering at the University of Kerbala. Flexural strength, denoted by the modulus of rupture, was determined through the analysis of data acquired from a simple beam subjected to a two-point load, as illustrated in **Figure (3.23)**. The calculation of the flexural strength of the specimens was employing the subsequent formula:

The following calculation may be used to evaluate the flexural strength in the event that a fracture occurs on the tension surface inside the middle third of the span's length:

$$F_r = \frac{PL}{bd^2} \quad \text{..... (3.2)}$$

Where:

- $\mathbf{F_r}$ = Modulus of Rupture (MPa).
- **P** = maximum value for the applied load (N).
- **L** = Span length for the sample, (mm).
- **b** = Average sample width (mm).
- **d** = Average sample depth (mm).

Figure (3.23): Machine of flexural tensile strength testing in this work.

3.9 Testing Procedure of the Beams

All specimens were tested using a machine with a maximum loading capacity of 2000kN. This apparatus was outfitted with a digital load cell and a data logger acquisition system, enabling the continuous recording of load and deflection data at one-second intervals and storing the data in an Excel spreadsheet. At the University of Kerbala's College of Engineering, specifically at the Structural Laboratory of the Department of Civil Engineering, the experimental setup was put up. A 1.5 m wide by 3.00 m tall frame operating in load-control mode was used to carry out the experiment. The crane, which is used to raise and place the beams under test, is supported by a steel I-section frame that was bolted and welded to the load frame. The specimen's test setup is shown schematically in **Figure (3.24).** Applying a modest pre-load then secured the location. There were 5 kN increments for lower loads and 2 kN increments for heavier ones. There was a 10-minute break between

each loading step. A Linear Variable Differential Transformer (LVDT) 150mm device was used to determine the vertical deflections at the mid-span under load; In contrast, a load cell was utilized to quantify the applied load.

Figure (3.24): Setup for testing specmines.

3.9.1 Beams test

Modest load increments were applied to each beam tested under a monotonic static load. Each increase in load amounts to 5 kN, and samples are observed until failure. The recorded readings were done manually, with each increment added to the data logger. The progression of cracks is indicated for each stage, with the crack width measurement done from one stage to the next. The testing of the specimen is illustrated in **Figure (3.25).**

Figure (3.25): Beam test machin.

3.9.2 Deflection measurements

One form of deflection measurement employed in the study involved the utilization of a linear displacement sensor known as LVDT-KTR-150mm, which was explicitly used to ascertain the deflections occurring at the mid-span. This measurement technique was instrumental in capturing the structural response to external forces, providing valuable insights into the system's behavior under varying loading conditions.

3.9.3 Strain indicator

Figure (3.26) shows the results of strain measurements taken using a bi-channel data logger. The device has a total of fifteen channels, eleven of which are specifically for strain gauges and four of which are reserved for LVDT-KTR-150 mm. The operational software integrated within the strain indicator allows for

recording each channel's reading at intervals of every five seconds; this feature proves to be highly beneficial in facilitating the acquisition of an accurate estimation of the behavior exhibited by the concrete surface currently under examination.

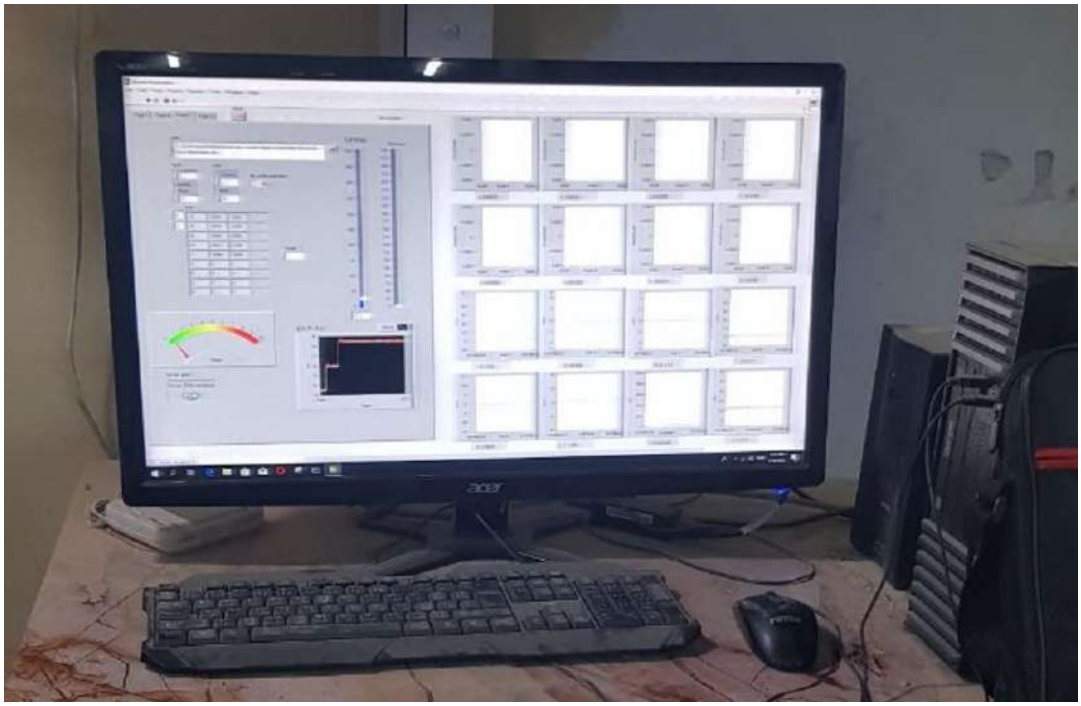

Figure (3.26): A device for measuring strain and a software interface for displaying the data were utilized.

3.9.4 Supports

All the beams that underwent testing were supported, with a pin support at one end and a roller support at the opposite end. The roller support consisted of a single steel shaft with a diameter of 25mm. Each beam was subjected to testing under two-point loading conditions. The specific support configurations can be observed in **Figure (3.27)**.

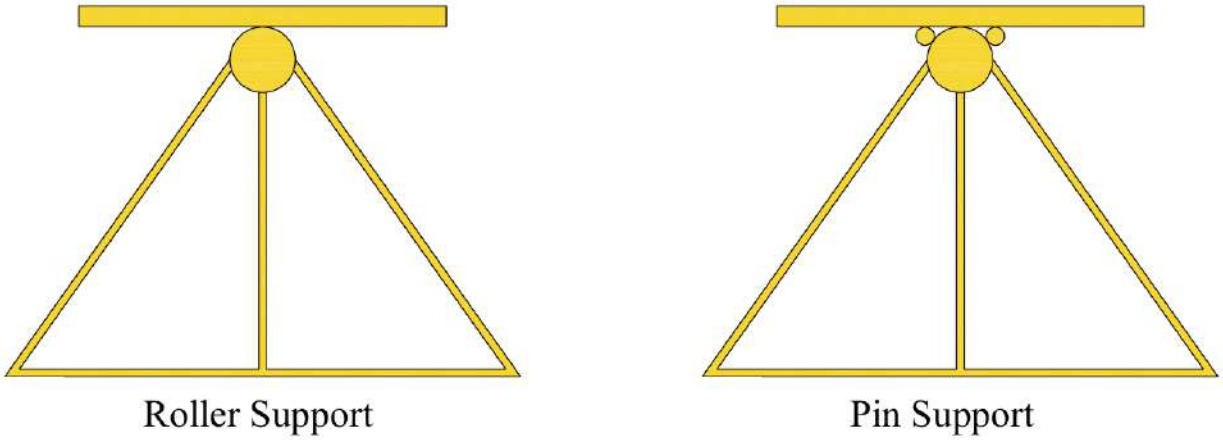

Figure (3.27): Roller and Pin Support.

Chapter Four: Results and Discussion (Experimental)

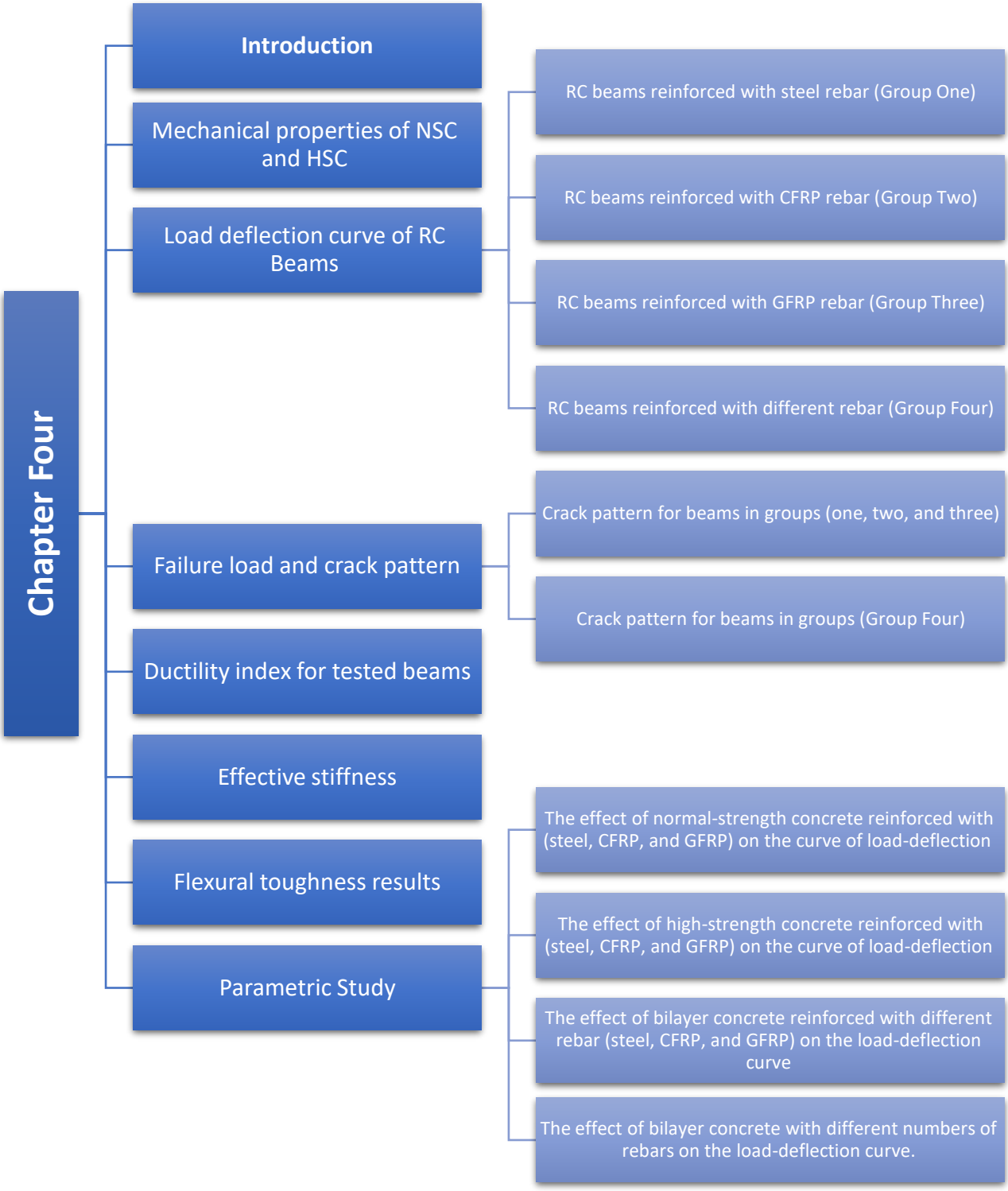

Chapter Four

Results and Discussion (Experimental)

4.1 Introduction

This thesis presents the overall behavior of bilayer beams with different reinforcement bars, focusing on normal concrete (NC) and high strength concrete (HC) mechanical properties. The detailed characteristics of these two types of concrete are thoroughly presented in this study. Furthermore, the experimental results from tests conducted on fifteen reinforced concrete beams are extensively reviewed and analyzed within this section. The structural response of the load-deflection curve is carefully scrutinized, along with the critical parameters such as the load at first crack initiation, crack propagation behavior, flexibility of the beams, and the ultimate load. In-depth examination and discussion of these critical aspects provide valuable insights into bilayer beams' performance and structural integrity under different loading conditions. The findings from this study contribute significantly to the existing body of knowledge on the behavior of reinforced concrete structures, particularly in the context of bilayer beam systems with various reinforcement configurations.

4.2 Mechanical properties of NSC and HSC

The mechanical properties of concrete after 28 days of curing are crucial for assessing its performance, with key parameters such as compressive strength, splitting tensile strength, and flexural strength being of particular interest. These properties indicate the material's ability to withstand various loading conditions, making them essential for structural design and durability evaluations. To ensure accuracy and reliability, the mean values of these mechanical characteristics have

been calculated based on these samples for each parameter, allowing for a comprehensive understanding of the concrete's overall behavior. The compressive strength of concrete is defined as its ability to resist a compressive force until the point of failure is reached. In **Table (4.1)**, Cubic Compressive Strength (f_{cu}). Splitting Tensile Strength (f_{st}): This examination has been meticulously crafted to assess the capacity of concrete to withstand the forces of tensile stress, a critical factor in determining the material's overall durability and structural integrity. The dimensions of the three cylindrical samples, each measuring 100*200 mm. Flexural strength (f_r), also known as the modulus of rupture test, is an alternative method for assessing the tensile strength of concrete. The experiment utilized a prism-shaped specimen measuring 100 mm by 100 mm by 500 mm and applied the load at a centrally positioned singular point.

Table (4.1): Mechanical Properties of NC and HC

Type of concrete	Fcu (MPa)	ft (MPa)	fr (MPa)	ft/fcu	fr/fcu
NC	38	4	4.5	0.112	0.125
HC	71	5.6	6	0.0889	0.0952

4.3 Load deflection curve of RC Beams

The experiment assessed the deflection of each specimen at the beam's midpoint over the span. Every beam displayed a similar crack pattern in its mid-span deflection as the load grew progressively. The specimens' deformations and deflections are shown alongside the earlier crack pattern figures. The main experimental results of specimens are presented in **Table (4.2)**.

Table (4.2): The Main Experimental Results of Specimens.

Group	Beams specimen	No. of layers	Maximum deflection (mm)	Ultimate load (KN)
Group 1	NS-1	Single	14	134
	HS-1	Single	20	148
	NHS-2	Bilayer	26.6	167
Group 2	NC-1	Single	17	119
	HC-1	Single	16.5	123
	NHC-2	Bilayer	18.7	145
Group 3	NG-1	Single	27	112
	HG-1	Single	26	146
	NHG-2	Bilayer	29	121
Group 4	SSC-2	Bilayer	26	157
	CCS-2	Bilayer	17	129
	SSG-2	Bilayer	21	160
	GGS-2	Bilayer	26.3	142
	CCG-2	Bilayer	25.257	118
	GGC-2	Bilayer	24.29	102

4.3.1 RC beams reinforced with steel rebar (Group One)

This group comprises three types of reinforcement concrete beams: normal-strength (NS-1), high-strength (HS-1), and a bilayer (with normal strength at the bottom and high strength at the top), known as NHS-2. **Figure (4.1)** presented the measured curves of load-deflection for beams (NS-1, HS-1, and NHS-2). While (NS-1) and HS-1 have a narrow plastic area range, the linear rising limb represents the elastic region and has a larger angle until it hits the linear limit value of (109, 115.3, and 120 kN) with a corresponding deflection of (5.8, 7.14, and 4.17 mm) accordingly. Maximal applied loads across the plastic area were (134, 148, and 167 kN) and maximum deflections at the mid-span of specimens (14, 20, and 26.6 mm) accordingly, as a result of increasing the layer compressive strength, which in turn raised the ultimate load. From zero load up to around 115.3 kN for (HS-1) and 120

kN for (NHS-2), high-strength and bilayer beams showed larger deflections than (NS-1) in the first stage. The reason is that bilayer beams are both more flexible and stronger than single-layer beams due to the use of high-strength concrete (HS-1) and bilayer systems (NHS-2) (at compression sections of plastic zones as compression-yielding material). Deflection rises quickly because fractures in typical concrete beams continue to spread, approaching compression zones. Contrarily, normal compression portions of high and bilayer beams cannot have these fractures at the same rate. This explains why, after the first stage, a normal beam experiences less deflection than HS-1 and NHS-2 under the same load. Additionally, it may be seen that bilayer beams have an enhanced ultimate load when compared to beams made entirely of regular concrete. **Table (4.2)** shows that flexural capacity for high-strength (HS-1) and bilayer beams (NHS-2) increases by an average of 9.46% and 19.76% relative to (NS-1) specimen. Relating to the normal concrete beam, this result is corroborated by the findings of **(Alogla & Rasheed, 2023)**, who documented improved flexural performance in reinforced concrete beams with layered concrete designs.

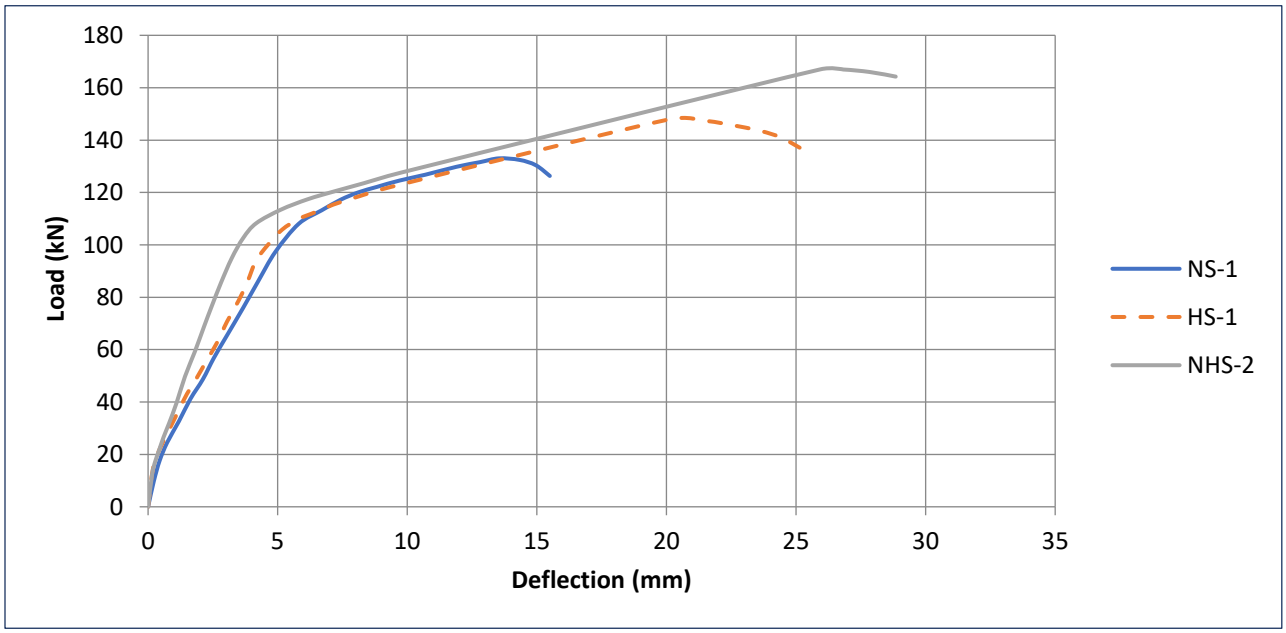

Figure (4.1): Load-deflection curve of specimens (Group One).

4.3.2 RC beams reinforced with CFRP rebar (Group Two)

The group consists of three types of reinforcing concrete beams: normal-strength (NC-1), high-strength (HC-1), and a bilayer (with normal strength at the bottom and high strength at the top) referred to as (NHC-2). **Figure (4.2)** displays the load-deflection curves at a middle span of the tested specimen's RC beams reinforced with CFRP rebar. A higher ultimate load resulted in a maximum applied load of 119, 123, and 145 kN across the plastic area, respectively, with a maximum deflection of 17, 16.5, and 18.7 mm at the mid-span of the specimens. The use of high-strength concrete for (HC-1) and bilayer systems for (NHC-2) (at compression parts of plastic zones as compression-yielding material) in bilayer beams gives them more flexibility and strength at the same time, which is why high-strength and bilayer beams showed higher deflections compared to (NC-1) in the first stage from zero load up to first crack load. Deflection rises quickly because fractures in ordinary concrete beams continue to spread, approaching compression zones. In contrast, these cracks cannot propagate at the same rate in the conventional compression regions of high and bilayer beams; hence, for the same load after the first stage, the deflection is lower for a typical beam than for HC-1 and NHC-2. Additionally, it may be seen that bilayer beams have an enhanced ultimate load when compared to beams made entirely of normal concrete (NC-1). Table (4-3) shows that compared to the regular concrete beam, the flexural capacity of high-strength (HC-1) and bilayer (NHC-2) beams increases by an average of 3.36% and 21.85%, respectively. this result is corroborated by the findings of **(Saad & Rasheed, 2018).**

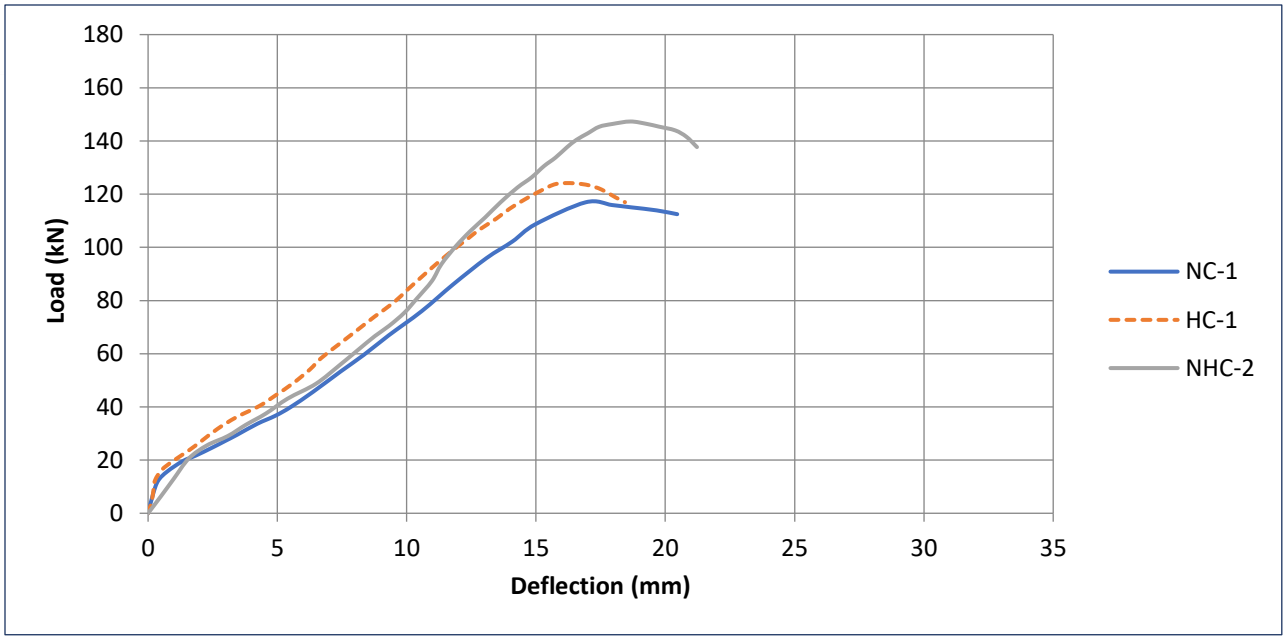

Figure (4.2): Load-deflection curve of specimens (Group Two).

4.3.3 RC beams reinforced with GFRP rebar (Group Three)

The group consists of three types of GFRP reinforcing beams: normal-strength (NG-1), high-strength (HG-1), and a bilayer (with normal strength at the bottom and high strength at the top) referred to as (NHG-2). **Figure (4.3)** presents the load-deflection curves at a middle span of the tested specimen's RC beams reinforced with GFRP rebar. The load-deflection curves of the NG-1 and HG-1 beams were linear to a load of 20 and 15 kN, respectively, before they cracked. The rigidity was diminished when it cracked. High beams (HG-1) deflected more than low beams (NG-1). As concrete beam cracks spread toward compression zones, deflection climbs fast. Up to 141.6 kN, the HG-1 specimen's concrete stiffness and crack distribution remained constant. After that, as additional cracks form in the concrete, the rigidity steadily decreases. However, crack dispersion across the concrete reached a load level of 111.6 kN in NG-1, but in NHG-2, the stiffness remained constant up to 120.6 KN. The ultimate load was raised, and the plastic area experienced a maximum applied load of (112, 146, and 121 kN), with the mid-section exhibiting the maximum deflection at the center span of specimens (27, 26,

and 29 mm), respectively. This behavior corresponds with previous research demonstrating that sand-coated GFRP bars may be increase adhesion with concrete, resulting in superior flexural strength and strain performance relative to steel-reinforced alternatives **(Jabbar & Farid, 2018)**.

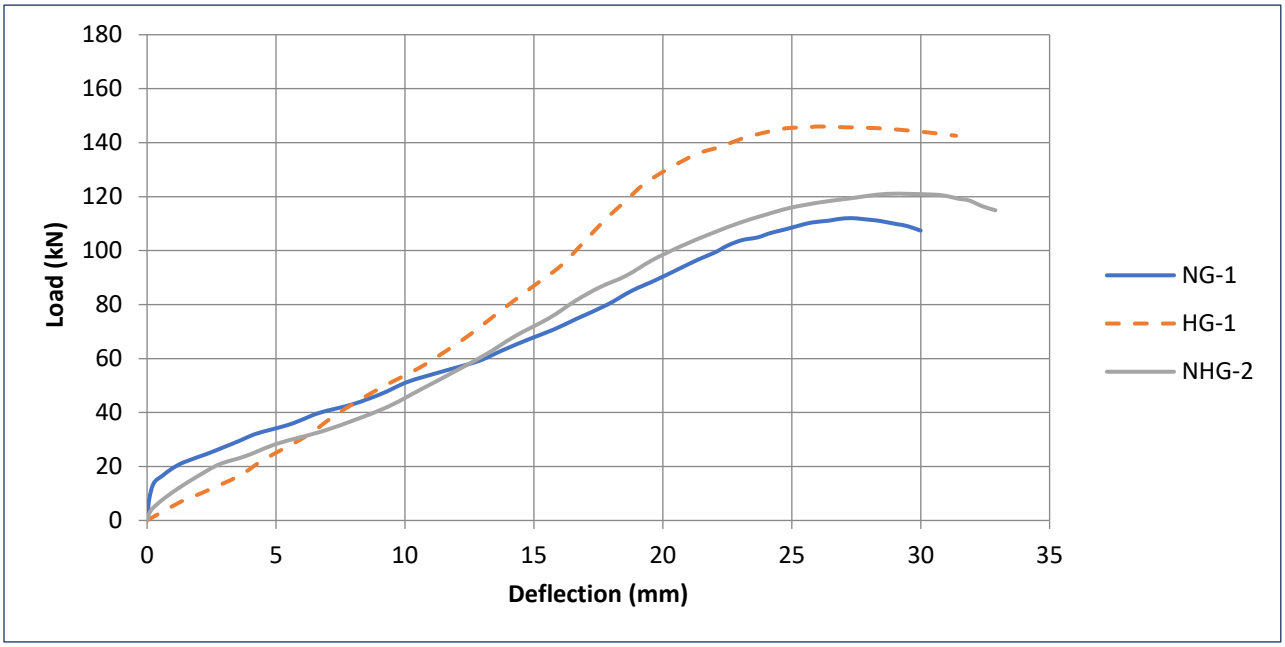

Figure (4.3): Load-deflection curve of specimens (Group Three).

4.3.4 RC beams reinforced with different rebar (Group Four)

This group comprises six specimens of bilayer concrete beams (with normal strength at the bottom and high strength at the top) reinforced with different types of rebars. The deflection was measured at mid-span. **Figure (4.4)** displays the load-deflection curves at a middle span of the tested specimens cast with a bilayer concrete and using different rebars of (Steel, CFRP, and GFRP). It was clear that the specimens for group four (SSC-2 and CCS-2) yielded according to their behavior until nearly at loads (91.4 and 127 kN), subsequently. Specimens experienced a maximum deflection of (17 mm and 129 kN) under the plastic region's maximum applied stress, respectively. The beams showed a decrease in the ultimate load by about 17.83%. This is because it uses two bars of steel with one bar of carbon for

the SSC-2 specimen, which gives them more flexibility and more strength at the same time. For the specimens (SSG-2 and GGS-2), at the mid-span of the specimens, the highest deflection was 26.3 mm, and the maximum applied load across the plastic area was 160 kN. The beams showed an increase in the ultimate load by about 11.25%. This is because it uses two bars of steel with one bar of glass for the SSG-2 specimen, which gives them more flexibility and more strength at the same time, according to the properties of the bars. The specimens (CCG-2 and GGC-2) had a plastic area that could bear 118 and 102 kN of stress and 25.25 and 24.29 mm of deflection at the center of the specimen span. The beams' ultimate load dropped 13.56 %. The CCG-2 specimen employs two carbon bars and one glass bar, which offers it extra flexibility and strength, depending on the bars' qualities. The above result shows the maximum ultimate load (SSG-2 and SSC-2) compared with the other specimens. Consequently, hybrid reinforced bars or hybrid systems demonstrated increased ductility in concrete beams. This observation aligns with the findings published by **(Ge et al., 2020)** and **(Said et al., 2021)**, who verified that hybrid reinforcement improves ductility in concrete beams.

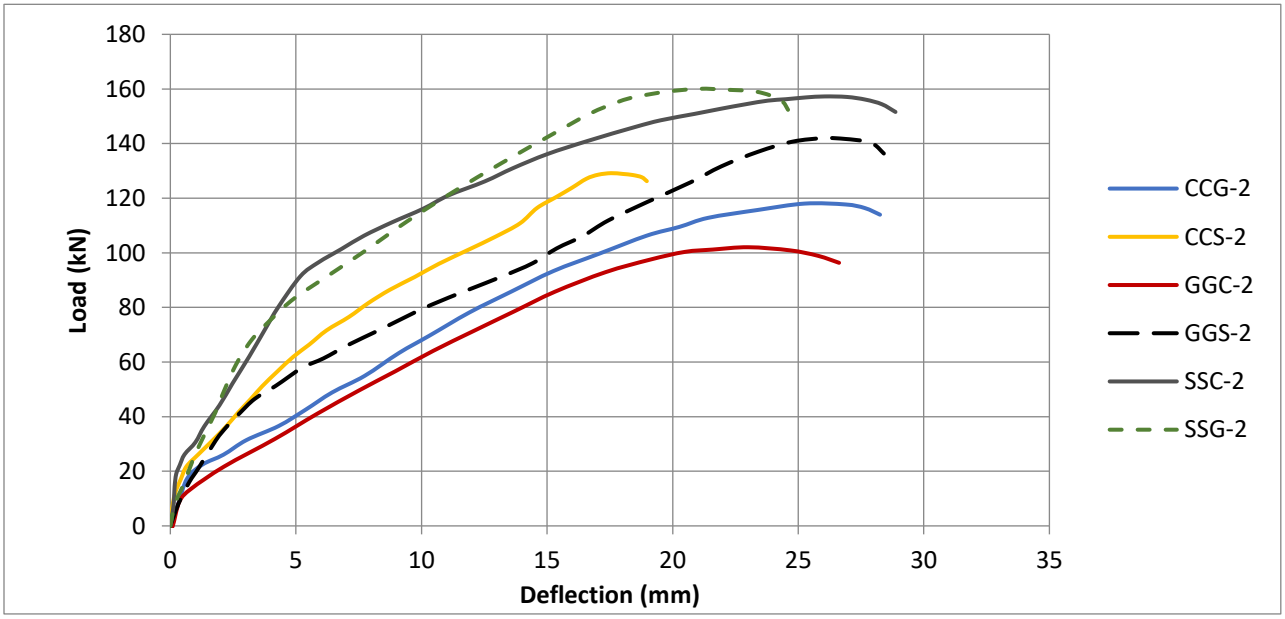

Figure (4.4): Load-deflection curve of specimens reinforced with different rebar (Group Four).

4.4 Failure load and crack patterns

Table (4.3) gives the beams' failure modes, first cracking value, Maximum deflection, and ultimate load. The behavior of the layered concrete beams in transmitting interface loads and propagating cracks was also evaluated by considering the cracking pattern and failure mechanism of certain of the beams.

Table (4.3): The Results of Tested Specimens.

Group	Specimen symbol	First Crack (kN)	Ultimate Load (kN)	Max. def (mm)	Failure Mode
group 1	NS-1	20	134	14	flexural
	HS-1	20	148	20	flexural
	NHS-2	35	167	26.6	flexural
group 2	NC-1	30	119	17	flexural-shear
	HC-1	20	123	16.5	flexural-shear
	NHC-2	20	145	18.7	flexural-shear
group 3	NG-1	20	112	27	flexural
	HG-1	20	146	26	flexural
	NHG-2	25	121	29	flexural
group 4	SSC-2	25	157	26	flexural
	CCS-2	20	129	17	flexural
	SSG-2	30	160	21	flexural
	GGS-2	20	142	26.3	flexural
	CCG-2	30	118	25.257	flexural-concrete crushing
	GGC-2	20	102	24.29	flexural-shear

To identify both small and large cracks, the surfaces that were going to be tested were first painted with a thin coat or two of white paint and then allowed to dry. **Figure (4.5)** shows that during the testing, microcracks were visually identified on the beam's lateral surface and then marked with a marker. The number of cracks visible in these specimens was logically smaller than those dimensions, since the specimens were designed with small dimensions to accommodate the load limitation of the universal testing machine, and because it is harder to detect cracks with the naked eye for smaller specimens.

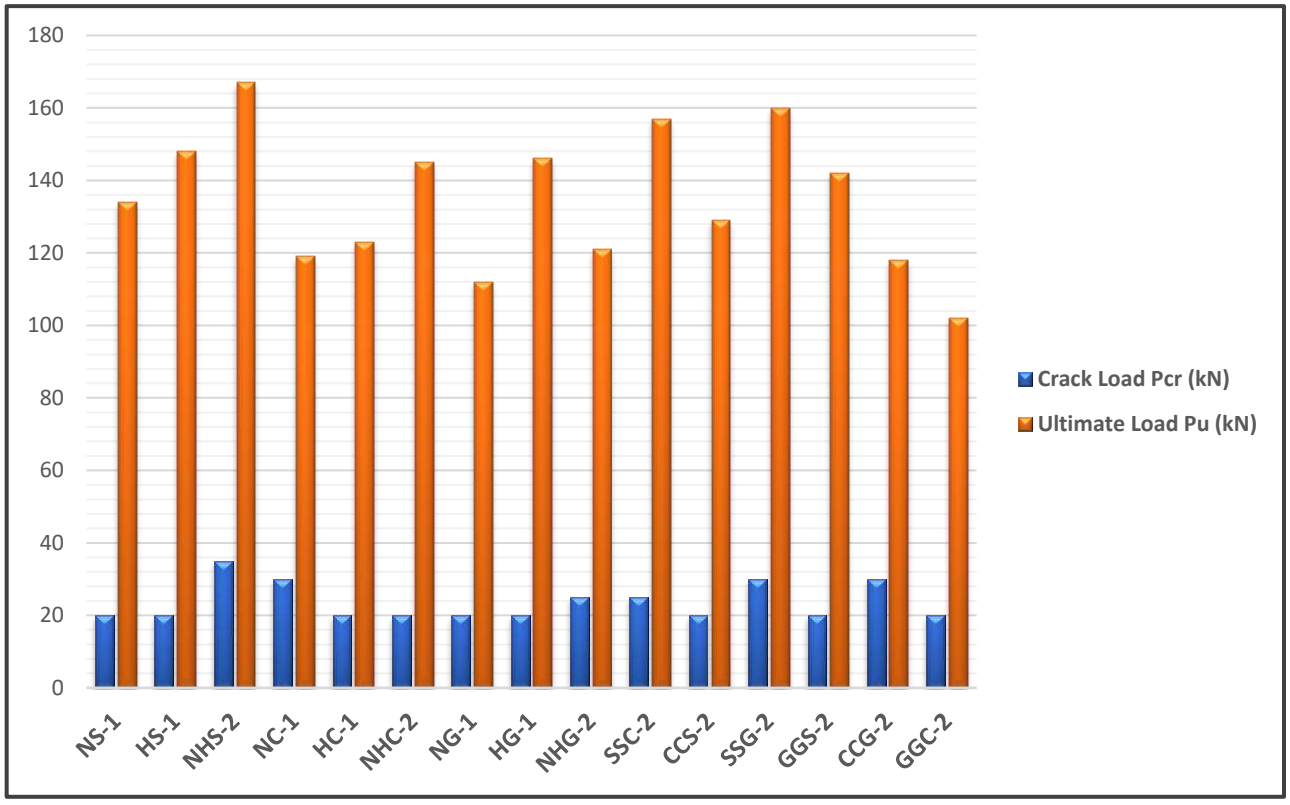

Figure (4.5): Ultimate Load and Crack Load for all specimens.

4.4.1 Crack pattern for beams in groups (one, two, and three)

According to the types of reinforcement, the tested specimens were divided into three groups. The first group includes three specimens of steel reinforcement, the last one cast in bilayer concrete (normal strength in the bottom zone and high strength in the top zone). The second group includes three beam specimens

reinforced with carbon bars, the last one cast in bilayer concrete (normal strength in the bottom zone and high strength in the top zone). The third group contains three specimens and the exact details as groups one and two, but reinforced with glass bars. The map of cracking for the conventional beam tested under a two-point loading is shown in **Figure (4.6)**. As usual, the first crack formed in the pure bending moment (B.M) zone at 20–35 kN midway during the span. Vertical cracks emerged at the maximum B.M. and shear zones as loading increased, but no additional cracks occurred up to 85 kN. Further cracks on both sides progressed toward the supports along decreasing angles. At (105 to 130) kN, the diagonal fracture occurred along the compression struts at an angle of 41.5 and advanced toward the beam's upper end point loads. However, crushing near the support preceded collapse. When loaded in a few locations, concrete may spall due to horizontal cracking at the compression face (112 to 150 kN). The beams collapsed in three modes, flexural, flexural-shear, and flexural-concrete crushing at the loads shown in **Table (4.3)**. The crack width in the hybrid beams was smaller than that of both beam types at all loading levels. This result is supported by the findings of **(Kheder et al., 2010).** The observed discrepancies in cracking patterns and ultimate load capabilities among the examined specimens might be ascribed to several reasons. The type of reinforcement was crucial; steel, carbon, and glass material demonstrated distinct mechanical properties that affected stiffness and load-bearing capacity. Integrating a bilayer concrete system enhanced stress distribution by positioning high-strength concrete in the compression zone, postponing crack initiation, and augmenting the failure load. The failure angles and fracture propagation patterns were closely correlated with the interplay of bending and shear forces, with bilayer beams transitioning to more ductile flexural behavior.

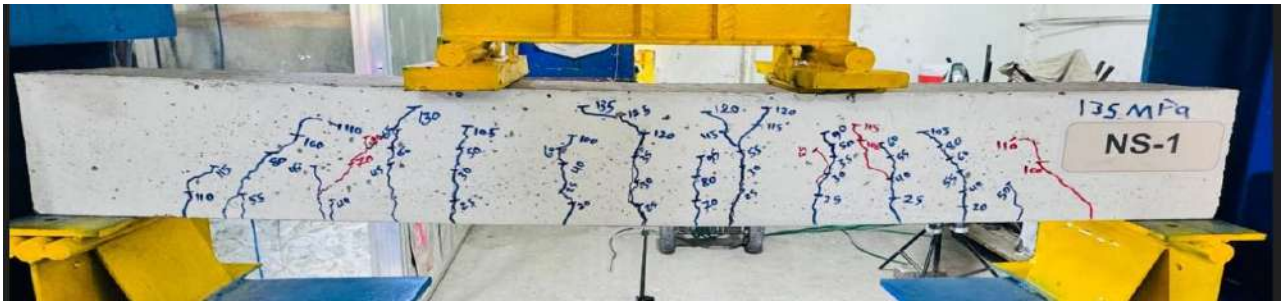

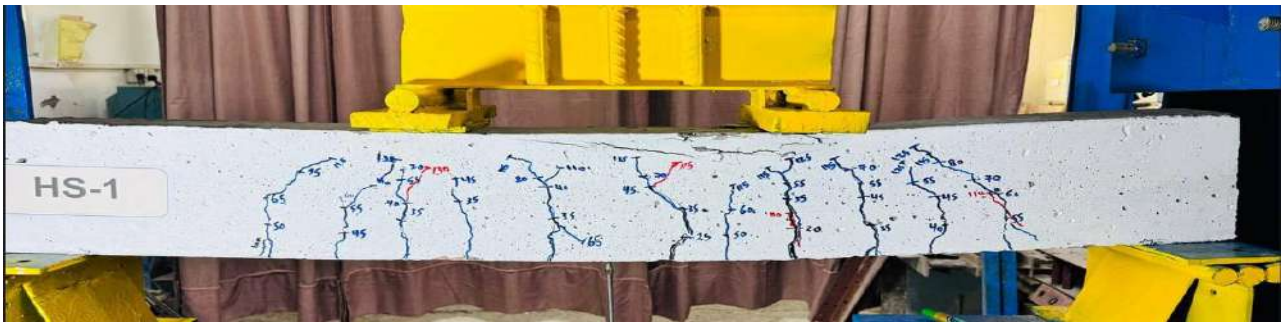

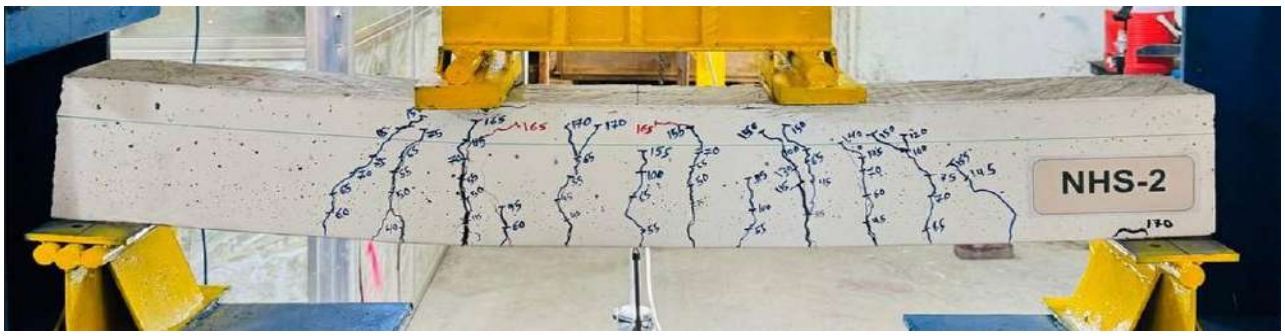

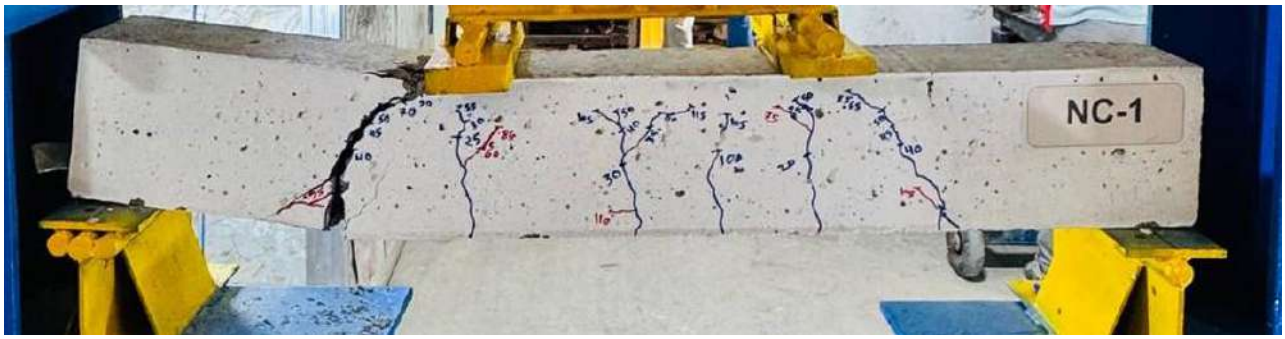

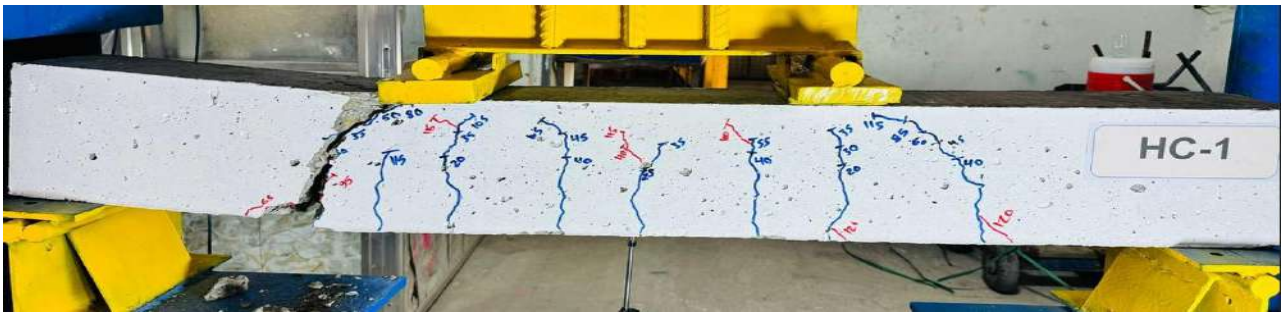

Continue...

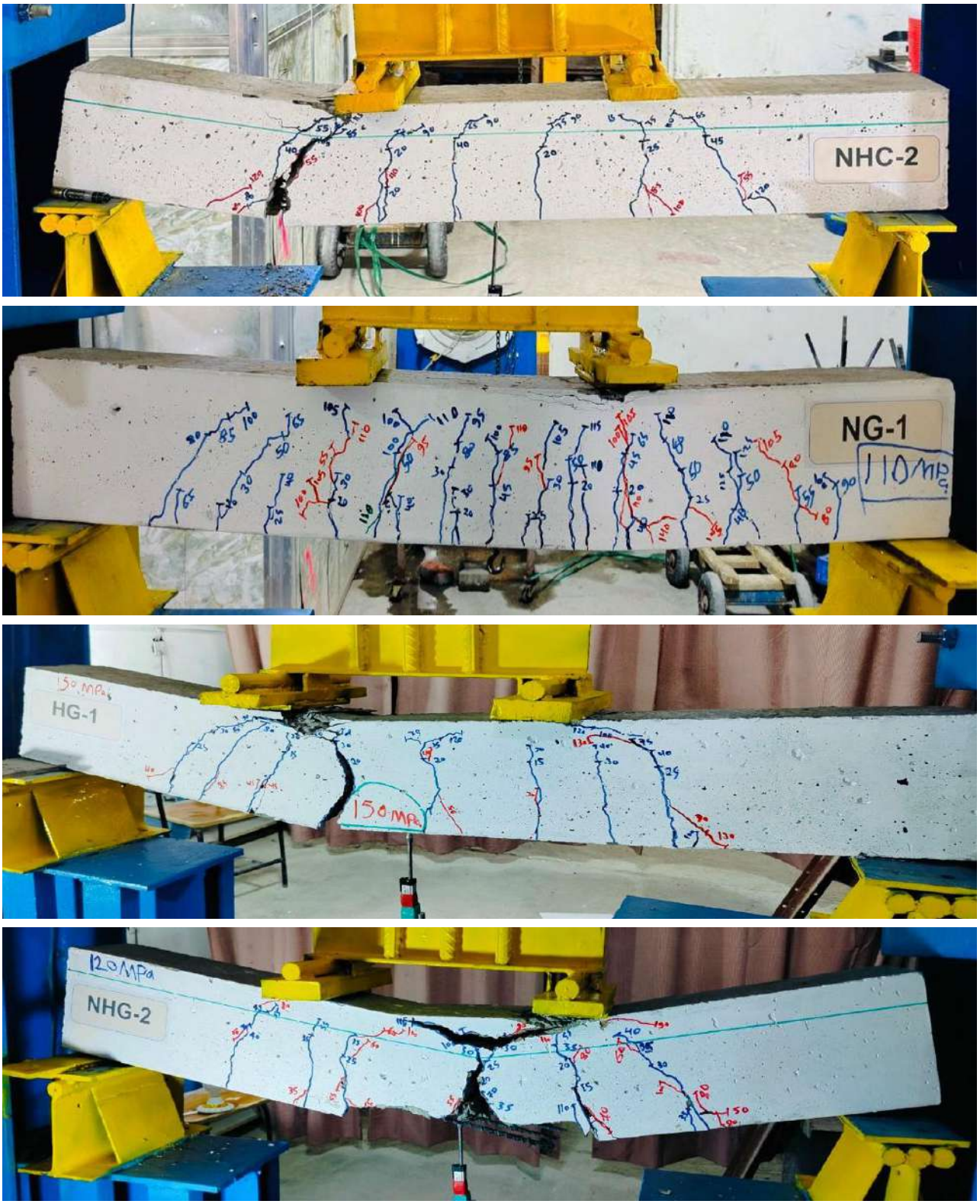

Figure (4.6): Cracking Pattern and Failure Mode for Beams Reinforced with One Type of Rebar.

4.4.2 Crack pattern for beams in groups (Group Four)

The tested specimens were divided into six subgroups, each cast with bilayer concrete (normal strength in the bottom zone and high strength in the top zone) and reinforced with different rebars using steel, CFRP, and GFRP bars (hybrid reinforcement). The plan for cracking the specimen is presented in **Figure (4.7)**. The first cracks appeared in the region of the high moment at the mid-span flexural area and began to appear with a load of (20 to 30 kN) spreading on both sides of the beam. A diagonal crack was initiated at (50 to 85 kN) and is inclined by an angle of (42^{o}), controlled by flexural cracking, approaching the supports. When cracks are subjected to progressive stress, they eventually reach the HSC and begin to slow down. Due to the development of shear-flexural cracks vertically under the loading point, the model generally collapsed at 105 kN. When comparing bilayer concrete beams with a single layer and one kind of reinforcement, it is worth noting that the capacity of the beams was increased by 3.32% when the beams were configured horizontally. This may be because the flexural resistance and strength of the compression block have been enhanced. One possible cause of the diagonal failure mode is the small distance between the point loads and the supports. It should be noted that, due to the rather high load concentration, crushing occurred at several supports. This reduce the specimen's overall capacity, potentially causing failure to occur before the section attains its full strength.. Thus, it is expected that if this local failure is avoided, a higher capacity may be obtained. The augmentation in capacity is mainly ascribed to the superior compressive strength conferred by the higher HSC layer and the better flexural performance resulting from hybrid reinforcement. The initial development of diagonal fractures is probably associated with the restricted shear span between the loading sites and supports, while localized crushing near the supports diminished the total capacity. Eradicating such isolated defects may enhance structural efficiency **(Yoon et al., 2011).**

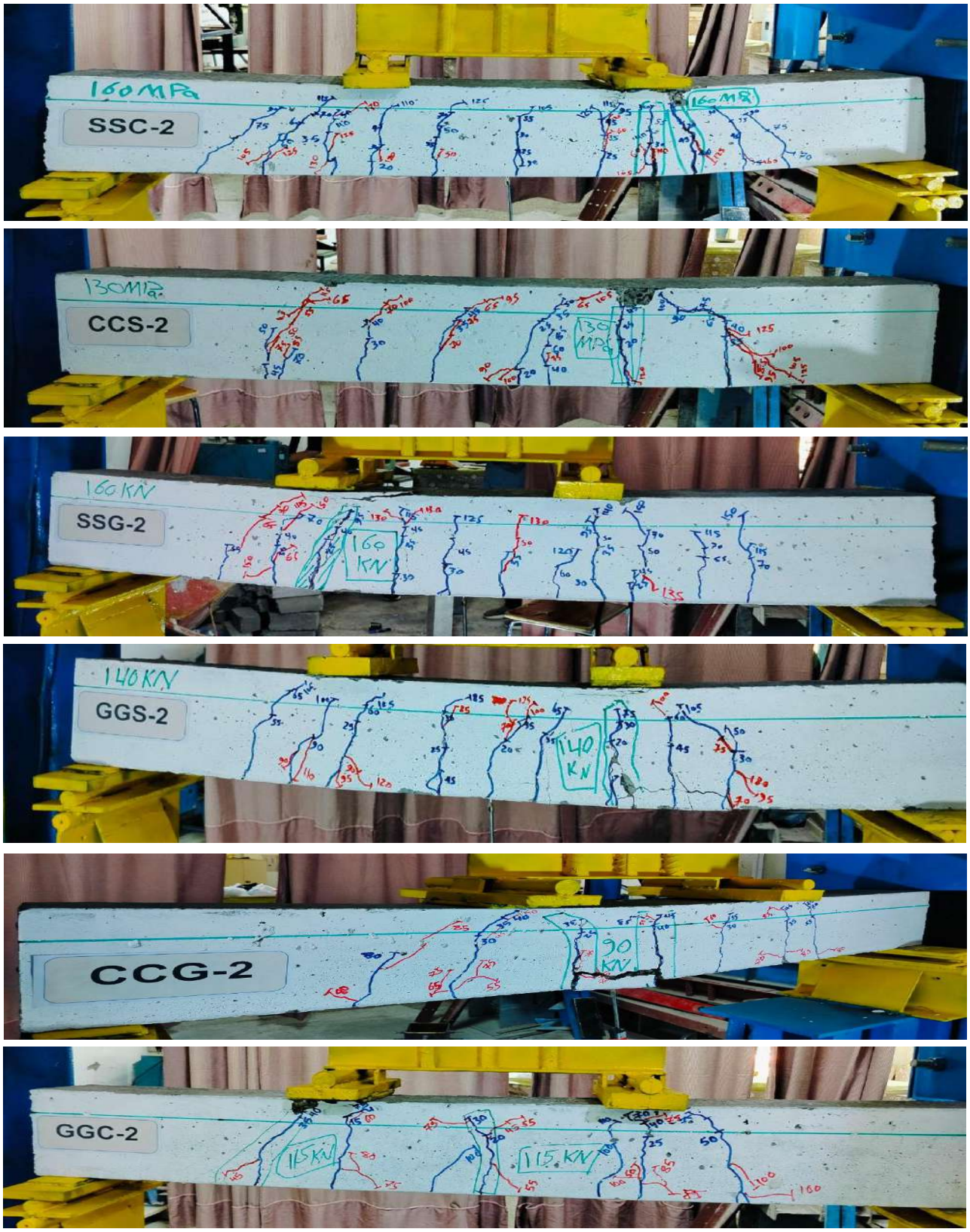

Figure (4.7): Cracking pattern and failure mode for bilayer concrete beam.

4.5 Ductility index for tested beams

Ductility refers to the capacity of RC components to withstand inelastic deformation without experiencing any reduction in their load-bearing capability until failure occurs. The ductility is the ratio between the ultimate deformation and the yield deformation. Deformation led to strains, curvatures, or deflections. The notional yield displacement (Δy) is where the two straight tangent lines connect on the load-displacement curves, one during the elastic stage and the other at the post-elastic stage **(Safaa, 2019)**. The ductility index in this research is defined as the deflection ratio at ultimate load to the yield deflection of the analogous elastoplastic system, as shown in **Figure (4.8)**.

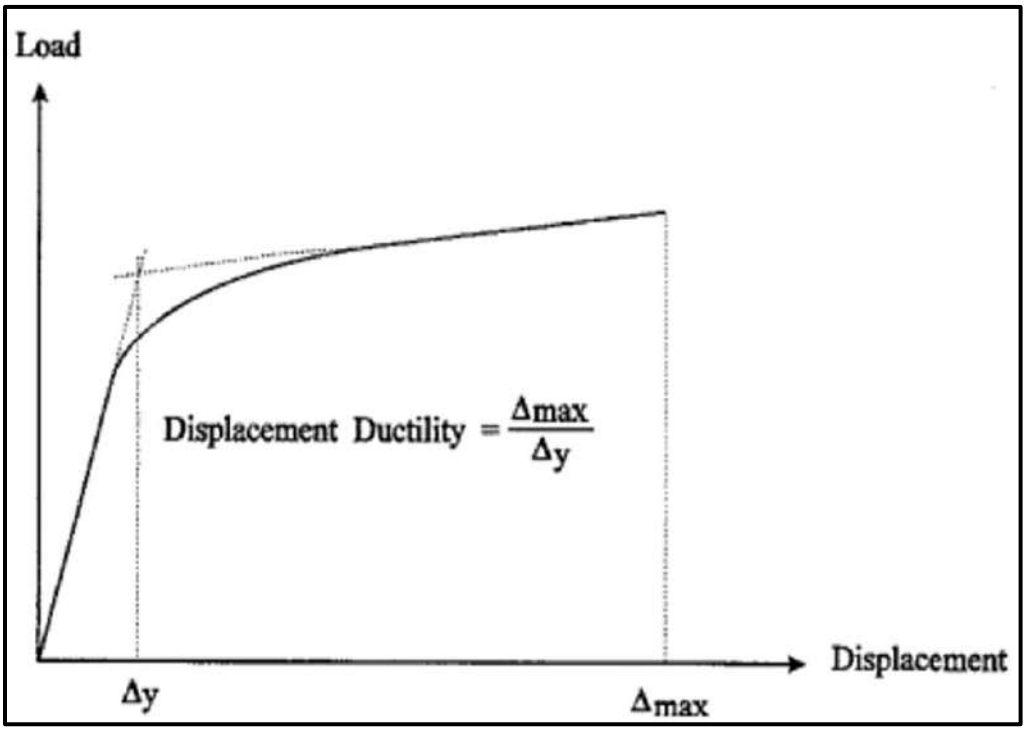

Figure (4.8): Definition of displacement ductility (Safaa, 2019).

The ductility index data for beams in this study are shown in **Table (4.4)**. To provide a clear explanation of how the ductility findings are calculated, the process of determining the displacement ductility using the technique specified for the (NS-

1) beam is shown in **Figures (4.9) to (4.13).** The tested beams exhibit minimal ductility mainly because the shape and dimensions of the cross-section of the structure affect its ductility, the type of materials used, and the reinforcement ratio. It is worth noting that the beams reinforced with steel bars (NHS-2) and bilayer concrete have a greater level of strengthening than others. For bilayer beams, concrete reinforced with various rebar can be a significant improvement in the (GGC-2) beam, which is reinforced with two glass and one carbon bars, as well as using a bilayer system; this improvement is because of the properties of bars and type of concrete layer.

Table (4.4): Ductility for tested beams specimens.

Group	Specimen designation	Yield deflection Δy(mm)	Ultimate deflection Δu (mm)	Ductility index=Δu/Δy
Group 1	NS-1	6.85	14	2.0437956
	HS-1	7.151	20	2.7968116
	NHS-2	6.129	26.6	4.3400228
Group 2	NC-1	15.732	17	1.0806001
	HC-1	15.147	16.5	1.0893246
	NHC-2	17.223	18.7	1.0857574
Group 3	NG-1	24.841	27	1.0869128
	HG-1	21.699	26	1.1982119
	NHG-2	24.234	29	1.1966658
Group 4	SSC-2	20.855	26	1.2467034
	CCS-2	15.211	17	1.1176123
	SSG-2	17.401	21	1.2068272
	GGS-2	24.145	26.3	1.0892524
	CCG-2	20.488	25.257	1.2327704
	GGC-2	18.257	24.29	1.3304486

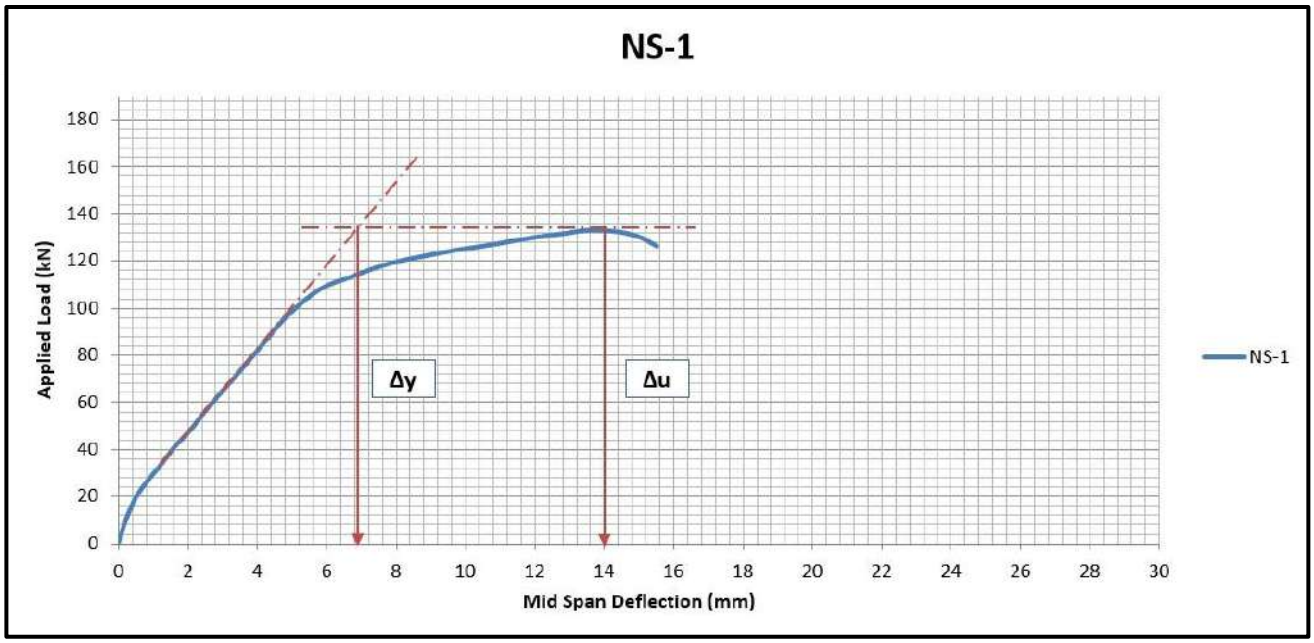

Figure (4.9): Typical diagram for determining the ductility of (NS-1) beams.

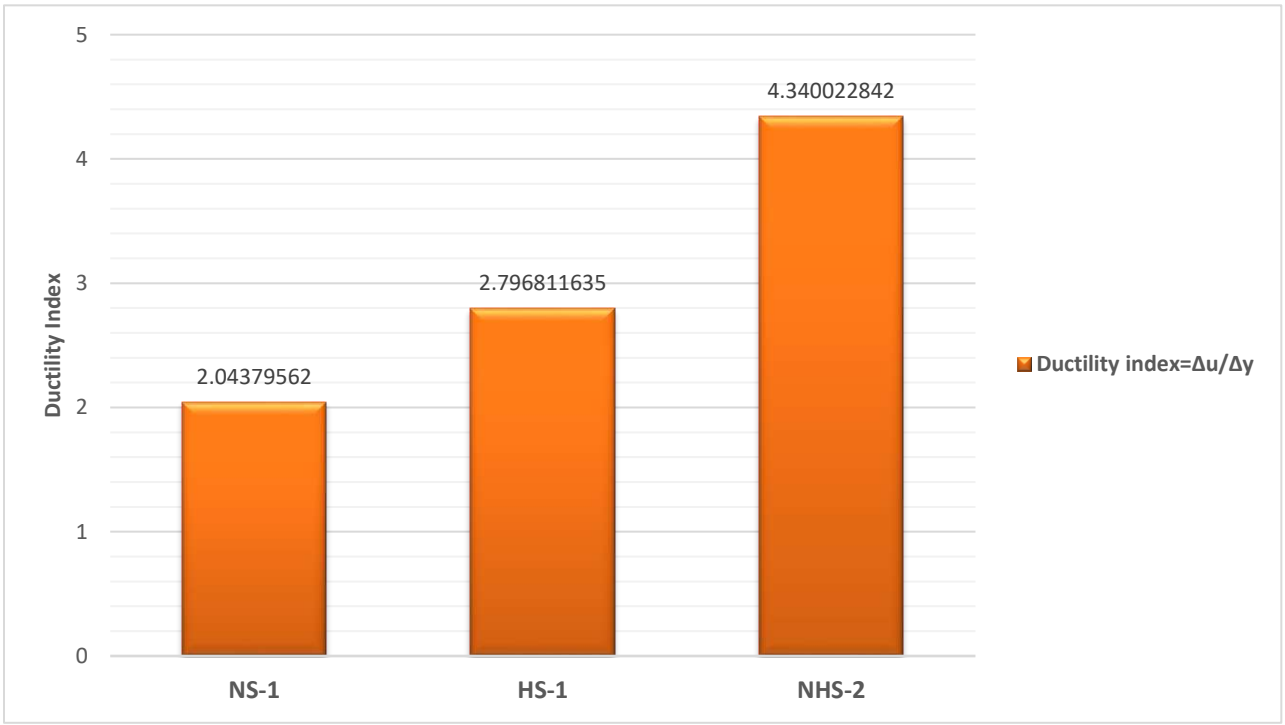

Figure (4.10): The ductility of (group 1) specimens.

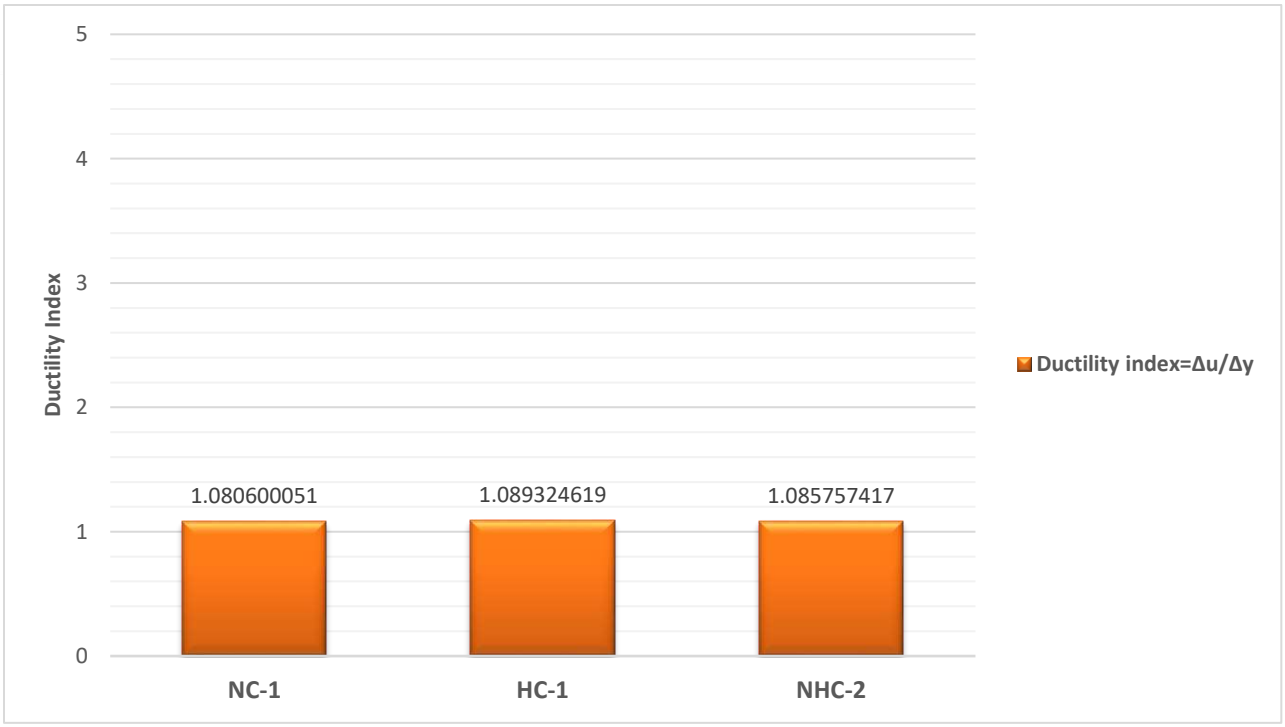

Figure (4.11): The ductility of (group 2) specimens.

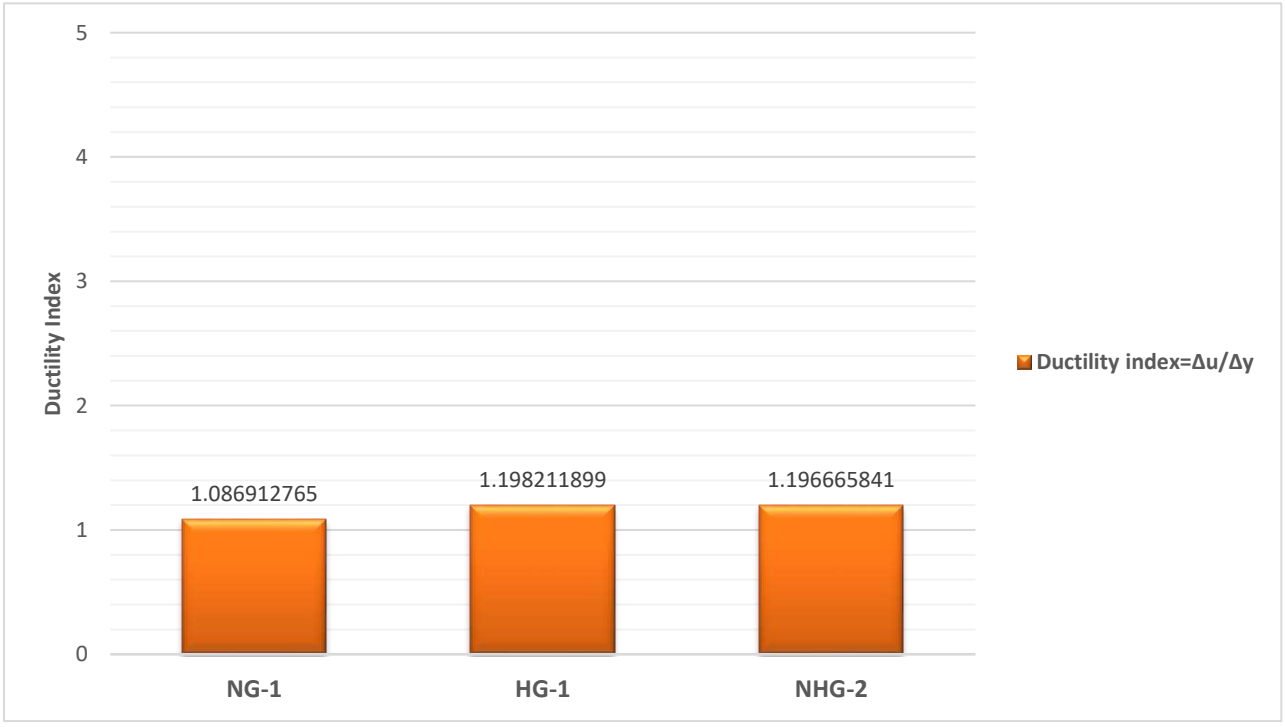

Figure (4.12): The ductility of (group 3) specimens.

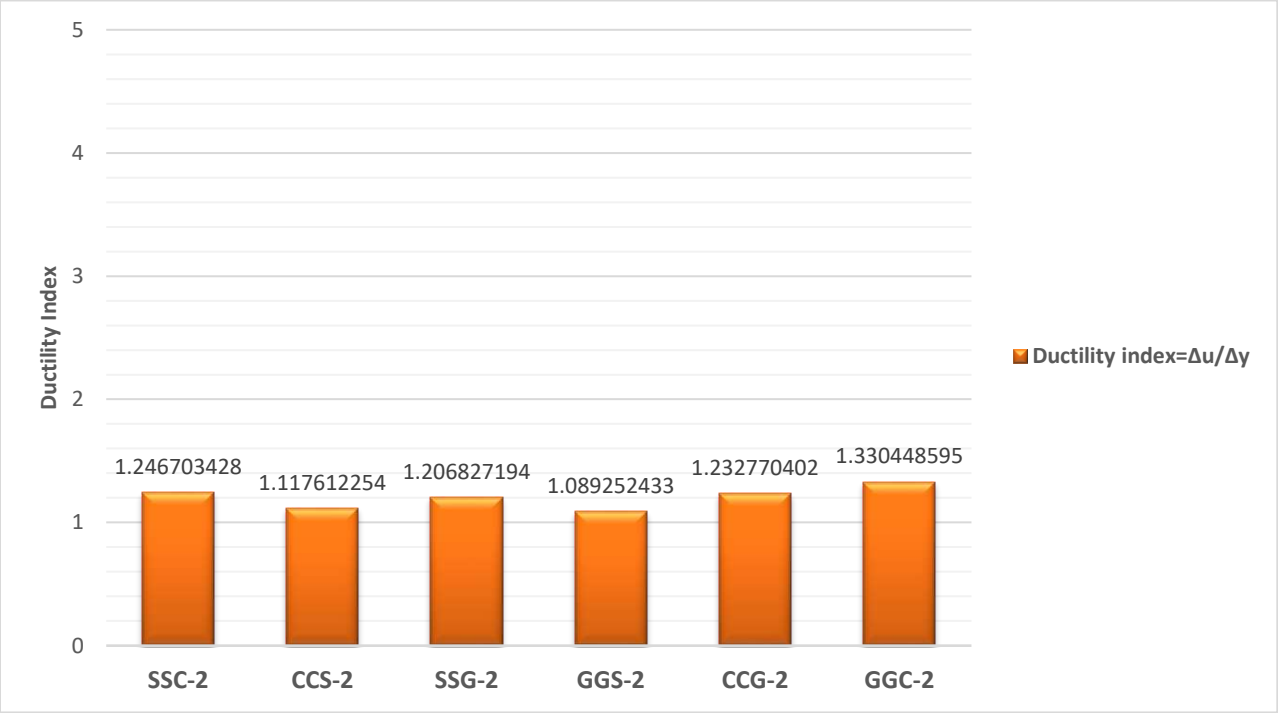

Figure (4.13): The ductility of (group 4) specimens.

4.6 Effective stiffness

An object's effective stiffness (k) quantifies the level of resistance that body of elastic presents to deformation. The notion of "effective stiffness" has been established, defined by the strength during the service load phase, which is 0.75 times the ultimate strength (Pu). Consequently, the effective stiffness (Ke), as shown in a **Figure (4.14)**, may be approximated using **Equation (4.1) (Shakir& Abd, 2020)**.

$$K_e = 0.75\, P_u/\Delta_{at(0.75\, P_u)} \quad \text{..... (4.1)}$$

Ke: the effective stiffness. (Pu): the ultimate load. Δ(0.75Pu): that represents the deflection corresponding to the load level of (0.75 Pu).

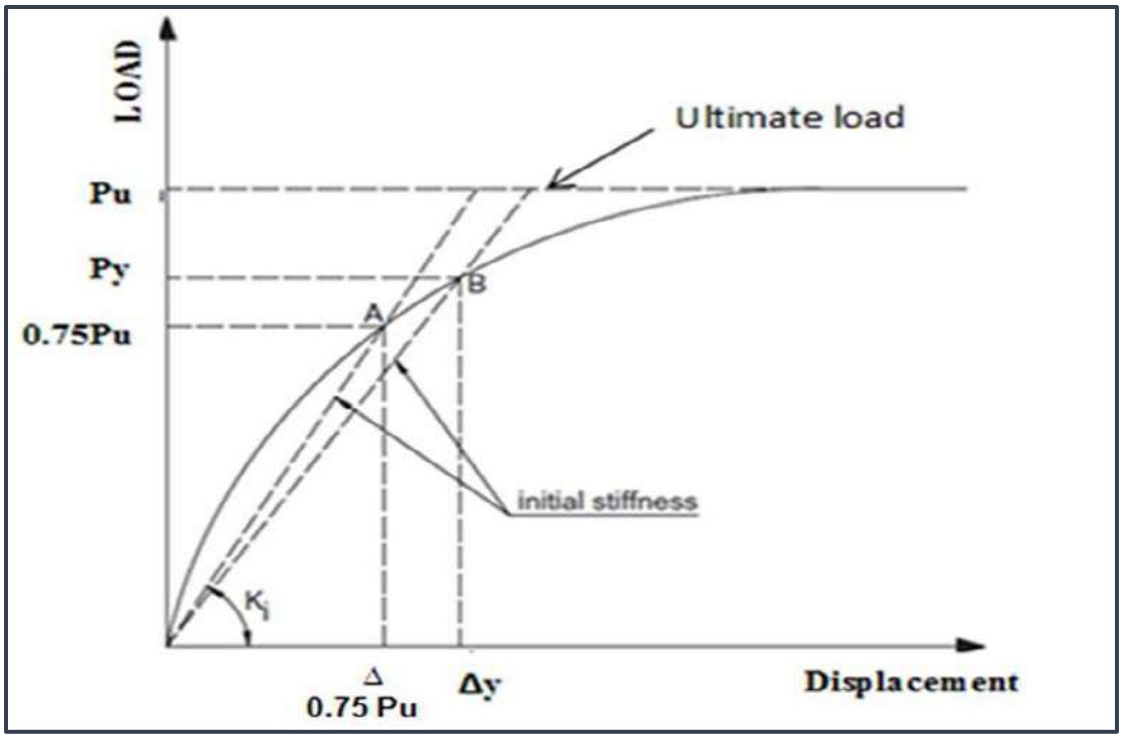

Figure (4.14): Effective Stiffness Determination (Shakir& Abd, 2020).

Table (4.5) displays the values of the stiffness of the tested beams. For steel specimens (group 1), The rigidity value was the highest among all specimens. Furthermore, it is noteworthy that the glass beams (group 3) exhibit the lowest stiffness, with a reduction of around 70.59% relative to the steel specimens, attributed to the efficacy of using HSC in the upper layer to enhance stiffness. It can also be noted that the bilayer beams reinforced with different rebar have a more significant value of stiffness compared with the other specimens because they use a bilayer system (high strength in the top zone and normal strength in the bottom zone) and different distributions of reinforcement and types of bars **Figure (4.15)** to **(4.18)** show the value of stiffness for all specimens.

Table (4.5): Stiffness Criteria of Beams.

Group	Specimen designation	Ultimate load, kN	0.75 Pu kN	Deflection at 0.75 Pu. (mm)	Stiffness, K (kN/mm)
group 1	NS-1	134	100.5	5.1	19.705882
	HS-1	148	111	5.3	20.943396
	NHS-2	167	125.25	8.4	14.910714
group 2	NC-1	119	89.25	12.7	7.0275591
	HC-1	123	92.25	10.4	8.8701923
	NHC-2	145	108.75	12.4	8.7701613
group 3	NG-1	112	84	16.5	5.0909091
	HG-1	146	109.5	17.4	6.2931034
	NHG-2	121	90.75	18.3	4.9590164
group 4	SSC-2	157	117.75	10.3	11.432039
	CCS-2	129	96.75	10.9	8.8761468
	SSG-2	160	120	11	10.909091
	GGS-2	142	106.5	16.2	6.5740741
	CCG-2	118	88.5	14.8	5.9797297
	GGC-2	102	76.5	11.4	6.7105263

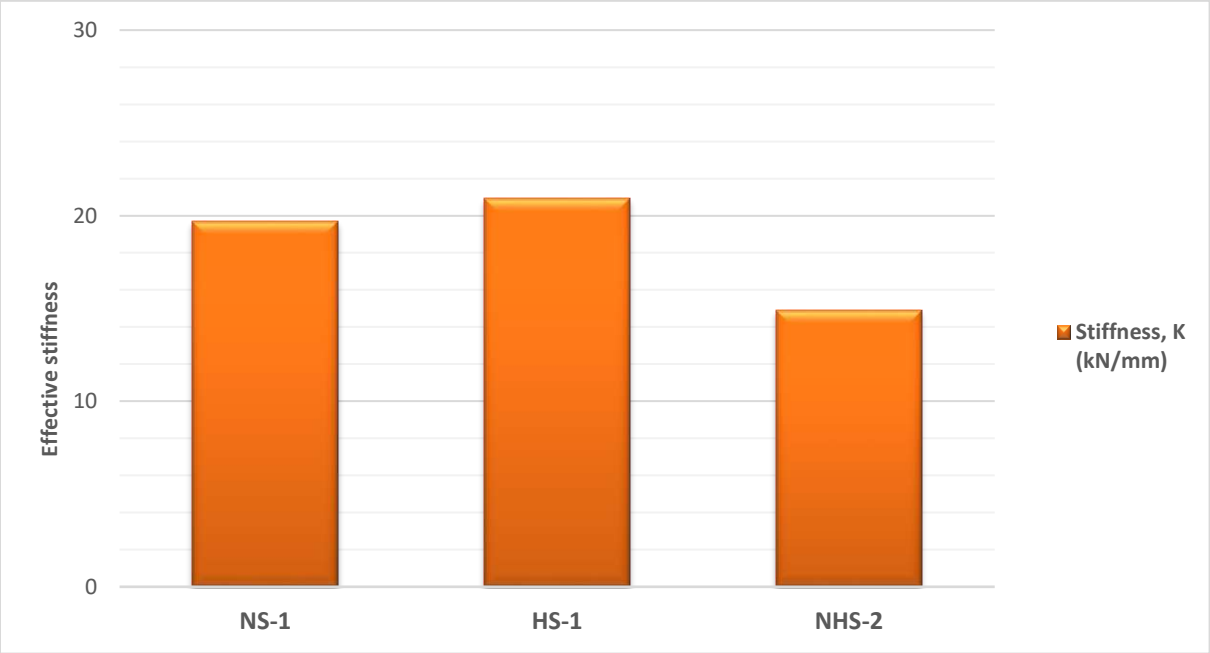

Figure (4.15): The effective stiffness for the specimens tested (group 1).

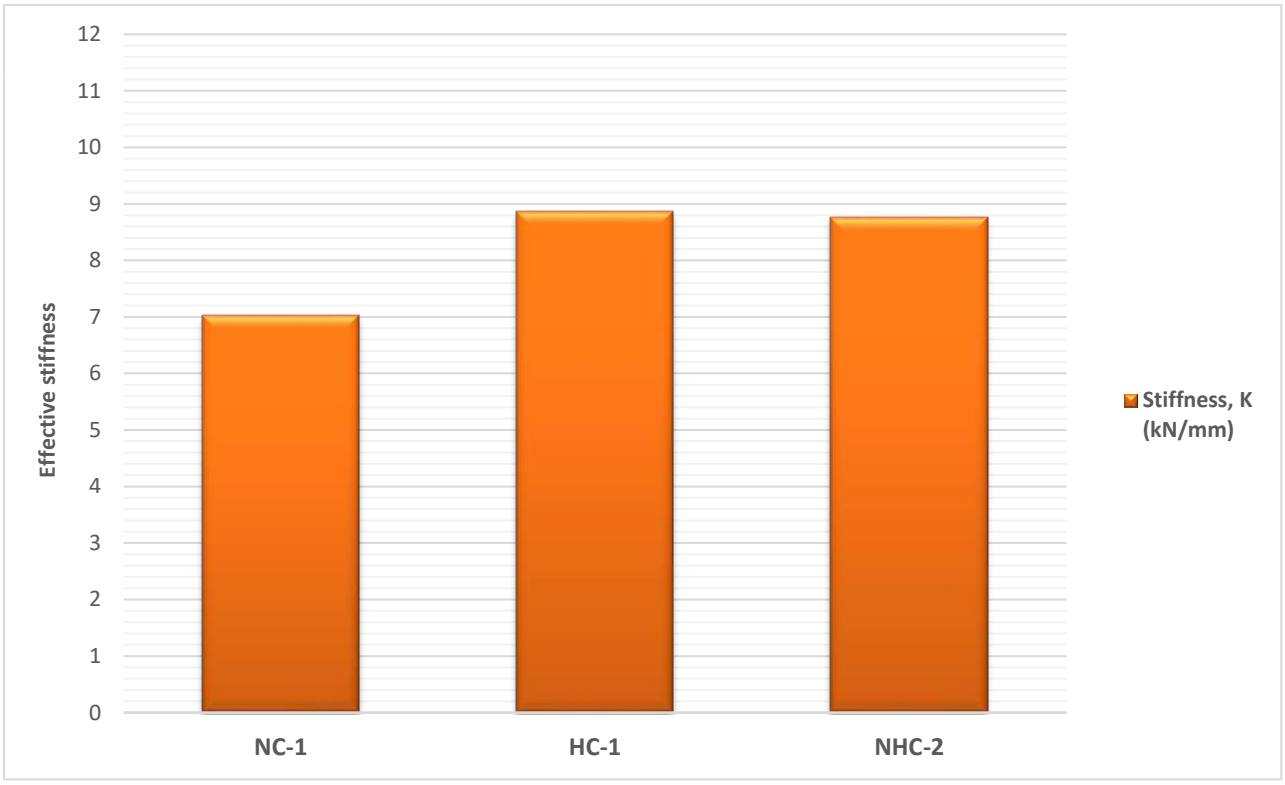

Figure (4.16): The effective stiffness for the specimens tested (group 2).

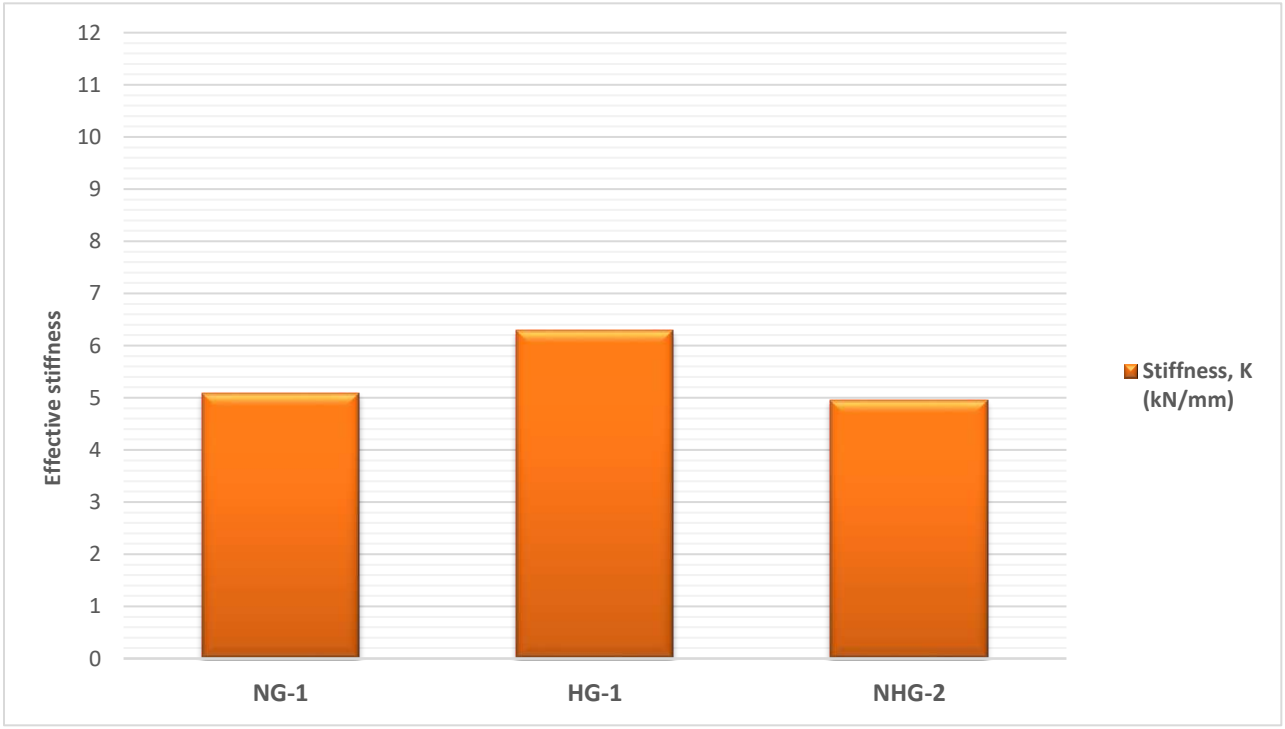

Figure (4.17): The effective stiffness for the specimens tested (group 3).

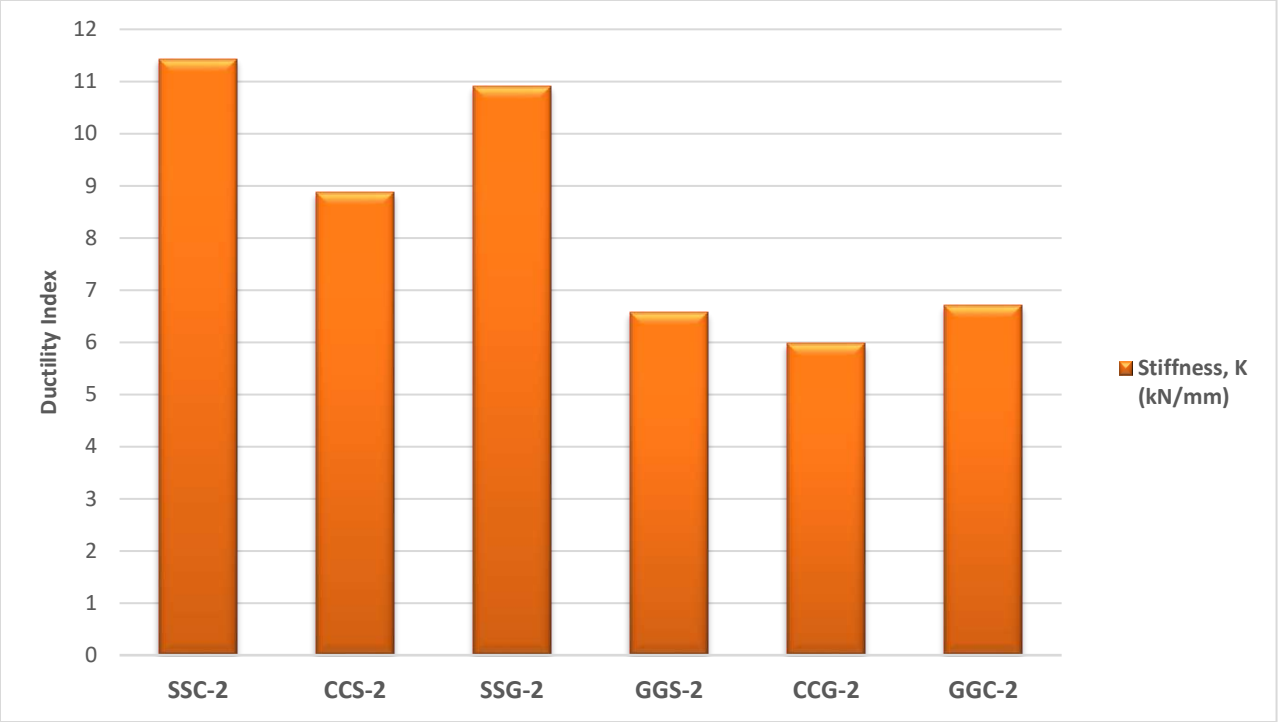

Figure (4.18): The effective stiffness for the specimens tested (group 4).

4.7 Flexural toughness results

Toughness is a quantitative measure of a component's ability to withstand deformations before it breaks or fails. It is determined by calculating the area under the load deflection curve when the stiffness is close to zero or equal to zero. Therefore, the energy the member generates gradually diminishes until it fails **(Ali & Abbas, 2016)**. Ductility and energy absorption capacity are essential for bilayer concrete beams and other statically indeterminate structures, especially under cyclic or recurrent loads. This is due to the augmentation of moment redistribution capability via the rotation of plastic hinges. **Table (4-6)** shows the toughness values for all beams tested under a two-point load, which showed improvement in flexural toughness noticeably and gradually when using normal, high, and bilayer systems. For the group, it can be seen that the lowest value in the (NS-1) specimen was (1568.7kN*mm); however, when using high-strength concrete, observed a

development in the toughness values by 90.04%, where the bending value was 565,444 kN*mm. Furthermore, when employing the bilayer system, it was evident that the increase was even more significant, at 142.34%, compared to sample NS-1. This can be attributed to using materials from two layers to target the strengths and weaknesses in the bending behavior of the structure. From this perspective, it is clear that the bilayer system is successful and possesses a higher bending strength than other elements. For group two, which uses carbon bars, I can see the lowest value in the (NC-1) specimen was (1468.69kN*mm). The increase in toughness values was evident and gradual; when using high-strength concrete, the increase was 4.42%, while with the use of a dual-layer system, the increase was 41.43%. This confirms the efficiency of using a bi-layer system, which provides greater bending strength and durability for the longevity and safety of the structure. It observes higher toughness values when using glass reinforcement than carbon and steel. This is attributed to the superior properties of glass, its high strength, and unique ductility. For instance, the toughness value for the specimen (NG-1) is (2077.24 kN*mm), the lowest value in the glass group but higher than that of the carbon and steel groups. It notes an increase of 33.19% when using high-strength concrete, while the increase was 43.34% with a bilayer system. For bilayer concrete beams reinforced with different rebar, it is observed that the highest value is (3504.13 kN*mm) for the model (SSC-2), which employs steel bars and a carbon bar cast in bilayers (the lower layer consists of normal-strength concrete, while the upper layer is high-strength concrete). Conversely, the lowest value was for the model (CCS-2), which recorded (1611.57 kN*mm). This is attributed to the use of carbon bars and a single steel bar, where the brittle properties of carbon led to a reduction in the toughness ratio **(Fallah & Nematzadeh,2022)** and **(Maranan et al., 2019)**. For the other models, notice a variation in the toughness ratios, as illustrated in **Table (4.6)**, where the ratios are

due to variations in the reinforcement ratio and the reinforcing used. **Figures (4.19)** to **(4.22)** show the value of flexural toughness for all specimens.

Table (4.6): Toughness results for the tested specimens.

Group	Specimen designation	Toughness (kN*mm)
Group 1	NS-1	1568.7
	HS-1	2981.14
	NHS-2	3801.67
Group 2	NC-1	1468.7
	HC-1	1403.79
	NHC-2	1813.3
Group 3	NG-1	2077.25
	HG-1	2766.65
	NHG-2	2977.44
Group 4	SSC-2	3504.14
	CCS-2	1611.58
	SSG-2	2891.97
	GGS-2	2664.93
	CCG-2	2325.32
	GGC-2	1858.12

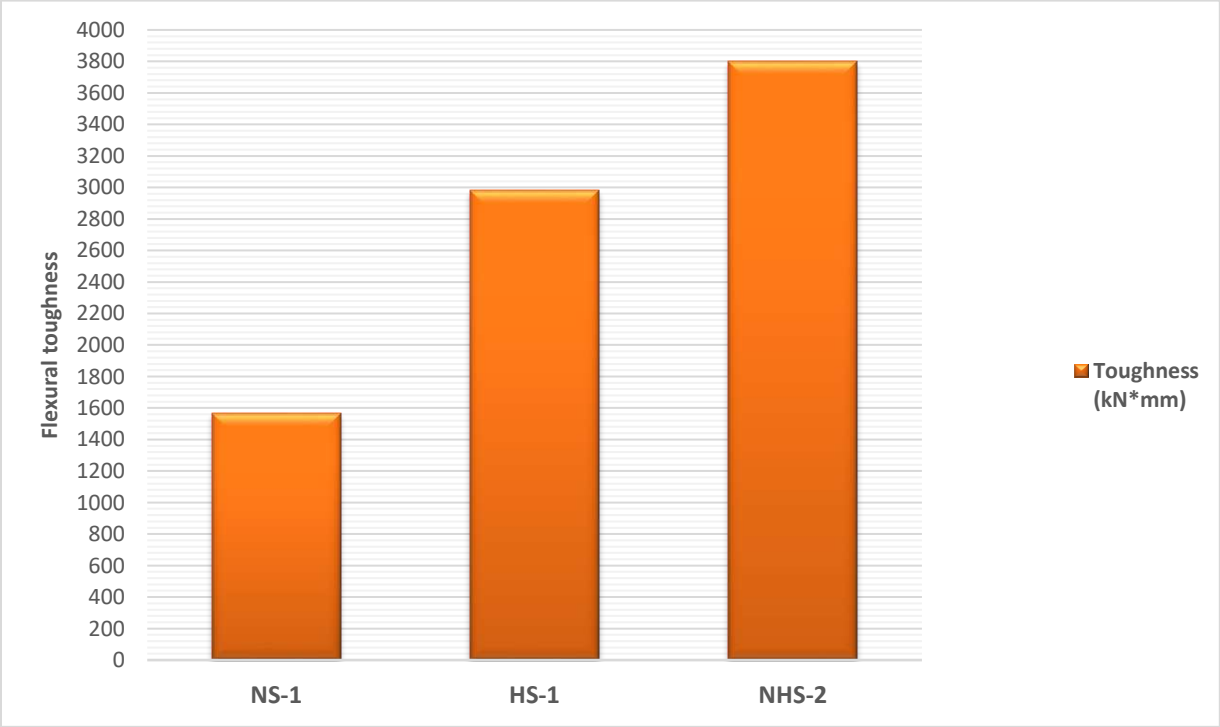

Figure (4.19): The flexural toughness of the specimens (group 1).

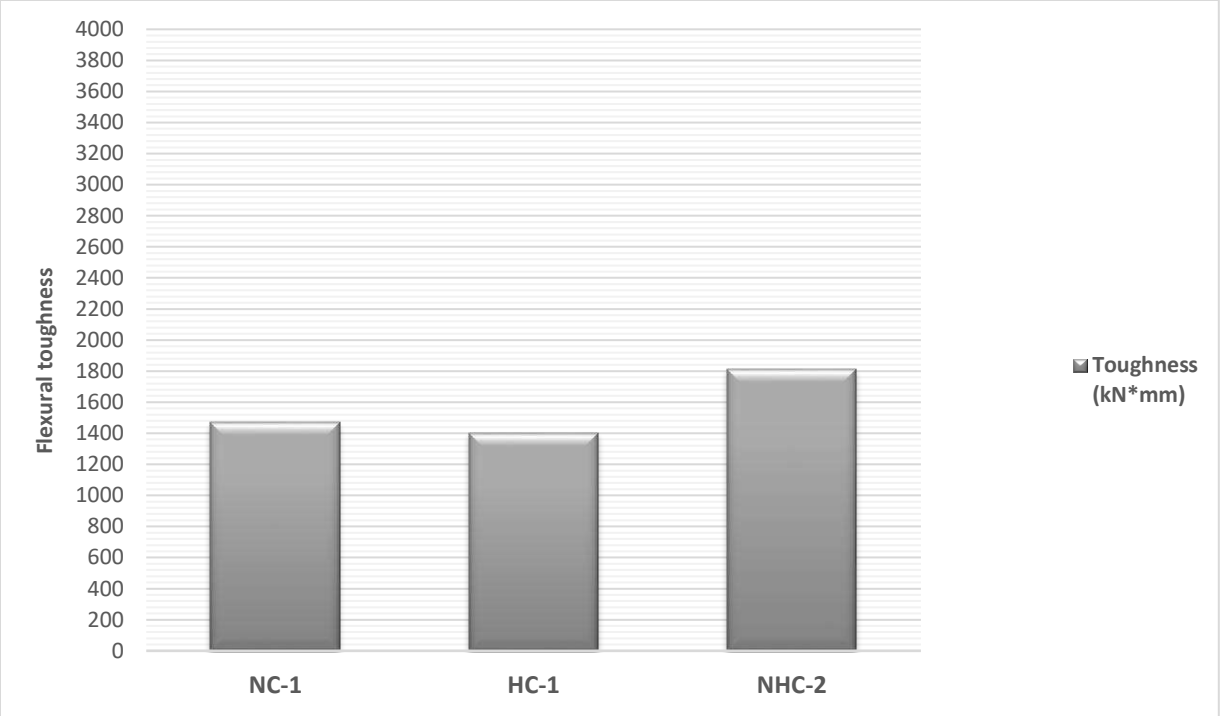

Figure (4.20): The flexural toughness of the specimens (group 2).

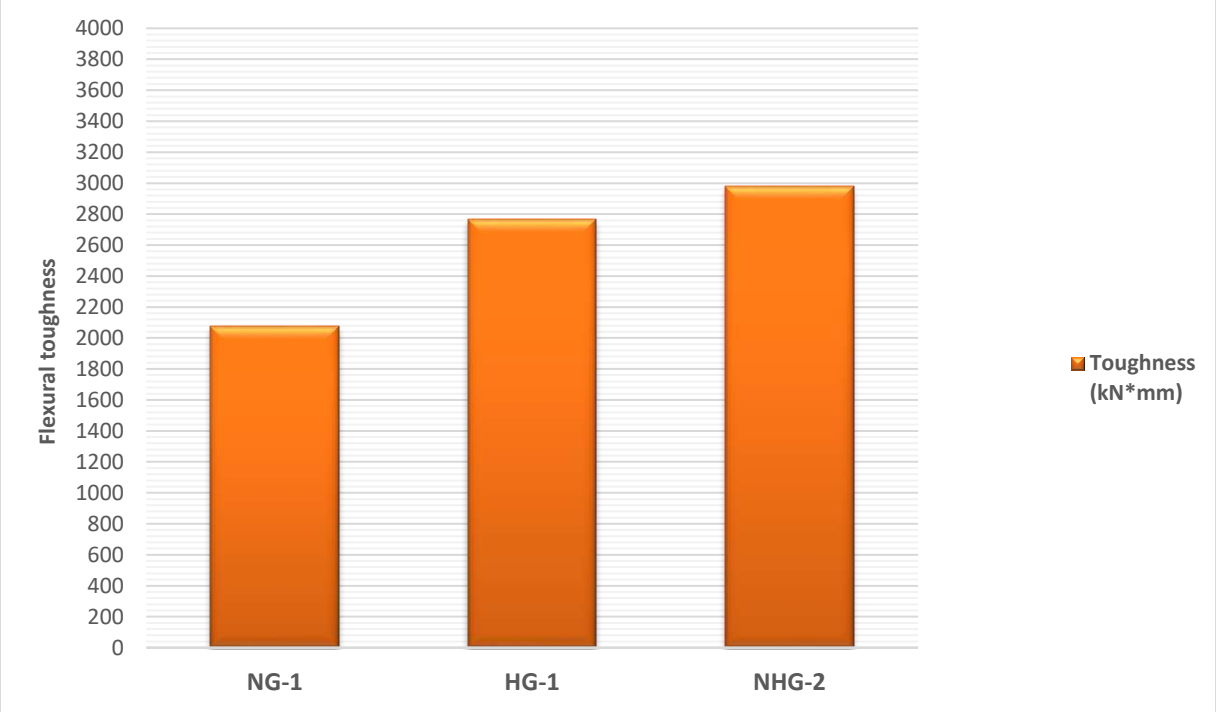

Figure (4.21): The flexural toughness of the specimens (group 3).

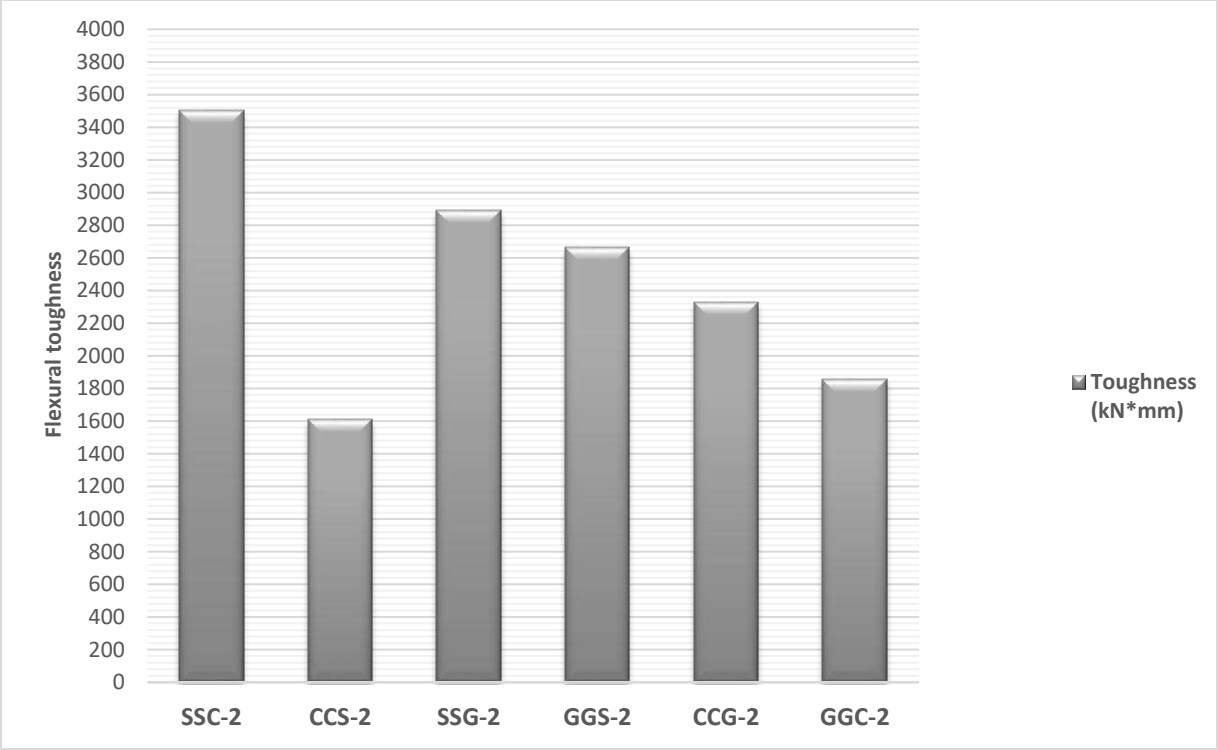

Figure (4.22): The flexural toughness of the specimens (group 4).

4.8 Comparison Between (Normal, High, Bilayer) Concrete Specimens

The research examined the impact of several factors on the behavior of bilayer beam capacity. The subsequent sections will analyze the correlation between these factors and the performance of the bilayer beam.

4.8.1 The effect of normal-strength concrete reinforced with (steel, CFRP, and GFRP) on the curve of load-deflection

Figure (4.23) shows the changes in load value and cracking for models that used a type of (steel, CFRP, and GFRP) reinforcement. The model (NS-1) exhibits the highest ultimate load at a value of (134 kN). Compared to the models reinforced with CFRP and GFRP bars, the percentage increase is (8.21%) and (16.42%), respectively. The reason for achieving a high load capacity in the model cast from normal-strength concrete reinforced with steel is due to steel's superior ductility compared to carbon and glass. This explanation holds when comparing carbon to

glass, as carbon possesses a higher ductility than glass, resulting in greater ultimate load values. Additionally, upon closer examination of **Figure (4.24)**, it is evident that the model (NS-1) has a curve with a steeper angle than the other models, indicating a lower crack value observed in this model. The lowest crack value recorded was (14mm) in the (NS-1) model, which then gradually increased in the models reinforced with carbon and glass at a percentage of (21.43%) and (91.22%) respectively. The load-deflection curve shape is almost similar for these models, with variations in the ultimate load value and the maximum cracking value, as shown in **Figure (4.24)**. This provides a good indicator of the integrity of the laboratory testing process for the samples that were locally poured, as well as the pouring process and the stages of curing and preservation from environmental conditions. In addition to the above, we observe that the principle of equal reinforcement diameters is well applied through the convergence of load values and the shapes of the load-deflection curves. This is a good indicator of the conformity of reinforcement data across all models.

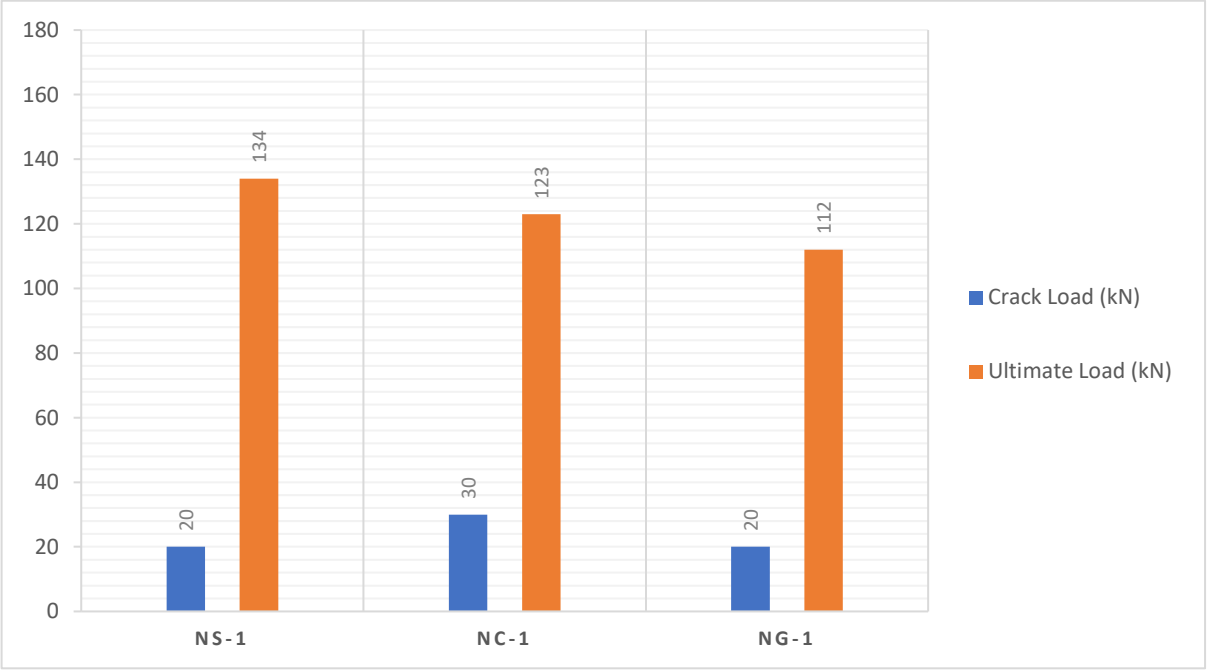

Figure (4.23): Compared load-deflection of the specimens (NS-1, NC-1, and NG-1).

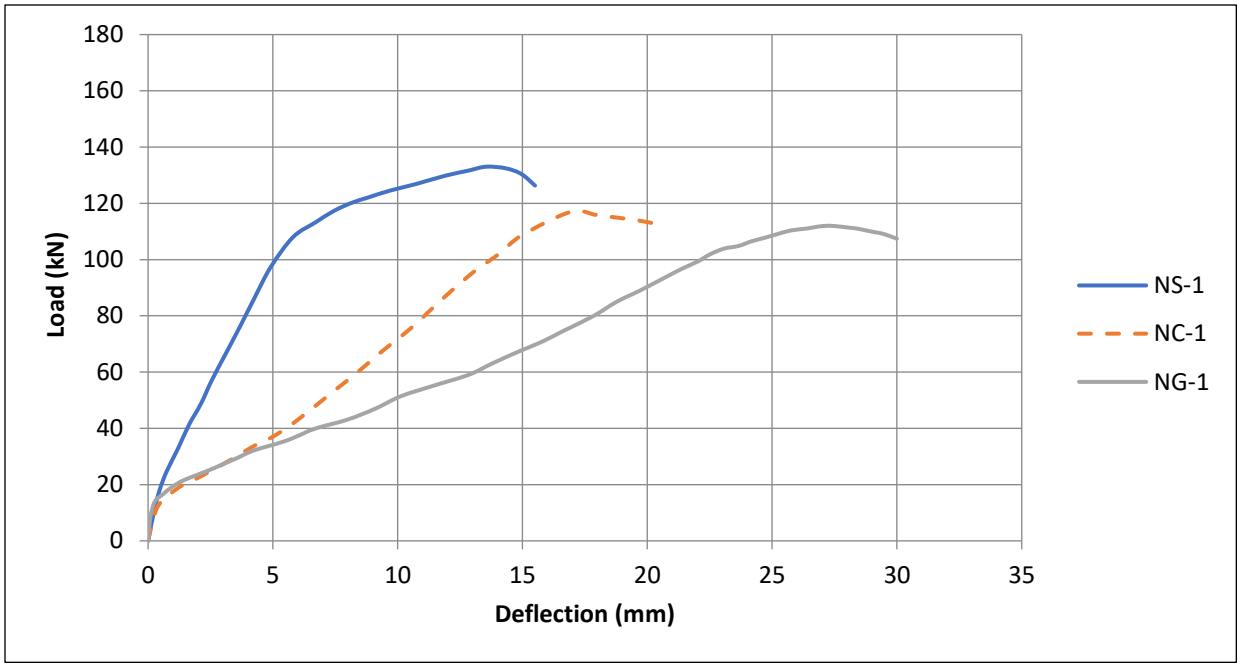

Figure (4.24): Load-deflection curve of specimens (NS-1, NC-1, and NG-1).

4.8.2 The effect of high-strength concrete reinforced with (steel, CFRP, and GFRP) on the curve of load-deflection

Figure (4.25), through the diagrams, there is a notable convergence in the models (HS-1) and (HG-1), which are cast from high strength concrete, with the first model reinforced with steel bars and the second with a glass bar. The convergence ratio is (1.37%). Additionally, from **Figure (4.26)**, it is observed that the similarity in the curves of these two models, as they exhibit very close ductility levels. However, the difference lies in the development and appearance of cracks, where the model reinforced with glass exhibits greater energy, a higher number of cracks, and more flexibility than the other models. These differences arise from the properties and characteristics of the materials used and the nature of the interaction between the glass rods and the concrete. As for the model (HC-1), which is cast from high strength concrete and reinforced with carbon bars, it shows a lower load capacity with a value of (15.07%) than (HS-1, and HG-1) and its load-deflection curve is similar to that of the model reinforced with glass bars, with a lower load and

deflection, as the maximum crack width was (16 mm). It can be concluded that the reinforcement bar equivalence process in all models was highly effective, resulting in significant convergence between the models in terms of failure load and cracking. The degree of variation in cracking is ascribed to the differing chemical and physical qualities of the various bars used in these models.

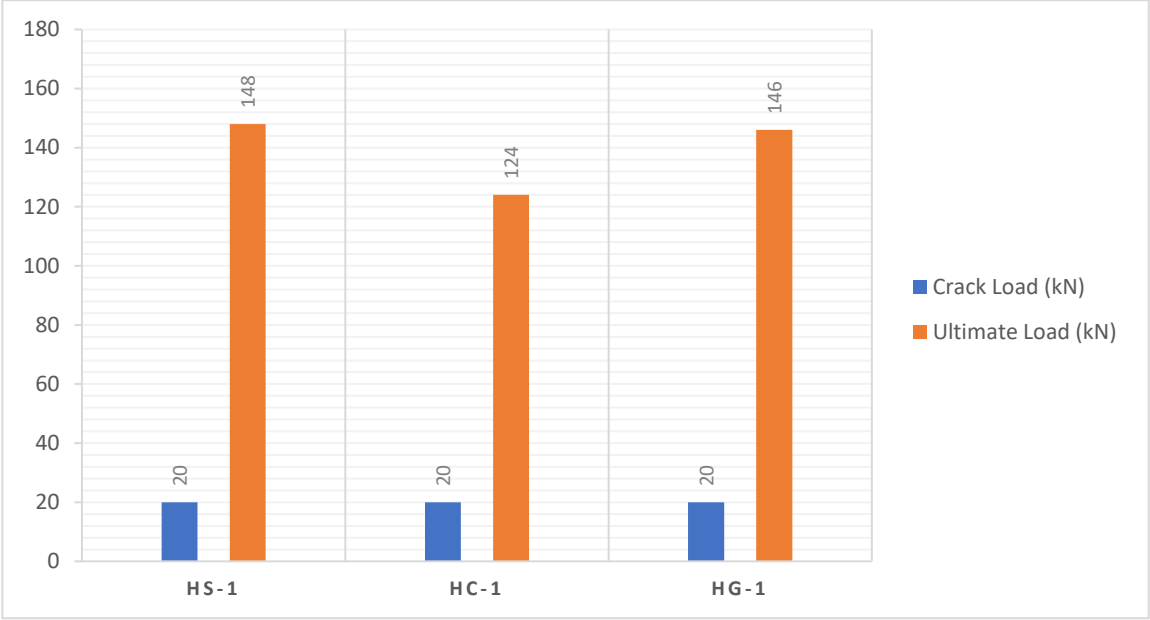

Figure (4.25): Compared load-deflection of the specimens (HS-1, HC-1, and HG-1).

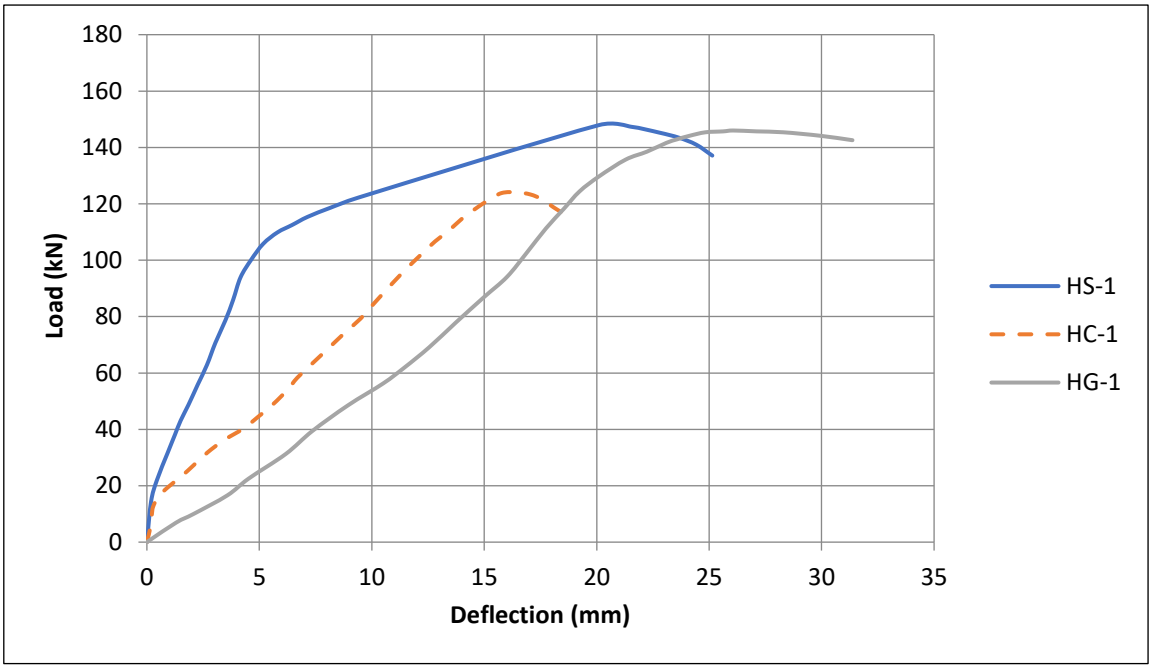

Figure (4.26): Load-deflection curve of specimens (HS-1, HC-1, and HG-1).

4.8.3 The effect of bilayer concrete reinforced with different rebar (steel, CFRP, and GFRP) on the load-deflection curve

Figures (4.27) and (4.28) illustrate the behavior of cast models with a bilayer concrete system (normal strength at the bottom and high strength at the top of the model section), reinforced with different types of rebar: steel for the first model and carbon and glass for the other two models. It is observed that the highest ultimate load is in model (NHS-2), which reached (166 kN), representing an increase of (11.45%) and (27.11%) when compared to the models reinforced with CFRP and GFRP rebar, respectively. This increase is attributed to the ductility property of the steel bars, resulting in a higher ultimate load than the other models. Additionally, there was an equivalence in the use of reinforcement bars, with steel bars of 10 mm diameter, CFRP bars of 6 mm diameter, and GFRP bars of 8 mm diameter, leading to a relative approximation among the models. From this, it concludes that the bilayer system is effective and provides better results and higher load-bearing capacity when used with steel reinforcement bars. Furthermore, the load-deflection curves exhibit a relatively gradual increase with varying climb angles due to the emergence of cracks and the maximum crack extent observed in the model (NHG-2), which reached (29.4mm), showing higher values compared to the steel and carbon models in ratio (11.56%) and (36.73%) when compared with the respective steel and carbon rebar models.

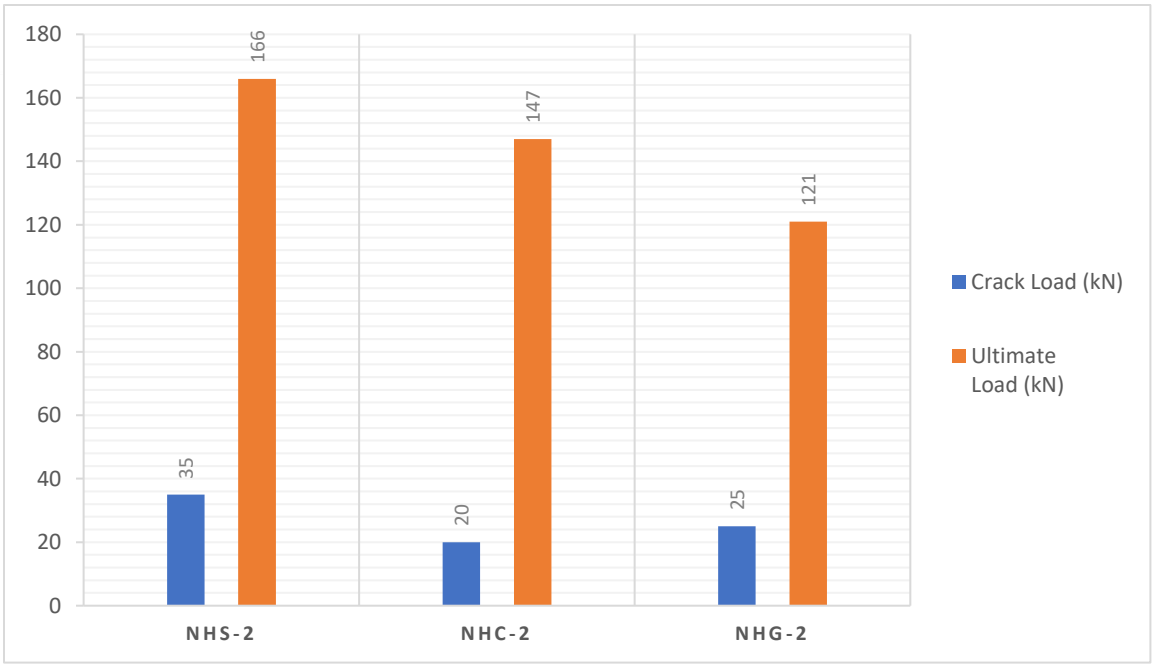

Figures (4.27): Compared load-deflection of the specimens (NHS-2, NHC-2, and NHG-2).

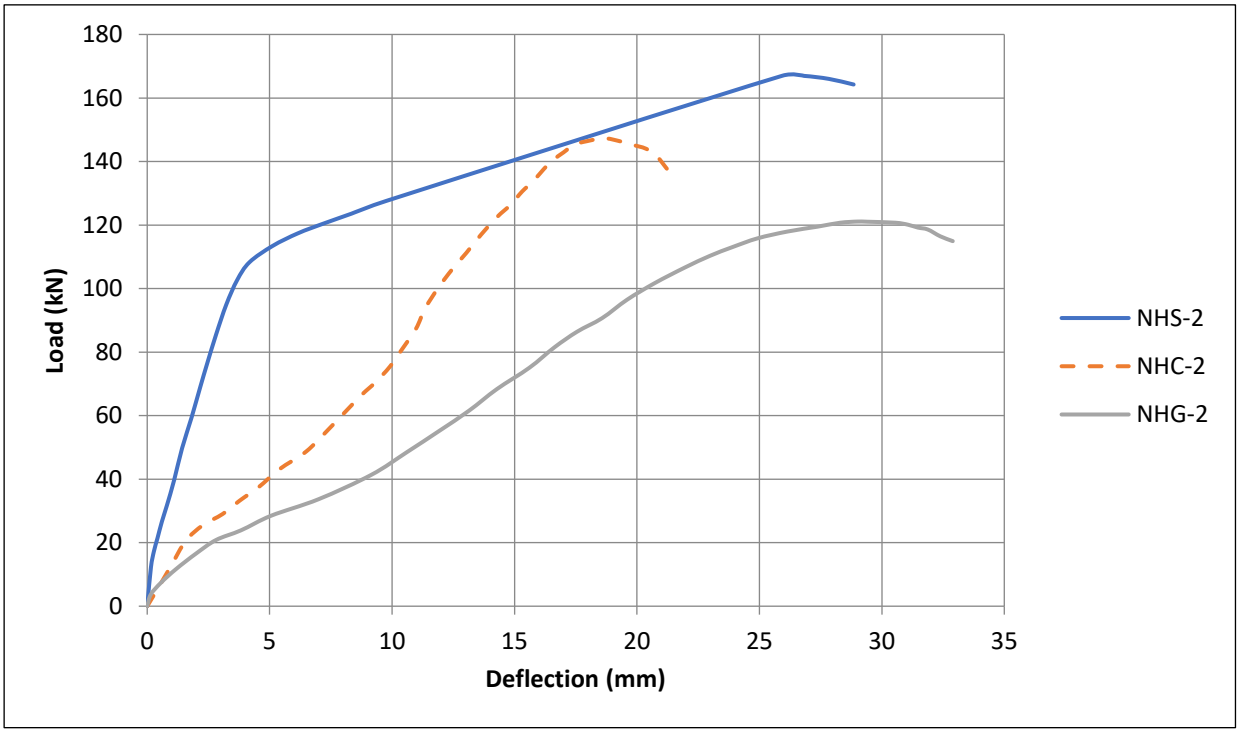

Figures (4.28): Load-deflection curve of specimens (NHS-2, NHC-2, and NHG-2).

4.8.4 The effect of bilayer concrete with different numbers of rebars on the load-deflection curve.

The deflection was measured at mid-span to investigate the influence of the strengthening processes on the stiffness of the tested beams. **Figure (4.29)** displays the load-deflection curves at a middle span of the tested specimens casting bilayer concrete with different rebar relative to deflection. This group comprises six models cast in a bilayer system (the lower layer of normal-strength concrete and the upper layer of high-strength concrete) and reinforced with various reinforcement bars (steel, CFRP, and GFRP). Laboratory testing was conducted by applying a gradual load to the model with a fixed increment, monitoring and recording the occurrence of cracks in real-time after each crack deflection instance in the structural element, and accurately plotting the load-deflection curve. The curve represents the connection between the load on the structure and the deflection, serving as an essential tool for analyzing the performance of materials and structural elements under loads. Initially, the curve was linear, with deflection increasing proportionally to the load. This phase indicates that the material behaves elastically and can return to its original shape after removing the load. Once the yield limit is exceeded, the curve begins to deform non-linearly. The material has surpassed the yield point at this stage, meaning it will retain permanent deformation even after the load is removed. As the load increases significantly, the material reaches the end of fracture or failure, where the curve levels off, leading to the collapse or breakage of the structural element. From **Figure (4.30)**, it can be observed that the highest load capacity was for the model (SSG-2), which consists of two layers of concrete reinforced with two steel bars and one glass bar, achieving a maximum load of (160 kN) and a deflection of (21 mm). In contrast, the model (GGC-2), also made of two layers of concrete but reinforced with two glass bars and one carbon bar, exhibited

the lowest load capacity, estimated at (102 kN) with a max. Deflection of (24.29 mm). It is observed that the elements that used the same type of reinforcement, albeit with varying reinforcement ratios and types of bars, exhibit similar load results compared to all other types. This is a positive indicator of the achievement of the concept of equivalence among the sections used.

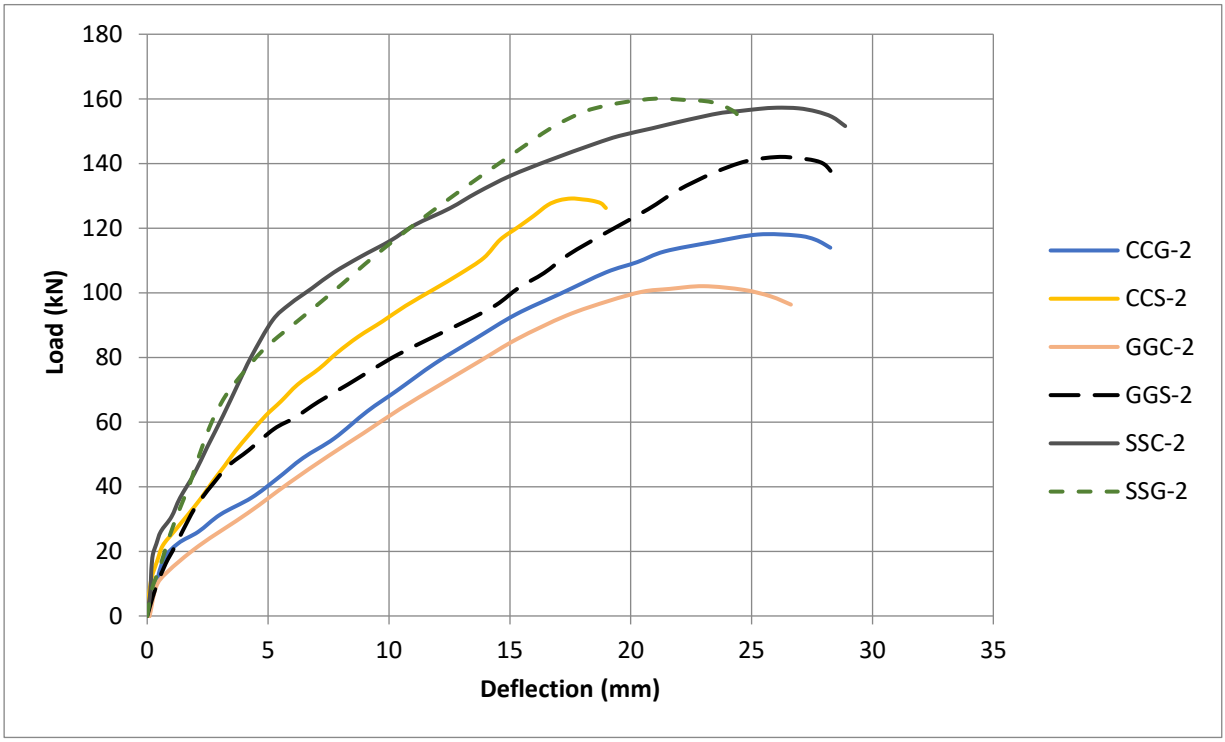

Figures (4.29): Load-deflection curve of bilayer specimens reinforced with different rebar.

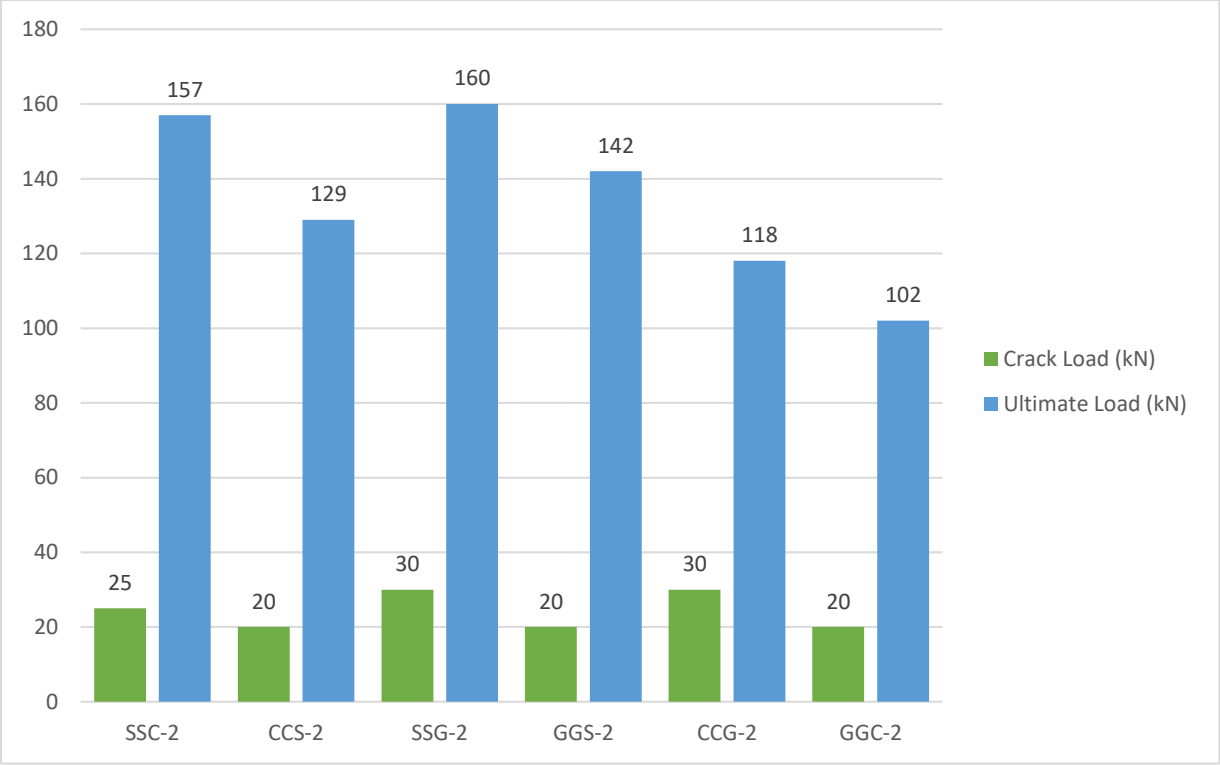

Figures (4.30): Compared load-deflection of bilayer specimens reinforced with different rebar.

Chapter Five: Finite Element Analysis

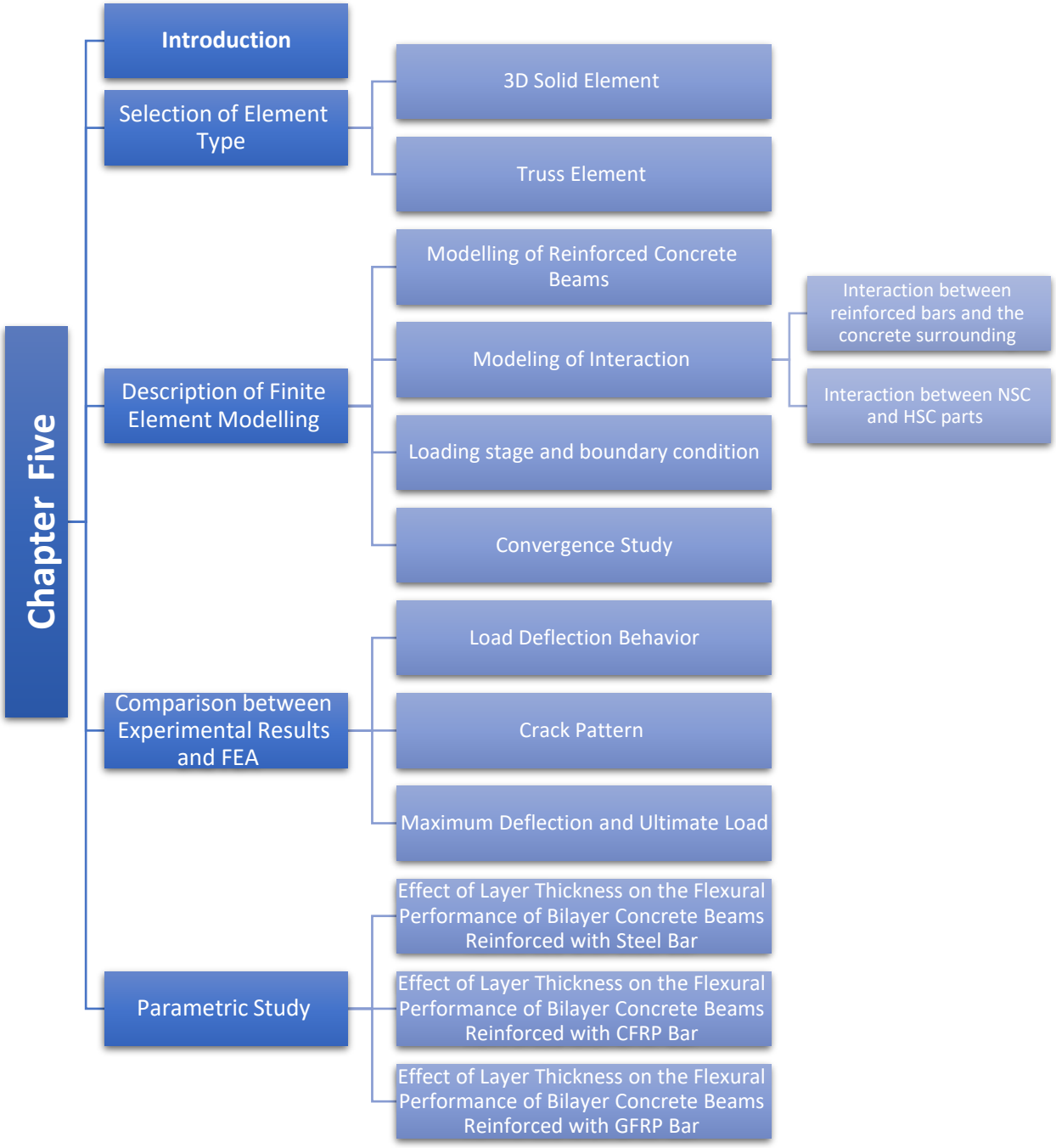

Chapter Five
Finite Element Analysis

5.1. Introduction

This part comprehensively compares the experimental data and the numerical analysis conducted using the finite element method. The study models the flexural performance of bilayer concrete beams reinforced with different types of rebars using ABAQUS/Standard 2017. Due to concrete's intricate composite nature, accurate modeling of its nonlinear behavior is essential for generating reliable simulations. The most direct approach for evaluating structural performance remains experimental testing. Nonetheless, numerical simulations serve as a valuable alternative due to the high costs and time demands of actual experiments. The finite element method provides a dependable tool for analyzing reinforced concrete structures, allowing for the consideration of critical factors such as load distribution, material anisotropy, and crack propagation.

This chapter purposes the expanding the research to include numerous cases that have not had the opportunity to be examined in the laboratory. Additionally, numerical model with experimental data to assess its accuracy. Essential components, such as element selection, material property specifications, and convergence criteria, are meticulously examined to ensure the simulation's accuracy. Furthermore, computer modeling is used to analyze the impact of concrete layers and reinforcement types on structural response. This study enhances our understanding of the flexural behavior of bilayer concrete beams and the comparative advantages of different reinforcement methods.

5.2. Selection of Element Type

This section is a compilation of the factors used to analyze the behavior of segregated reinforced concrete beams.

5.2.1. 3D Solid Element

A three-dimensional solid element is recommended for the concrete component in Finite Element analysis since it more accurately represents the structure's geometry and localized stress distribution. The ABAQUS element package comprises the following elements: 20-node quadratic brick, 10-node quadratic tetrahedron, 15-node quadratic triangular prism, 6-node linear triangular prism, 8-node linear brick, and 10-node quadratic tetrahedron. When using the same mesh density **(Chung and Sotelino, 2006)**. This research employed 8-node linear brick components (C3D8R), as shown in **Figure (5.1)**.

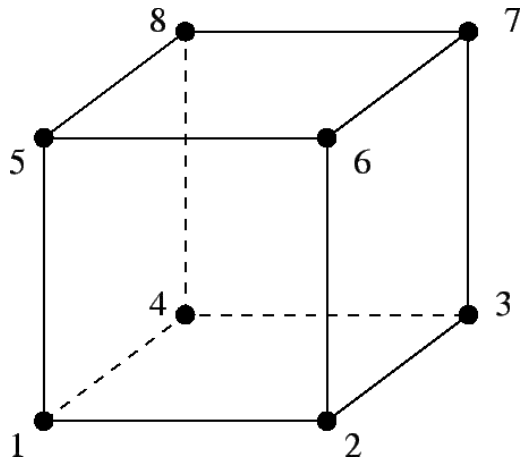

Figure (5.1): Element Type (C3D8R).

5.2.2. Truss Element

A linear, three-dimensional, two-node truss element (T3D2) was used to represent the reinforcing steel bars in the reinforced concrete beams. The T3D2 is present in **Figure (5.2)**.

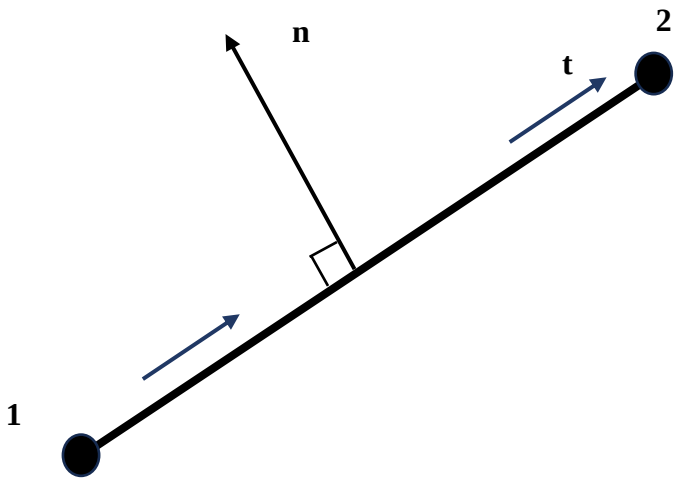

Figure (5.2): Type Element (T3D2).

***Appendix C: Material used in ABAQUS 2017**

5.3. Description of Finite Element Modelling

This section analyzed the geometry of the evaluated beams, boundary conditions, and loads used in the present investigation.

5.3.1. Modelling of Reinforced Concrete Beams

The reinforced concrete beam was modeled using finite element analysis, replicating the real study's geometry, material properties, stresses, and boundary conditions.

The modeling of the fifteen reinforced concrete beams typically had seven components. The components included steel plates used for loading and supports, CFRP bars, GFRP bars, flexural reinforcement (steel bars), shear reinforcement, and two varieties of concrete (normal and high) strength characteristics. The assembly of the specimen model necessitated the separate illustration of each component, as seen in **Figure (5.3**). Upon assembly of the components, embedded region restrictions must be used to connect them when the steel is integrated into the concrete and ensure adhesion between the concrete layers. **Figures (5.4) and (5.5)** illustrate the assembly components of the single and bilayer concrete models.

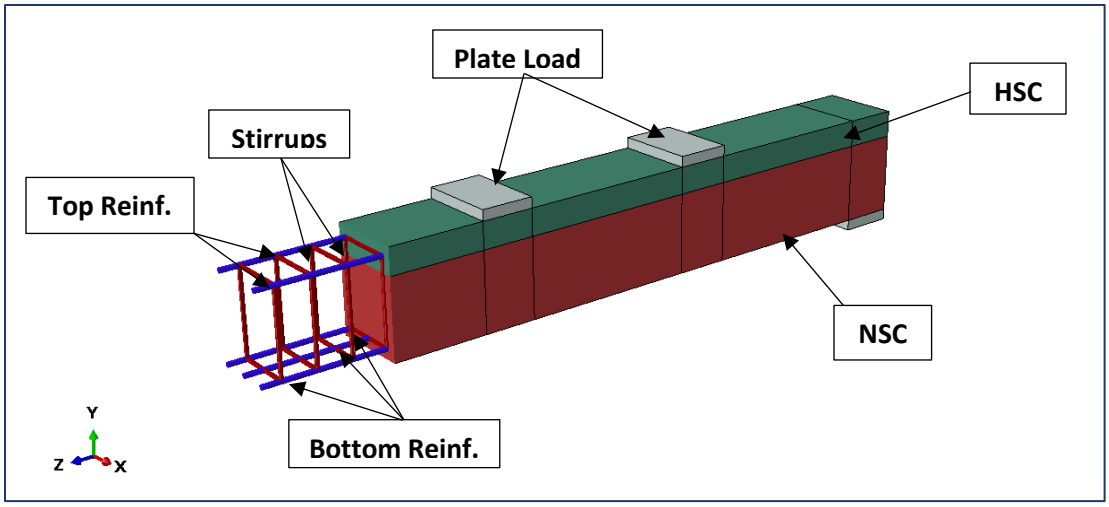

Figure (5.3): Details of the concrete beam.

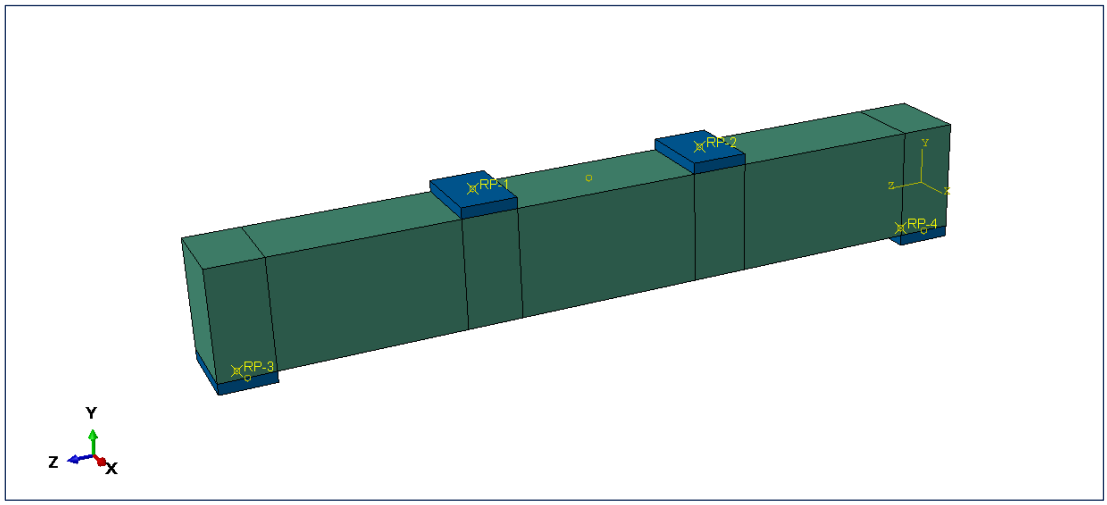

Figure (5.4): Assembly parts of single concrete model.

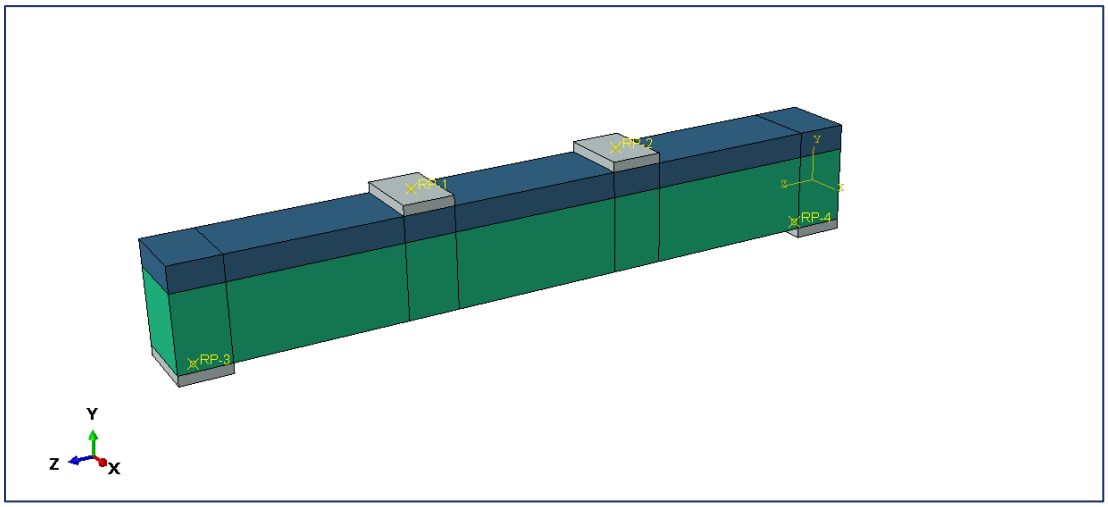

Figure (5.5): Assembly parts of bilayer concrete model.

5.3.2. Modeling of Interaction

ABAQUS offers many methodologies for modeling interactions among model components. These configurations facilitate the model's proximity to accurately reproduce the test's experimental behavior and the beam specimens seen during the experiment.

5.3.2.1. Interaction between reinforced bars and the concrete surrounding

This study used the truss components to characterize the reinforcing bars. As seen in **Figure (5.6)**, they were confined to concrete solid components (the "host" continuum) using an embedded region restriction in ABAQUS. Each reinforcing element node may be accurately linked to the nearest concrete node by embedding. The slip effects of concrete beam reinforcements are excluded from this bonding type; nevertheless, concrete tension softening has partially considered that influence. **(Malm, 2006)**.

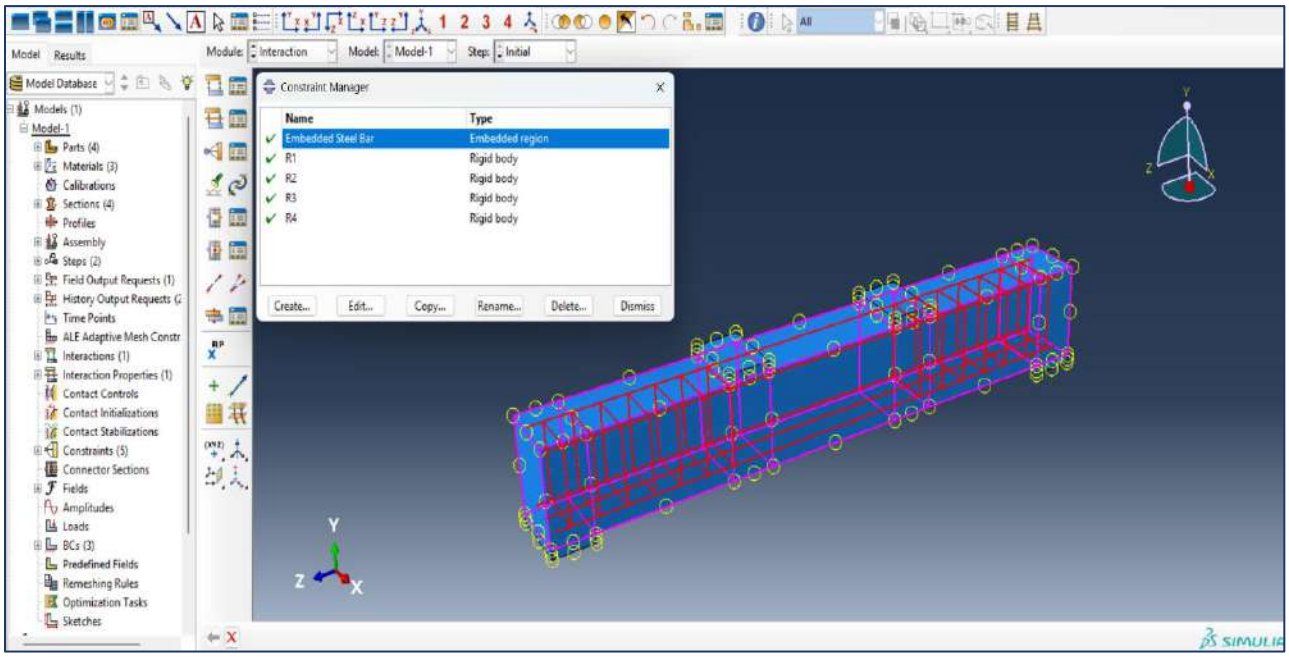

.

Figure (5.6): Interaction between reinforced bars and the concrete surrounding.

5.3.2.2. Interaction between NSC and HSC parts

As experimental studies have shown, the contact form between NSC and HSC is strong enough to prevent isolation, so using the "Tie contact technique" to replicate this state is appropriate. In ABAQUS, this is referred to as full contact restrictions. As shown in **Figure (5.7)**, the master surface and the slave surface must be appropriately defined so that both surfaces make full contact with the neighboring nodes on these surfaces.

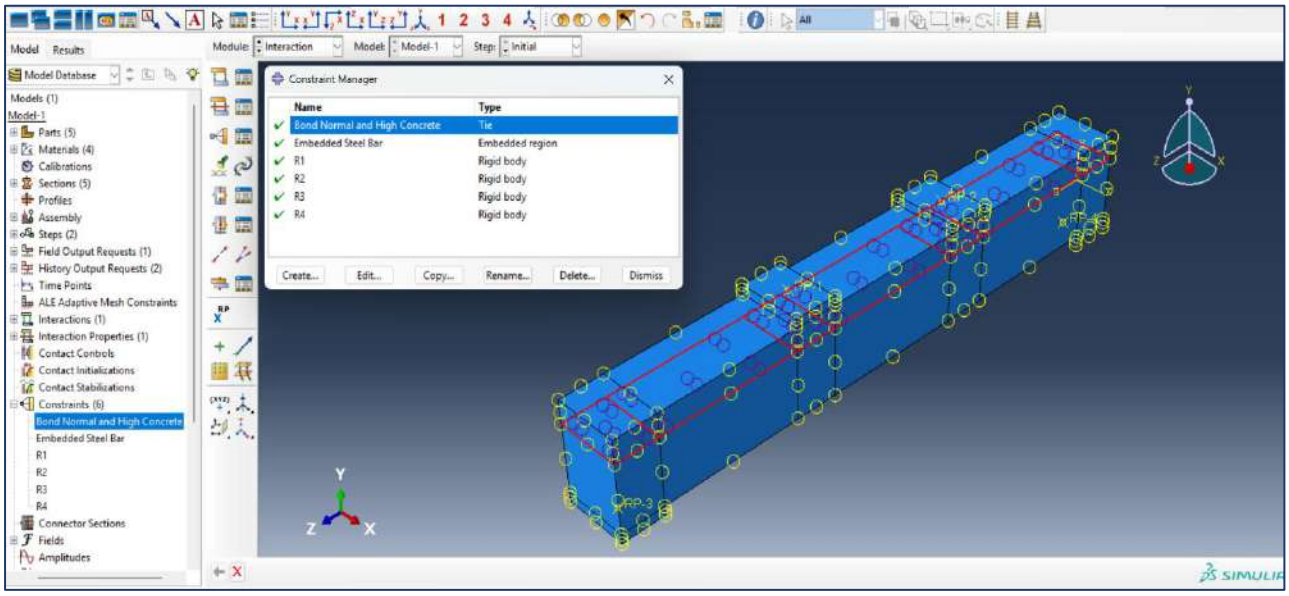

Figure (5.7): Interaction between NSC and HSC parts.

5.3.3. Loading stage and boundary condition

The experimental examination systematically applied loads to each tested beam at two distinct sites. Two-point loads were applied to the specimens throughout the experimental tests. **Figure (5.8)** illustrates that two steel plates, each measuring (100 x 150 x 20 mm), were used to transfer the loads to the beam.

The most precise findings were achieved by implementing a boundary condition displacement across all reinforced concrete specimen models. Constrained models at the hinge support (Uz=Uy=Ux=0) are shown in **Figure (5.9)**

Also, models with constraints on the roller support are used (Uy=Ux=0).

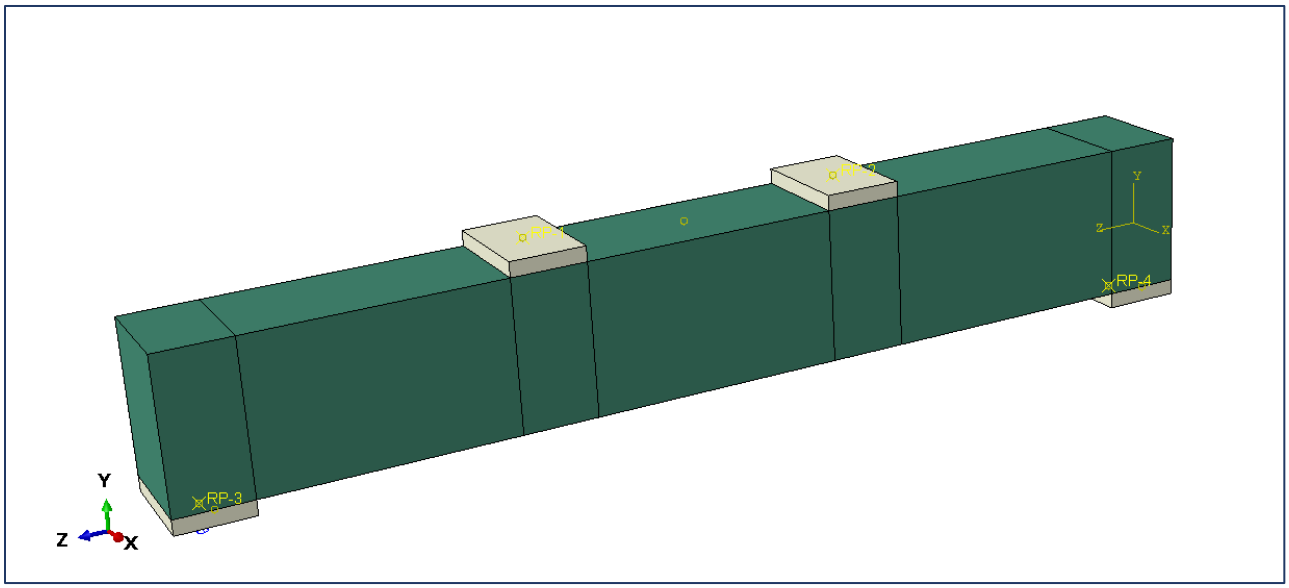

Figure (5.8): Applied load on steel plates.

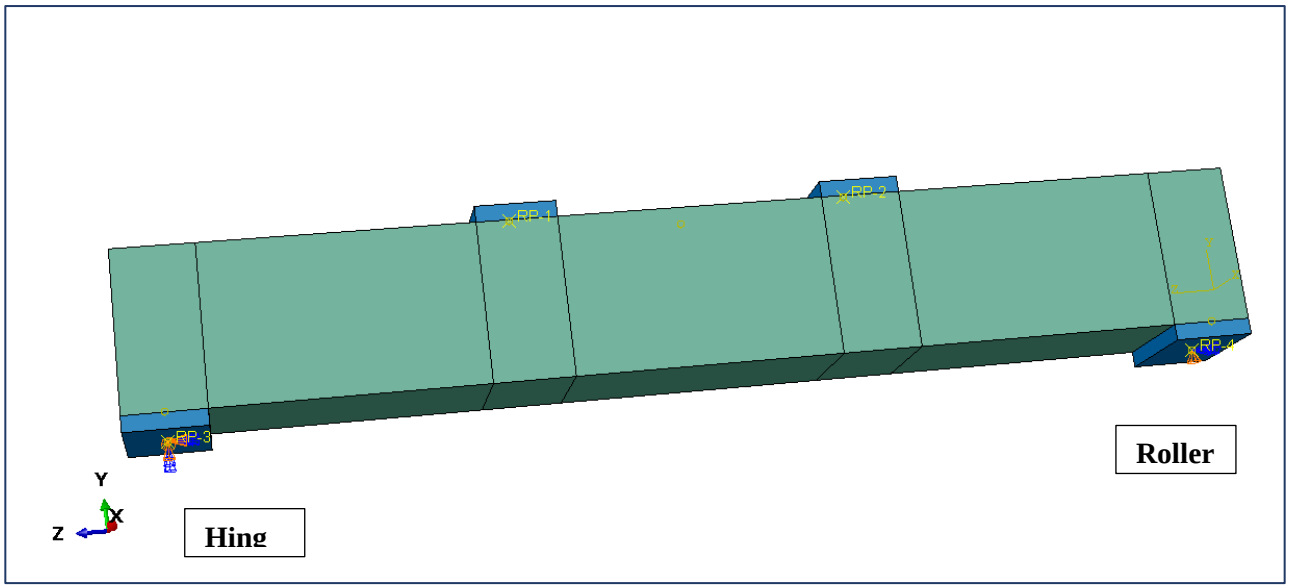

Figure (5.9): Roller and hing supports (Boundary conditions).

5.3.4. Convergence Study

Four mesh sizes that yielded the closest convergence were used to (NS-1) specimen to determine the optimal mesh size. **Figure (5.10)** illustrates a convergence analysis to determine the optimal element sizes of 30, 25, 20, and 15

mm for the control beam mesh. The alteration in load may be ignored when decreased the mesh size is from 25 to 15. The 20 mm mesh size yields more precise results, as seen in Table (5.1). The mesh dimension of all the beams was 20 mm for this purpose. The mesh density for finite element analysis is shown in **Figure (5.11).**

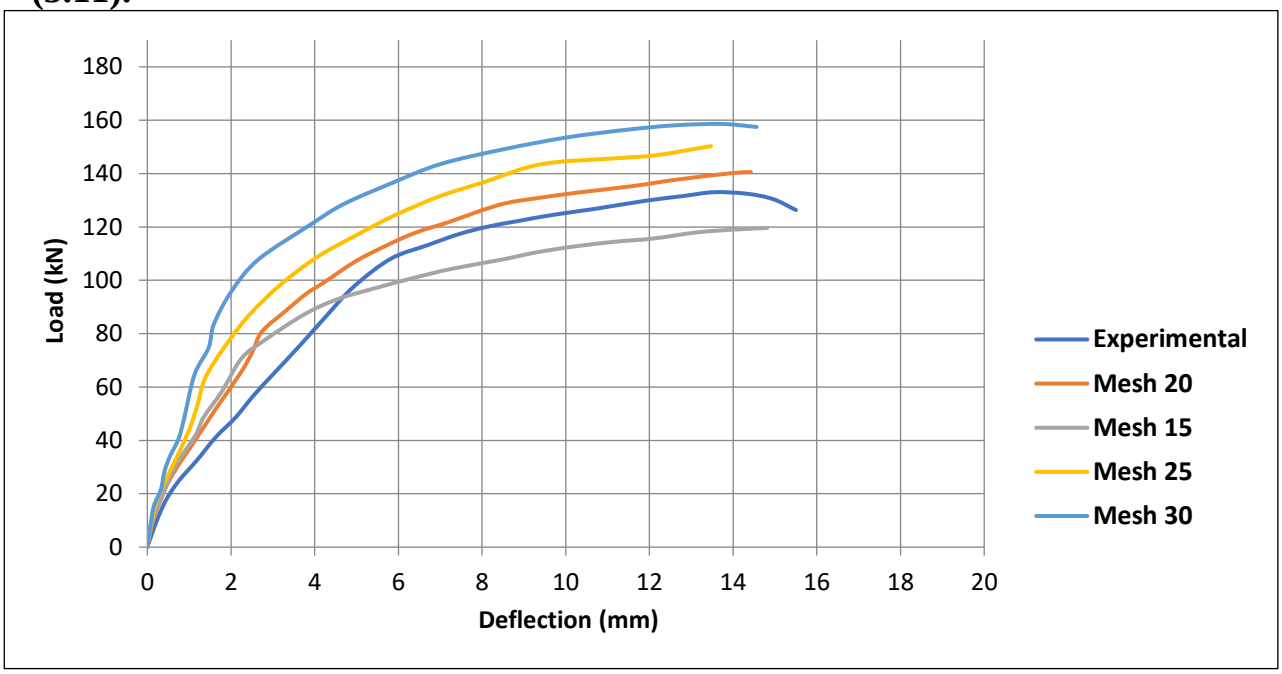

Figure (5.10): The Effect of Mesh Size on the Deflection of the Mid Span Load Curve.

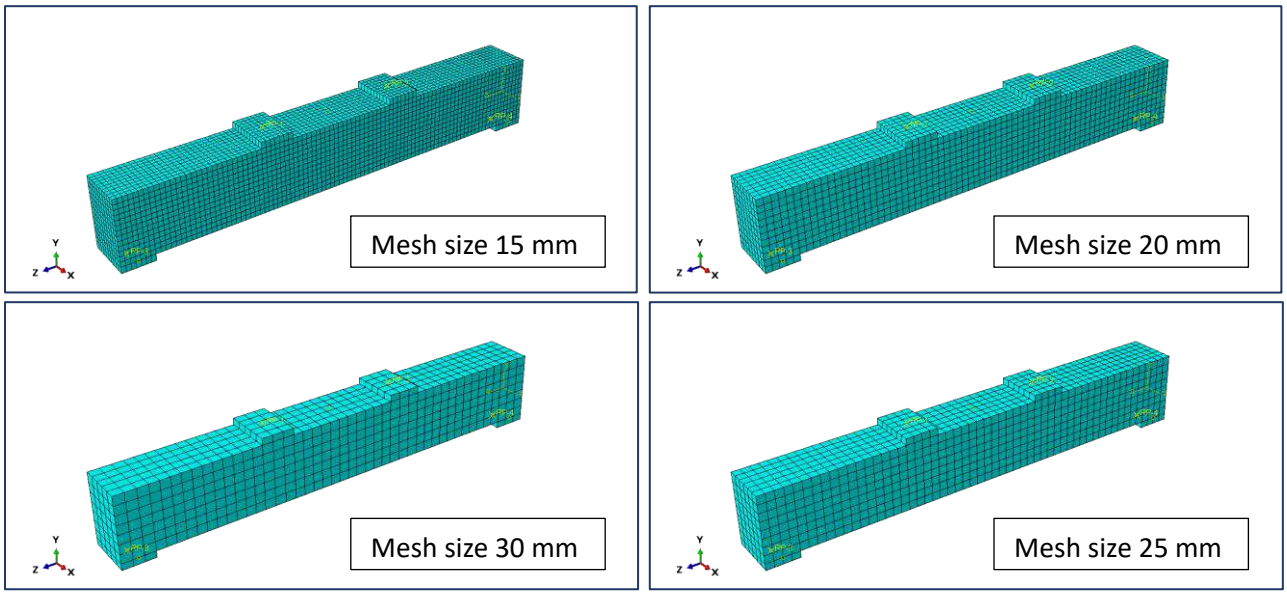

Figure (5.11): Finite Element Mesh Sizes.

Table (5.1): The Changing Mesh Sizes Outcome.

Element size		Ultimate load (kN)	Maximum deflection (mm)
15	Exp	134	14
	FEA	119	14.8
20	Exp	134	14
	FEA	140	14.39
25	Exp	134	14
	FEA	153	15.03
30	Exp	134	14
	FEA	157.49	15.96

5.4. Comparison between Experimental Results and FEA

This section analyses the relationship between experimental results and finite element analysis (FEA) outcomes. The comparison emphasizes essential aspects like ultimate load capacity, peak deflection, failure crack patterns, and the load-deflection relationship. Analyzing these parameters evaluates the correctness of the finite element model in simulating structural behavior, confirming its efficacy in performance prediction.

5.4.1. Load Deflection Behavior

Figures (5.12) to (5.26) compare the load-deflection curves derived from numerical simulations with experimental data. Deflection measurements were documented at the center of the span of all specimens evaluated in the laboratory investigation. The results demonstrate a robust association between the numerical predictions produced by the ABAQUS program and the experimental outcomes. The results are detailed in Chapter 4 and demonstrate the reliability of the

numerical analysis. **Appendix C: Stresses distribution of the specimens in ABAQUS**.

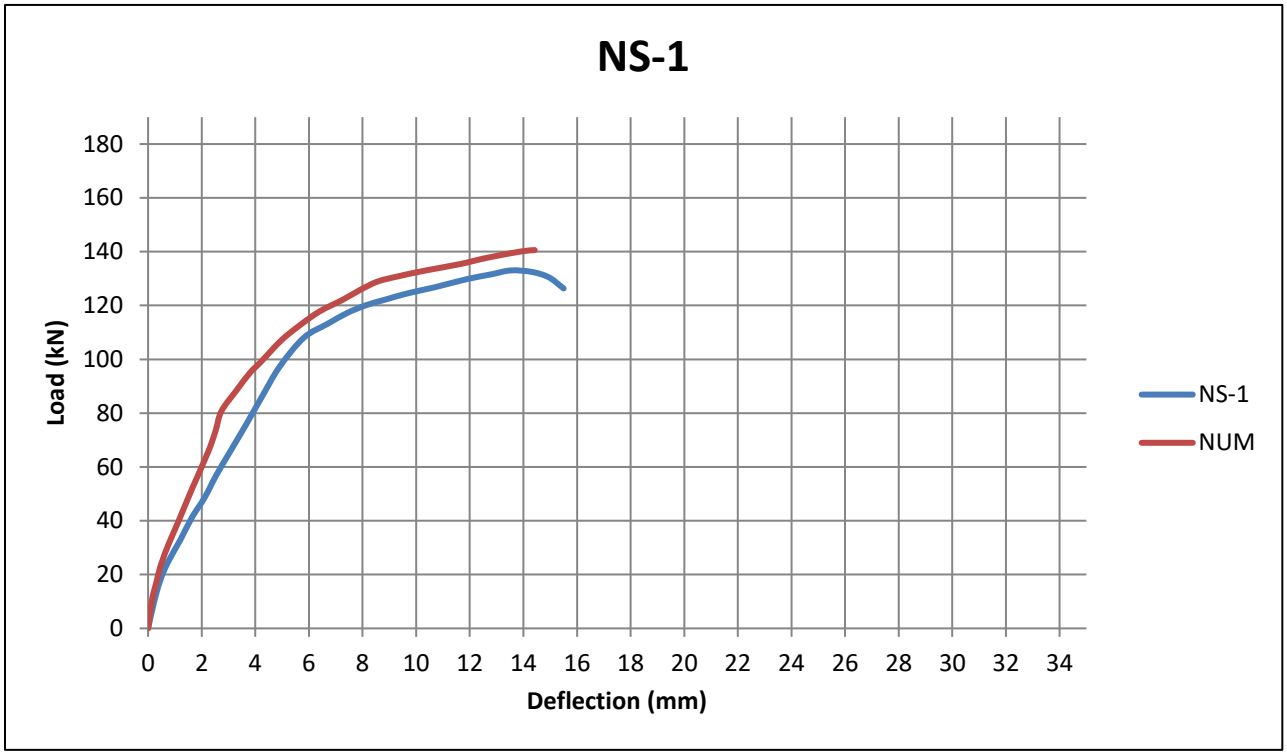

Figure (5.12): Numerical and experimental load-deflection curves for (NS-1) model.

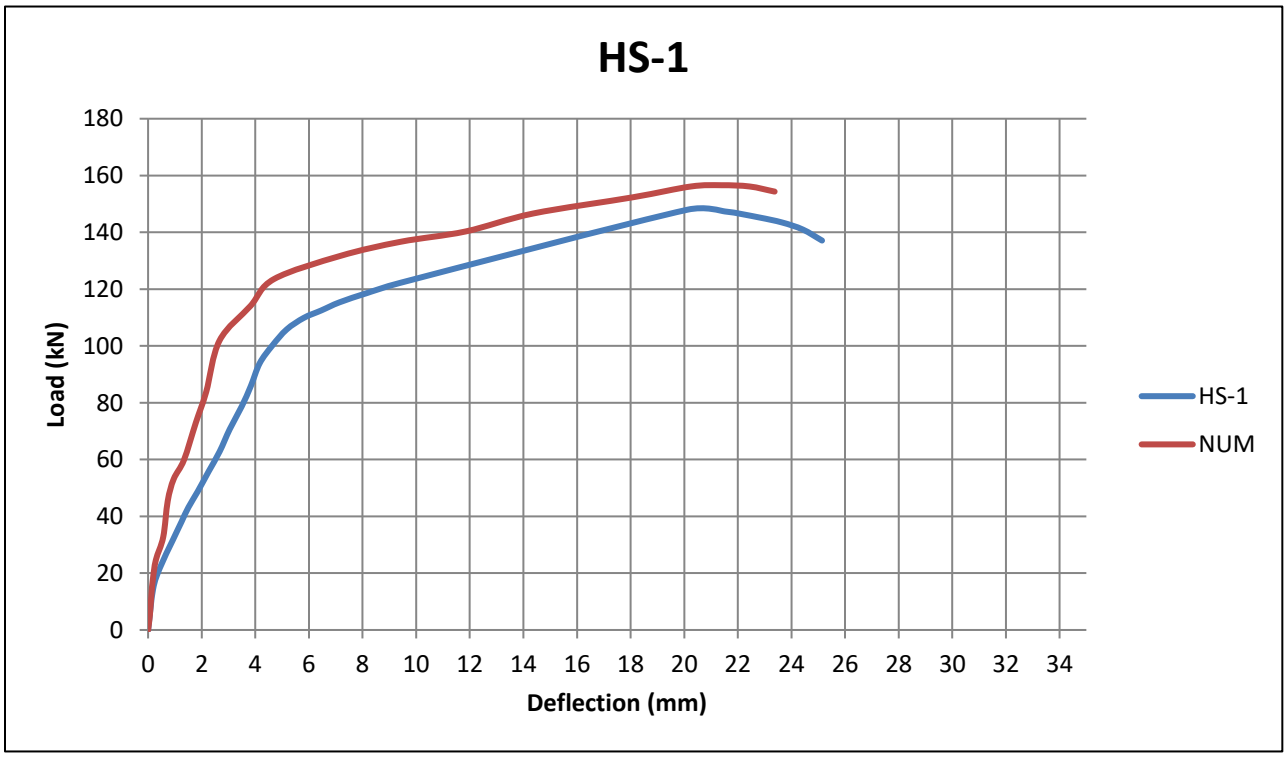

Figure (5.13): Numerical and experimental load-deflection curves for (HS-1) model.

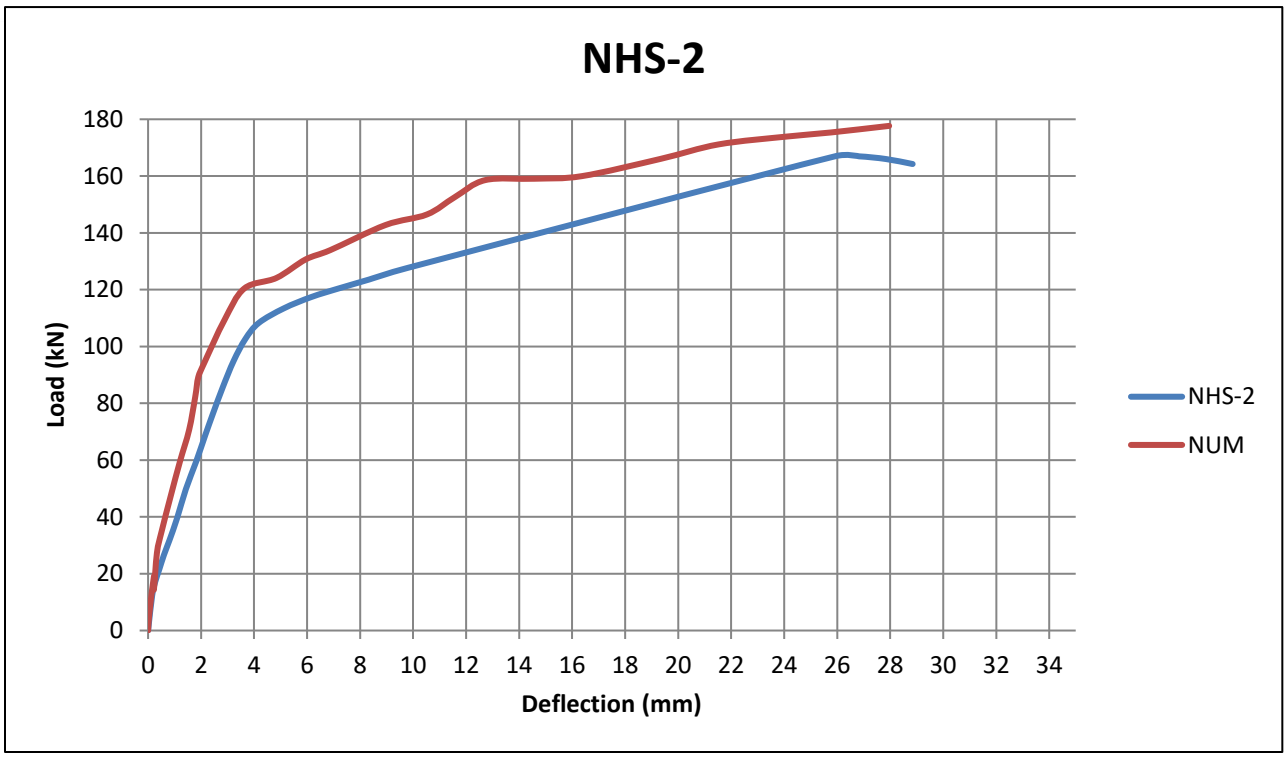

Figure (5.14): Numerical and experimental load-deflection curves for (NHS-2) model.

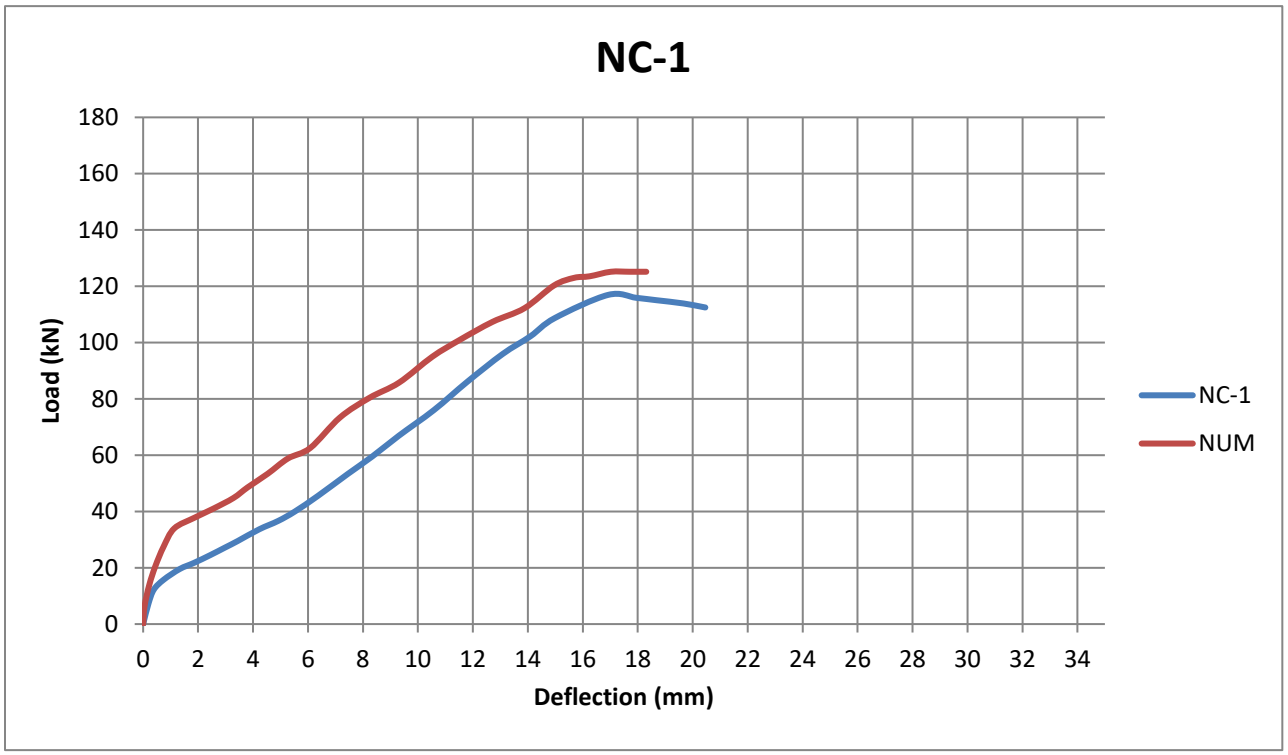

Figure (5.15): Numerical and experimental load-deflection curves for (NC-1) model.

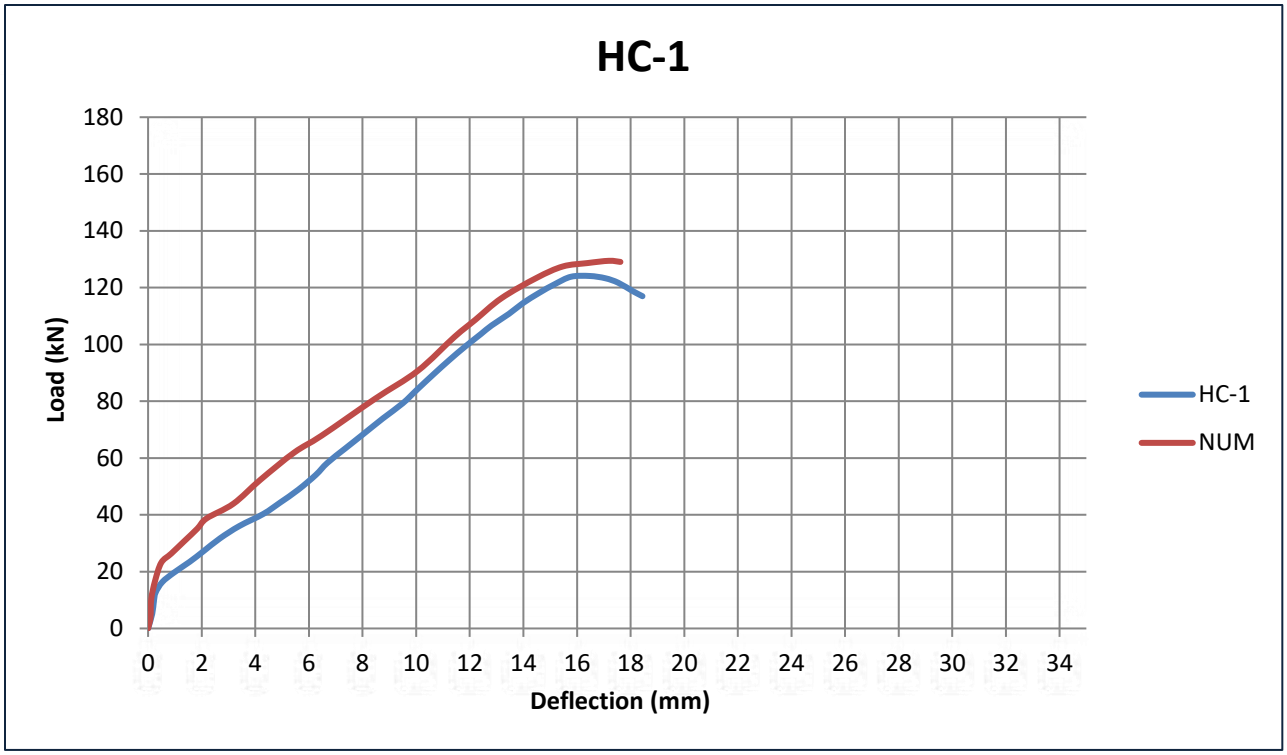

Figure (5.16): Numerical and experimental load-deflection curves for (HC-1) model.

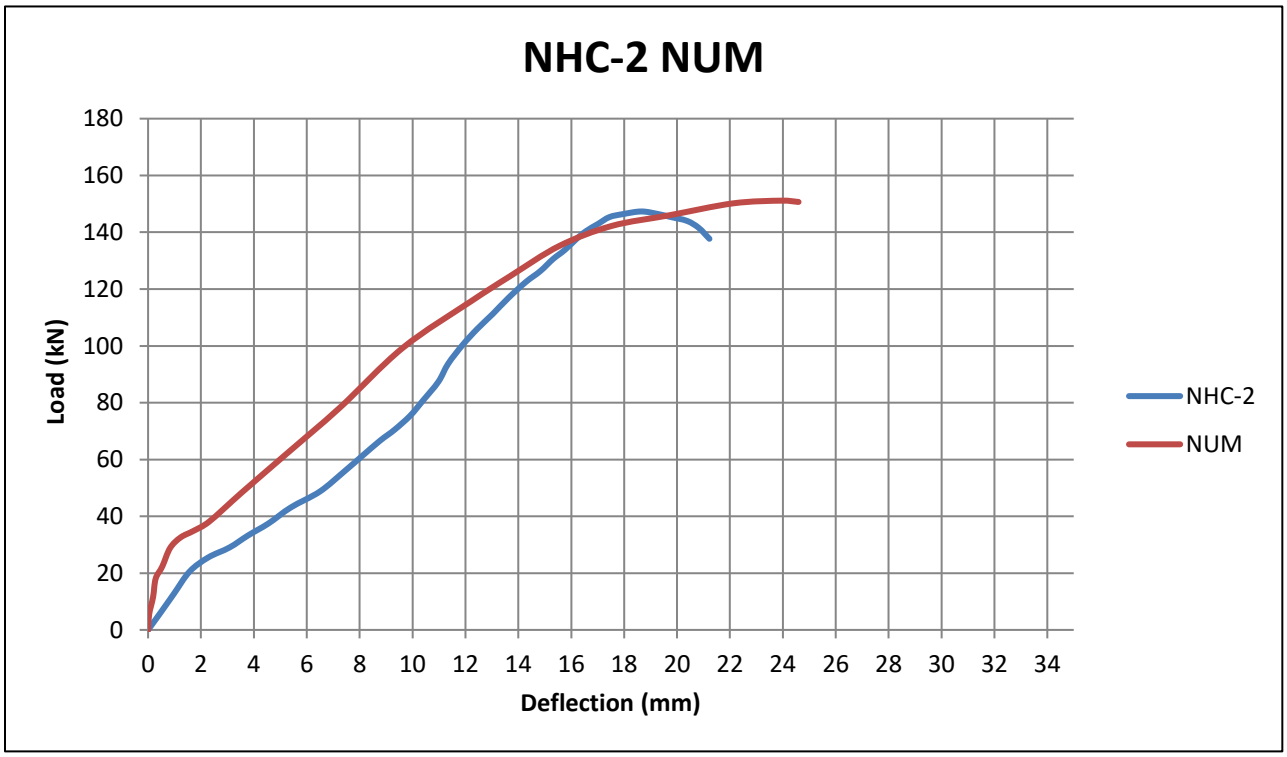

Figure (5.17): Numerical and experimental load-deflection curves for (NHC-2) model.

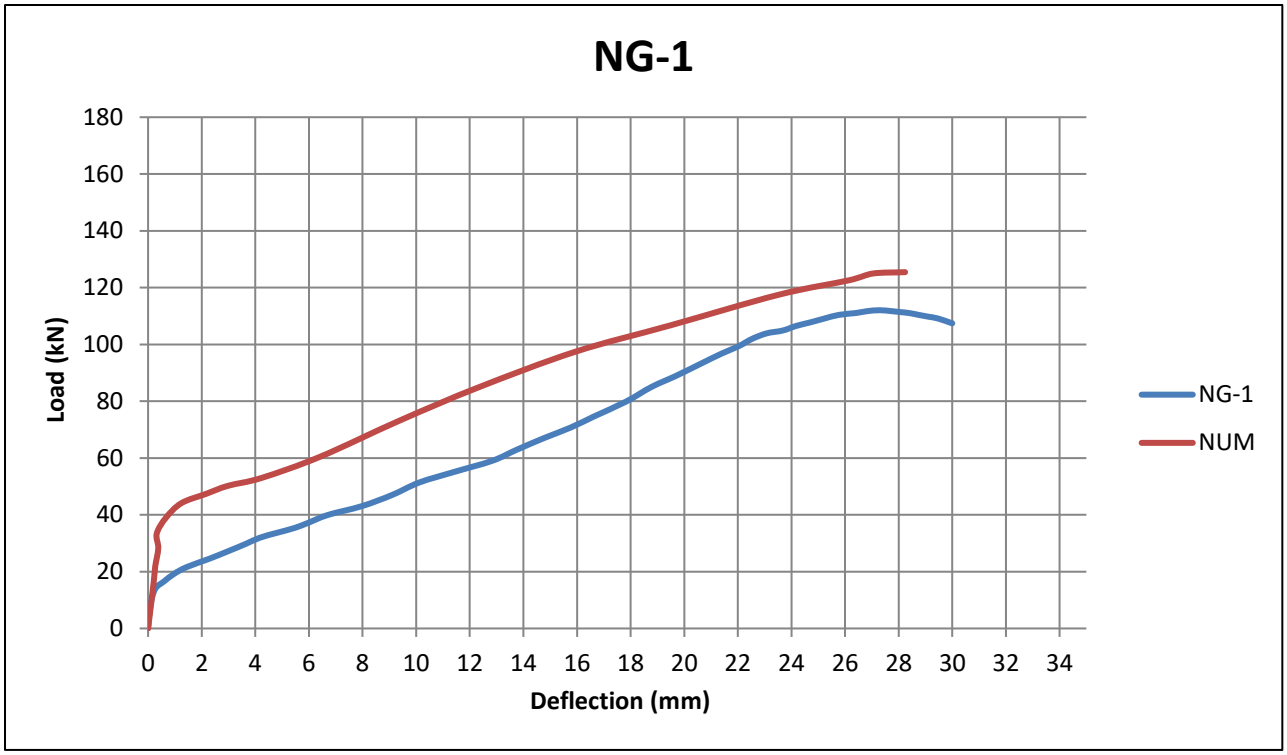

Figure (5.18): Numerical and experimental load-deflection curves for (NG-1) model.

Figure (5.19): Numerical and experimental load-deflection curves for the (HG-1) model

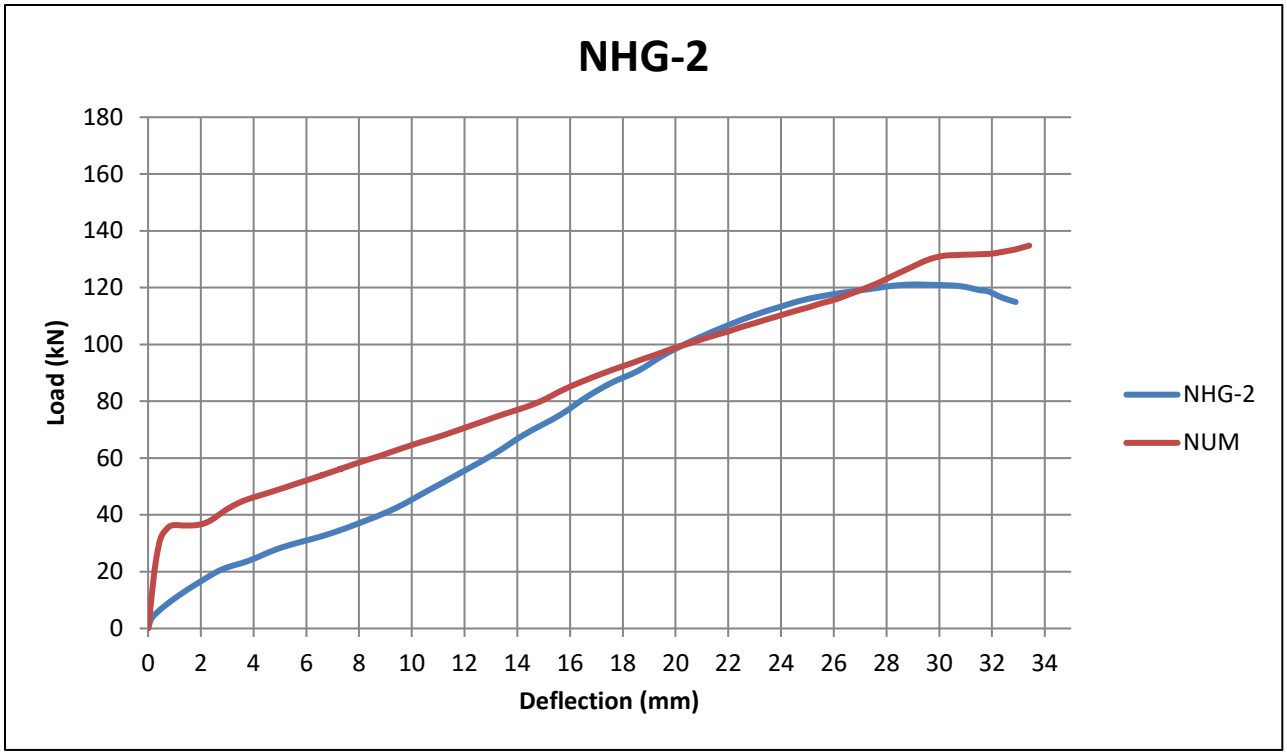

Figure (5.20): Numerical and experimental load-deflection curves for (NHG-2) model

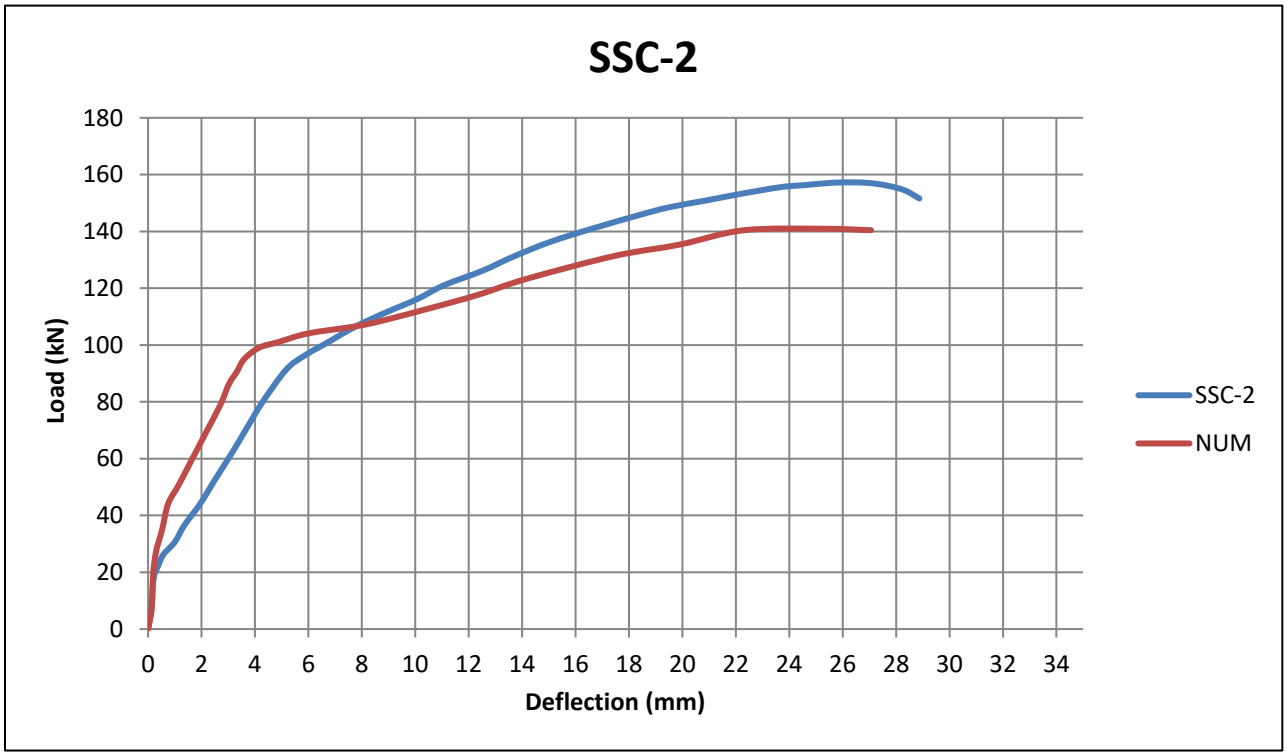

Figure (5.21): Numerical and experimental load-deflection curves for (SSC-2) model.

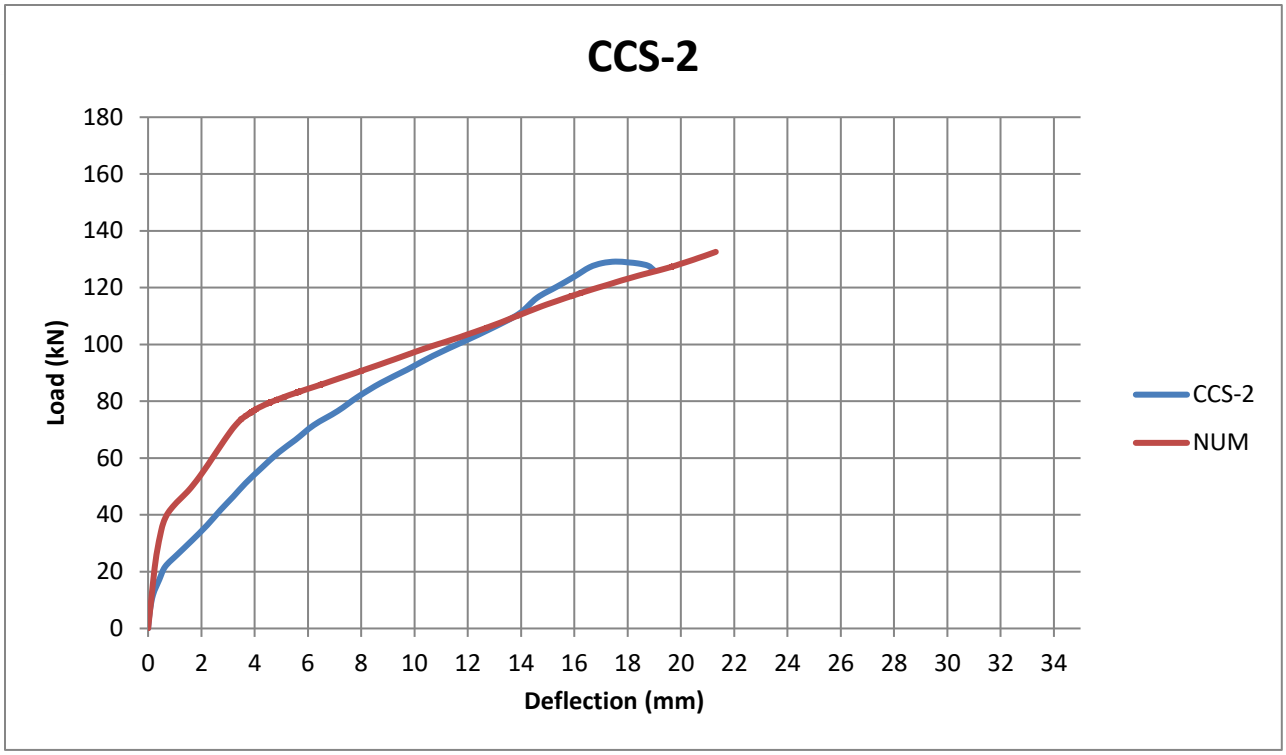

Figure (5.22): Numerical and experimental load-deflection curves for (CCS-2) model.

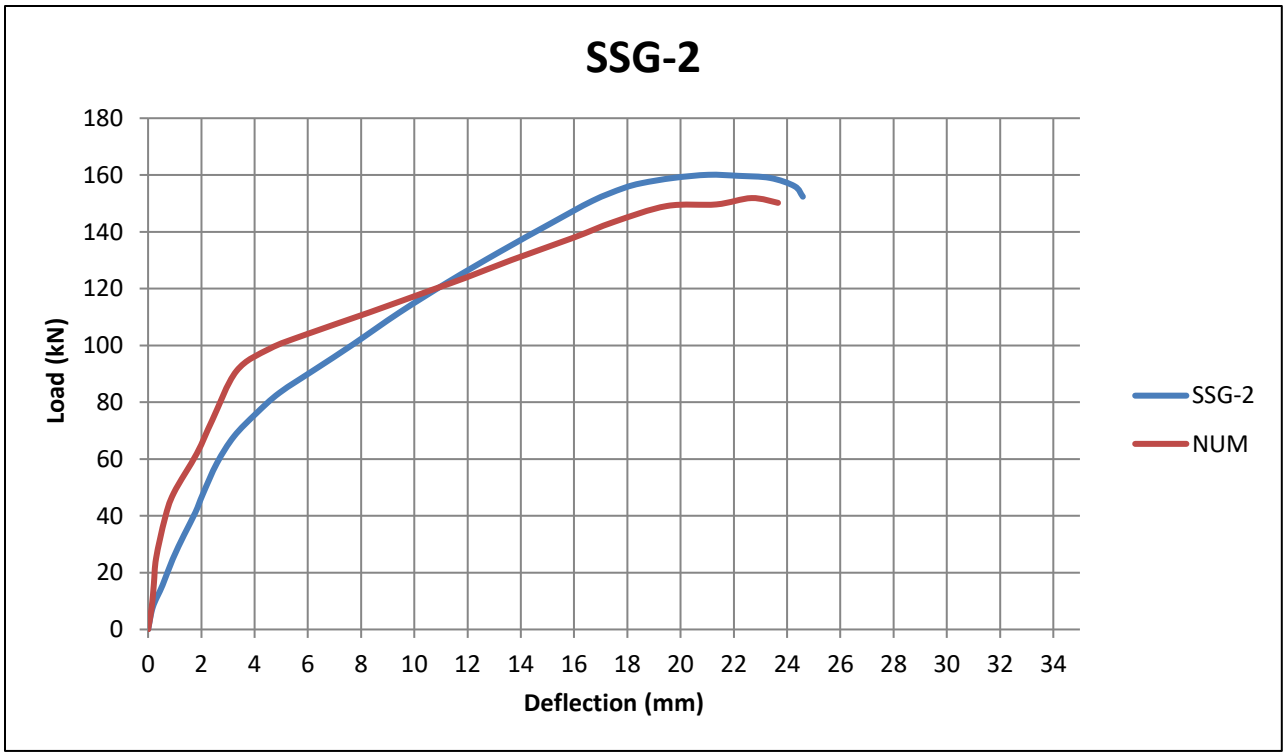

Figure (5.23): Numerical and experimental load-deflection curves for (SSG-2) model.

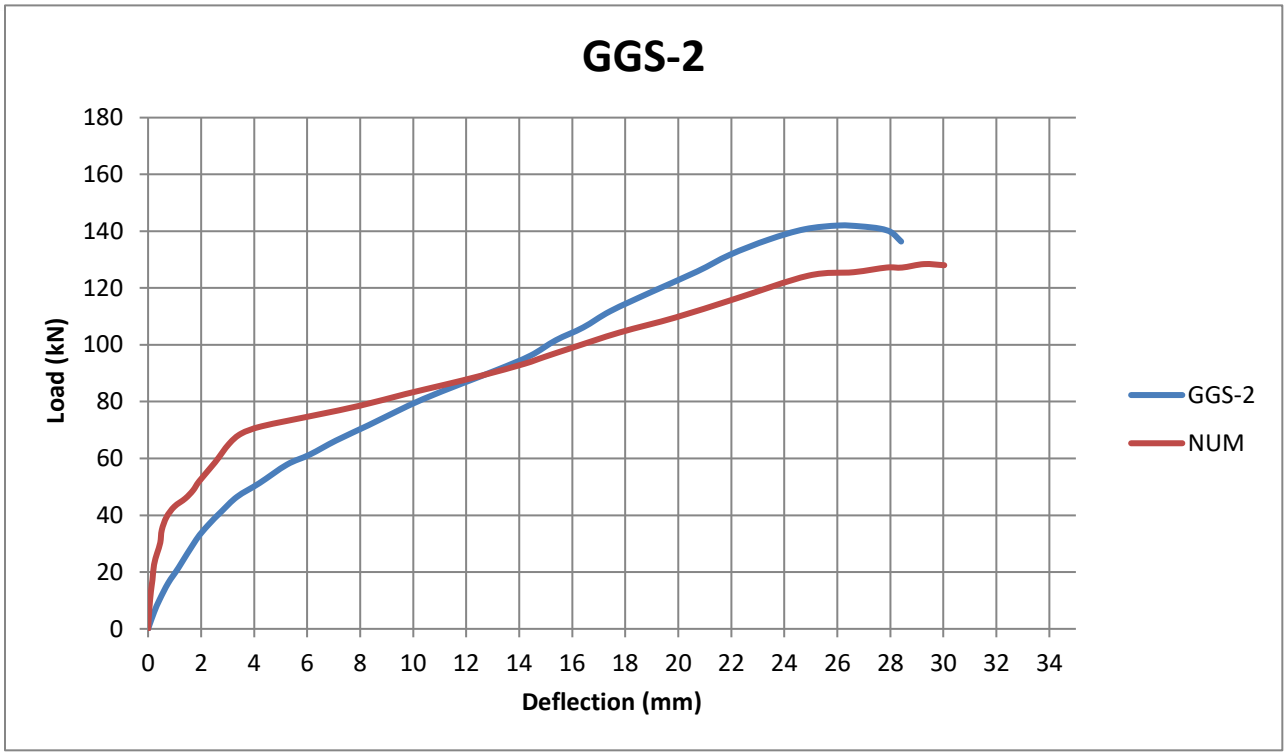

Figure (5.24): Numerical and experimental load-deflection curves for (GGS-2) model.

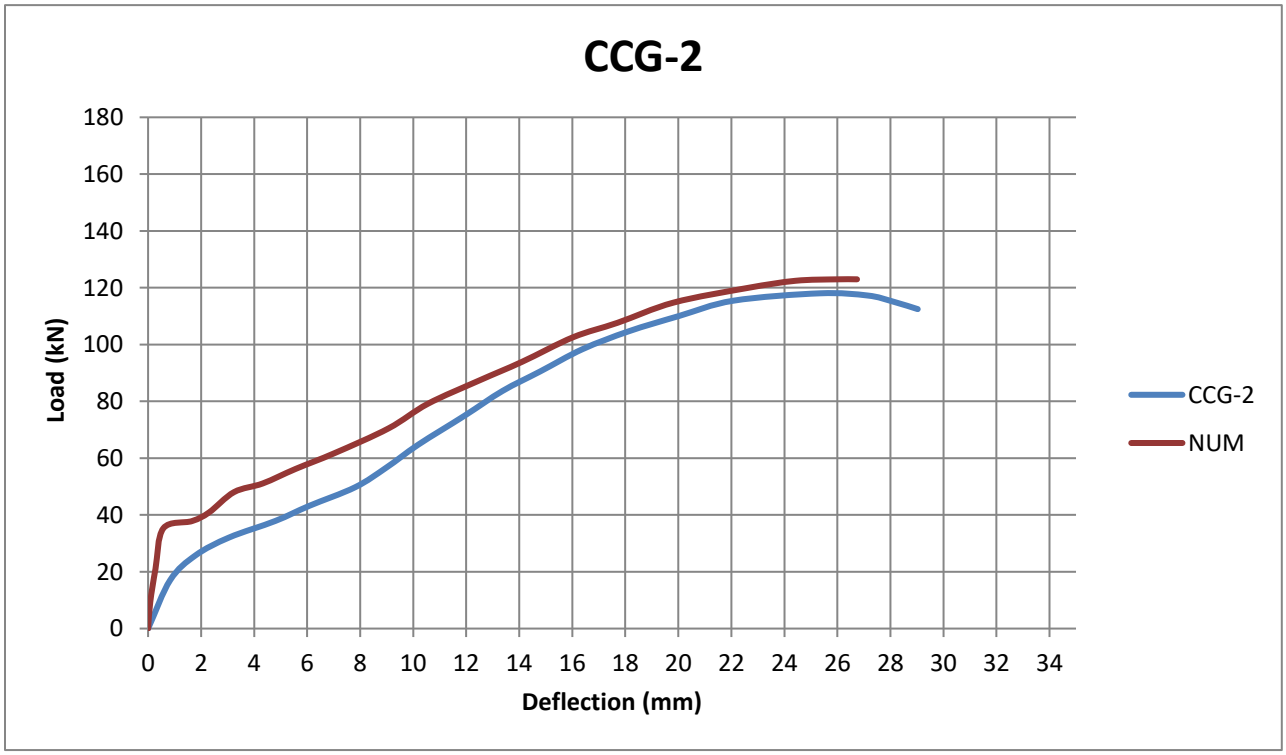

Figure (5.25): Numerical and experimental load-deflection curves for (CCG-2) model.

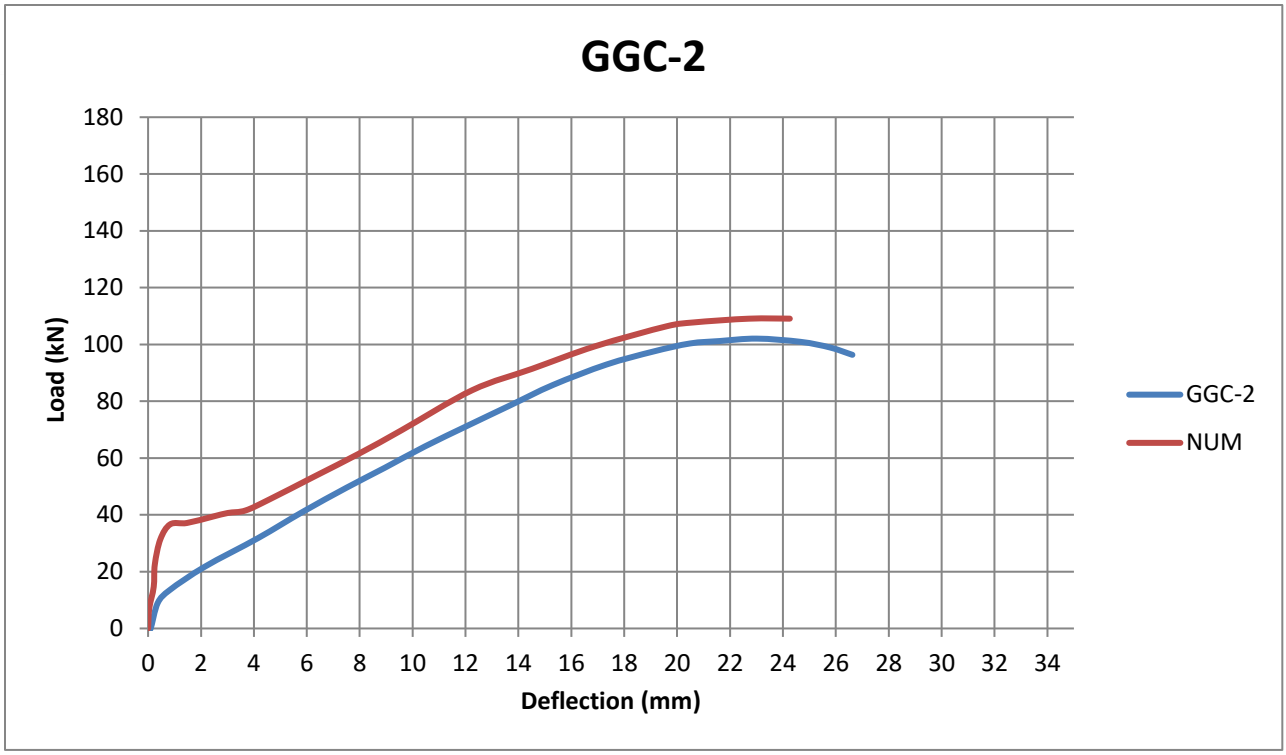

Figure (5.26): Numerical and experimental load-deflection curves for (GGC-2) model.

5.4.2. Crack Pattern

The crack patterns shown in **Figures (5.27) to (5.41)** found in the experimental specimens were juxtaposed with those produced by the numerical models in the ABAQUS software. The data exhibited a robust association between the numerical simulations and the experimental findings, indicating a significant consistency between the two methodologies.

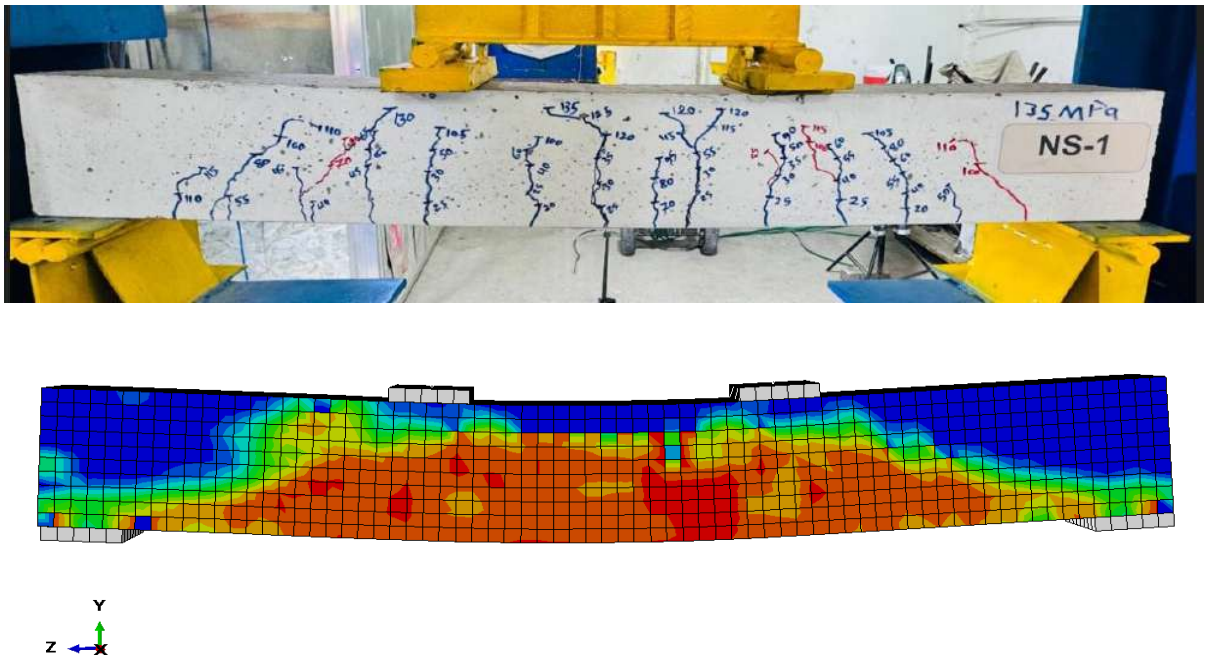

Figure (5.27): Experimental and numerical cracks propagation for (NS-1) model.

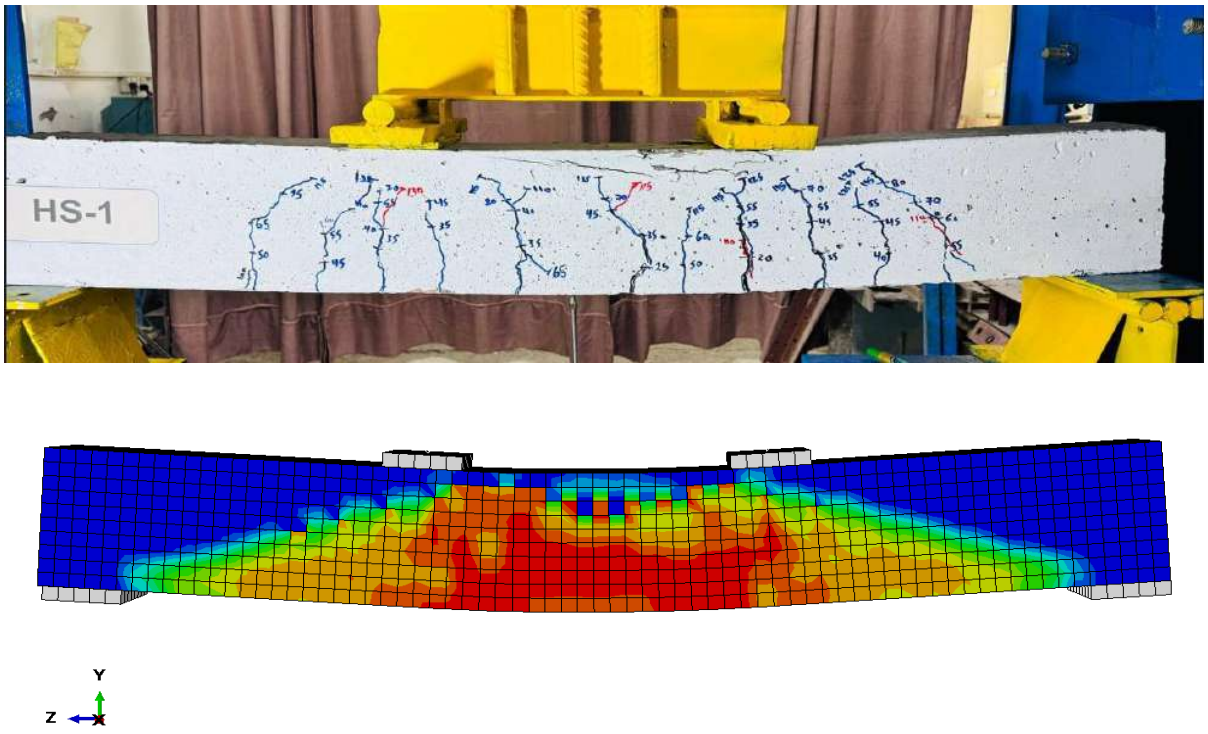

Figure (5.28): Experimental and numerical cracks propagation for (HS-1) model.

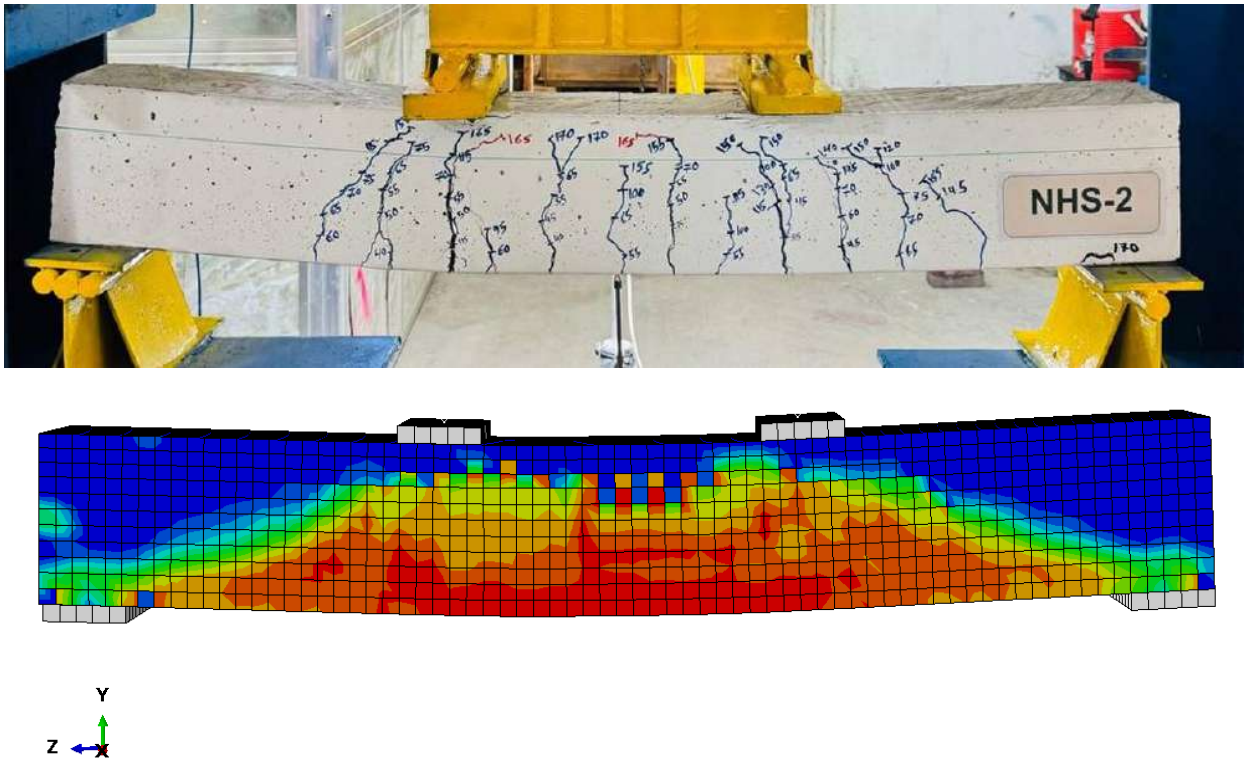

Figure (5.29): Experimental and numerical cracks propagation for (NHS-2) model.

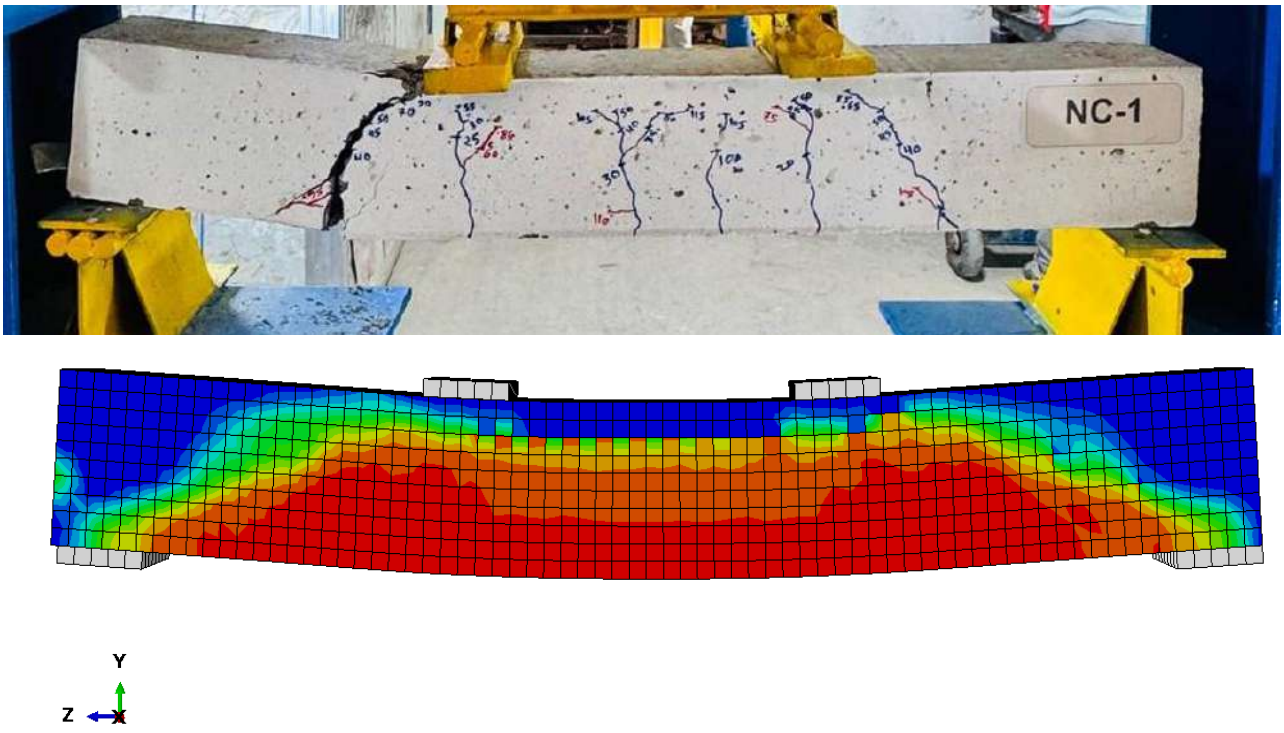

Figure (5.30): Experimental and numerical cracks propagation for (NC-1) model.

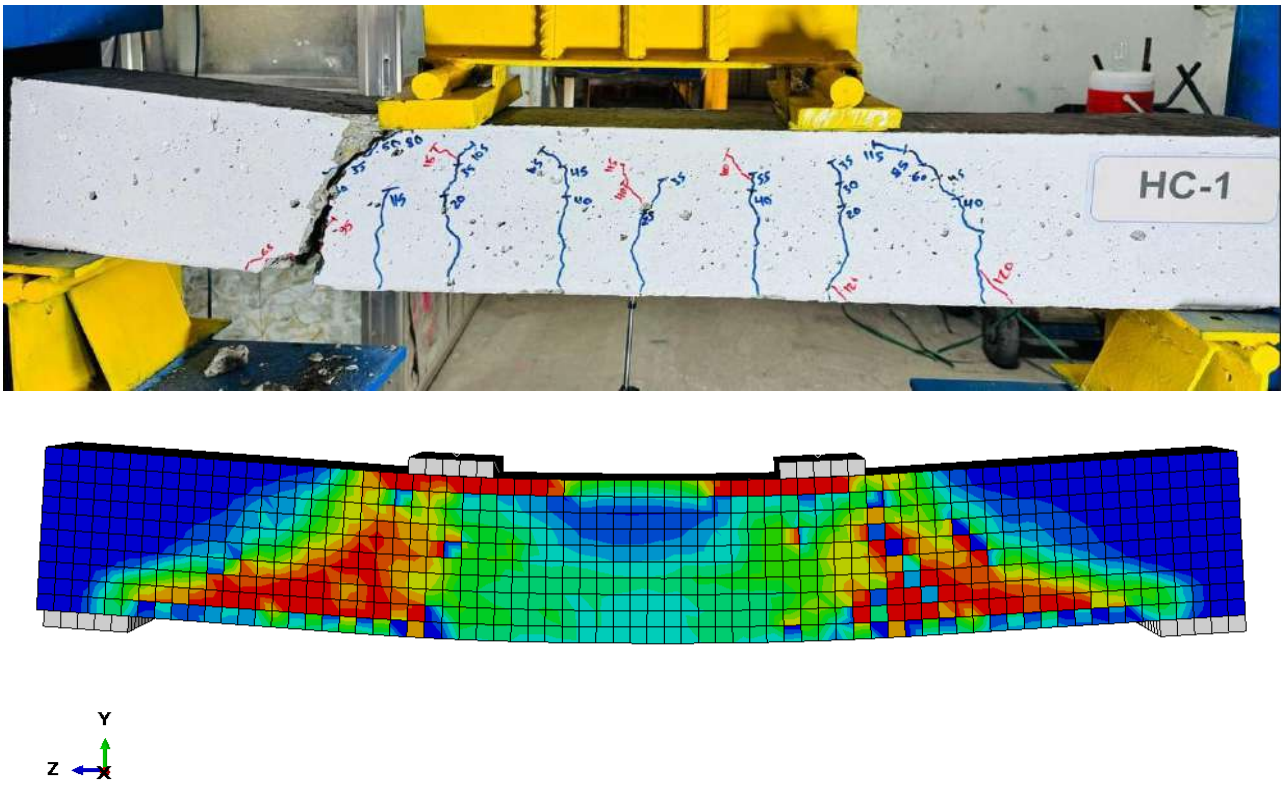

Figure (5.31): Experimental and numerical cracks propagation for (HC-1) model.

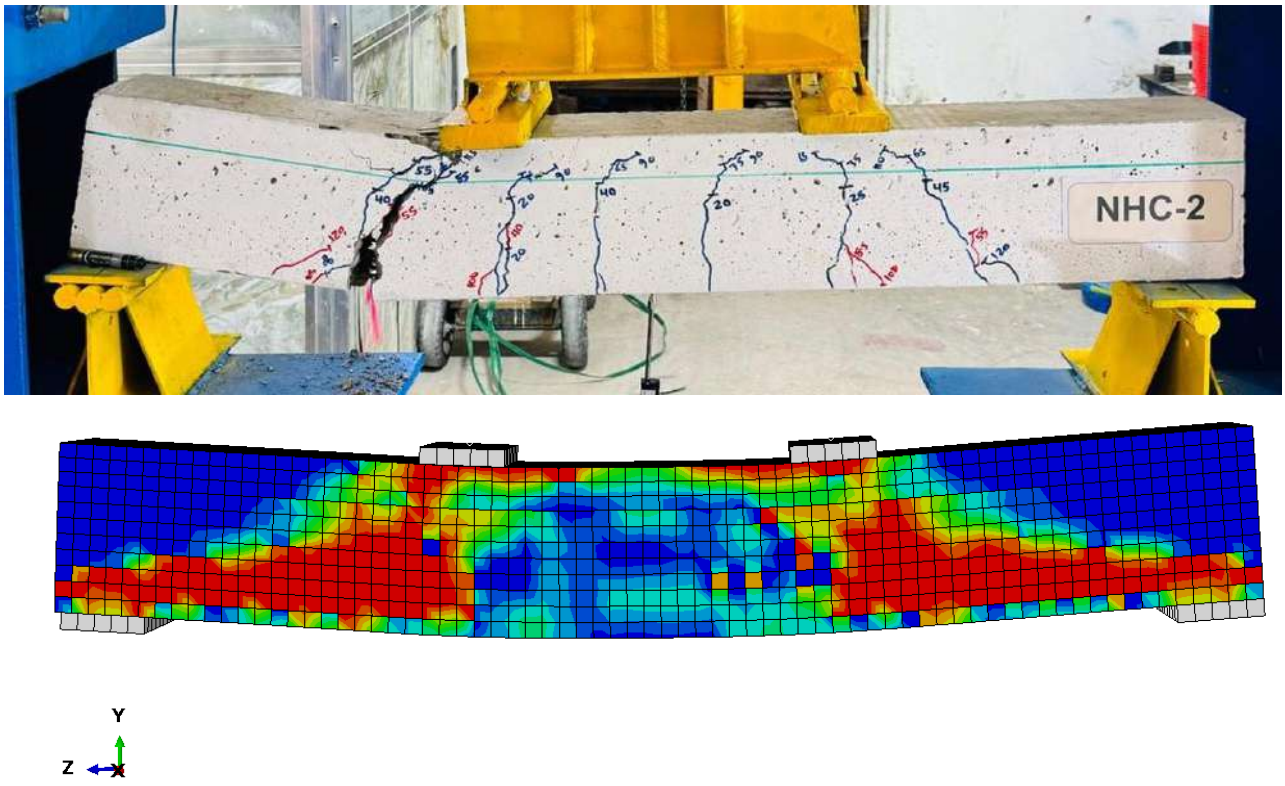

Figure (5.32): Experimental and numerical cracks propagation for (NHC-2) model.

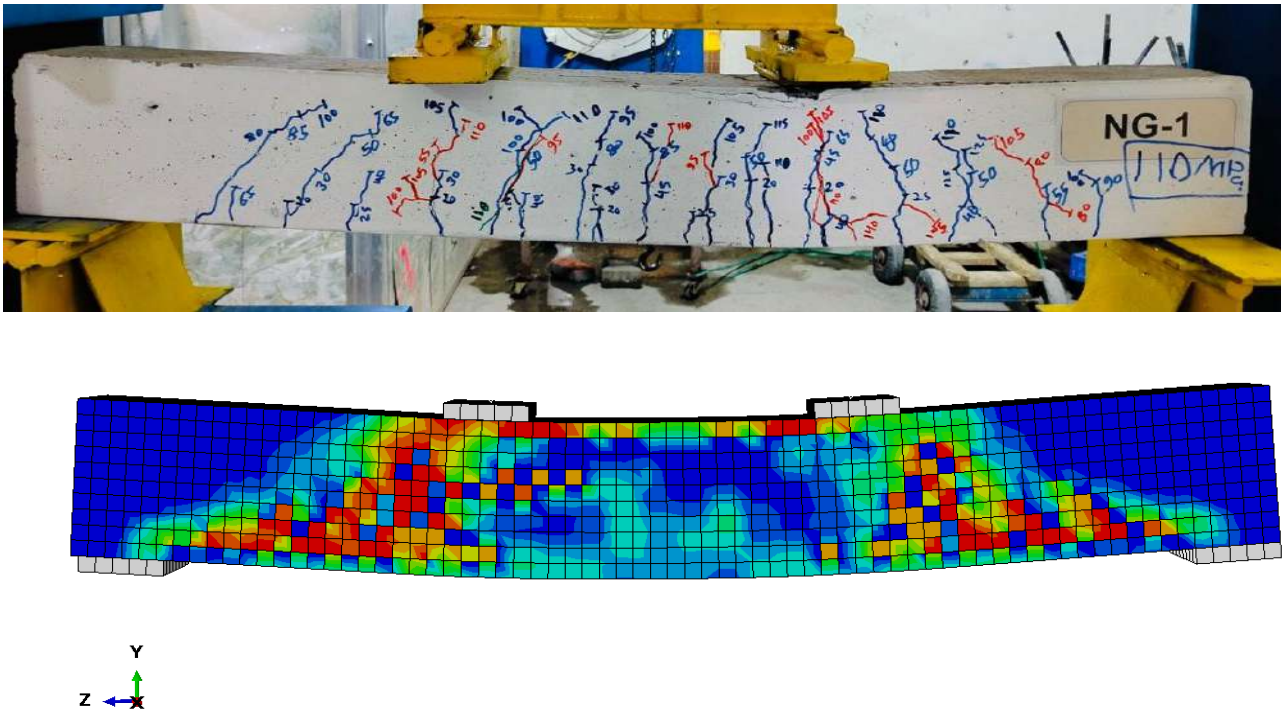

Figure (5.33): Experimental and numerical cracks propagation for (NG-1) model.

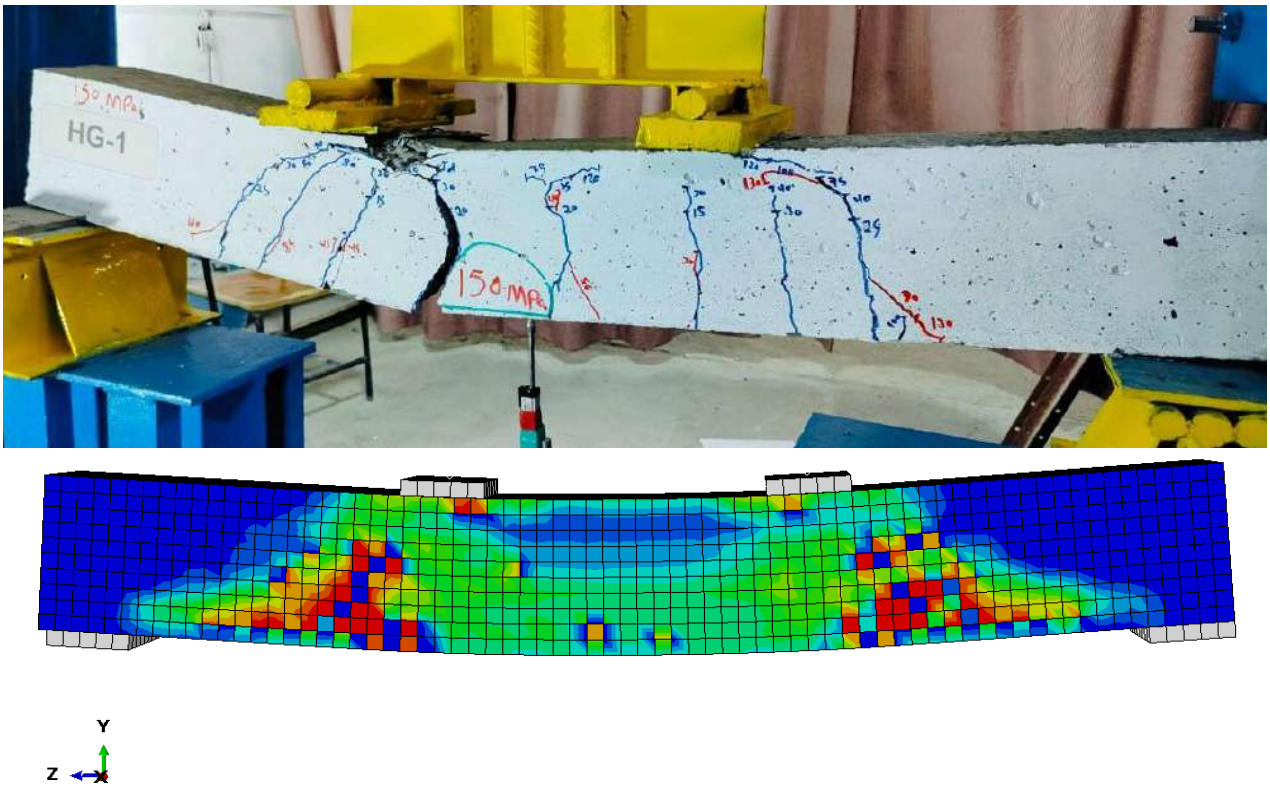

Figure (5.34): Experimental and numerical cracks propagation for (HG-1) model.

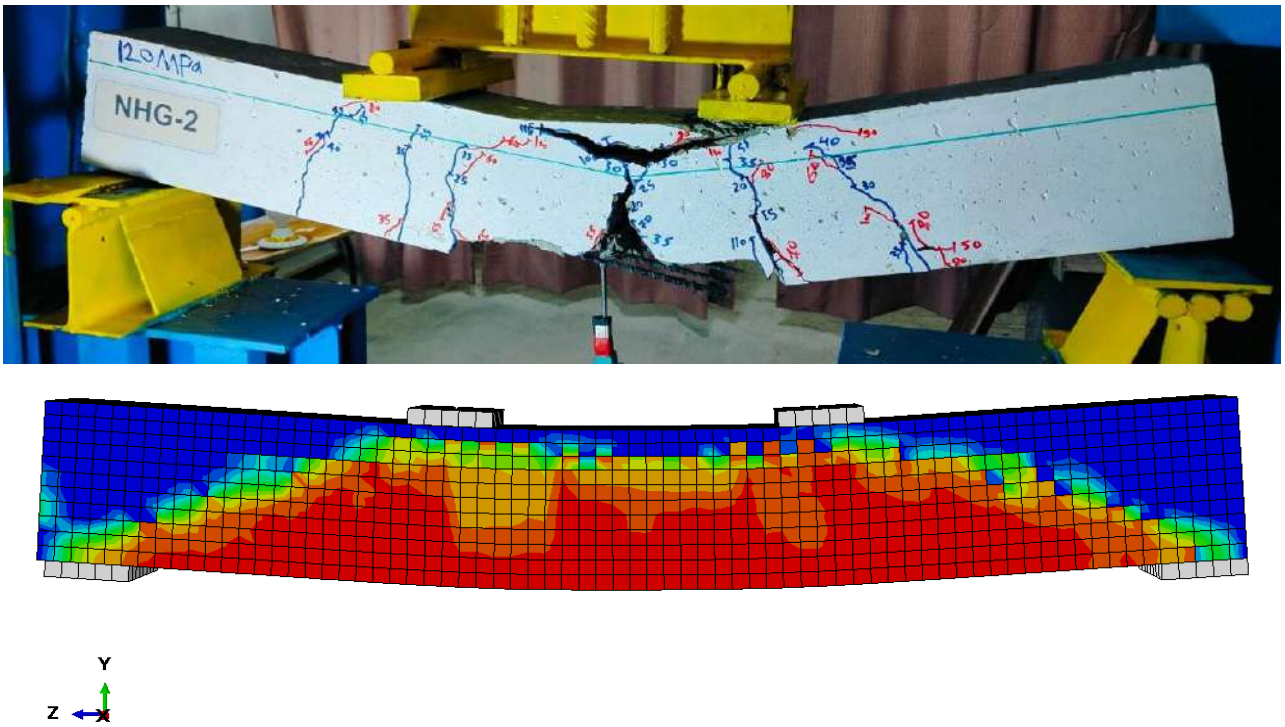

Figure (5.35): Experimental and numerical cracks propagation for (NHG-2) model.

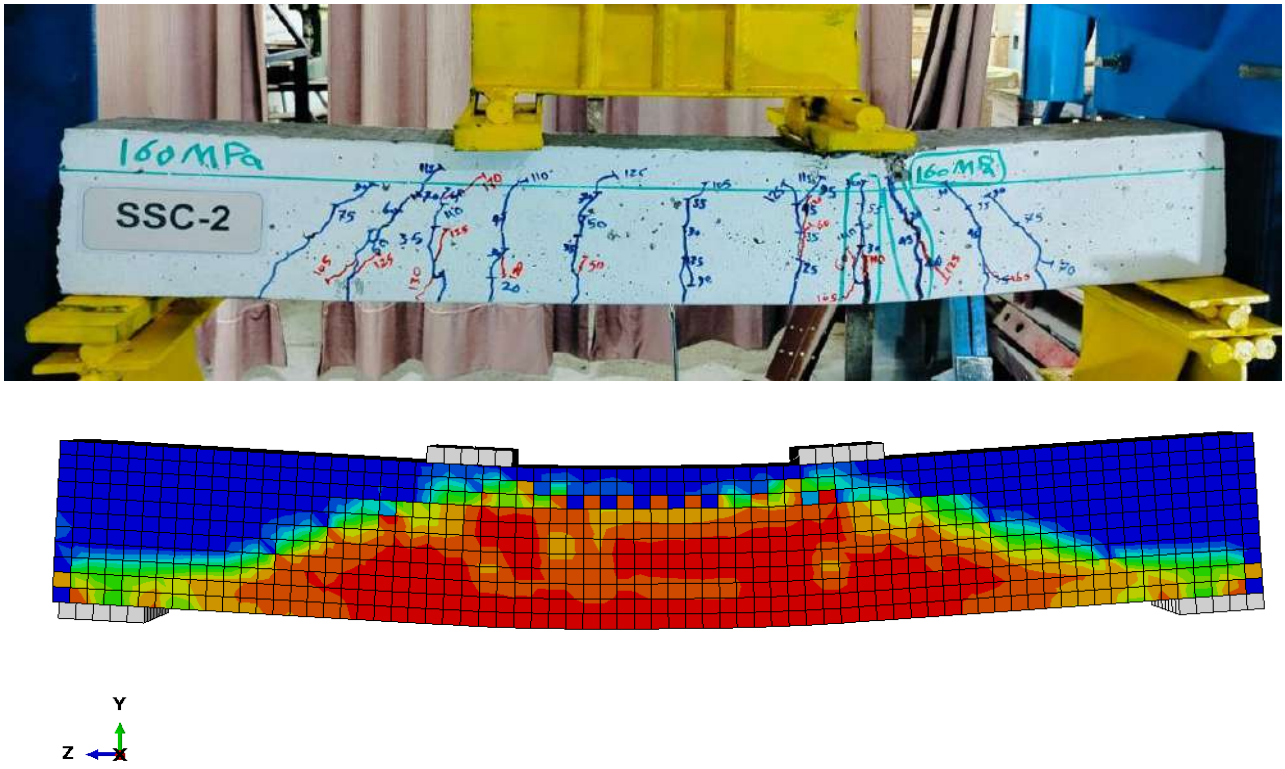

Figure (5.36): Experimental and numerical cracks propagation for (SSC-2) model.

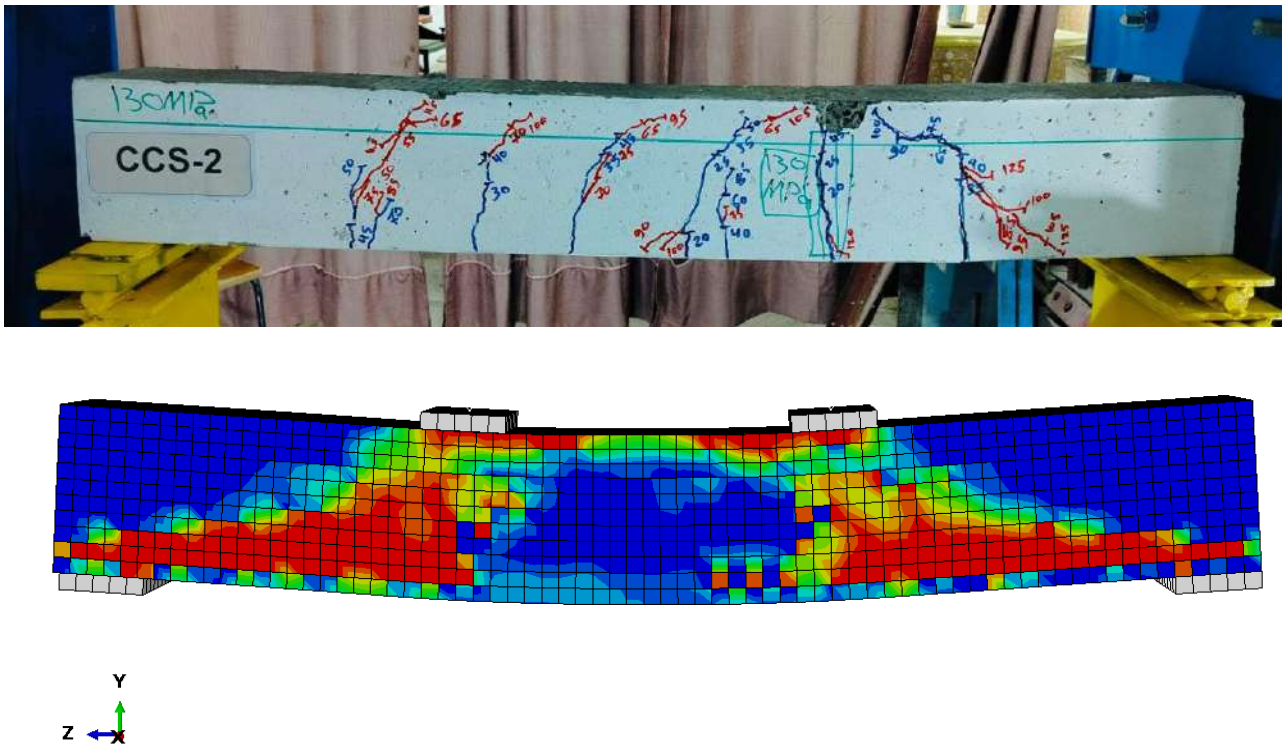

Figure (5.37): Experimental and numerical cracks propagation for (CCS-2) model.

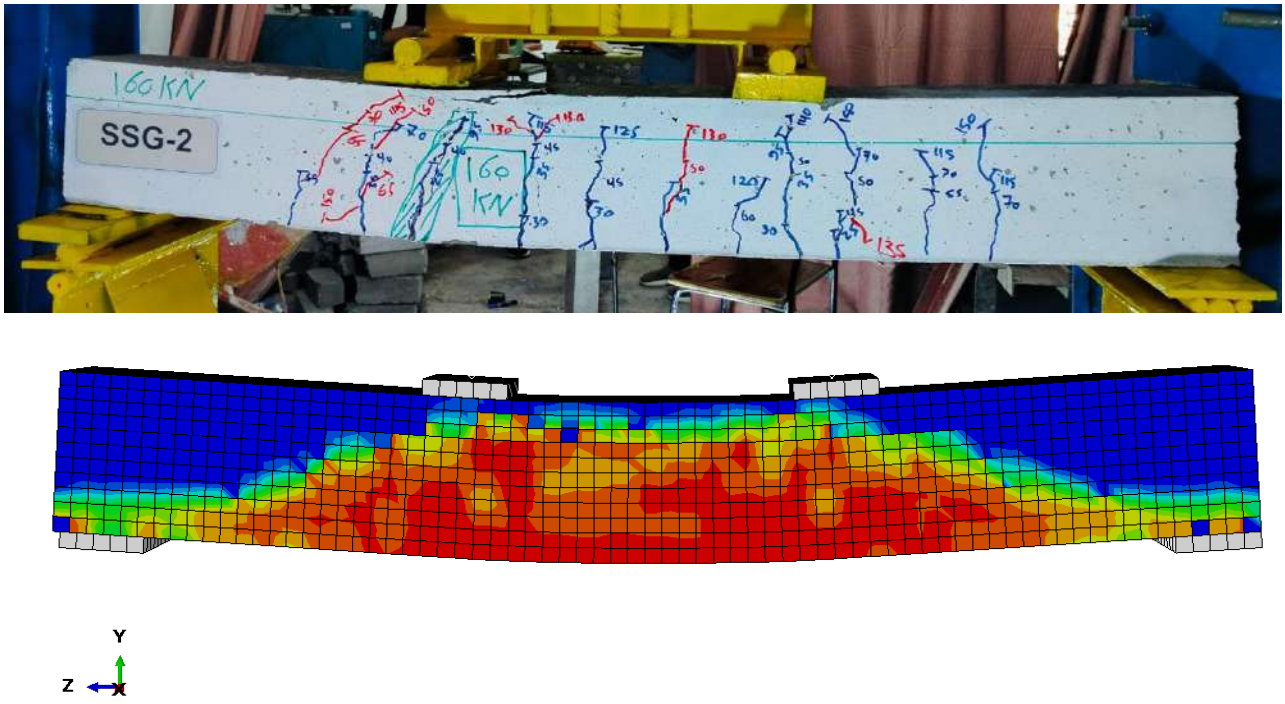

Figure (5.38): Experimental and numerical cracks propagation for (SSG-2) model.

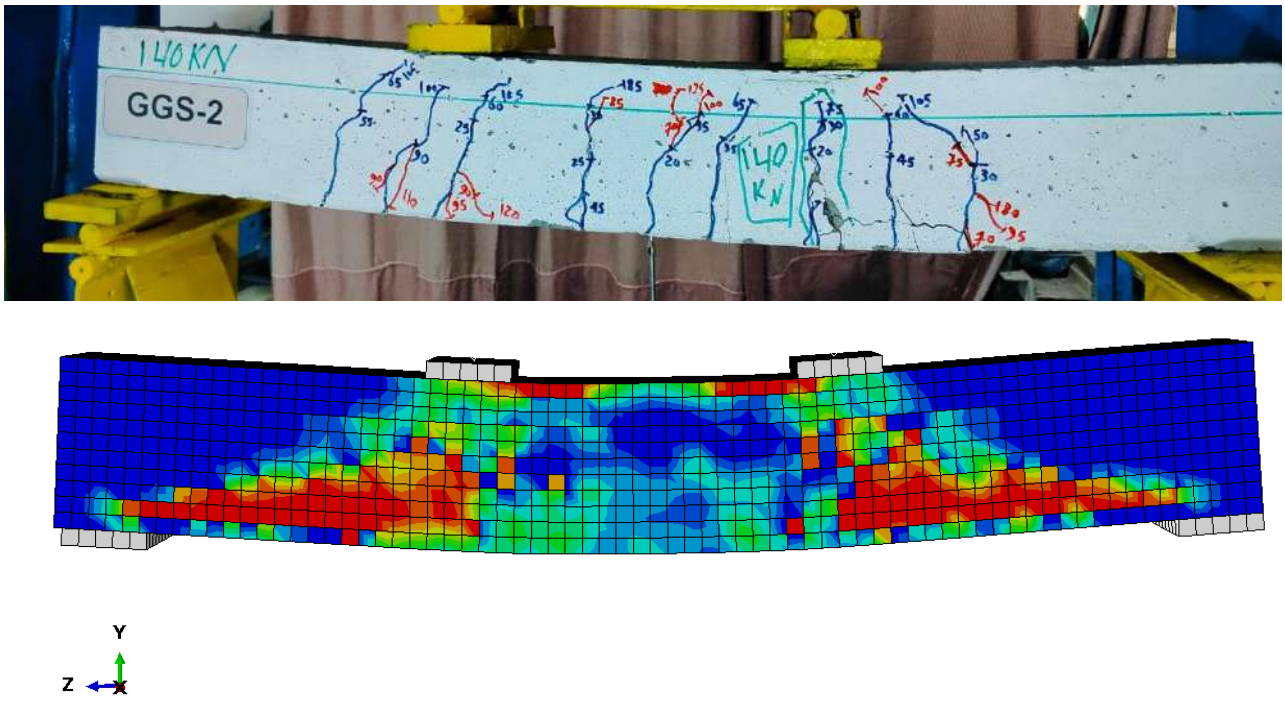

Figure (5.39): Experimental and numerical cracks propagation for (GGS-2) model.

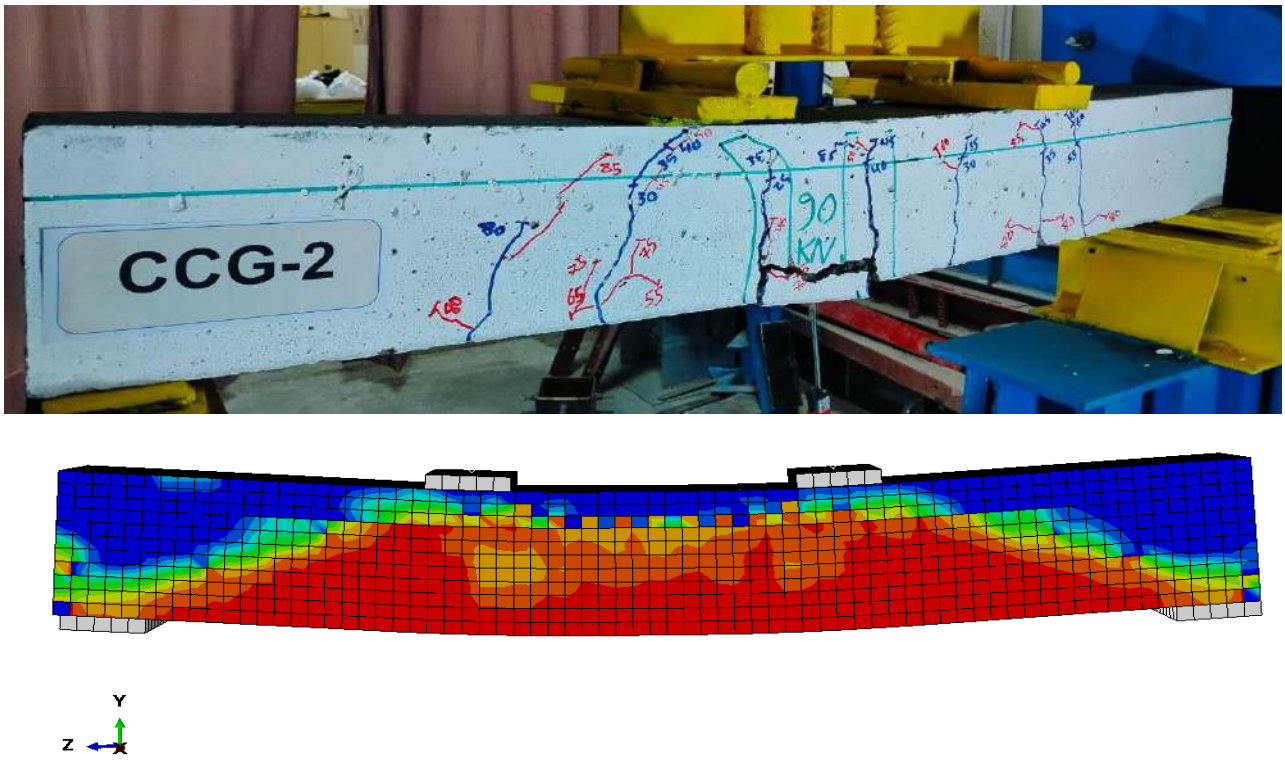

Figure (5.40): Experimental and numerical cracks propagation for (CCG-2) model.

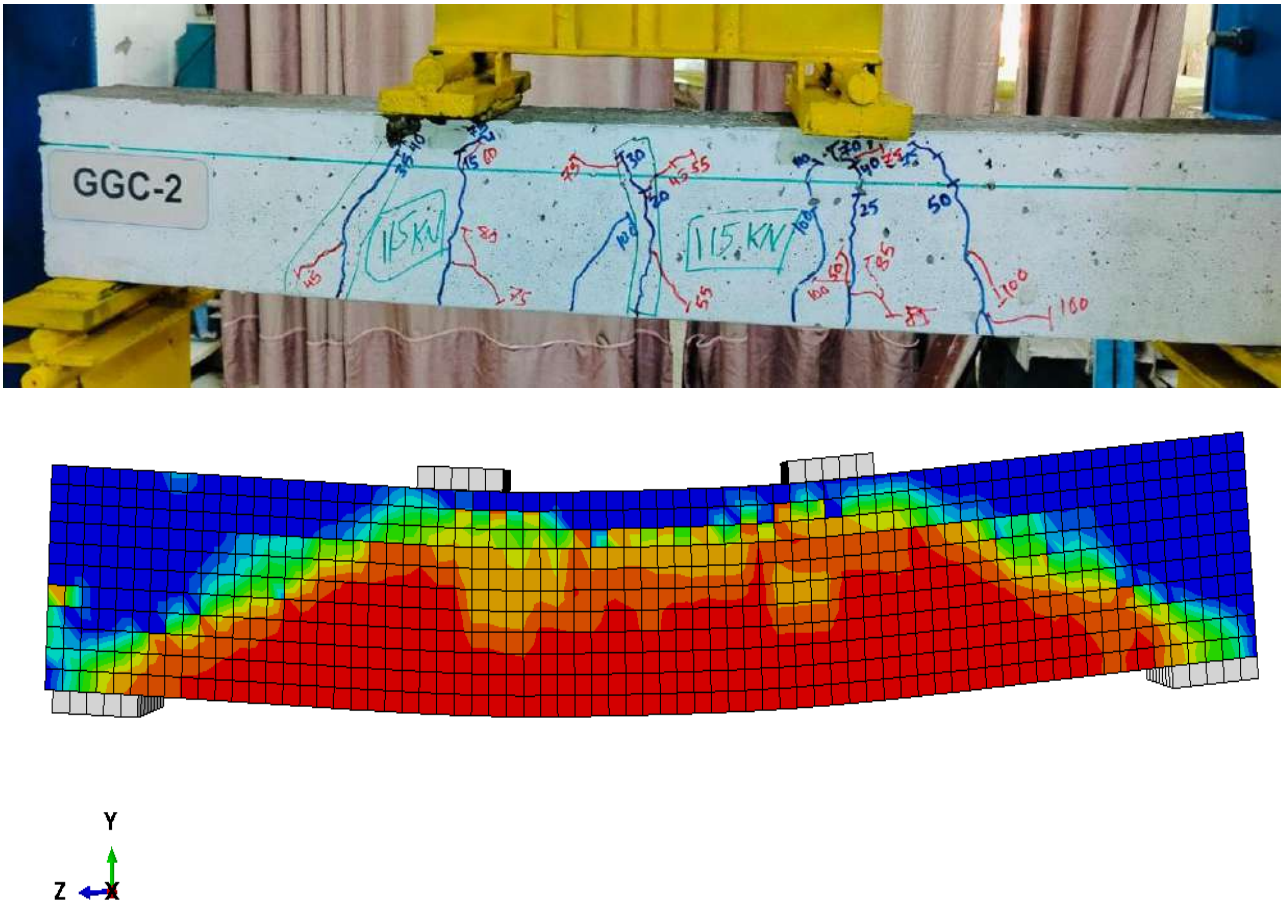

Figure (5.41): Experimental and numerical cracks propagation for (GGC-2) model.

5.4.3. Maximum Deflection and Ultimate Load

A comparison is made between the experimental load and maximum deflection, and the similar computational data generated by the ABAQUS algorithm, shown in **Table (5.2)**. With variations of 5.99% for the ultimate load and 6.31% for the maximum deflection, the study reveals a significant concordance between the information gained from numerical analysis and the data collected from the experiments. It is possible to conclude, on the basis of the results, that the numerical model can produce accurate predictions, making it a trustworthy instrument for carrying out more research.

Table (5.2): Numerical and Experimental Results of the Tested Specimens

Group	Specimens symbol	load (kN)		Different percentages of ultimate load %	Maximum deflection (mm)	Different percentage of deflection %
Group 1	NS-1	EXP	134	4.55	14	3
		FEA	140.10		14.42	
	HS-1	EXP	148	5.78	20	9.20
		FEA	156.56		21.84	
	NHS-2	EXP	167	6.35	27	5.11
		FEA	177.60		27.96	
Group 2	NC-1	EXP	119	5.17	17	7.65
		FEA	125.15		18.30	
	HC-1	EXP	123	5.24	17	6.73
		FEA	129.44		17.61	
	NHC-2	EXP	145	4.23	19	8.66
		FEA	151.13		20.32	
Group 3	NG-1	EXP	112	9.02	27	4.56
		FEA	122.10		28.23	
	HG-1	EXP	146	2.60	26	6.31
		FEA	149.80		27.64	
	NHG-2	EXP	121	8.15	29	3.31
		FEA	130.86		29.96	

Group 4	SSC-2	EXP	157	-9.53	26	4.08
		FEA	142.04		27.06	
	CCS-2	EXP	129	2.46	17	9.41
		FEA	132.18		18.60	
	SSG-2	EXP	160	-6.13	21	7.24
		FEA	150.20		19.48	
	GGS-2	EXP	142	-9.58	26	8.86
		FEA	128.40		28.63	
	CCG-2	EXP	118	4.20	25	5.87
		FEA	122.96		26.74	
	GGC-2	EXP	102	6.93	24.29	0.21
		FEA	109.07		24.34	

5.5. Parametric Study

In this study, the ABAQUS software was used to conduct a parametric analysis to evaluate the influence of layer thickness on the structural performance of bilayer concrete beams reinforced with different bars. The beams underwent testing using a two-point loading configuration. The following section delineates the main parameters examined in this chapter.

1. Effect of layer thickness on the flexural performance of bilayer concrete beams reinforced with steel bars.
2. Effect of layer thickness on the flexural performance of bilayer concrete beams reinforced with CFRP bar.
3. Effect of layer thickness on the flexural performance of bilayer concrete beams reinforced with GFRP bar.

5.5.1. Effect of Layer Thickness on the Flexural Performance of Bilayer Concrete Beams Reinforced with Steel Bar

This group has four types, with the compression layer regulated and adjusted in varying relative amounts. Each model consists of two layers: the top layer is composed of high-strength concrete, and the bottom layer is constructed from normal-strength concrete. Reinforcement steel was used. Table (5.3) and **Figure (5.42)** provide the thicknesses of the layers used, the ultimate load, and the maximum deflection, which were 50, 75, 100, and 150 mm thick. They underwent two load points using identical support types and adhering to the same operating principles as the genuine laboratory models. It was noted that an increase in layer thickness results in a significant alteration in the ultimate load. The model with a layer thickness of 75 mm demonstrated a 3.67% increase in ultimate load relative to the laboratory model with a thickness of 50 mm. Correspondingly, the other thicknesses exhibited comparatively elevated ultimate load ratios of 5.72% and 10.33% for the models with thicknesses of 100 mm and 150 mm, respectively. This suggests that increased layer thickness correlates with enhanced ultimate load strength of structural parts in comparison to single-layer models.

Table (5.3): Effect of upper layers' thickness on RC steel Bars.

Group	Upper layer thickness (mm)	Ultimate load (kN)	Maximum deflection (mm)
Steel Bars	50	177	27.9
	75	183.5	28.30
	100	187.13	27.16
	150	195.29	29.39

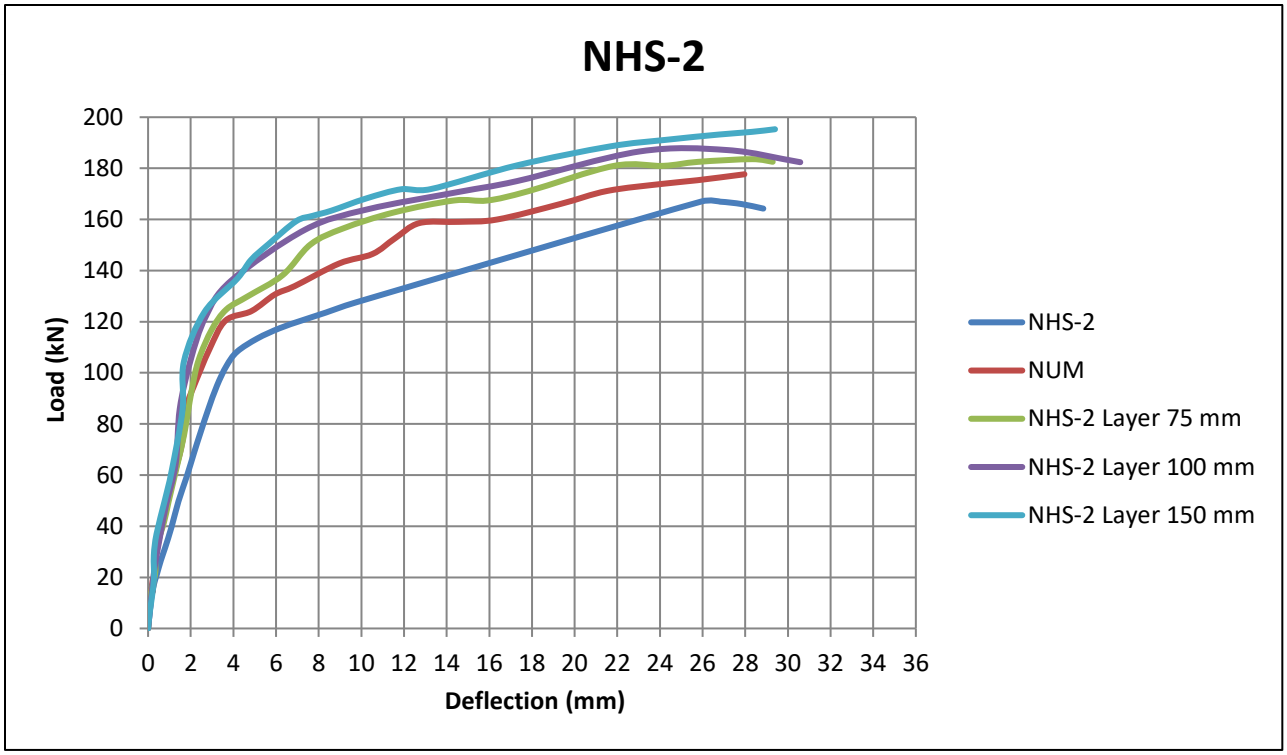

Figure (5.42): Effect of upper layers' thickness on RC steel Bars.

5.5.2. Effect of Layer Thickness on the Flexural Performance of Bilayer Concrete Beams Reinforced with CFRP Bar

This set comprises four models, and the thickness of the compression layer systematically varied in different amounts. Each model has a bilayer structure, including high-strength concrete in the top layer and normal-strength concrete in the bottom layer. CFRP reinforcement was used consistently. The layer thicknesses, together with the associated load and deflection values, are specified in Table (5.4) and shown in **Figure (5.43)**. The evaluated layer thicknesses were 50 mm, 75 mm, 100 mm, and 150 mm. The models underwent two-point loading under uniform support circumstances, mirroring the configuration of the real laboratory tests. The findings demonstrate a distinct relationship between layer thickness and maximum load capacity. The model with a 75 mm layer thickness demonstrated a 3.02% enhancement in ultimate load relative to the 50 mm model.

Likewise, the 100 mm and 150 mm versions exhibited further improvements of 8.05% and 12%, respectively. The results indicate that augmenting the thickness of the compression layer improves the ultimate load capacity of the structural components relative to single-layer designs.

Table (5.4): Effect of upper layers' thickness on RC CFRP Bars.

Group	Upper layer thickness (mm)	Ultimate load (kN)	Maximum deflection (mm)
CFRP Bars	50	151.13	20.3
	75	155.7	24.21
	100	163.3	26.42
	150	169.27	26.40

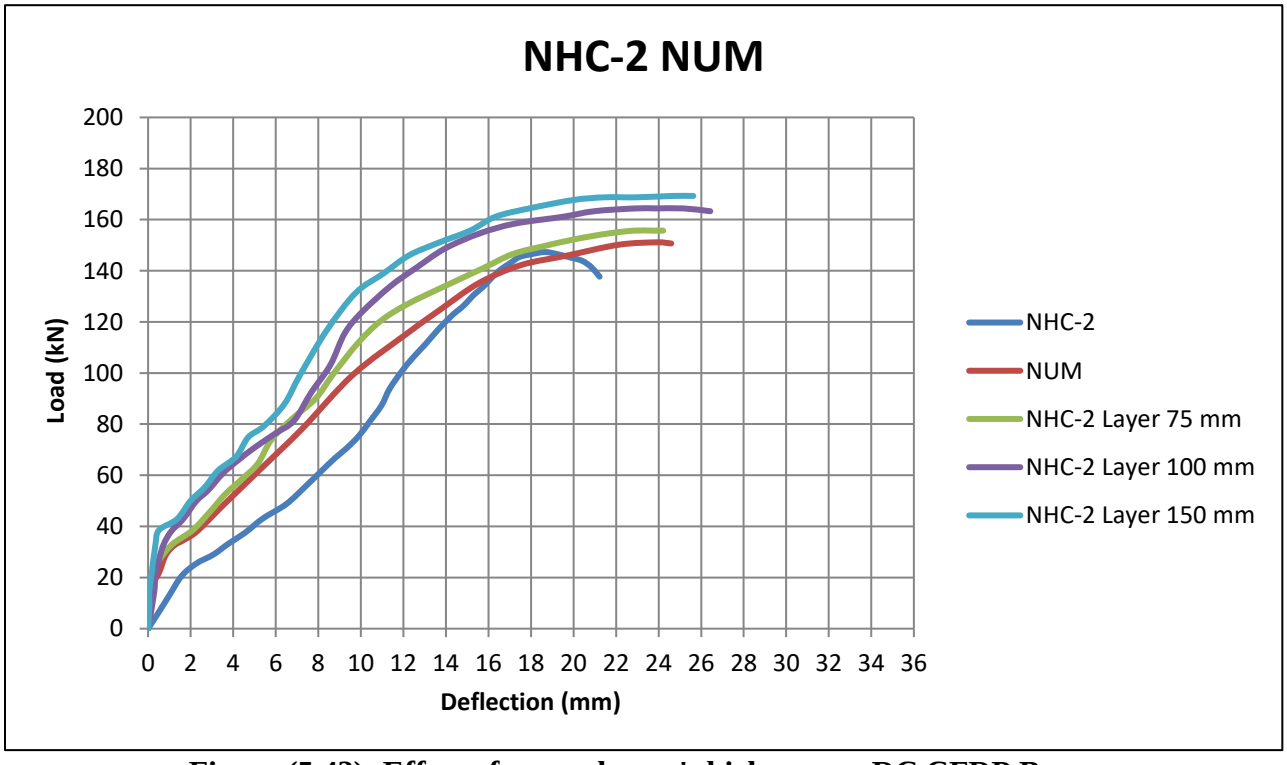

Figure (5.43): Effect of upper layers' thickness on RC CFRP Bars.

5.5.3. Effect of Layer Thickness on the Flexural Performance of Bilayer Concrete Beams Reinforced with GFRP Bar

This research has four models, each constructed with differing thicknesses of the compression layer. All versions consist of a bilayer concrete structure, including high-strength concrete in the top layer and normal-strength concrete in the bottom layer, reinforced by GFRP bars. Table (5.5) presents the specifics of layer thicknesses, load, and deflection, which are also shown in **Figure (5.44)**. The investigated thicknesses were 50 mm, 75 mm, 100 mm, and 150 mm. Each model underwent two-point loading under uniform support circumstances, mirroring the configuration used in the experimental testing. The findings indicate a definitive correlation between the thickness of the compression layer and structural performance. The model with a 75 mm layer thickness demonstrated a 3.2% enhancement in ultimate load relative to the 50 mm model. Correspondingly, the models with 100 mm and 150 mm layers exhibited further increases of 5.87% and 8.03%, respectively. These data indicate that increasing the thickness of the compression layer significantly enhances load-bearing capability in comparison to single-layer structural elements.

Table (5.5): Effect of upper layers' thickness on RC GFRP Bars.

Group	Upper layer thickness (mm)	Ultimate load (kN)	Maximum deflection (mm)
GFRP Bars	50	130.86	29.96
	75	135.054	31.4425
	100	138.54	32.01
	150	141.3664	32.45

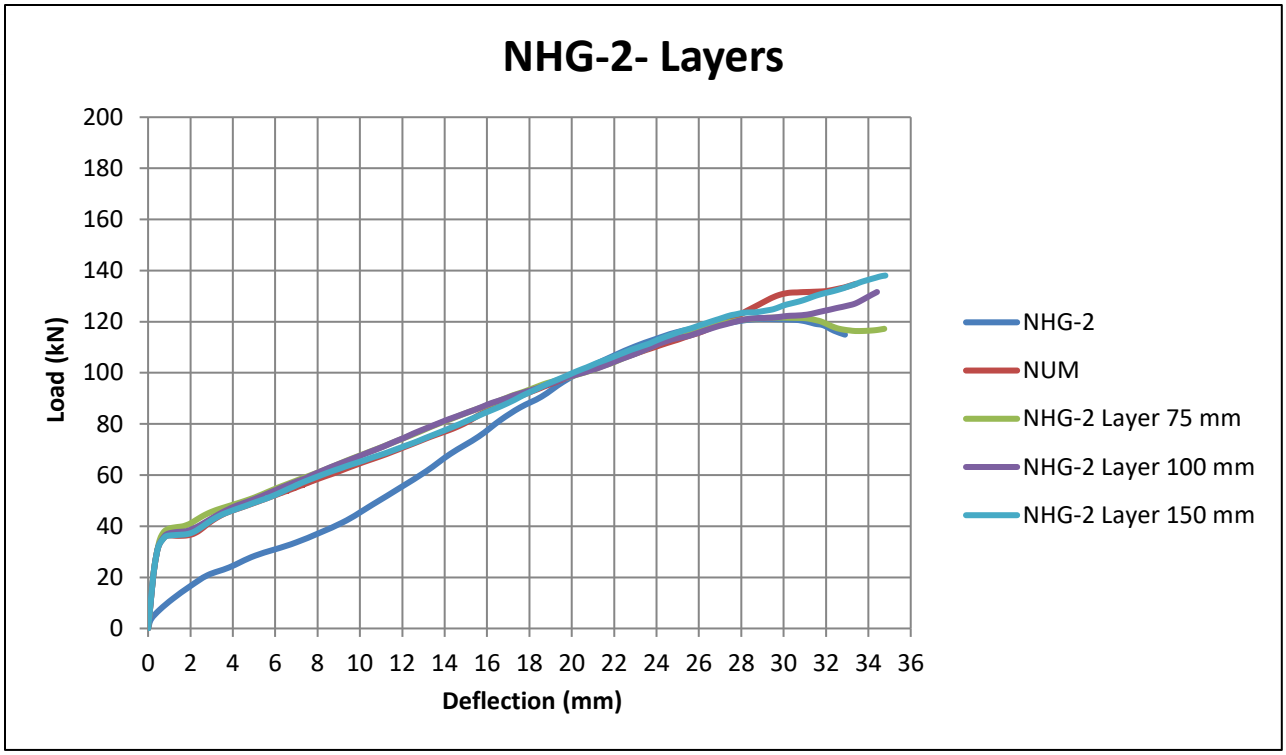

Figure (5.44): Effect of upper layers' thickness on RC GFRP Bars.

Chapter Six: Conclusions and Recommendations

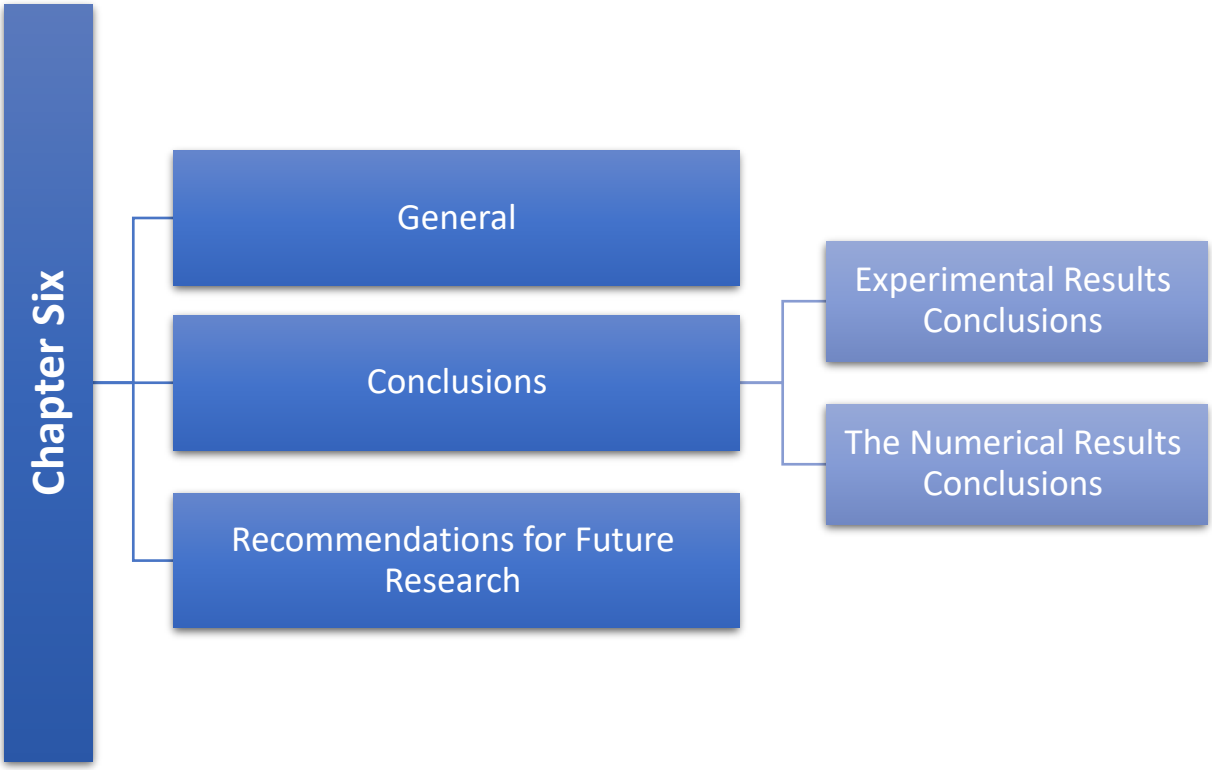

Chapter Six
Conclusions and Recommendations

6.1 General

This research evaluates and contrasts the flexural performance of bilayer concrete beams reinforced with various materials (steel, CFRP, and GFRP) using different compressive strengths of concrete (normal at the bottom and high at the top). This study uses an experimental program and a nonlinear finite element model to examine the beams' flexural behavior. This chapter employs experimental and analytical findings to conclude. Recommendations for future projects are also offered.

6.2 Conclusions

This part lays out the key findings from the current experimental and numerical investigations.

6.2.1. Experimental Results Conclusions

1. The bilayer concrete system models demonstrated an increase in ultimate load and the intensity of first crack load by 12.77 % and 30.95 %, respectively, relative to models constructed with a single layer of concrete.
2. Composed of a bilayer system using steel reinforcement bars, shows a significant increase in both maximum load and maximum crack value by 24.63 % and 42.86 %, respectively, compared to the model which consists of a single layer of normal-strength concrete and an even more significant increase of (12.84% and 33.1%) compared to a model which is made of high-strength concrete.
3. A bilayer concrete beam incorporating various types of rebar demonstrated enhancements in ultimate load and initial cracking load. The configuration

featuring two steel bars alongside a glass bar, as well as the model comprising two steel bars with a carbon bar, exhibited the most significant improvements in ultimate load and first crack load, with increases of 22.56 % and 18.18 %, respectively, in comparison to models using different types of reinforcement.

4. Flexural failure predominated; other specimens exhibited flexural-shear or concrete crushing. Flexural-shear failure was more common in CFRP bar and bilayer steel bar models, indicating shear demand and reinforcing arrangement. Only one specimen bilayer—two CFRP bars and one GFRP bar—exhibited concrete crushing and flexural failure. Failure patterns match expected behaviors based on loading and reward.
5. Using a bilayer system has significantly improved the structural element's behavior in its ultimate load by up to 24.4% in some models. Additionally, using composite materials and reinforcement with different types of bars has changed the failure mode from simple bending to combined bending failure, indicating improved ductility and distribution of internal stresses.
6. Specific groups showed considerable improvements in the ductility index. The bilayer system cast with a steel bar had the highest ductility index (4.34), an increase of 112% over the reference one-layer specimen. The GFRP bar system had moderate improvements, 19% greater than the one-layer specimen. Ductility indices for carbon group specimens ranged from 1.08 to 1.09, indicating consistent but mild ductility.
7. A bilayer concrete beam with varied rebar specimens had moderate to high ductility indices of 1.09 to 1.33. Two GFRP bars and one CFRP bar had the highest ductility index (1.33), 22% higher than two GFRP bars and one steel bar.
8. For effective stiffness, the models reinforced with steel and one layer of high-strength material had a higher value of about 20.9, while the bilayer model

strengthened with glass had the lowest stiffness value of 4.95. On the other hand, the hardness of the carbon-reinforced models varied by only 2.5%.

9. The bilayer concrete beam reinforced with two steel bars and one CFRP bar had a higher effective stiffness magnitude, 47.77 %, compared with the bilayer model reinforced with two CFRP bars and one GFRP bar.
10. For flexural toughness, the bilayer model with steel reinforcement had a high magnitude (3801.67 kN.mm), but the bilayer model with the carbon group had the lowest value at about (1813.3 kN.mm). However, the other models show a relative convergence in flexural toughness value.
11. Compared to the bilayer model reinforced with two CFRP bars and one steel bar, the bilayer concrete beam reinforced with two steel bars and one CFRP bar had a higher level of flexural toughness (54.01%).

6.2.2. The Numerical Results Conclusions

1. The finite element analysis (FEA) was effectively executed, exhibiting superior convergence for ultimate load, deflection, and failure mode for bilayer concrete beams reinforced with various kinds of rebar. This encompasses beams augmented with steel, CFRP, and GFRP, in addition to hybrid reinforcement arrangements. The numerical results closely matched the experimental data, validating the dependability of the created model in modeling the structural behavior of these beams.
2. The comparison between the experimental data and finite element analysis (FEA) indicated an average discrepancy of roughly 2.1% in ultimate load and 4.93% in maximum deflection. The scores signify a high degree of accuracy in the numerical model, illustrating its dependability in forecasting the structural behavior of the evaluated specimens.

3. The finite element study indicates that augmenting the layer thickness in the bilayer system models improves their ultimate load and maximum deflection by 6.33 % and 9.01 %, respectively.

6.3 Recommendations for Future Research

1. Further investigations might examine the implementation of hybrid reinforcement systems using diverse fiber-reinforced polymer (FRP) types, such as basalt or aramid, to evaluate their influence on flexural performance.
2. Future studies should concentrate on the endurance and long-term performance of bilayer concrete beams subjected to environmental conditions, including freeze-thaw cycles, elevated humidity, and chemical exposure.
3. Examining the behavior of bilayer concrete beams under dynamic and seismic stress conditions may be beneficial for earthquake-resistant structural applications.
4. Future research may investigate improved reinforcing techniques, such as the integration of prestressed FRP reinforcements or novel grouting materials, to improve the structural efficiency of bilayer beams.

References

ACI Committee 363. (1992). State-of-the-art report on high-strength concrete (ACI 363R-92). American Concrete Institute.

ACI Committee 440. (2015). Guide for the design and construction of structural concrete reinforced with fiber-reinforced polymer (FRP) bars (ACI 440.1R-15). American Concrete Institute.

ACI Committee-363, "State of the Art Report on High Strength Concrete (ACI 363R-92)", American Concrete Institute, Detroit, 1997.

Adam, M. A., Said, M., Mahmoud, A. A., & Shanour, A. S. (2015). Analytical and experimental flexural behavior of concrete beams reinforced with glass fiber reinforced polymers bars. Construction and building materials, 84, 354-366.

Aiello, M. A., & Ombres, L. (2002). Structural performances of concrete beams with hybrid (fiber-reinforced polymer-steel) reinforcements. Journal of Composites for Construction, 6(2), 133-140.

Al-Amry, M. G. (2013). Experimental Investigation and Nonlinear Analysis of Hybrid Reinforced Concrete Deep Beams (M. SC thesis, Univ. of Babylon).

Ali, Y., & Abbas, A. A. (2016). Structural behavior of reinforced lightweight concrete corbels strengthened with NSM-CFRP bars. International Journal of Civil Engineering and Technology, 7(6), 380–392.

AL-Khafaji, A. G. A., Al-Mamoori, A. H. N., & Abd Aoun, A. M. (2018, June). Improvement of flexural strength of precast concrete spliced girder using reactive powder concrete in splice region. In Structures (Vol. 14, pp. 197-208). Elsevier.

Alkhrdaji, T., Fyfe, E. R., Korff, J., Schupack, M., Bakis, C. E., Gentry, T. R., ... & Shield, C. K. (2006). Guide for the design and construction of structural concrete reinforced with FRP bars. Proceedings of the American Concrete Institute (ACI) committee, 440.

Alogla, K., & Rasheed, L. S. (2023). Effect of the location of reactive powder concrete layer on the behaviour of hybrid deep beams. *International Journal of Structural Engineering*, *13*(3), 368-385.

ASTM C39/C39M-15a, "Standard Test Method for Compressive Strength of Cylindrical Test Specimens", Annual Book of ASTM Standards, 2015.

ASTM C494/C494M-13. ASTM International. (2013): Standard specification for chemical admixtures for concrete. Annual Book of ASTM Standards.

ASTM International. (2010). ASTM C78: Standard test method for flexural strength of concrete (using simple beam with third-point loading). American Society for Testing and Materials, 100, 12959–19428.

ASTM International. (2011). ASTM C496/C496M-11: Standard test method for splitting tensile strength of cylindrical concrete specimens. Annual Book of ASTM Standards.

Aziz, O. Q., & Taha, B. O. (2013). Flexure behavior of high strength concrete (HSC) beams reinforced with carbon fiber reinforced polymer (CFRP) rebars with and without chopped carbon fiber (CCF). Int J Sci Res, 1(6), 123-139.

Barris, C., Sala, P., Gómez, J., & Torres, L. 2020. Flexural behavior of FRP reinforced concrete beams strengthened with NSM CFRP strips. Composite Structures, v. 241, 112059.

Bank, L. C. (2013). Progressive failure and ductility of FRP composites for construction. *Journal of Composites for Construction*, *17*(3), 406-419.

BS 1881-116,"Method for Determination of Compressive Strength of Concrete Cubes", British Standards Institute, London, 1983.

Canadian Standards Association. (2012). *CSA S806-12: Design and construction of building structures with fibre-reinforced polymers*. CSA Group.

Carreira, D. J., & Kuang-Han Chu. (1985). Stress-Strain Relatonship for Reinforced Concrete in Compression. ACI Structural Journal, November December, 797–804.

Cheung, M. M., & Tsang, T. K. (2010). The behavior of concrete beams reinforced with hybrid FRP composite rebar. Advances in Structural Engineering, 13(1), 81-93.

Chung, W., & Sotelino, E. D. (2006). Three-dimensional finite element modeling of composite girder bridges. Engineering Structures, 28(1), 63–71. https://doi.org/10.1016/j.engstruct.2005.05.019

Duthinh, D. and Starnes, M., 2001, "Strength and Ductility of Concrete Beams Reinforced with FRP and Steel", National Institute of Standards and Technology, NISTIR 6830, 16 P.

El Refai, A., Abed, F., & Al-Rahmani, A. (2015). Structural performance and serviceability of concrete beams reinforced with hybrid (GFRP and steel) bars. Construction and Building Materials, 96, 518-529.

El-Nemr, A., ElSafty, A., & Benmokrane, B. (2016). Flexural behavior of concrete beams reinforced with GFRP bars of different grades. In International Conference on Structural and Geotechnical Engineering.

Fallah-Valukolaee, S., Hashemi, S. K., & Nematzadeh, M. (2022, May). Effect of steel fiber on flexural performance of bilayer concrete beams with steel and GFRP rebars: experiments and predictions. In Structures (Vol. 39, pp. 405-418). Elsevier.

G Karayannis, C., K Kosmidou, P. M., & E Chalioris, C. 2018. Reinforced concrete beams with carbon-fiber-reinforced polymer bars—Experimental study. Fibers, 6(4), 99.

Ge, W. J., Ashour, A. F., Yu, J., Gao, P., Cao, D. F., Cai, C., & Ji, X. (2019). Flexural behavior of ECC–concrete hybrid composite beams reinforced with FRP and steel bars. Journal of Composites for Construction, 23(1), 04018069.

Ge, W., Wang, Y., Ashour, A., Lu, W., & Cao, D. (2020). Flexural performance of concrete beams reinforced with steel–FRP composite bars. Archives of Civil and Mechanical Engineering, 20(2), 56.

Ge, W., Zhang, J., Cao, D., & Tu, Y. (2015). Flexural behaviors of hybrid concrete beams reinforced with BFRP bars and steel bars. Construction and Building Materials, 87, 28-37.

Grepstad, L., & Overli, J. A. (2007). Hybrid Concrete Structures–Experimental and Numerical Investigation of Beams with Lightweight Concrete and Fiber-Reinforcement. The Concrete Innovation Centre, COIN.

Harris, H. G., Somboonsong, W., & Ko, F. K. (1998). A new ductile hybrid FRP reinforcing bar is for concrete structures. Journal of composites for construction, 2(1), 28-37.

Hassan, H. F. (2015). The behavior of hybrid deep beams containing ultra-high performance and conventional concretes. Engineering and Technology Journal, 33(1), 30-50.

Hassan, S. A., & Faroun, G. A. (2016). The behavior of hybrid reinforced concrete deep beams under repeated loading. Civil and Environmental Research, 8(10), 14-37.

Hassan, S. A., Hemzah, S., & Alyhya, W. (2020). Structural behavior of self-compacted concrete box girders with in-place openings (Doctoral dissertation, University of Kerbala). University of Kerbala.

Hawileh, R. A. (2015). Finite element modeling of reinforced concrete beams with a hybrid combination of steel and aramid reinforcement. Materials & Design (1980-2015), 65, 831-839.

Hosseini, A. S., & Sadeghian, P. (2025). Assessing compressive properties of gfrp bars: novel test fixture and statistical analysis. *Journal of Composites for Construction*, *29*(2), 04025011.

Iskhakov, I., & Ribakov, Y. (2007). A design method for two-layer beams consisting of normal and fibered high strength concrete. Materials & Design, 28(5), 1672-1677.

Iskhakov, I., & Ribakov, Y. (2013). Two-layer concrete bridge beams as composite elements. *Structural Concrete*, *14*(3), 271-277.

Kabashi, N., Krasniqi, C., Sustersic, J., Dautaj, A., Krasniqi, E., & Morina, H. (2018). Flexural behavior and cracks in concrete beams reinforced with GFRP bars. In International Congress on Polymers in Concrete (ICPIC 2018) Polymers

for Resilient and Sustainable Concrete Infrastructure 16 (pp. 617-625). Springer International Publishing.

Kalpana, V. G., & Subramanian, K. (2011). Behavior of concrete beams reinforced with GFRP BARS. Journal of reinforced plastics and composites, 30(23), 1915-1922.

Kara, I. F., Ashour, A. F., & Köroğlu, M. A. (2015). Flexural behavior of hybrid FRP/steel reinforced concrete beams. Composite Structures, 129, 111-121.

Kheder, G. F., Al Kafaji, J. M., & Dhiab, R. M. (2010). Flexural strength and cracking behavior of hybrid strength concrete beams. Materials and structures, 43, 1097-1111.

Kreger, M. E., & Linbeck, L. (1986). Behavior of Reinforced Concrete Columns Subjected To Lateral and Axial Load Reversals. June, 1475–1486.

Lamanna, A., Bank, L. C. and Scott, D. W. 2004. "Flexural Strengthening of Reinforced Concrete Beams by Mechanically Attaching FiberReinforced Polymer Strips", Journal of Composites for Construction, Vol. 8, No. 3, June 1, p. 203-210.

Lau, D., & Pam, H. J. (2010). Experimental study of hybrid FRP reinforced concrete beams. Engineering Structures, 32(12), 3857-3865.

Ma, K., Qi, T., Liu, H., & Wang, H. (2018). Shear behavior of hybrid fiber reinforced concrete deep beams. Materials, 11(10), 2023.

Malm, R. (2006). Shear cracks in concrete structures subjected to in-plane stresses (Licentiate thesis). Royal Institute of Technology (KTH).

Maranan, G. B., Manalo, A. C., Benmokrane, B., Karunasena, W., Mendis, P., & Nguyen, T. Q. (2019). Flexural behavior of geopolymer-concrete beams

longitudinally reinforced with GFRP and steel hybrid reinforcements. Engineering Structures, 182, 141-152.

Martin Perry Associates. (2022). Investigation of reinforced concrete (pp. 1–3). Retrieved from https://mperryassociates.com.

Miàs Oller, C., Torres Llinàs, L., Turon Travesa, A., & Barris Peña, C. (2013). Experimental study of immediate and time-dependent deflections of GFRP reinforced concrete beams. © Composite Structures, 2013, vol. 96, p. 279-285.

Mohammed, A. H. (2020). Torsional Capacity of Hybrid Reinforced Concrete Beams.

Mustafa, S. A., & Hassan, H. A. (2018). Behavior of concrete beams reinforced with hybrid steel and FRP composites. HBRC Journal, 14(3), 300-308.

Nachiappan, P., SmithaGopinath, A., Iyer, N., & Manju, T. (2014). Experimental Studies on Hybrid Beam Reinforced with Steel and BFRP Bar. International Journal of Scientific and Engineering Research, 5(6), 60-63.

Najm, H. B., & Fahmi Rasheed, M. H. (2023). Flexural Behavior of Two-layers Reinforced Concrete Beams. Polytechnic Journal, 12(2), 20.

Nematzadeh, M., & Fallah-Valukolaee, S. (2021). Experimental and analytical investigation on structural behavior of two-layer fiber-reinforced concrete beams reinforced with steel and GFRP rebars. Construction and Building Materials, 273, 121933.

Newman J., and Choo B.S., "Advanced Concrete Technology," 1st Edition, Elsevier Ltd., UK 2003, pp.(616)

Osman, M., Ismail, H., & Atya, H. (2016). Study of Flexure Behavior of Beams Reinforced with Different Hybrid Percent of Glass and Carbon Bars. British Journal of Applied Science & Technology, 18(3), 1-12.

P. Valerio. 2009. “Realistic Shear Assessment and Novel Strengthening of Existing Concrete Bridges,” PhD Thesis, Dep. Archit. Civ. Eng., BATH University, p. 240, November.

Pang, L., Qu, W., Zhu, P., & Xu, J. (2016). Design propositions for hybrid FRP-steel reinforced concrete beams. Journal of Composites for Construction, 20(4), 04015086.

Qu, W., Zhang, X., & Huang, H. (2009). Flexural behavior of concrete beams reinforced with hybrid (GFRP and steel) bars. Journal of Composites for construction, 13(5), 350-359.

Ramakrishnan, S., Selvakumar, A., Nandagopalan, K. R., and Vivekanandan, R. (2019, July). A study on shear strength of beam reinforced with basalt fiber bars (BFRP). In AIP Conference Proceedings (Vol. 2128, No. 1). AIP Publishing.

Saad, A. Y., & Rasheed, L. S. (2018, November). Behaviours of hybrid deep beams with RPC Layers in the tension region. In *IOP Conference Series: Materials Science and Engineering* (Vol. 433, No. 1, p. 012032). IOP Publishing.

Sada, M. J. (2021, February). Shear performance of hybrid concrete deep beams of trapezoidal section. In IOP Conference Series: Materials Science and Engineering (Vol. 1067, No. 1, p. 012015). IOP Publishing.

Safaa H. Abboud, and P. D. A. Y. A. (2019). Behavior of Reinforced Concrete Thin Beams with Vertical and Horizontal Openings (p. 8).

Said, M., Shanour, A. S., Mustafa, T. S., Abdel-Kareem, A. H., & Khalil, M. M. (2021). Experimental flexural performance of concrete beams reinforced with an innovative hybrid bars. *Engineering Structures*, *226*, 111348.

Sam, A. R. M., & Swamy, R. N. (2005). Flexural behaviour of concrete beams reinforced with glass fibre reinforced polymer bars. Malaysian Journal of Civil Engineering, 17(1), 49-57.

Sarsam, K. F., & Mohammed, M. H. (2014). Load-deflection behavior of hybrid beams containing reactive powder concrete and conventional concrete. Journal of Engineering and Sustainable Development, 18(3), 118-147.

Shakir, Q. M. & Abd, B. B. (2020). "Retrofitting of Self Compacting RC Half Joints with Internal Deficiencies by CFRP Fabrics", Jurnal Teknologi, Vol.82, No.6.

Specification, I.S., "Aggregate From Natural Sources For Concrete and Construction". No. 5 of 1984.

Specification, I.S., "Portland Cement", The Central Organization for Standardization and Quality Control, Baghdad. IQS No. 5/2019.

Sudheer, R & Ramana, R (2011). Evaluation of Shear Resistance of High Strength Concrete Beam without Web Reinforcement Using Ansys

Sun, Z., Fu, L., Feng, D. C., Vatuloka, A. R., Wei, Y., & Wu, G. (2019). Experimental study on the flexural behavior of concrete beams reinforced with bundled hybrid steel/FRP bars. Engineering Structures, 197, 109443.

Szabó, Z. K. (2013). Bond Characteristics of NSM Reinforcements Based on Advanced Test Methods (Doctoral dissertation, Budapest University of Technology and Economics (Hungary).

Vijayan, D. S., Sivasuriyan, A., Devarajan, P., Stefańska, A., Wodzyński, Ł., & Koda, E. (2023). Carbon fibre-reinforced polymer (CFRP) composites in civil engineering application—a comprehensive review. *Buildings*, *13*(6), 1509.

Wei, B., He, X., Zhou, M., Wang, H., & He, J. (2024). Experimental study on flexural behaviors of FRP and steel bars hybrid reinforced concrete beams. *Case Studies in Construction Materials*, *20*, e02759.

Yoon, Y. S., Yang, J. M., Min, K. H., & Shin, H. O. (2011). Flexural strength and deflection characteristics of high-strength concrete beams with hybrid FRP and steel bar reinforcement. Special Publication, 275, 1-22.

Appendix A

Design of Beam (NS-1)

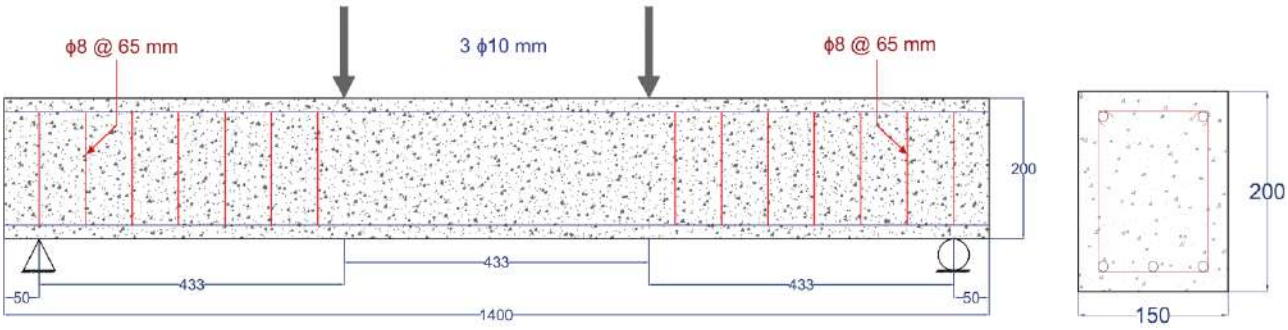

A.1 Calculation of flexural capacity for the beam

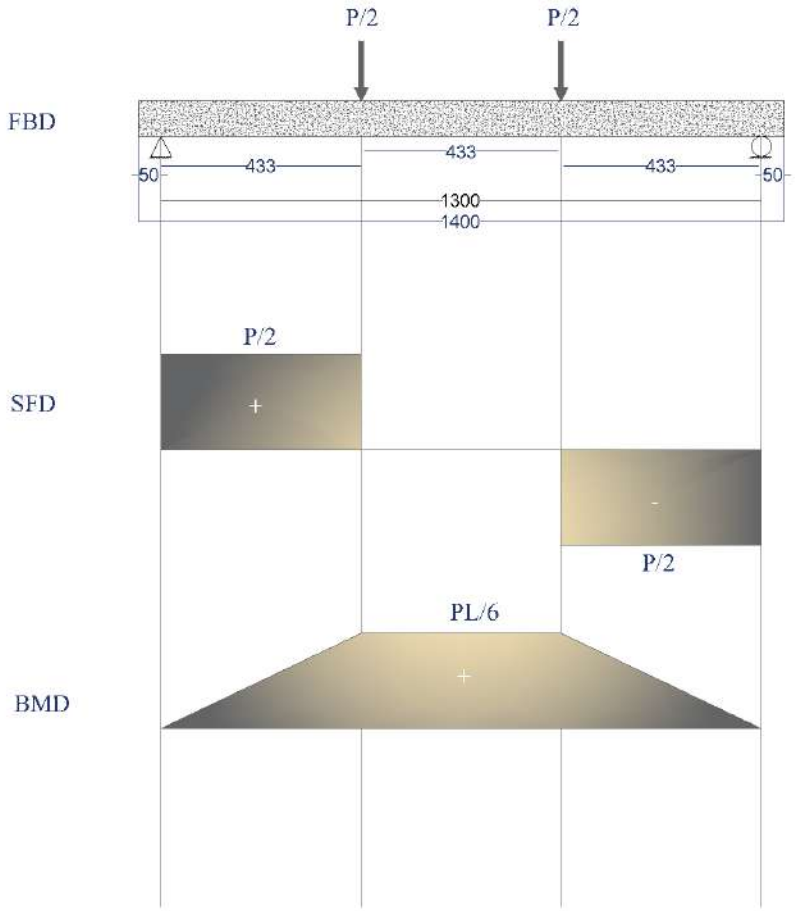

Beam Data

- Beam total span (L) ⟶ 1400 mm
- Beam clear span (L) ⟶ 1300 mm
- Yield strength for steel (Fy) ⟶ 547 MPa
- Concrete strength (f'c) ⟶ 30 MPa
- Height of beam section (h) ⟶ 200 mm
- Width of beam section (b) ⟶ 150 mm
- Cover (Top, bottom, and sides) ⟶ 20 mm
- Effective depth (d) ⟶ 166 mm
- The diameter for top reinforcement is ⟶ 10 mm
- The diameter for bottom reinforcement is ⟶ 10 mm
- The diameter of shear reinforcement is ⟶ 8 mm

Use bar 3 Ø10 for the main reinforcement

$$A_{s\,provide} = 3 \times \frac{\pi\,(\varphi)^2}{4} = 3 \times \frac{\pi\,(10)^2}{4} = 235.62\ mm^2$$

$$\rho_{provide} = \frac{A_{s\,provide}}{b \times d} = 0.00946$$

$$\rho_{max} = 0.85\beta_1 \times \frac{f'c}{fy}\ \frac{\varepsilon_{cu}}{\varepsilon_{cu}+0.004}$$

$$\beta_1 = 0.85 - \frac{f'c - 28}{7} \times 0.05 = 0.835$$

$$\rho_{max} = 0.01668$$

$$\rho_{min} = 0.25 \times \frac{\sqrt{f'c}}{fy} = 0.002503$$

$$\therefore \rho_{min.} < \rho_{provide} < \rho_{max.}$$ ok

- **Find moment capacity:**

$$M_n = A_s \times F_y \times \left(d - \frac{a}{2}\right)$$

$$a = \beta_1 \times C$$

From equilibrium T = C …… get

$$a = \frac{A_s \times F_y}{0.85 \times fc' \times b} = \frac{235.62 \times 547}{0.85 \times 30 \times 150} = 33.7\ mm$$

$$\therefore M_n = 19.22\ kN.m$$

Now find …. $M_u = \varphi M_n$

Find φ from strain diagram

$$\frac{\varepsilon_{cu}}{C} = \frac{\varepsilon_t}{d - C}$$

$$C = \frac{a}{\beta_1} = 35.410\ mm$$

$$\varepsilon_t = 0.00933 > 0.005 \rightarrow \varphi = 0.9$$

∴ M_u = 17.3 kN.m

$$M_u = \frac{P \times L}{6} \rightarrow P_u = 74.14\ kN$$

A.2 Calculation of shear capacity for beam

VC = Nominal shear strength provided by concrete, KN

VS = Nominal shear strength provided by shear reinforcement, KN

Vn = Nominal shear strength, KN

Vu = Shear strength at critical section, KN

Note: Vu at d effective depth = 30.32 KN = Vu applied

$$\varphi V_C = \varphi \times 0.17 \times \sqrt{fc'} \times b \times d$$

φ in shear reinforcement $= 0.75$

$$\varphi V_C = 17.4\ \text{kN} \rightarrow V_C = 23.2\ kN$$

$$\varphi V_u = \varphi V_c + \varphi V_s \rightarrow V_s = \frac{V_u - \varphi V_c}{\varphi} = 17.22\ kN$$

- **Check the dimensions of concrete section:**

Vs < 4 Vc Vs = 17.22 kN, 4Vc = 92.8 kN

17.22 kN < 92.8 kN

∴ The dimension of the concrete section is adequate

Vu > Ø Vc → 30.32 > 17.4 kN …….. we need shear reinforcement

To calculate the shear spacing design:

Region	Vu > Ø Vc
S Theoretical	2Vc = 46.4 KN, Vs < 2 Vc
S for Av minimum	$S = \frac{A_v \times f_y \times d}{V_S}$ Av = No. of legs × Abs = 100.53 mm2 …… **S = 407 mm**
S maximum	Vs < 2Vc 17.22 < 2 × 23.2 = 46.4 KN ok Min. (d 2 or 600 mm) Min. (83 mm or 600 mm)
S required	Min. (S theoretical or S for Av minimum or S maximum) Min. (407 mm, 804.24 mm, 83 mm) S required = 83 mm For safety, use Ø 8 mm @ 65 mm for shear reinforcement

Appendix B

Materials properties (Test Result and Data Sheet for Material Used in Experimental Program)

B.1 Cement

Table B.1: Test Result for Chemical Analysis of Cement

Compound composition	Chemical composition	Weight (%)	Iraqi Limitations No. 5/2019
Lime	**Cao**	61.17	….
Silica	**SiO2**	19.83	….
Alumina	**Al2O3**	3.96	….
Iron oxide	**Fe2O3**	3.62	….
Magnesia	**MgO**	2.31	≤ 5%
Sulfate	**SO3**	2.23	≤2.5%if C3A< 5% ≤2.5%if C3A> 5%
Loss on ignition	**L.O.I**	2.04	≤ 4%
Insoluble residue	**I.R**	0.84	≤ 1.5 %
Lime saturation factor	**L.S.F**	0.79	0.66-1.02
Tricalcium aluminates	**C3A**	2.75	≤ 3.5
Tricalcium silicate	**C3S**	40.26	….
Diacalcium silicate	**C2S**	29.4	….
Tricalcium alumoma ferrite	**C4AF**	8.74	….

*** These results were performed in the Karbala Construction Laboratory.**

Table B.2: Test Result for physical properties of the cement.

Physical Properties	Test Result	Iraqi Limitations No. 5/2019
Fineness (Blaine method) in (m^2/kg)	349	≥ 300
Initial Setting (minute)	142	≥ 45
Final Setting (minute)	193.2	≤ 600
Soundness -Le Chatle(mm)	0.47	≤ 10
Compressive strength at two days (MPa)	22.8	≥ 20
Compressive strength at twenty-eight days (MPa)	43.4	≥ 42.5
Specific gravity	3.15	-

*** These results were performed in the Karbala Construction Laboratory.**

B.3 Fine Aggregate (sand)

Table B.3: Fine Aggregate Test Results.

Sieve size (mm)	Cumulative Passing %	Passing accumulated %Limits of Iraqi specifications No. 45/1984, zone (3)
10	100	100
4.75	99	90 - 100
2.36	89	85 - 100
1.18	80	75 - 90
0.6	69	60 - 79
0.3	40	12 - 40 %
0.15	10	0 - 10
Materials passing from sieve 75 µ %= 3.6% (specification requirements up to 5%)		
SO3 content=0.105% (specification requirements up to 0.5%)		

*** These results were performed in the Karbala Construction Laboratory.**

B.4 Coarse Aggregate (Gravel)

Table B.4: Coarse Aggregate Test Result.

Sieve size (mm)	Passing %	Passing accumulated %Limits of Iraqi specifications No. 45/1984, zone (3)
37.5 (1.5 in)	….	….
19 (3/4 in)	100	100
12.5 (1/2 in)	98	90 - 100
10 (3/8 in)	50	50 - 85
4.75 (No. 4)	3	0 - 10
Mechanical wear =16.1% ((specification requirements up to 35%)		
Materials passing from sieve 75 µ %= 0.29% (specification requirements up to 3%)		
SO3 content=0.03% (specification requirements up to 0.1%)		

*** These results were performed in the Karbala Construction Laboratory.**

B.5 Superplasticizer (SP)

Table B.5: Properties of Super Plasticizer.

Property	Name	Color	Relative density	PH
value	Master Glenium 54	Light green	1.07	8 - 5

B.6 Glass Fiber Reinforced Polymer GFRP Rebar properties

Product Data:

GFRP Rebar Technical Data (General)																		
Diameter(mm)	3	4	6	8	10	12	14	16	18	20	22	25	28	30	32	34	36	40
Cross section(mm^2)	7	12	28	50	73	103	134	180	248	278	355	478	590	671	740	857	961	1190
Density(g/cm^3)	2.2	2.2	2.2	2.2	2.2	2.1	2.1	2.1	2.1	2.1	2.1	2.1	2.1	2.1	2.1	2.1	2.1	2.1
Weight(g/m)	16	28	62	111	173	237	323	422	534	659	798	1030	1292	1484	1688	1906	2136	2638
Ultimate tensile(KN)	13.5	18	36	54	72	99	117	149	189	225	270	342	432	450	504	540	585	640
Ultimate tensile strength (Mpa)	1900	1500	1280	1080	980	870	764	752	744	716	695	675	650	637	626	595	575	509
Ultimate shear strength (Mpa)	>150	>150	>150	>150	>150	>150	>150	>150	>150	>150	>150	>150	>150	>150	>150	>150	>150	>150
E-modulus(GPa)	>40	>40	>40	>40	>40	>40	>40	>40	>40	>40	>40	>40	>40	>40	>40	>40	>40	>40

High Property GFRP Rebar						
Diameter(mm)	10	16	20	22	25	32
Cross section(mm^2)	73	180	278	355	478	740
Density(g/cm)	2.2	2.1	2.1	2.1	2.1	2.1
Weight(g/m)	173	422	659	798	1030	1688
Ultimate tensile (KN)	85	180	310	390	450	640
Ultimate tensile strength (Mpa)	1000	1000	1000	1000	900	850
Ultimate shear strength (Mpa)	>150	>150	>150	>150	>150	>150
E-modulus(GPa)	>45	>45	>45	>45	>45	>45



Fig. B. 1. Glass Fiber Reinforced Polymer GFRP Rebar (According to the Manufacturer**).**

B.7 Carbon Fiber Reinforced Polymer CFRP Rebar properties

Product Data:

DIAMETER:	4-26 mm
TENSILE STRENGTH:	1800-2200 Mpa
ELASTIC MODULUS:	140-155 Gpa
ELONGATION:	1.3-1.5%
DENSITY:	1.6-1.8g/m^3
COEFFICIENT OF THERMAL EXPANSION	0 (x10-6/° C)
SURFACE:	Ribbed/wrapped/sand coated
MATERIAL:	Carbon Roving & Epoxy Additives

Fig. B. 2. Carbon Fiber Reinforced Polymer CFRP Rebar (According to the Manufacturer**).**

Appendix C

ABAQUS Requirements

C.1 Material used in ABAQUS 2017 :

Table C.1: General properties of concrete

Group	Specimen designation	Compressive strength (MPa)	Young modulus (MPa)	Poisson Ratio
group 1	NS-1	For normal strength = **30.12 Mpa** For high strength = **57 Mpa**	For normal strength = **28839.01 Mpa** For high strength = **35484.22 Mpa**	For normal strength = **0.18** For high strength = **0.2**
	HS-1			
	NHS-2			
group 2	NC-1			
	HC-1			
	NHC-2			
group 3	NG-1			
	HG-1			
	NHG-2			
group 4	SSC-2			
	CCS-2			
	SSG-2			
	GGS-2			
	CCG-2			
	GGC-2			
Parameter Study	NHS-2 Layers			
	NHC-2 Layers			
	NHG-2 Layers			

Table C.2: Parameters of concrete damaged plasticity

Type	Dilation angle	Eccentricity	Fb0/fc0	k	Viscosity parameter
Normal strength	35	0.1	1.16	0.67	0.003
High strength	40	0.1	1.16	0.67	0.003

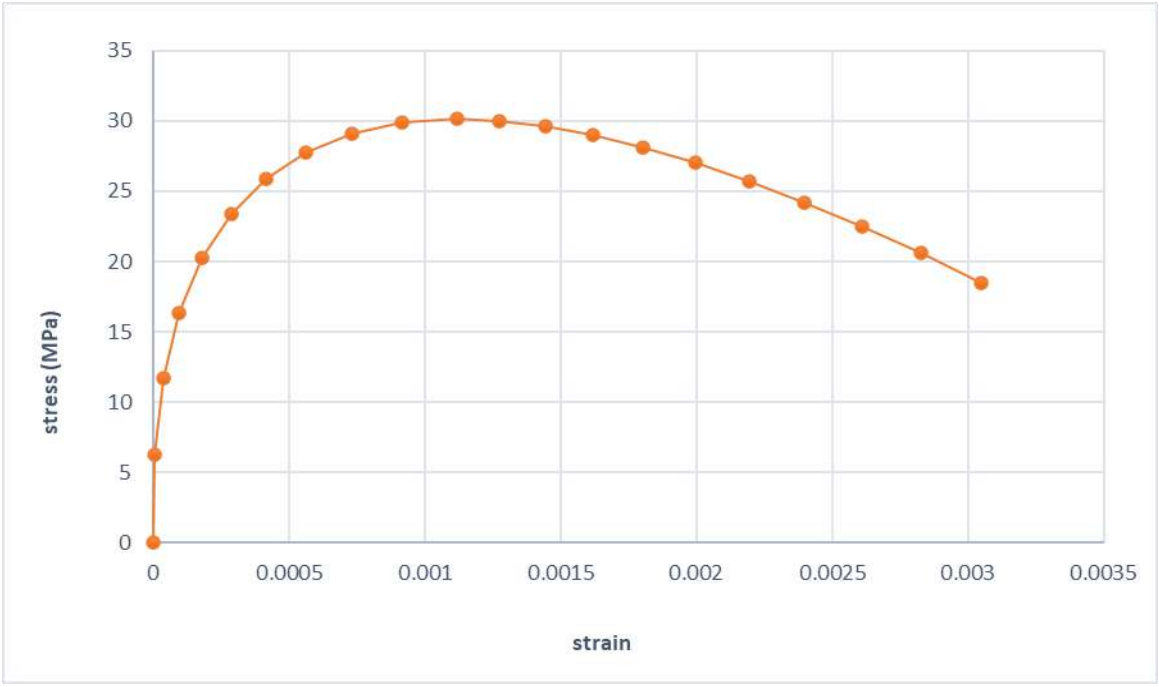

Fig. C. 1. Model of stress-strain relationship used for Normal strength concrete (Hassan et al.,2020).

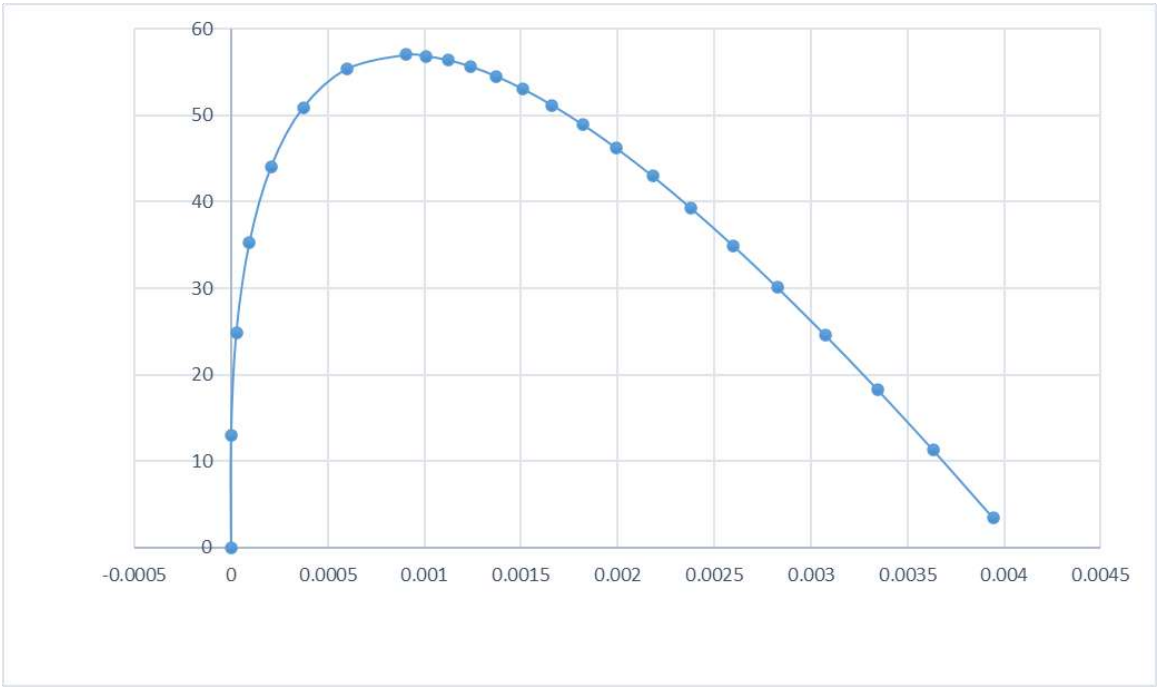

Fig. C. 2. Model of stress-strain relationship used for High strength concrete (Hassan et al.,2020).

Table C.3: Stress-strain relationship for compressive behavior for normal and high strength used in this study for normal concrete (Carreira & Kuang-Han Chu, 1985).

For normal strength		
Number	Yield stress (MPA)	Plastic strain (mm)
1	0	0
2	6.298886803	0.000209986
3	11.73255911	0.000419973
4	16.35954345	0.000629959
5	20.23320411	0.000839945
6	23.40230005	0.001049931
7	25.91147119	0.001259918
8	27.80166436	0.001469904
9	29.11050751	0.00167989
10	29.87263927	0.001889876
11	30.12	0.002099863
12	29.9888818	0.002255365
13	29.60287877	0.002410867
14	28.97256097	0.002566369
15	28.10792198	0.002721872
16	27.01841766	0.002877374
17	25.71300185	0.003032876
18	24.20015924	0.003188378
19	22.48793571	0.003343881
20	20.58396632	0.003499383
21	18.49550121	0.003654885

For high strength		
Number	Yield stress (MPA)	Plastic strain (mm)
1	0	0
2	13.04337812	0
3	24.87992091	2.71075E-05
4	35.3100683	9.48576E-05
5	44.08769504	0.000207169
6	50.90568749	0.000372325
7	55.37580542	0.000600792
8	57	0.000906003
9	56.85533565	0.001009544
10	56.40916975	0.001121215
11	55.64206588	0.001241541
12	54.53288036	0.001371091
13	53.05857046	0.001510487
14	51.1939764	0.001660407
15	48.91157245	0.001821594
16	46.18118213	0.001994861
17	42.96965127	0.002181103
18	39.24047144	0.002381304
19	34.95334471	0.00259655
20	30.06367893	0.002828044
21	24.522	0.00307712
22	11.25605624	0.003634128
23	3.401630185	0.00394557

➢ Stresses distribution for concrete and reinforcement:

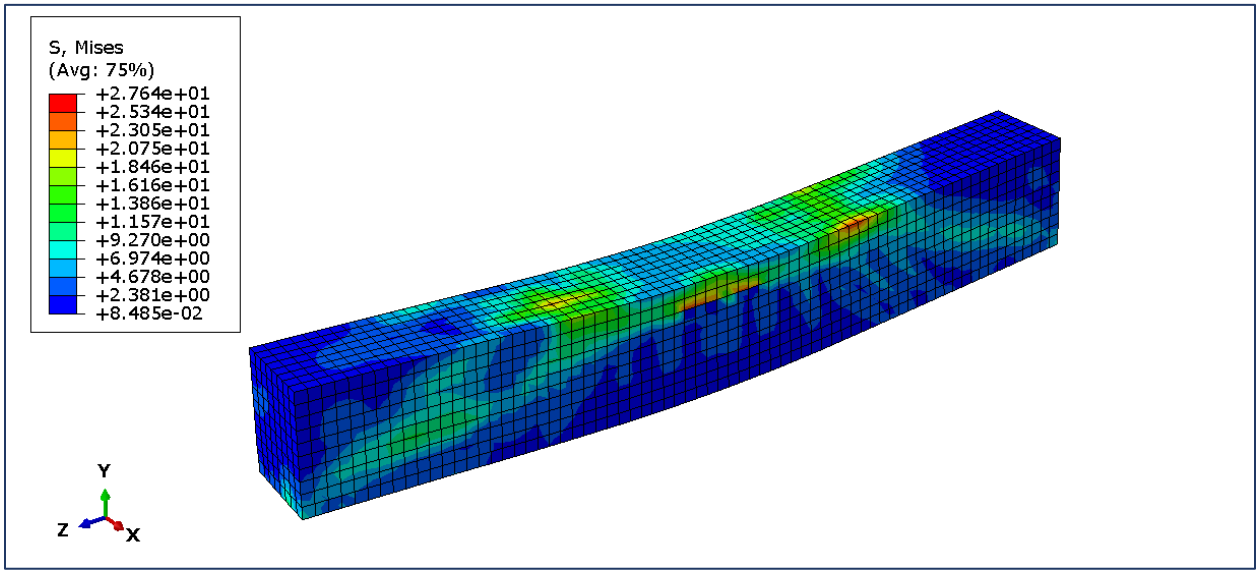

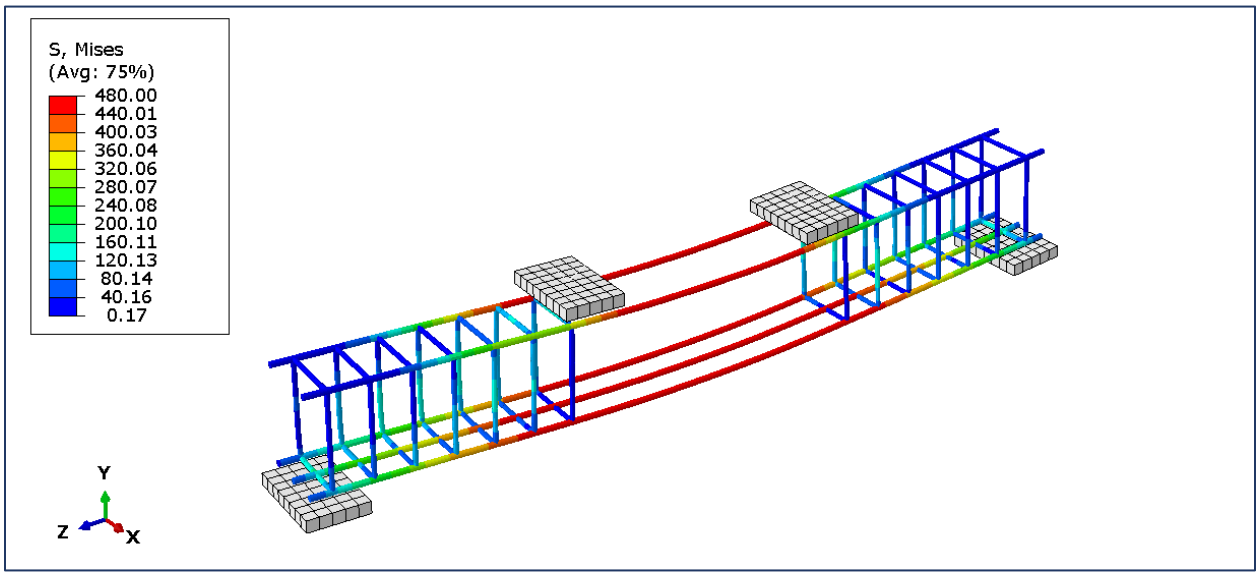

Fig. C. 3. Stress distribution for concrete and reinforcement in (NS-1).

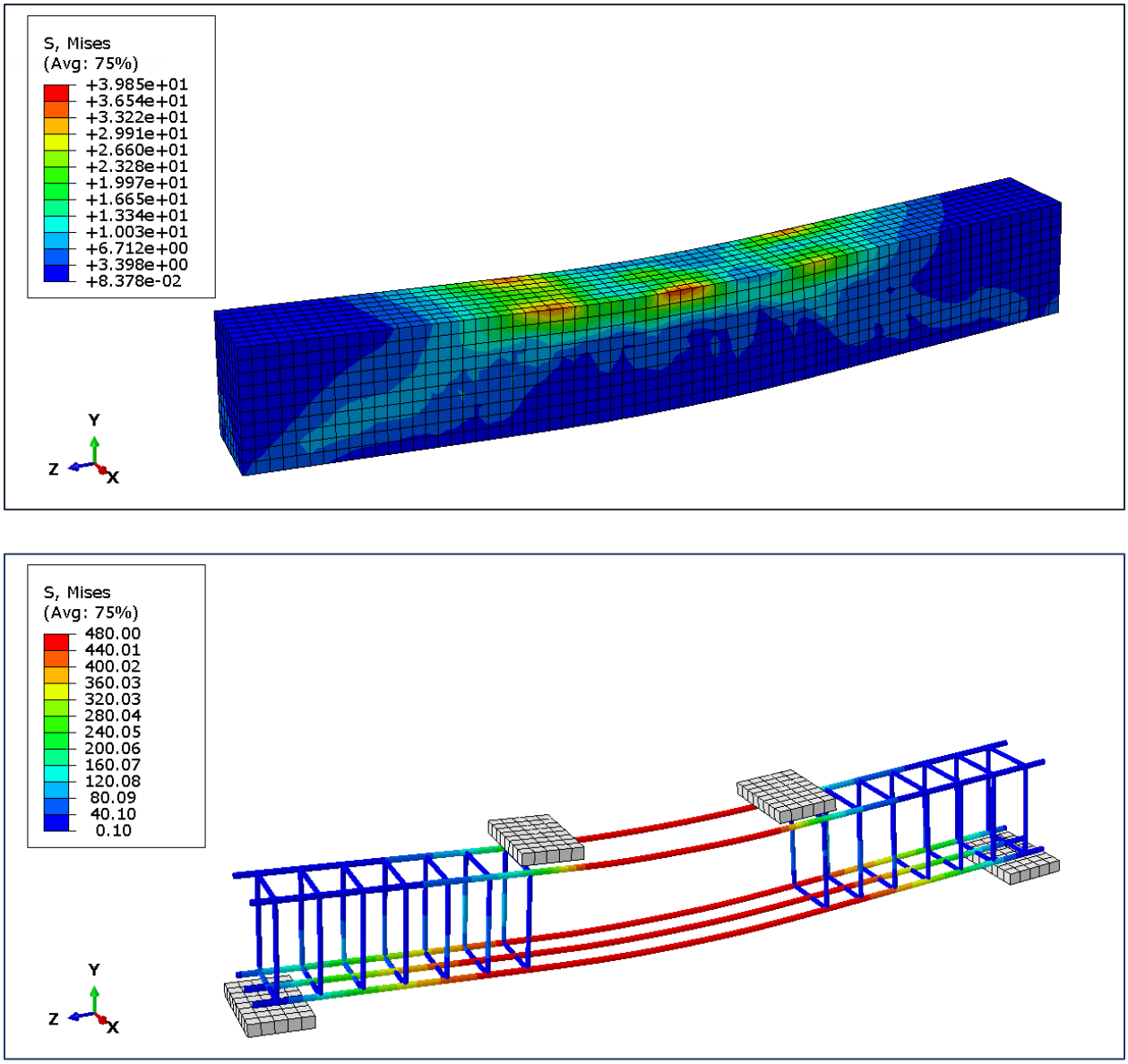

Fig. C. 4. Stress distribution for concrete and reinforcement in (HS-1).

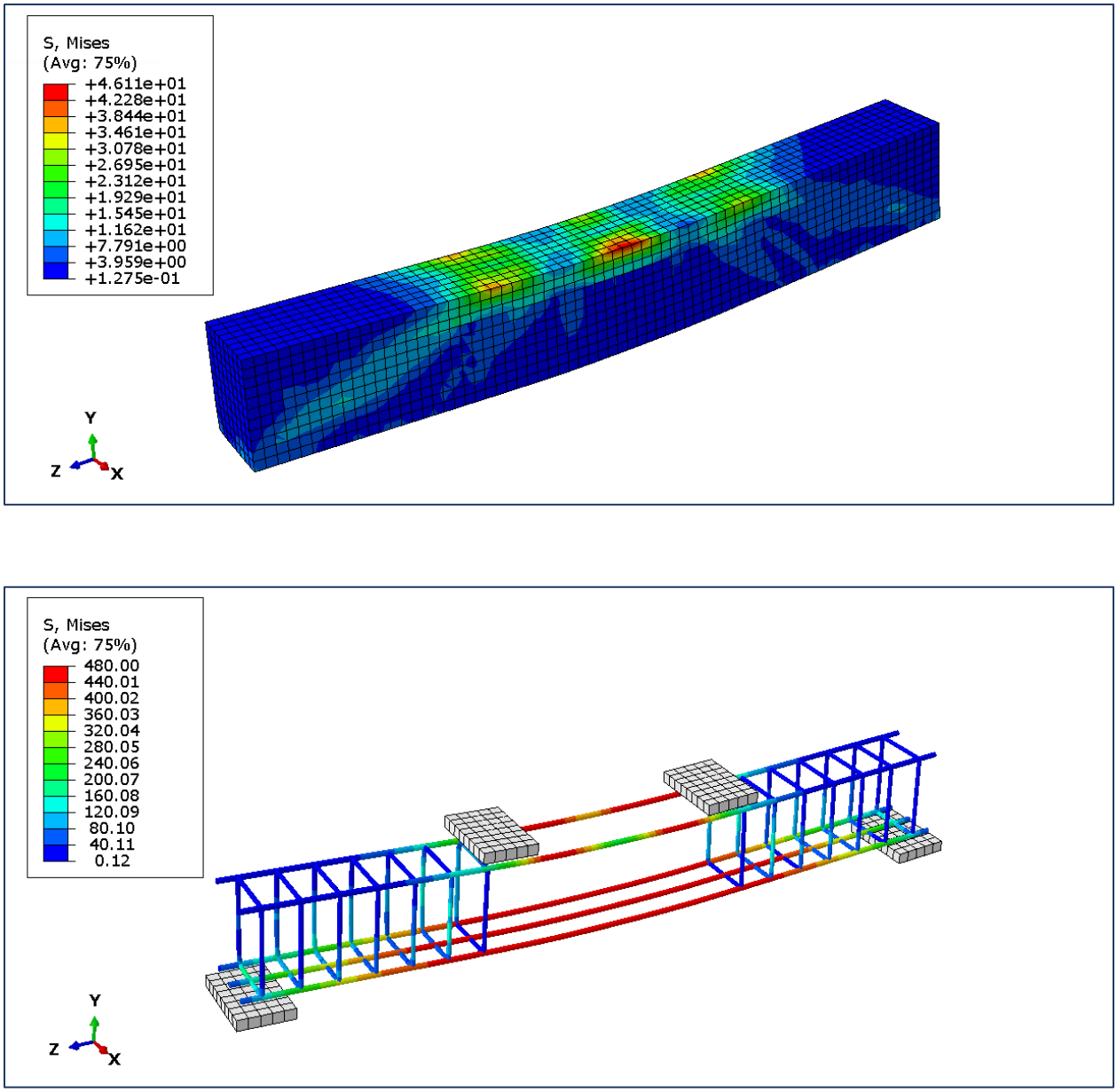

Fig. C. 5. Stress distribution for concrete and reinforcement in (NHS-2).

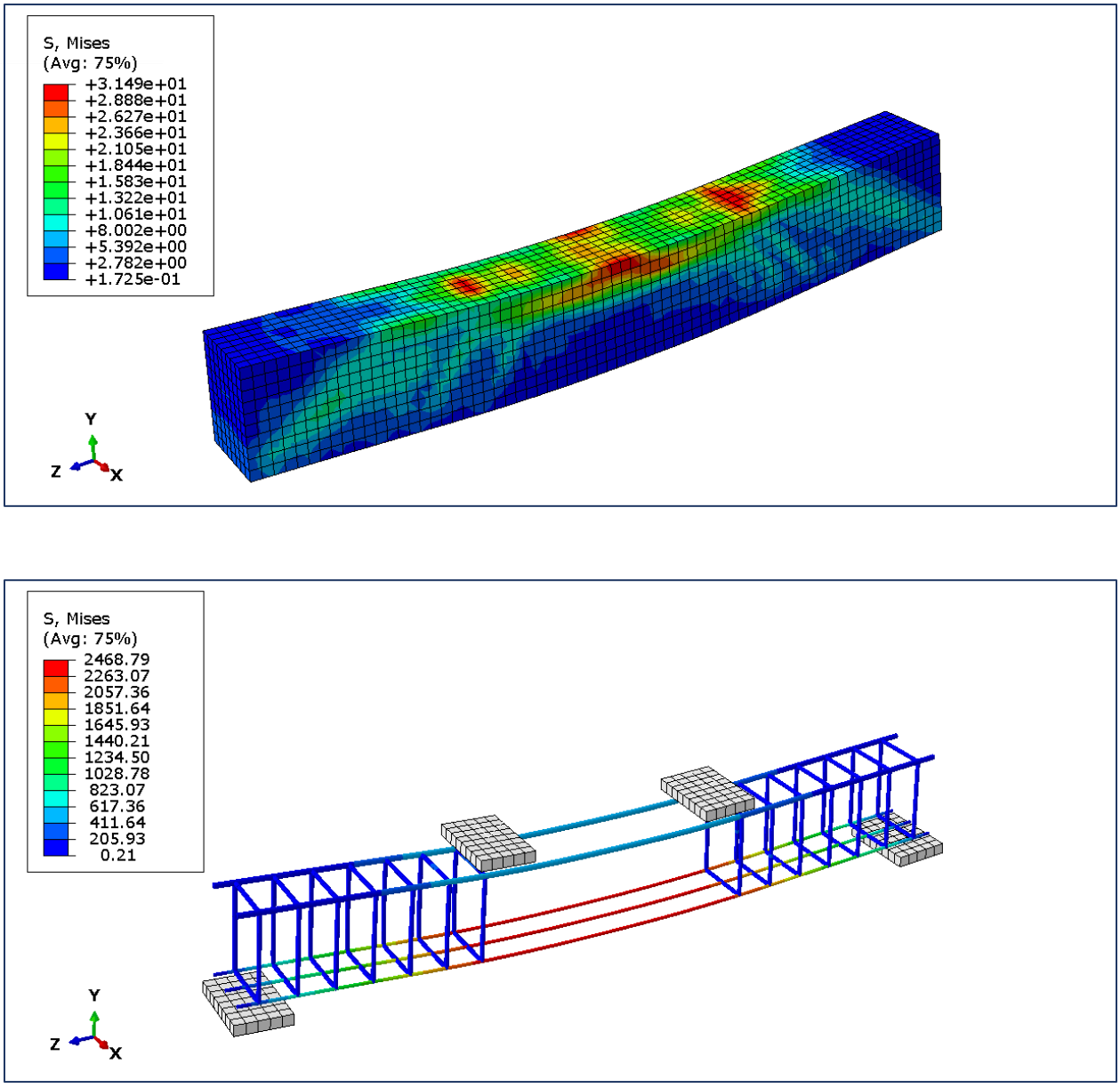

Fig. C. 6. Stress distribution for concrete and reinforcement in (NC-1).

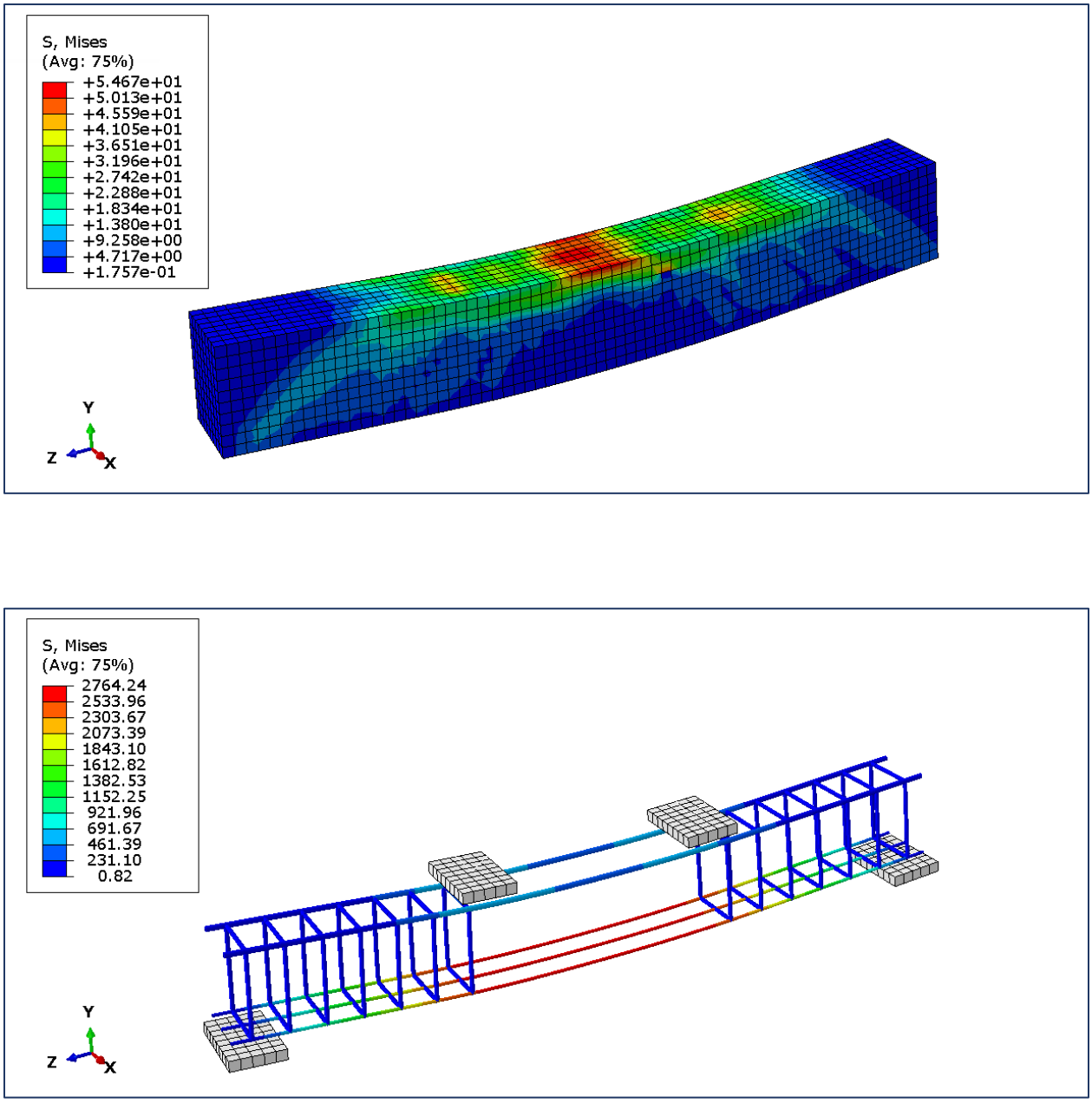

Fig. C. 7. Stress distribution for concrete and reinforcement in (HC-1).

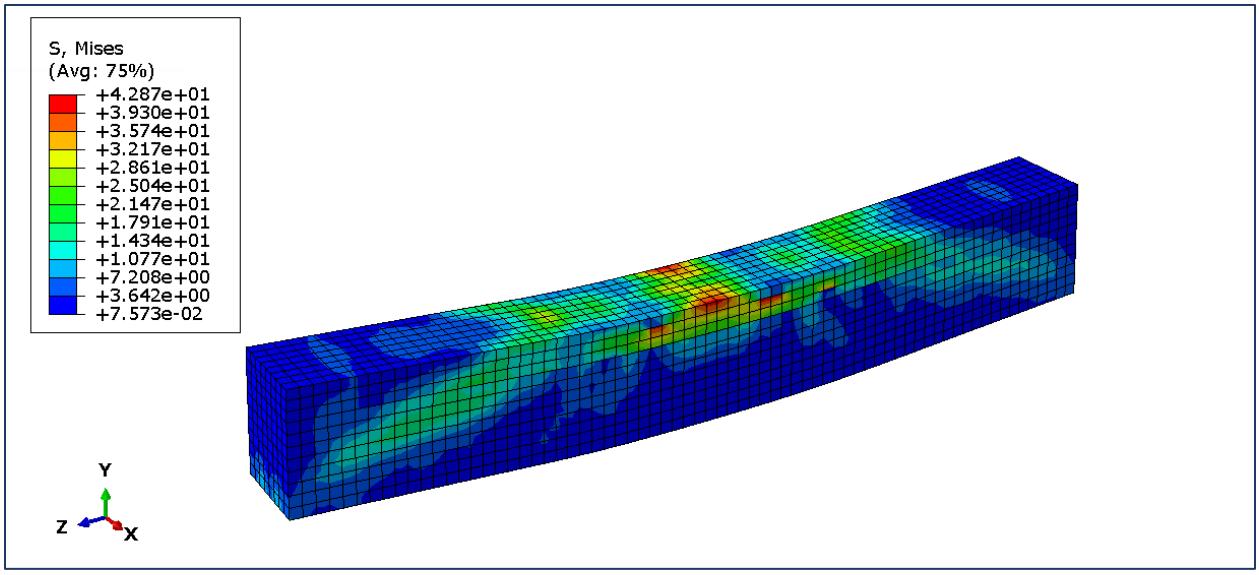

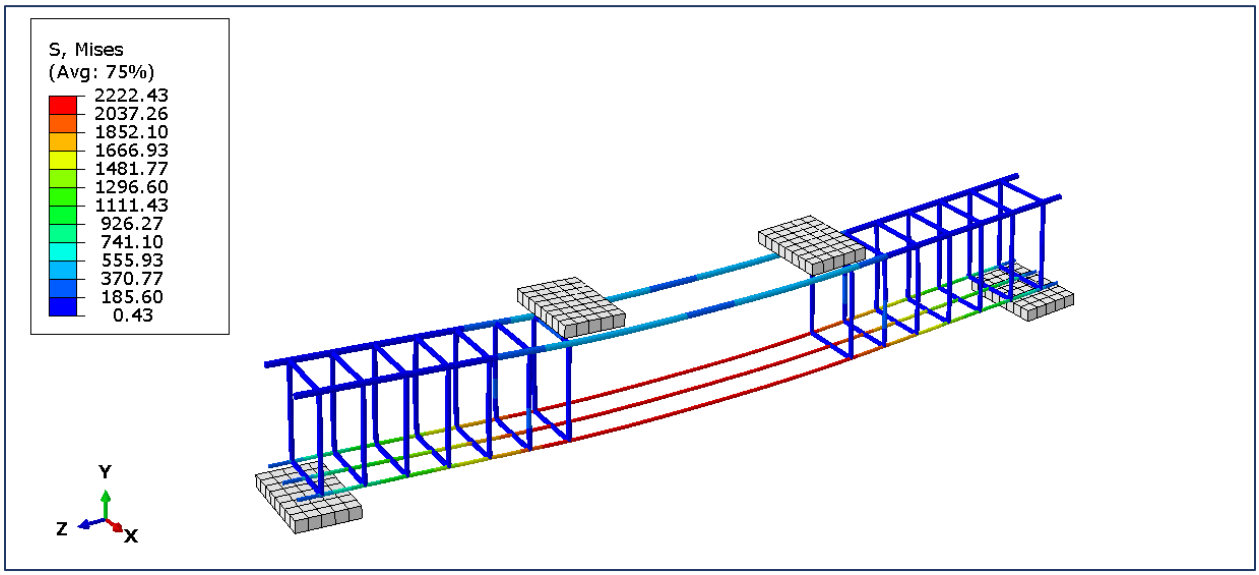

Fig. C. 8. Stress distribution for concrete and reinforcement in (NHC-2).

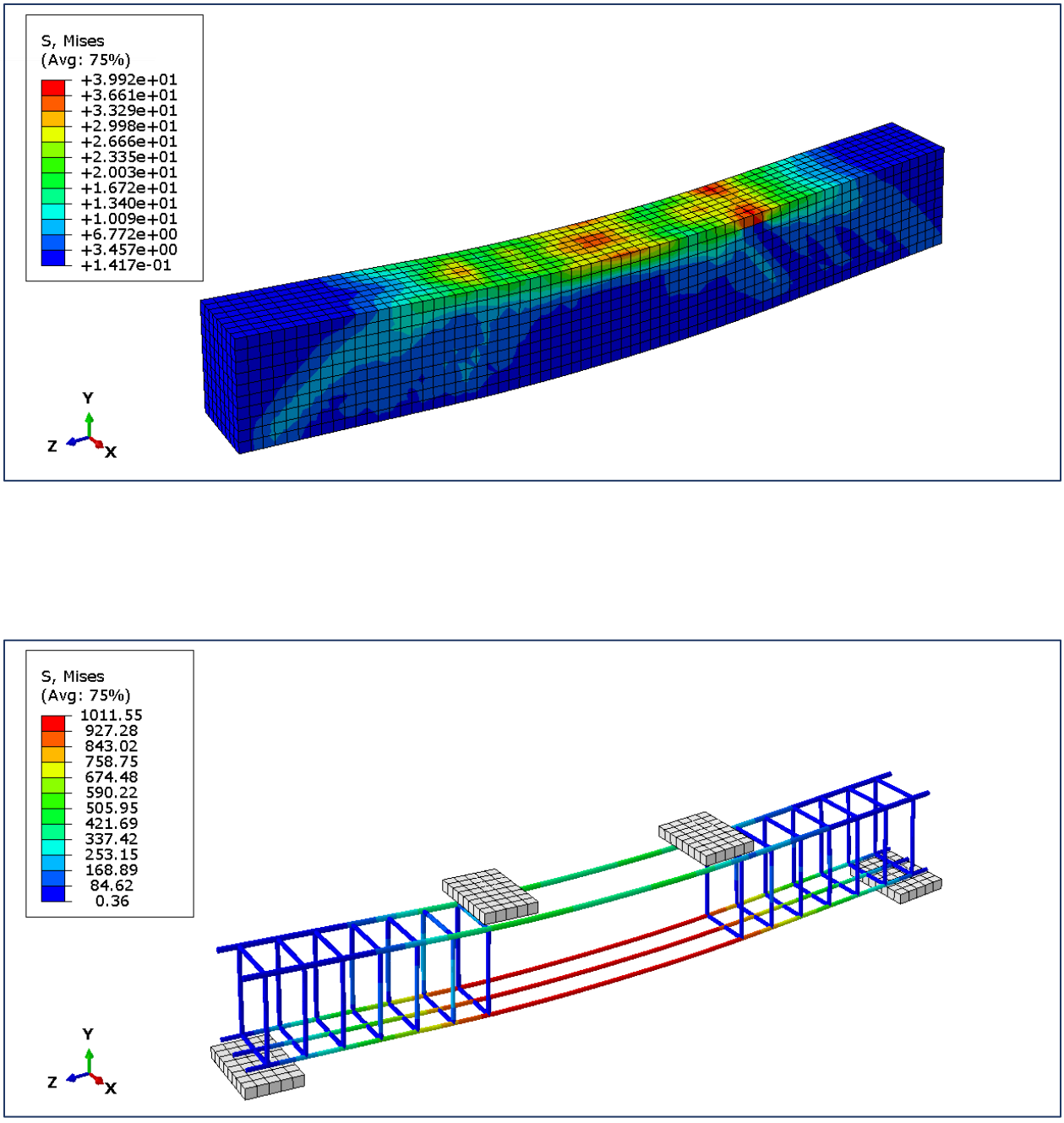

Fig. C. 9. Stress distribution for concrete and reinforcement in (NG-1).

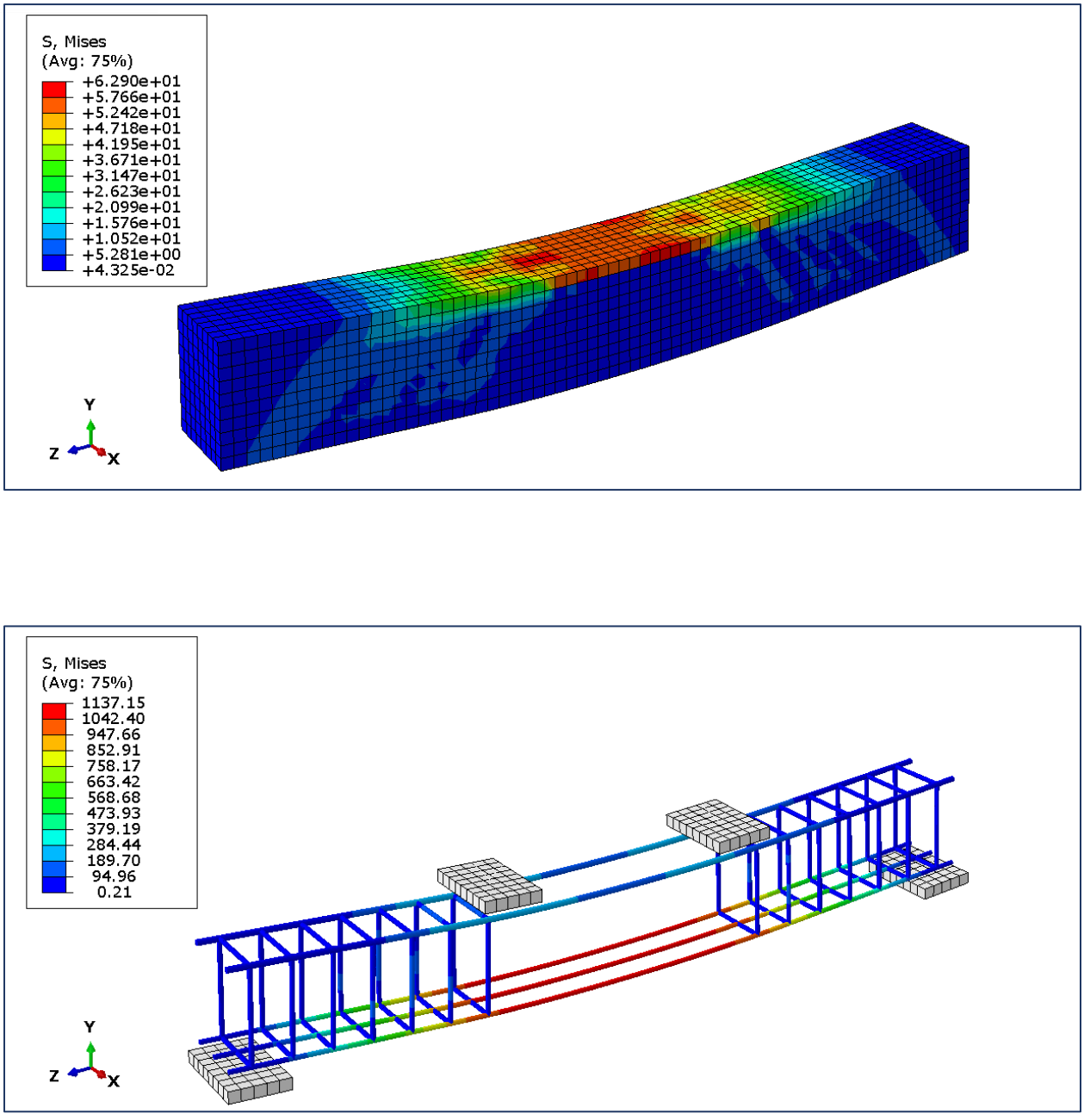

Fig. C. 10. Stress distribution for concrete and reinforcement in (HG-1).

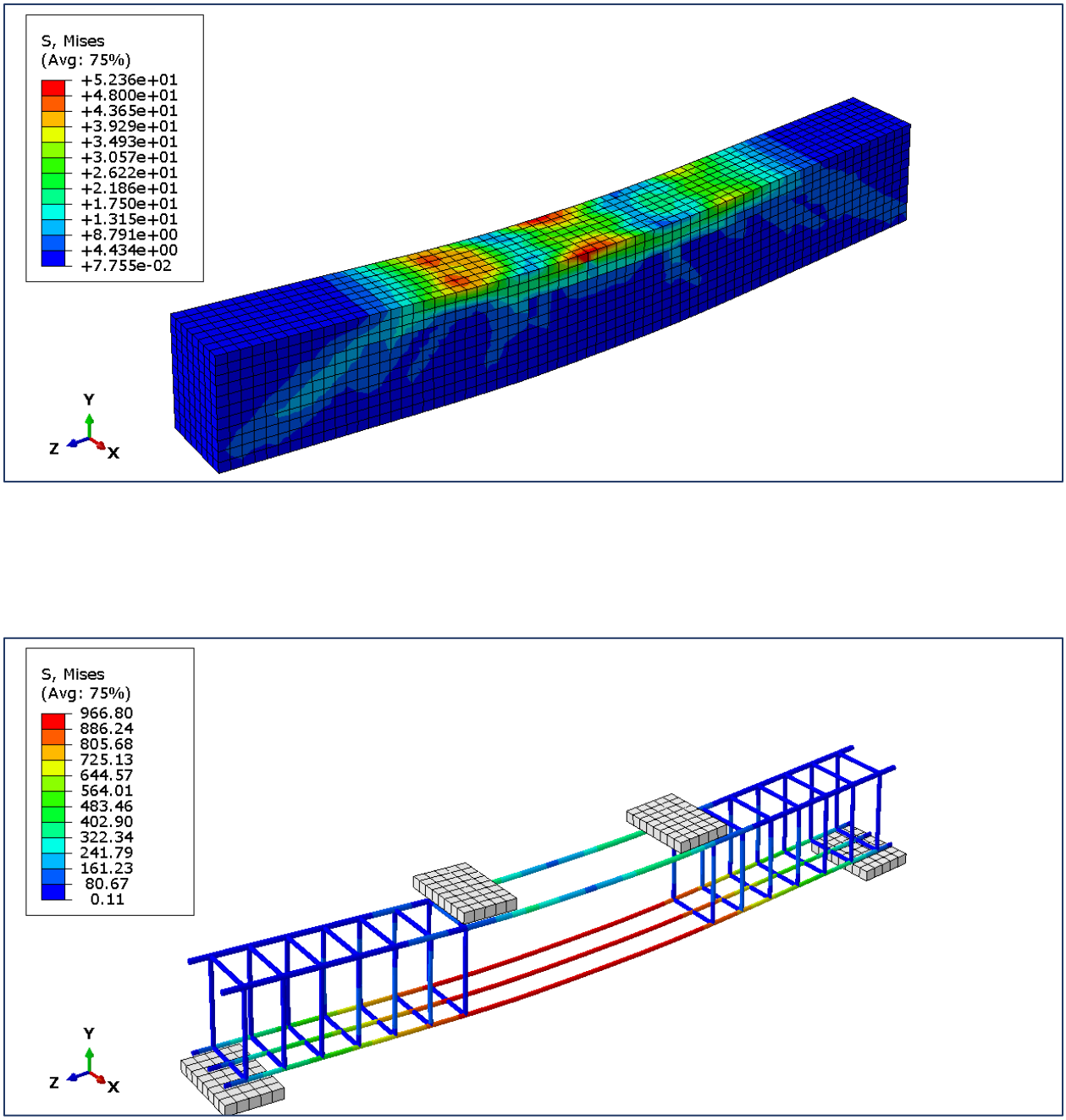

Fig. C. 11. Stress distribution for concrete and reinforcement in (NHG-2).

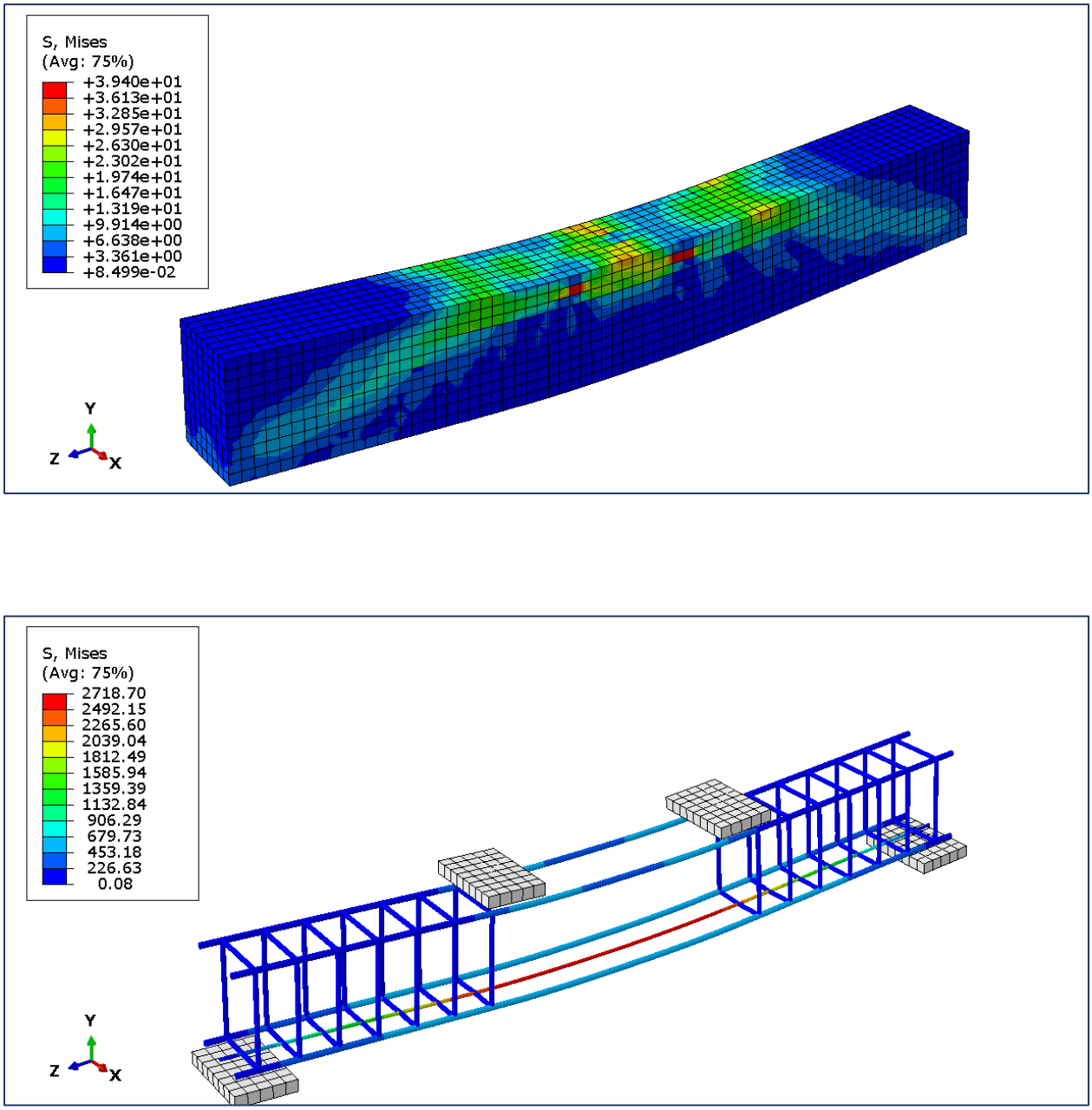

Fig. C. 12. Stress distribution for concrete and reinforcement in (SSC-2).

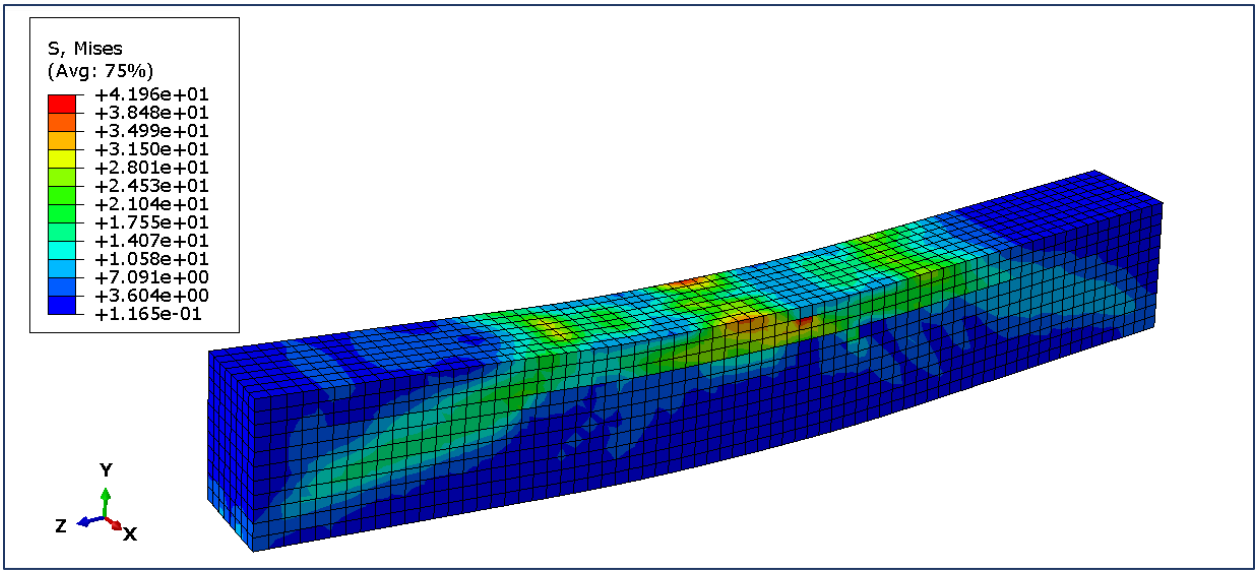

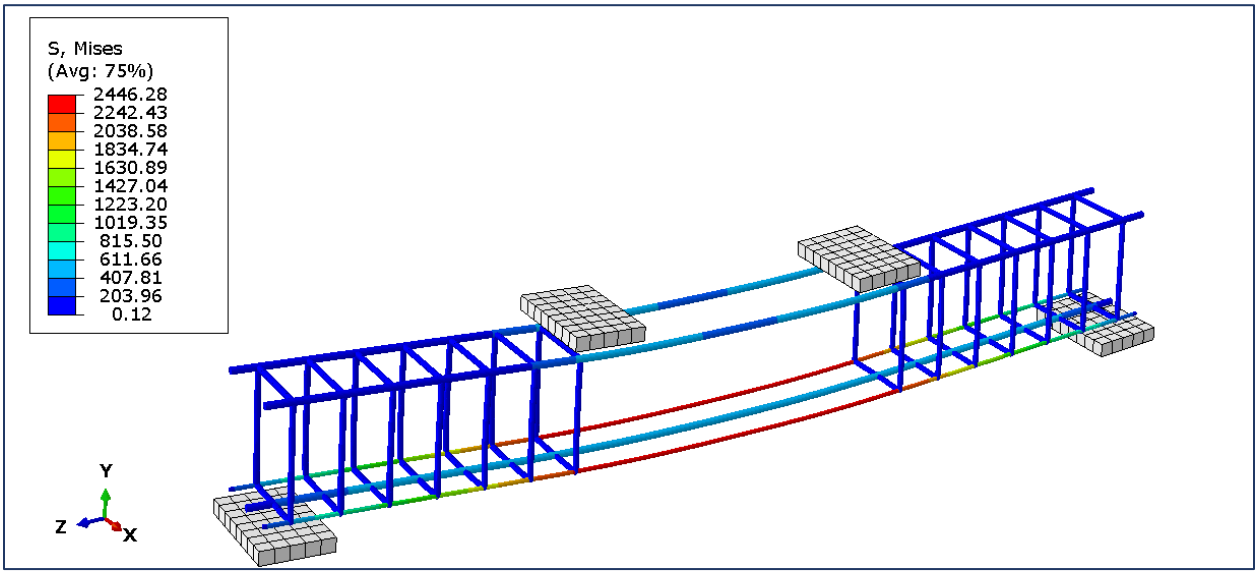

Fig. C. 13. Stress distribution for concrete and reinforcement in (CCS-2).

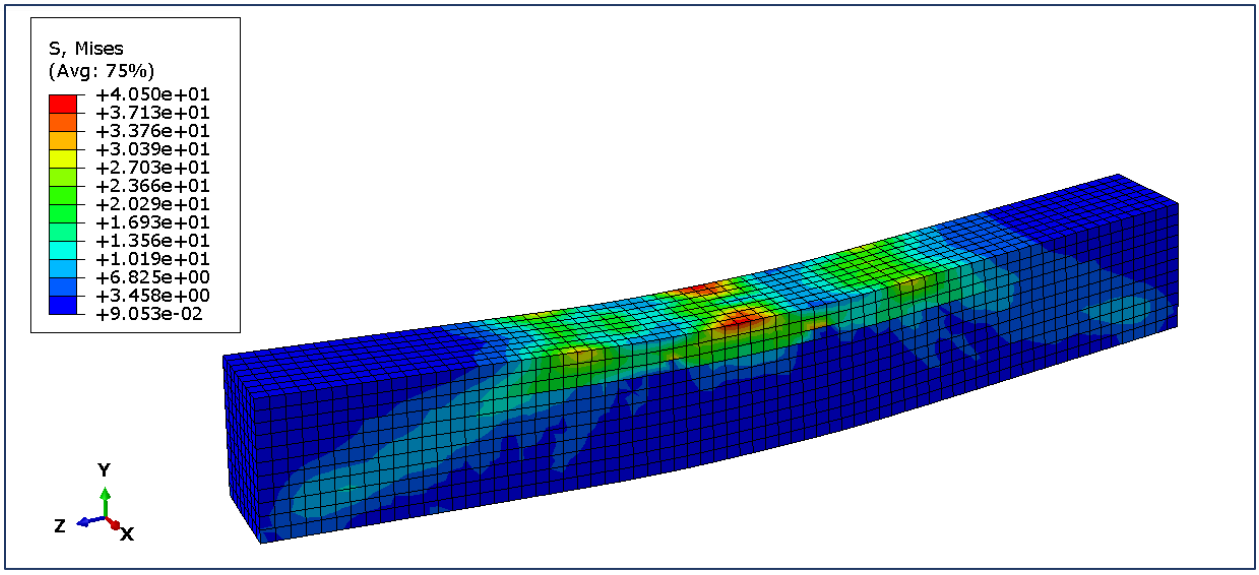

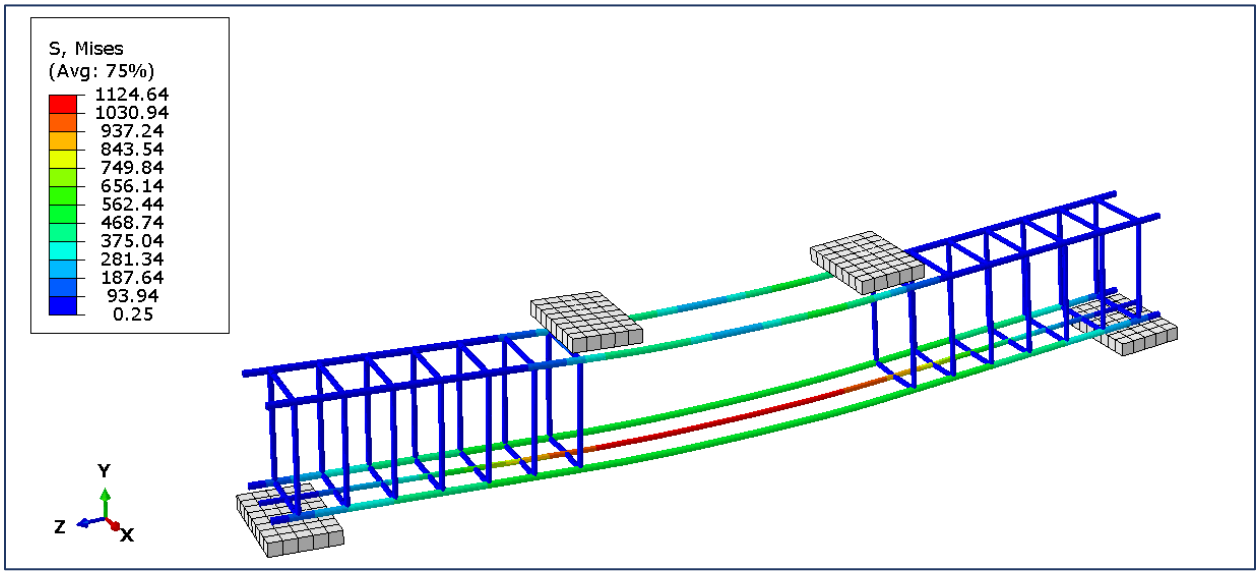

Fig. C. 14. Stress distribution for concrete and reinforcement in (SSG-2).

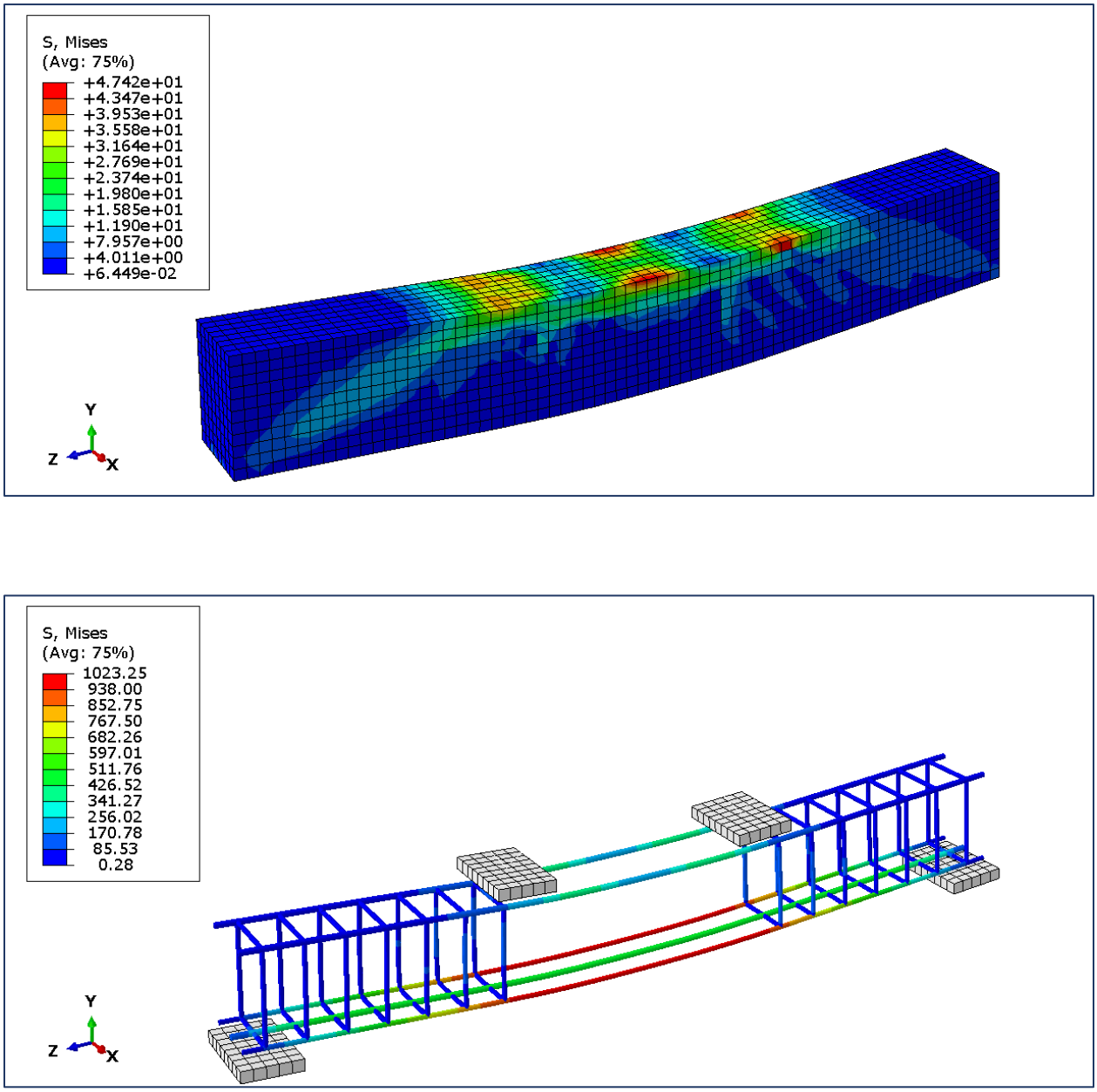

Fig. C. 15. Stress distribution for concrete and reinforcement in (GGS-2).

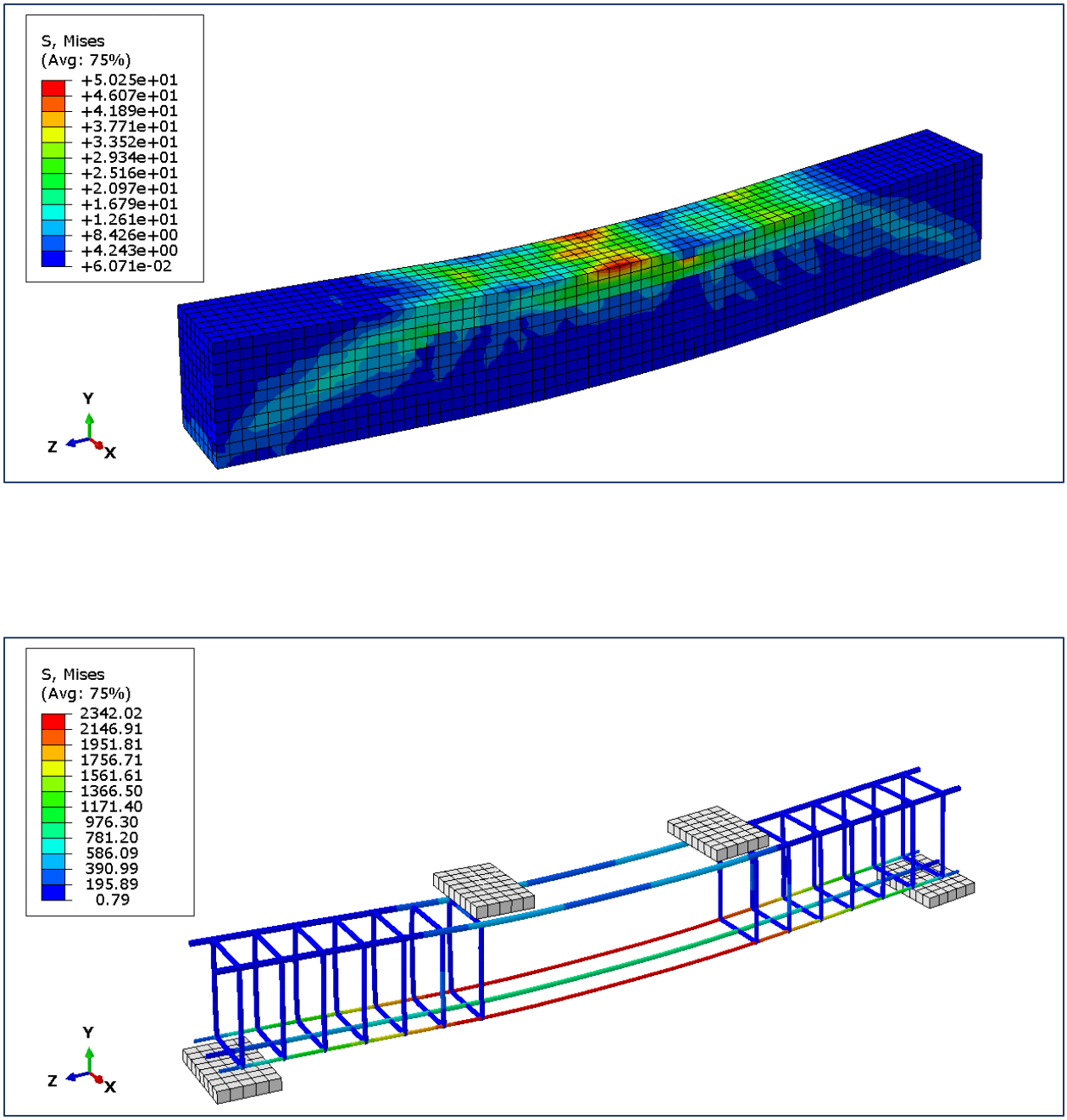

Fig. C. 16. Stress distribution for concrete and reinforcement in (CCG-2).

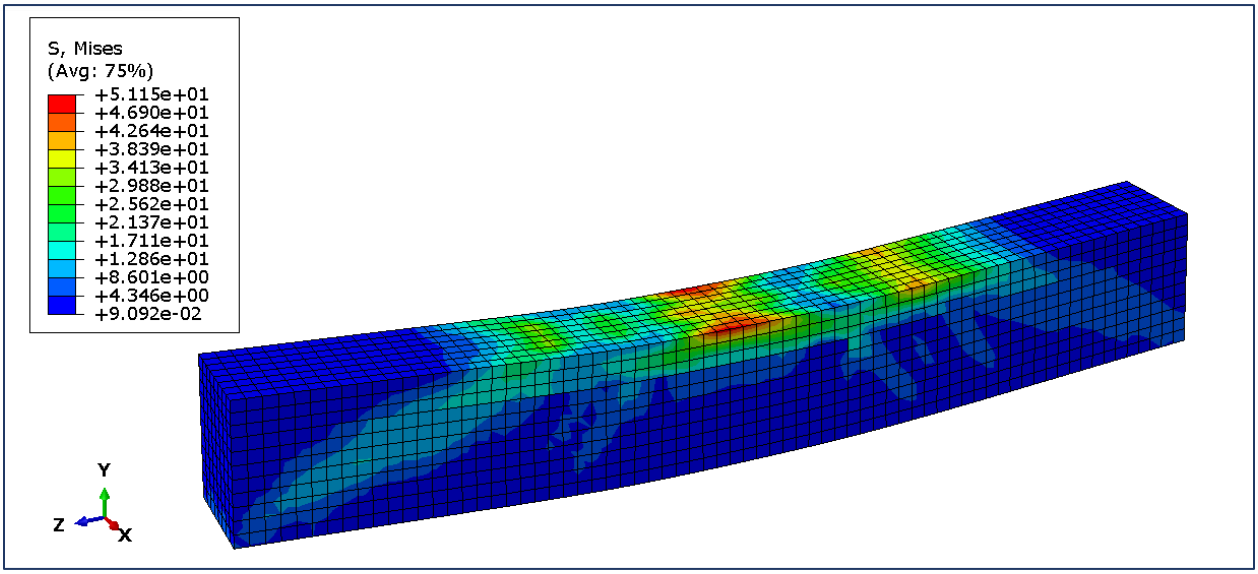

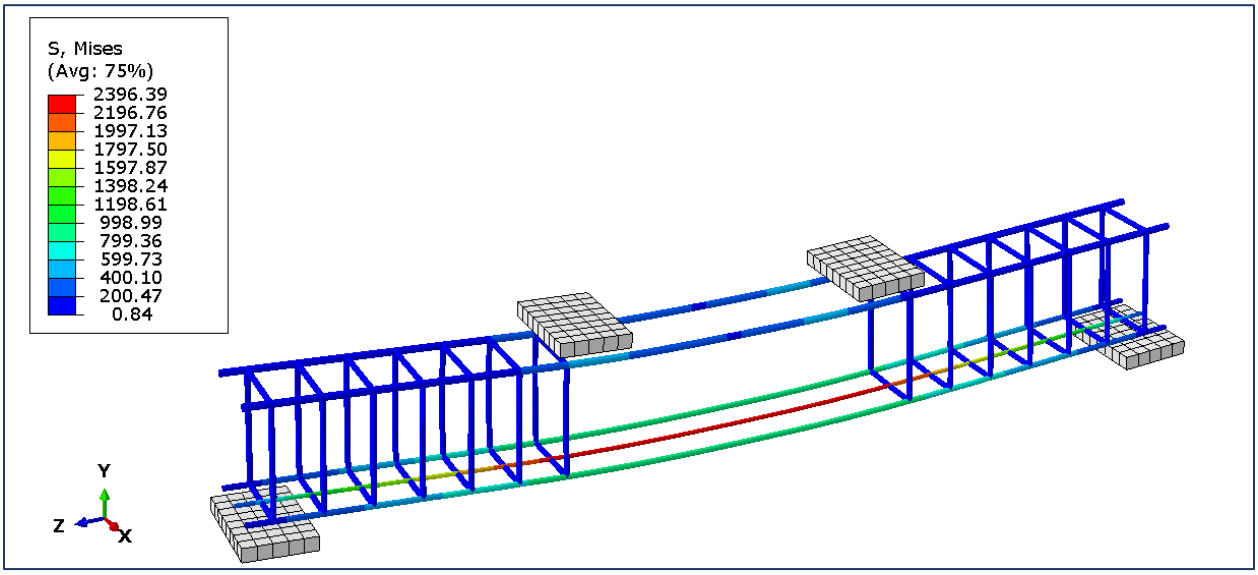

Fig. C. 17. Stress distribution for concrete and reinforcement in (GGC-2).

الخلاصـــــــة

تُعد العتبة الخرسانية ثنائية الطبقة عنصراً إنشائياً متخصصاً يتكوّن من طبقتين مختلفتين من الخرسانة، وقد صُممت هذه البنية لتحسين الكفاءة الإنشائية من خلال تعزيز مقاومة الانثناء، والمتانة، والقدرة النهائية على التحمل تحت ظروف تشغيلية متعددة. وقد أثبت الجمع بين التسليح بالألياف الزجاجية والكربونية المدعّمة بالبوليمر(GFRP, CFRP) ، والتسليح الفولاذي، والتسليح الهجين في العتبات الخرسانية ثنائية الطبقة أنه بديل مناسب للتسليح الفولاذي التقليدي، لما يتمتع به من نسبة عالية بين المقاومة والوزن، بالإضافة إلى تحسين الأداء الانثنائي ومقاومة التشقق. يهدف هذا البحث إلى تقييم الأداء الانثنائي (القدرة على التحمل، انتشار التشققات، والانحراف) للعتبات الخرسانية ثنائية الطبقة والمسلحة بأنواع مختلفة من قضبان التسليح (حديد، CFRP، GFRP، أو تسليح هجين)، وذلك من خلال الدراسة التجريبية والتحليل العددي تحت حمل نقطتين. تم تصنيع خمسة عشر نموذجاً بأبعاد (150×200×1400 ملم) في الموقع، حيث شملت ستة نماذج بطبقة خرسانية واحدة، بينما تكوّنت التسعة الأخرى من طبقتين خرسانيتين. استُخدمت الخرسانة الاعتيادية المقاومة (NSC)في منطقة الشد، بينما وُظّفت الخرسانة عالية المقاومة (HSC) في منطقة الضغط بهدف تحسين خصائص المادة والسلوك الإنشائي. تم تصنيف النماذج إلى أربع مجموعات اعتماداً على نوع التسليح المستخدم: قضبان (الحديد، CFRP، GFRP، والتسليح الهجين). وقد تم تمثيل السلوك غير الخطي للعتبات باستخدام برنامج ABAQUS للتحليل العددي. أظهرت النتائج تقارباً جيداً بين النماذج العددية والقياسات المختبرية، بمتوسط الفرق في الحمل الأقصى حوالي 2.1% وفي هبوط اقصى 4.93%. كما بينت النتائج أن النماذج ثنائية الطبقة سجلت تحسناً في الحمل الأقصى بنسبة 12.77%، وفي حمل التشقق الأول بنسبة 30.95% مقارنة بالنماذج أحادية الطبقة. كذلك، أظهرت النماذج ذات التسليح الهجين زيادة في المطيلية بنسبة 7.3% مقارنة بتلك المسلحة بنوع واحد من القضبان. تُشير هذه النتائج إلى أن التصاميم الهجينة المقترحة تُحسّن الأداء الإنشائي، وتقدّم حلاً واعداً لبناء منظومات خرسانية أكثر استدامة وكفاءة.

جمهورية العراق

وزارة التعليم العالي و البحث العلمي

جامعة كربلاء

كلية الهندسة

قسم الهندسة المدنية

أداء الانثناء للأعتاب الخرسانية ثنائية الطبقة المسلحة بقضبان مختلفة الأنواع

رسالة مقدمة الى

مجلس كلية الهندسة جامعة كربلاء وهي جزء من متطلبات نيل درجة الماجستير في علوم الهندسة المدنية

المؤلف:

سلام حسين مدلول

(بكالوريوس هندسة مدنية – الجامعة المستنصرية – 2019)

باشراف :

أ.م.د زينب محمد رضا عبد الرسول

أ.م.د مشتاق صادق راضي

شوال - 1446 نيسان - 2025